Synthesis and Characterisation of Stimulus-responsive Diblock Copolymer Nano-objects Prepared by RAFT Aqueous Dispersion Polymerisation

Sarah Jayne Wilson

Department of Chemistry
The University of Sheffield

Submitted to the University of Sheffield in fulfilment of the requirements for the award of Doctor of Philosophy

September 2019

The work described in this thesis was undertaken at the University of Sheffield under the supervision of Professor Steven P. Armes between October 2015 and September 2019 and has not been submitted, either wholly or in part, for this or any other degree. All the work is the original work of the author, except where acknowledged.

Signature: _____

Sarah Jayne Wilson

September 2019

Acknowledgements

I feel very lucky to have been surrounded by supportive and encouraging people throughout the ups and downs that have led to the completion of this thesis. Firstly, I would like to express my gratitude to my supervisor, Prof. Steve Armes FRS. Thank you for allowing me to undertake this research in your group. I am extremely grateful for all of the unforgettable, amazing experiences that I have had in the past four years including the opportunity to attend several international conferences and to publish three research papers. Your dedication to this piece of research is truly appreciated.

I would like to acknowledge BASF for the partial funding of this project and in particular my industrial supervisor, Dr Adam Blanazs, for his time and advice and for allowing me to visit Germany.

The CDT in polymers, soft matter and colloids and the EPSRC are thanked for partial funding of this project with special thanks to Dr Joe Gaunt for his guidance.

I'd like to thank Svetomir Tzokov and Christopher Hill for their TEM expertise, Sandra van Meurs and Craig Robertson for their NMR spectroscopy advice and for conducting several NMR experiments and Denise Richards and Louise Brown-Leng for always going above and beyond to sort out any finance and admin issues.

Cate O'Brien, Dr Matthew Derry and Dr Oleksandr Mykhaylyk are thanked for collecting and analysing the SAXS data and for sharing their SAXS expertise.

To the members of the Armes, Spain and Ryan/Mykhaylyk groups, past and present, thank you for making my time in the upstairs and downstairs offices so enjoyable. Special thanks to Cate, Nick, Matt R and Matt D for taking the time to answer all of my chemistry-related questions!

I am extremely thankful to the members of Fitmums and Friends running group and my friends at parkrun for providing a healthy distraction, excellent conversion and for making running enjoyable.

To Louise, Sam, Chelsea and Shaun I thank you for your support and constant supply of evenings filled with food. To my dear friends, Jessica, Jonathan, Victoria, Josh, Cate and Matt thank you for being there whenever I need you.

To Jason and Rebecca, I am deeply grateful for your love and constant support and encouragement.

To my father, mother, father-in-law and mother-in-law, this wouldn't have been possible without you. I hope I have made you all proud.

Finally, I dedicate this Thesis to my husband James who supports me in everything that I do.

Publications

S. J. Byard, M. Williams, B. E. Mckenzie, A. Blanazs and S. P. Armes, Macromolecules, 2017, 50, 1482–1493.

S. J. Byard, A. Blanazs, J. Miller and S. P. Armes, Langmuir, 2019, 35, 14348–14357.

S. J. Byard, C. T. O'Brien, M. J. Derry, M. Williams, O. O. Mykhaylyk, A. Blanazs and S. P. Armes, Chem. Sci., 2020, 11, 396–402.

T. J. Neal, D. L. Beattie, **S. J. Byard**, G. N. Smith, M. W. Murray, N. S. J. Williams, S. N. Emmett, S. P. Armes, S. G. Spain and O. O. Mykhaylyk, Macromolecules, 2018, 51, 1474–1487.

Conferences

The 258th National Meeting & Exposition of the American Chemical Society (ACS), San Diego, March 2018, **Conference Talk**

European Colloid and Interface Society (ECIS), Ljubljana, September 2018, **Conference Talk**

The 255th National Meeting & Exposition of the American Chemical Society (ACS), New Orleans, March 2018, **Conference Talk**

The 254th National Meeting & Exposition of the American Chemical Society (ACS), Washington, August 2017, **Conference Talk**

The 12th International Conference on Advanced Polymers *via* Macromolecular Engineering, Ghent, May 2017, **Poster Presentation**

Macro Group Young Researchers Meeting, Edinburgh, June 2017, **Poster Presentation**

Macro Group Young Researchers Meeting, Liverpool, April 2016, **Poster Presentation**

Abstract

This Thesis focuses on the preparation of stimulus-responsive nano-objects prepared by polymerisation-induced self-assembly using reversible addition-fragmentation chain transfer aqueous dispersion polymerisation. Firstly, an experimental phase diagram has been constructed for the reproducible synthesis of poly(*N*,*N*-dimethylacrylamide)-poly(diacetone acrylamide) (PDMAC-PDAAM) diblock copolymer spheres, worms and vesicles. Dynamic light scattering (DLS) indicates that, in most cases, these PDMAC-PDAAM nano-objects are surprisingly resistant to changes in either solution pH or temperature. However, $PDMAC_{40}$-$PDAAM_{99}$ worms do undergo partial dissociation to form a mixture of relatively short worms and spheres on adjusting the solution pH from pH 2-3 to around pH 9 at 20 °C. Moreover, a change in copolymer morphology from worms to a mixture of short worms and vesicles is observed on heating this worm dispersion to 50 °C. Post-polymerisation cross-linking of concentrated aqueous dispersions of PDMAC-PDAAM nano-objects has been performed at 20 °C using adipic acid dihydrazide (ADH).

A new amphiphilic diblock copolymer that can form spheres, worms, vesicles or lamellae in aqueous solution simply by raising the solution temperature from 1 °C (spheres) to 25 °C (worms) to 50 °C (vesicles) to 70 °C (lamellae) has been synthesised by chain extension of a PDMAC precursor with 4-hydroxybutyl acrylate (HBA) (80 mol%) and DAAM (20 mol%). The first two transitions exhibit excellent reversibility as judged by rheology studies but the lamellae-to-vesicle transition shows hysteresis on cooling. A statistical copolymer of HBA and DAAM was used for the nanoparticle core to enable ADH crosslinking of this hydrophobic block, thus facilitating TEM analysis of the four nanoparticle morphologies.

Chain extension of a cationic poly(2-(acryloyloxy)ethyl trimethylammonium chloride) (PATAC) precursor with DAAM produces cationic spherical nanoparticles whose size can be adjusted by systematic variation of the mean degree of polymerisation (DP) of the PDAAM block. Remarkably, $PATAC_{100}$-$PDAAM_{1500}$ spheres remain colloidally stable in the presence of either 4 M KCl or 3 M ammonium sulfate for at least 115 days at 20 °C. Moreover, these nanoparticles also remain stable in 3 M KCl at 90 °C for six days. Using binary mixtures of PATAC and PDMAC precursors enables the cationic character of such spheres to be tuned. DLS analysis shows that a PATAC-rich stabiliser layer is required for high salt tolerance. Moreover, cationic diblock copolymer worms and vesicles can be prepared by utilising a relatively low mole fraction of the PATAC block in the stabiliser layer. These latter dispersions also exhibit reasonably good salt tolerance: the worms remained colloidally stable in the presence of up to 2 M KCl while vesicles resisted flocculation up to 1 M KCl.

Finally, $PATAC_{100}$-$PDMAC_y$ diblock copolymer nanoparticles have been prepared at 10 % w/w solids in 2 M ammonium sulfate, with DLS studies indicating relatively large sphere-equivalent diameters. DLS and ^{1}H NMR spectroscopy analysis indicate that a four-fold dilution of such dispersions with water results in nanoparticle dissociation to afford molecularly-dissolved copolymer chains. For a PDMAC DP of 2000 or above, such dissociation leads to a significant increase in solution viscosity. A monomer-starved feed protocol has been used to prepare a low-viscosity dispersion of $PDMAC_{100}$-$PDMAC_{10000}$ nanoparticles at 40 % w/w solids. Dilution-triggered dissociation of this dispersion results in the formation of a transparent, free-standing gel.

Abbreviations

^{1}H NMR	Proton nuclear magnetic resonance
AA	Acrylic acid
ACVA	4,4′-azobis(4-cyanovaleric acid)
ADH	Adipic acid dihydrazide
AEAM	2-aminoethylacrylamide hydrochloride
AIBA	2,2′-azobis(2-methylpropionamidine)dihydrochloride
AIBN	Azobisisobutyronitrile
AMPS	Sodium 2-acrylamido-2-methylpropanesulfonate
AscAc	Ascorbic acid
ATAC	2-(acryloyloxy)ethyl trimethylammonium chloride
ATRP	Atom transfer radical polymerisation
CDT	Critical degelation temperature
CGT	Critical gelation temperature
CMC	Critical micelle concentration
CPDB	2-cyano-2-propyl dithiobenzoate
CTA	Chain transfer agent
DAAM	Diacetone acrylamide
DCC	*N*,*N*'-dicyclohexylcarbodiimide
DDMAT	2-(dodecylthiocarbonothioylthio)-2-methylpropionic acid
DEAAM	*N*,*N*-diethylacrylamide
DLS	Dynamic light scattering
$Đ_M$	Molar mass dispersity
DMAC	*N*,*N*-dimethylacrylamide
DMAP	4-dimethylaminopyridine
DP	Degree of polymerisation
EA	Ethyl acrylate
EDL	Electrical double layer
FRP	Free radical polymerisation
FT-IR	Fourier-transform infrared spectroscopy
GlyMA	Glycidyl methacrylate
GMA	Glycerol monomethacrylate
GPC	Gel permeation chromatography
HBA	4-hydroxybutyl acrylate
HEA	2-hydroxyethyl acrylate
HPMA	2-hydroxypropyl methacrylate

HPMAC	2-hydroxypropylmethacrylamide
KPS	Potassium persulfate
KSPMA	Potassium 3-sulfopropyl methacrylate
LAM	Less activated monomer
LCST	Lower critical solution temperature
MADIX	Macromolecular design by the interchange of xanthates
MAM	More activated monomers
MATAC	[2-(Methacryloyloxy)ethyl]trimethylammonium chloride
MEA	2-methoxyethyl acrylate
Me-DDMAT	2-(dodecylthiocarbonothioylthio)-2-methylpropionate
M_n	Number average molecular weight
MPC	2-(methacryloyloxy)ethylphosphorylcholine
M_w	Weight average molecular weight
MWD	Molecular weight distribution
NAEP	2-(*N*-acryloyloxy)ethylpyrrolidone
NAGA	*N*-acryloylglycinamide
NIPAM	*N*-isopropylacrylamide
NMEP	*N*-(2-methacryloyloxy)ethyl pyrrolidone
NMP	Nitroxide-mediated polymerisation
NVP	*N*-vinyl pyrrolidone
ODT	Order-disorder transition
PDI	Dynamic light scattering polydispersity
PEG	Poly(ethylene oxide)
PISA	Polymerisation-induced self-assembly
PITSA	Polymerisation-induced thermal self-assembly
RAFT	Reversible addition-fragmentation chain-transfer
RDRP	Reversible-deactivation radical polymerisation
SAXS	Small-angle X-ray Scattering
SIPLI	Shear-induced polarised light imaging
SSL	Strong segregation limit
TEM	Transmission electron microscopy
UCST	Upper critical solution temperature
VA	Vinyl alcohol
VA-044	2,2'-azobis[2-(2-imidazolin-2-yl)propane] dihydrochloride
VAc	Vinyl acetate

Contents

Contents

Chapter 1

Introduction

1.1 General Concepts of Polymer Science

In 1920 Staudinger first suggested that polymers were high molecular weight, long-chain macromolecules.[1] Before this, it was thought that very large covalently-bonded molecules could not exist.[2] However, it wasn't until a series of experiments were conducted by Carothers in 1929 that Staudinger's concept was finally accepted by the wider scientific community.[3] It is now well-established that polymers are long-chain molecules formed from many repeat units which are known as monomers. The range of monomers that can be used to synthesise polymers is extensive. Consequently, polymers with a vast range of properties can be designed. Over 80% of global polymer production comprises commodity polymers such as polyethylene, polypropylene, poly(ethylene terephthalate), polystyrene, poly(vinyl chloride) and polyurethane which are used in applications such as packaging, building and construction, the automotive industry, electrical insulation and appliances, household products, agriculture, drug excipients and medical devices. However, speciality polymers with specific architectures, properties and functionality are becoming more prevalent as we move into an era of targeted drug delivery, implantable medical devices, 3D printing, electric vehicles, renewable energy and enhanced oil recovery.

1.2 Polymer Architectures

Polymers prepared from a single type of monomer are termed homopolymers. However, more complex architectures can be obtained by copolymerisation of two or more different monomers. A copolymer is a polymer containing two or more different monomers. Copolymers composed of two chemically different monomers can be categorised as block, gradient, alternating, statistical (for which random copolymers are a specific case) or graft copolymers (Figure 1.1).

Fig.1.1. Schematic representation of (a) a block copolymer (b) a gradient copolymer, (c) an alternating copolymer, (d) a random copolymer and (e) a graft copolymer formed from monomers A and B.

Sequential polymerisation of monomer A followed by monomer B results in an AB diblock copolymer. Gradient copolymers exhibit a gradual change in composition from monomer A to monomer B. An alternating copolymer is composed of strictly alternating monomer units of A and B in an equimolar ratio. Statistical copolymers have compositions that depend on the relative reactivities of the respective comonomers. A random copolymer is a statistical copolymer in which the probability of finding monomer A or B at a particular point in the chain are independent of each other. A copolymer is known as a graft copolymer when monomer B forms branches from the main polymer backbone composed of monomer A.[4]

This Thesis focuses exclusively on the synthesis and characterisation of AB diblock copolymers and A(B-*stat*-C) block copolymers (where the second block is a statistical copolymer composed of monomers B and C).

1.3 Polymer Classification

In 1929, Carothers classified polymers into condensation and addition polymers.[4] Condensation polymers are formed from monomers with the elimination of a small molecule during the reaction. Conversely, addition polymers are formed without the elimination of small molecules during polymerisation. The polymerisation of vinyl monomers (i.e. those which contain a carbon-carbon double bond) produces addition polymers since the chains are formed by reaction of the vinyl groups to form saturated C=C backbones without the loss of a small molecule. For addition polymers, the repeat unit has the same elemental composition as the corresponding monomer. However, this early classification of polymers is now considered outdated because there are some polymers such as polyurethanes that would be classified incorrectly according to these simple guidelines.[4]

In 1953, Flory noted the various mechanisms by which polymers are built up from monomers.[5] His observations led to a new classification system: either step or chain polymerisation. In a step polymerisation, monomers first react to form dimers. These dimers can react with another monomer unit or with another dimer to form trimers or tetramers, respectively. These trimers and tetramers can then react further with monomer, dimers or other trimers and tetramers. This slow, stepwise build-up of molecular weight continues throughout the polymerisation. High molecular weight polymers are not formed until near the end of the polymerisation reaction, see Figure 1.2. It is noteworthy that this nomenclature does not make the distinction between step polymerisations which proceed with the formation of a small molecule by-product and those that do not. IUPAC encourages the use of the terms *polycondensation* to describe the former and *polyaddition* for the latter.

In a chain polymerisation, an initiator or catalyst is used to produce an active site that reacts rapidly with one monomer unit at a time, with the regeneration of the active site after each monomer addition. Propagation ceases when the active centre is destroyed in a termination reaction. Unlike step polymerisation, high molecular weight polymers are produced even at low monomer conversions. The average molecular weight decreases slightly towards the end of the reaction as the reaction becomes starved of monomer resulting in shorter polymer chains, see Figure 1.2. Chain polymerisations are exclusively discussed throughout this Thesis.
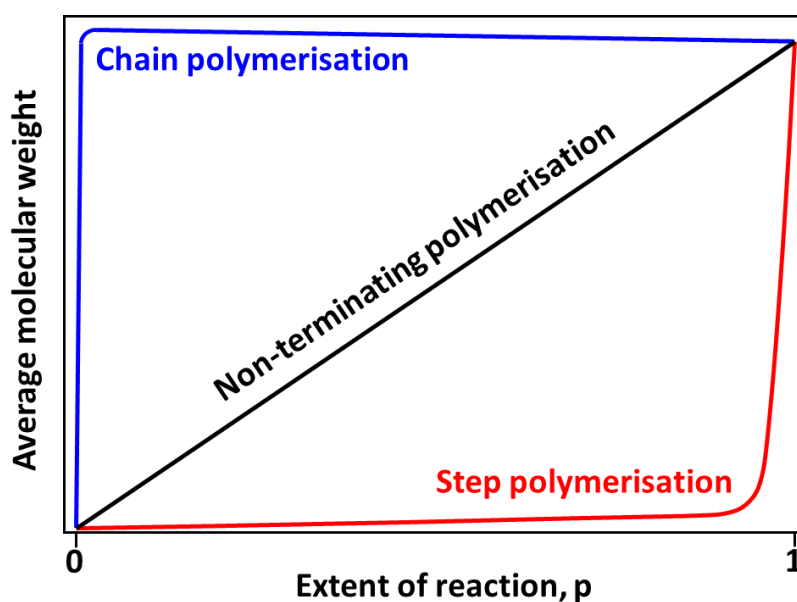
Fig. 1.2. Schematic representation of the average molecular weight against the extent of reaction, *p* for a chain polymerisation, a step polymerisation and a non-terminating polymerisation.

In both step and chain polymerisation, the final polymer comprises chains of varying lengths. Hence, the resulting polymer does not possess a unique molecular weight but rather a molecular weight distribution (MWD). Therefore, an average molecular weight must be used to describe the polymer. There are several different average molecular

weights that can be used. In this Thesis, the number-average molecular weight (M_n) and the weight-average molecular weight (M_w) will be used to describe the polymers. These parameters can be calculated using Equations 1.1 and 1.2 below.

$$M_n = \frac{\sum n_i M_i}{\sum n_i} \qquad\qquad 1.1$$

$$M_w = \frac{\sum n_i M_i{}^2}{\sum n_i\, M_i} \qquad\qquad 1.2$$

Here n_i is the number of molecules of a given species and M_i is the molecular weight of a given species. Consequently, M_w is always greater than M_n.

Ideally, the whole MWD should be determined because, in principle, two polymers with the same M_n could possess different MWDs. IUPAC recommends using the term molar mass dispersity ($Đ_M$), for which molecular weight dispersity or dispersity are acceptable synonyms, to describe the breadth of the MWD. $Đ_M$ is expressed in terms of M_w and M_n according to Equation 1.3. If every polymer chain had exactly the same chain length then $Đ_M$ would be equal to unity. IUPAC recommends that such polymers are called 'uniform polymers'. Polymers for which $Đ_M$ exceeds unity are to be called 'non-uniform polymers'. To avoid confusion, M_w/M_n will be used as a measurement of the width of the MWD of the polymers synthesised in this thesis.

$$Đ_M = \frac{M_w}{M_n} \qquad\qquad 1.3$$

1.4 Polymerisation Techniques

1.4.1 Living Anionic Polymerisation

In 1956, Szwarc introduced the concept of 'living polymerisation' through the anionic polymerisation of styrene in THF using a sodium-naphthalene complex.[6] In the first step of the reaction, naphthalide undergoes an electron transfer reaction with styrene to produce a negative monomer ion (1) or (2) in Figure 1.3. Either end of species (1) and (2) can propagate with further monomer, one end growing as a radical, the other as a carbanion to produce either species (3) or (4). The radicals do not live long and quickly undergo dimerisation to produce species such as (5). (5) continues to propagate with further monomer units from either end of the species until all the monomer is consumed.
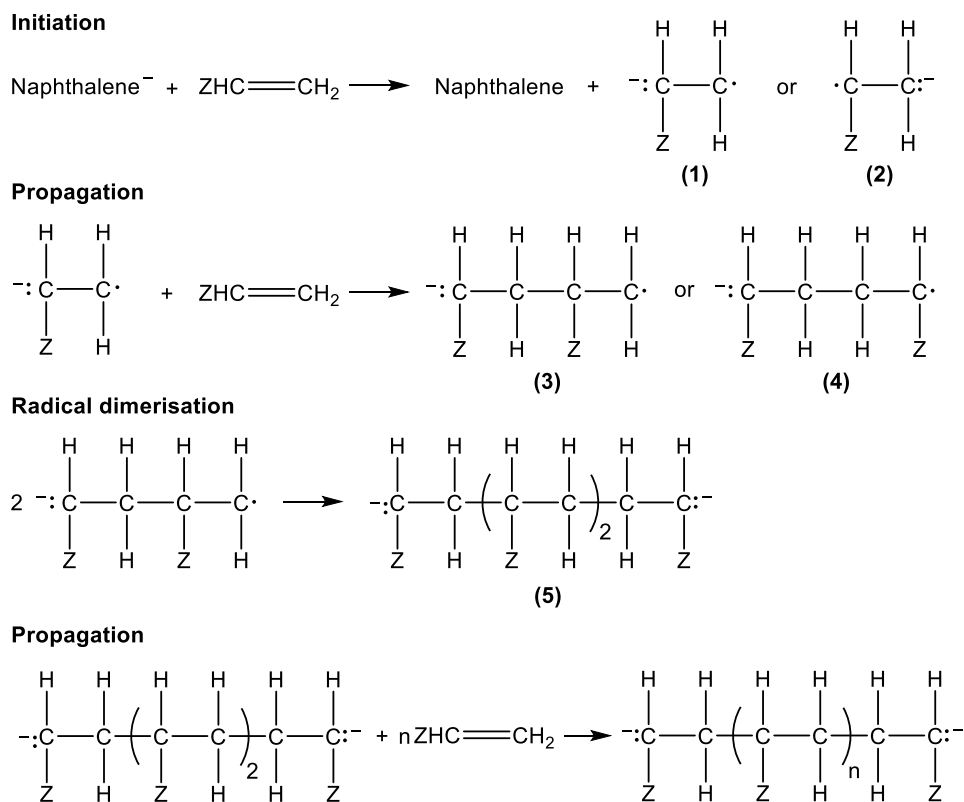
Fig. 1.3. The mechanism for the anionic polymerisation of styrene using a sodium-naphthalene complex initiator. $Z = C_6H_5$.[7]

For a polymerisation to be termed 'living' it must possess no intrinsic termination reactions. This is indeed the case with anionic polymerisation since the propagating carbanions cannot react with each other.

Once the supply of monomer is exhausted the polymer chains stop growing. However, the living carbanion chain-ends remain intact. Further polymerisation can be achieved by the addition of a second charge of monomer. Szwarc demonstrated this through the addition of isoprene to living polystyrene chains that had been initiated with a sodium-naphthalene complex. This resulted in a polyisoprene-*b*-polystyrene-*b*-polyisoprene triblock copolymer being formed.[7] Using *n*-butyllithium as an initiator for anionic polymerisations results in the formation of monofunctional propagating species of the form shown in Figure 1.4 which can be used to produce AB-type block copolymers.[8,9]
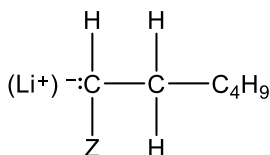
Fig. 1.4. Monofunctional propagating species formed when *n*-butyllithium is used as an initiator for anionic polymerisations.[8,9]

For such polymerisations the final degree of polymerisation (DP) of the polymer can be calculated using Equation 1.4 where [M] is the concentration of monomer, [I] is the concentration of the initiator and *c* is the fractional monomer conversion.[10]

$$DP = \frac{[M]}{[I]} \times c \qquad\qquad 1.4$$

In an ideal anionic polymerisation, initiation is essentially complete before any propagation occurs. Thus, all chains grow uniformly throughout the reaction. This results

in a linear increase in M_n with conversion, see Figure 1.2. Moreover, Schulz demonstrated that polymers with very narrow MWDs can be produced using living anionic polymerisation ($M_w/M_n \sim 1.06$).[10]

However, living anionic polymerisation has some intrinsic drawbacks: it cannot be conducted in protic solvents or non-polar solvents that do not solvate the ions that are formed. Rigorous and exhaustive removal of monomer impurities, moisture and oxygen is essential to avoid premature termination. Lastly, it is particularly difficult to polymerise polar monomers or those containing acidic or electrophilic substituents.[6,7,10,11] Even with such drawbacks, the technology was quickly adopted by industry to produce well-defined block copolymers which can be used as thermoplastic elastomers.[12]

1.4.2 Free Radical Polymerisation

Free radical polymerisation (FRP) is an example of a chain polymerisation. It is a versatile method that allows polymerisation of many functional monomers including those containing acid and hydroxyl groups.[4,13] Although in most cases FRP must be conducted under an inert atmosphere, FRP is not hindered by water or protic solvents and minimal purification of monomers and solvents is required.[13]

The FRP mechanism consists of three elementary steps: initiation, propagation, and termination, Figure 1.5.[4,14]
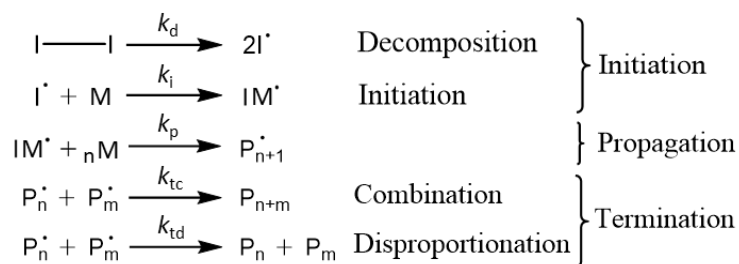
Fig. 1.5. Three elementary steps in free radical polymerisation.[4]

Initiation begins with the production of free radicals (I·) by decomposition of a radical source (I). Figure 1.5 depicts the polymerisation mechanism when two radicals are produced from the decomposition of a radical source which is the most common outcome. However, this may not be the case for all initiators. For example, some redox couples decompose with the formation of only one radical.[15] Decomposition of the initiator is usually the rate-determining step for the polymerisation, with typical values for the rate constant k_d being of the order of 10^{-5} s^{-1}.

Once radicals are formed, they react rapidly with monomer (M) to form an adduct with an active centre (IM·). The rate constant for initiation, k_i, is of the order of 10^4 M^{-1} s^{-1}. The rate of initiator decomposition is relatively slow compared to the rate of reaction of radicals with monomer. Therefore, the rate of initiation, R_i, is given by Equation 1.5, where f is the initiator efficiency (which is the fractional probability that the radical actually initiates monomer).

$$R_i = \frac{d[IM\cdot]}{dt} = 2fk_d[I] \qquad\qquad 1.5$$

The active centres propagate quickly by reaction with monomer units (propagation rate constant, $k_p \sim 10^2$ - 10^4 M^{-1} s^{-1}). This results in high molecular weight polymer chains being formed early in the reaction. The rate of propagation, R_p, is assumed to be independent of the polymer chain length.[16] Consequently, R_p can be expressed as:

$$R_p = -\frac{d[M]}{dt} = k_p[M][P_n\cdot] \qquad\qquad 1.6$$

Propagation continues until termination occurs by either recombination or disproportionation with another propagating active centre (P$_m$·). Termination is relatively fast with the termination rate constant approaching the diffusion-controlled limit, $k_t \sim 10^8$ M^{-1} s^{-1}.[13] The overall rate of termination is given by:

$$R_t = 2k_t[P_n{}^{\cdot}]^2 \qquad\qquad 1.7$$

The instantaneous concentration of free radicals is small and becomes constant within a very short time scale. Therefore, the steady-state approximation can be applied, such that $R_t = R_i$, Equation 1.8.

$$2fk_d[I] = 2k_t[P_n{}^{\cdot}]^2 \qquad\qquad 1.8$$

Rearranging Equation 1.8 gives Equation 1.9.

$$[P_n{}^{\cdot}] = \sqrt{\frac{fk_d[I]}{k_t}} \qquad\qquad 1.9$$

The overall rate of polymerisation, R_{poly} can be expressed by Equation 1.10

$$R_{poly} = -\frac{d[M]}{dt} = R_i + R_p \qquad\qquad 1.10$$

Since R_p is much faster than R_i, it can be assumed that the number of monomers consumed during initiation is negligible compared to the number of monomers consumed during propagation, therefore $R_i + R_p \approx R_p$, so R_{poly} can be expressed by Equation 1.11.

$$1.11$$
$$R_{poly} = [M]\sqrt{\frac{fk_d[I]}{k_t}}$$

The kinetic chain length (D_k) is the average number of monomer units consumed by each radical and is defined by Equation 1.12.

$$D_k = \frac{R_p}{R_i} = \frac{R_p}{R_t} = \frac{k_p[M][P_n{}^{\cdot}]}{2(k_t)[P_n{}^{\cdot}]^2} = \frac{k_p[M]}{2(k_t)[IM^{\cdot}]} = \frac{k_p[M]}{2\sqrt{fk_dk_t[I]}} \qquad 1.12$$

From Equation 1.11, it is clear that the rate of polymerisation can be increased by increasing either the monomer or initiator concentration. However, high molecular weight polymers are only produced when low initiator concentrations are used. Therefore, it is difficult to produce high molecular weight polymers using solution-based FRP.

Usually, various chain transfer side reactions also occur during FRP, whereby the active centre can react with either monomer, solvent, initiator or polymer. Combined with the slow rate of initiator decomposition which results in the generation of new active centres throughout the polymerisation, this produces polymers with broad MWDs ($M_w/M_n > 1.50$). Moreover, the relatively short lifetime of the propagating polymer radical prevents the synthesis of block copolymers and other complex polymer architectures.[12] Nevertheless, FRP is widely used in industry for the synthesis of polymers such as polyethylene, polystyrene, poly(vinyl chloride), poly(meth)acrylates, polyacrylamides and poly(vinyl alcohol).[13]

1.4.3 Reversible-Deactivation Radical Polymerisation

Reversible-deactivation radical polymerisation (RDRP), often referred to in the literature as controlled radical polymerisation, combines the versatility of FRP with some of the advantages of living anionic polymerisation. Like FRP, RDRP can be carried out in the bulk (i.e. in the absence of any solvent) or in a range of solvents (including protic solvents such as water) under a range of conditions and temperatures.[12,17–22] RDRPs are pseudo living polymerisations which means that termination events are not removed entirely but their frequency is significantly reduced. This is achieved by reversibly trapping the growing polymer radicals as dormant species.[23] Since the chains remain active after all of the monomer is consumed, block copolymers and complex copolymer architectures can be prepared.

The three main RDRP techniques are nitroxide-mediated polymerisation (NMP), atom transfer radical polymerisation (ATRP) and reversible addition-fragmentation chain-transfer/macromolecular design by the interchange of xanthates (RAFT/MADIX) polymerisation.

1.5 RAFT/MADIX Polymerisation

Of the three RDRP techniques, RAFT/MADIX is the most versatile in terms of monomer choice and solvent selection. RAFT polymerisation was developed by CSIRO scientists in Melbourne, Australia in the late 1990s.[24] Concurrently, Rhodia scientists utilised xanthates to produce polymers with pseudo-living characteristics *via* MADIX polymerisation.[25,26] The RAFT and MADIX polymerisation mechanisms are essentially identical (Figure 1.6).[27] MADIX involves the use of xanthate-based CTAs, which are not the focus of this work. Instead, trithiocarbonate RAFT CTAs have been used throughout this Thesis.

According to the RAFT mechanism, initiation and termination occur just like FRP.[27] After initiation, a propagating radical is formed, $P_n\cdot$, that can continue to propagate by reaction with monomer, (M), or react reversibly with a CTA, (1), to produce a radical intermediate, (2). Fragmentation of this intermediate either reforms the propagating radical ($P_n\cdot$) or a new radical, ($R\cdot$) and a dormant thiocarbonylthio species, (3). If a new radical is formed ($R\cdot$) this can reinitiate polymerisation to form a new propagating radical, $P_m\cdot$. The CTA R group is chosen so that fragmentation favours the formation of the propagating radical however, new radicals are still formed which rapidly converts the original CTA into a polymeric CTA, (4). In an effective system, addition-fragmentation is faster than propagation so there is on average less than one monomer unit added per addition-fragmentation cycle. This rapid equilibrium ensures that chains grow with equal probability. Importantly this enables the mean DP and M_n to be calculated using Equations 1.13 and 1.14 respectively. Here [M] and [CTA] are the concentrations of monomer and CTA respectively, MW(M) and MW(CTA) are the molecular masses of the monomer and CTA respectively and c is the fractional conversion.

$$DP = \frac{[M]}{[CTA]} \times c \qquad\qquad 1.13$$

$$M_n = \left[\frac{[M]}{[CTA]} \times MW(M) \times c\right] + MW(CTA) \qquad\qquad 1.14$$

The mechanism outlined in Figure 1.6 represents the ideal case where the CTA behaves as a perfect chain transfer agent. In reality, a number of undesirable chain transfer reactions also occur. Despite such side reactions and some background termination reactions, judicious choice of the CTA and optimised reaction conditions enables the synthesis of low dispersity polymers *via* RAFT polymerisation ($M_w/M_n < 1.30$).[28]

Initiation

Reversible chain transfer/propagation

Reinitiation

Chain equilibration/propagation

Termination
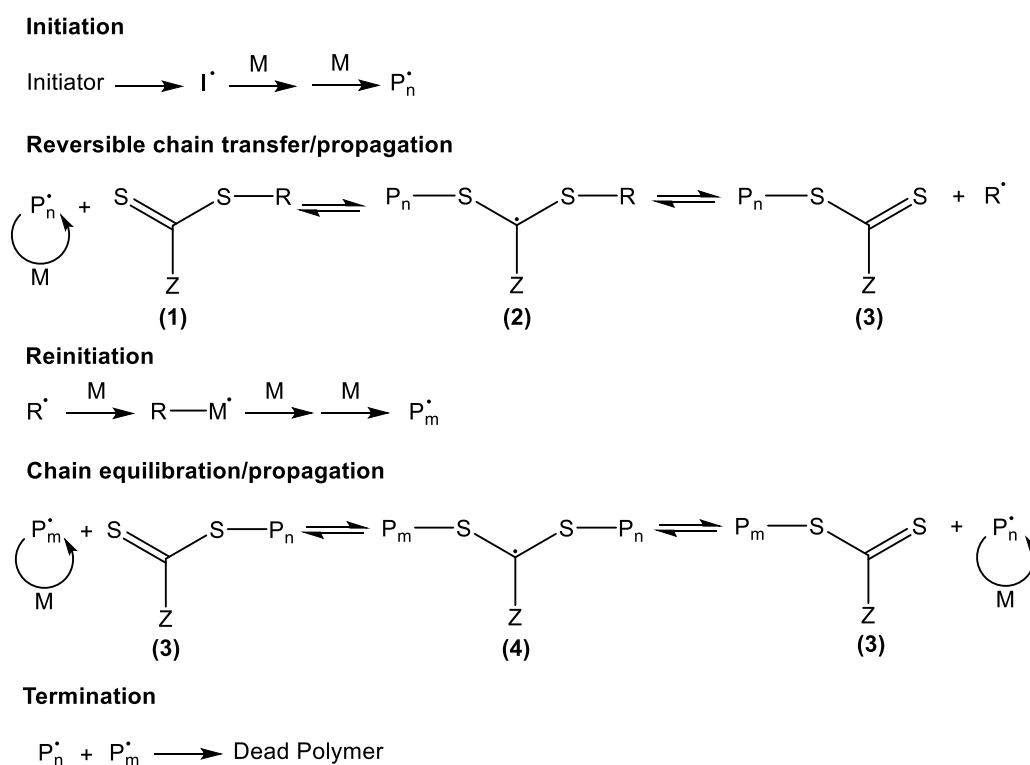
Fig. 1.6. RAFT polymerisation mechanism according to Moad, Rizzardo and Thang.[27]

1.5.1 Choice of RAFT CTA

The general structure for the CTA used in a RAFT polymerisation is given in Figure 1.7. Such polymerisations can be optimised by carefully selecting the R and Z groups on the CTA to suit the monomer type and the reaction conditions.
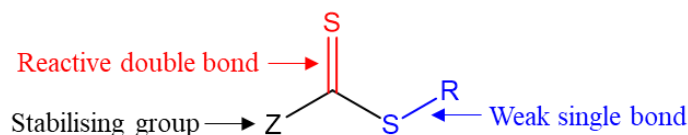
Fig. 1.7. Generic chemical structure of a RAFT CTA indicating its key components.

The R group should be a suitable radical leaving group that can reinitiate polymerisation.[29,30] The Z group influences the stability of the radical intermediates (2) and (4) shown in Figure 1.6 and dictates the reactivity of the C=S bond towards radical attack.[27] General guidelines for selection of the R and Z groups have been provided by Moad, Rizzardo and Thang and are reproduced in Figure 1.8.[21,31]
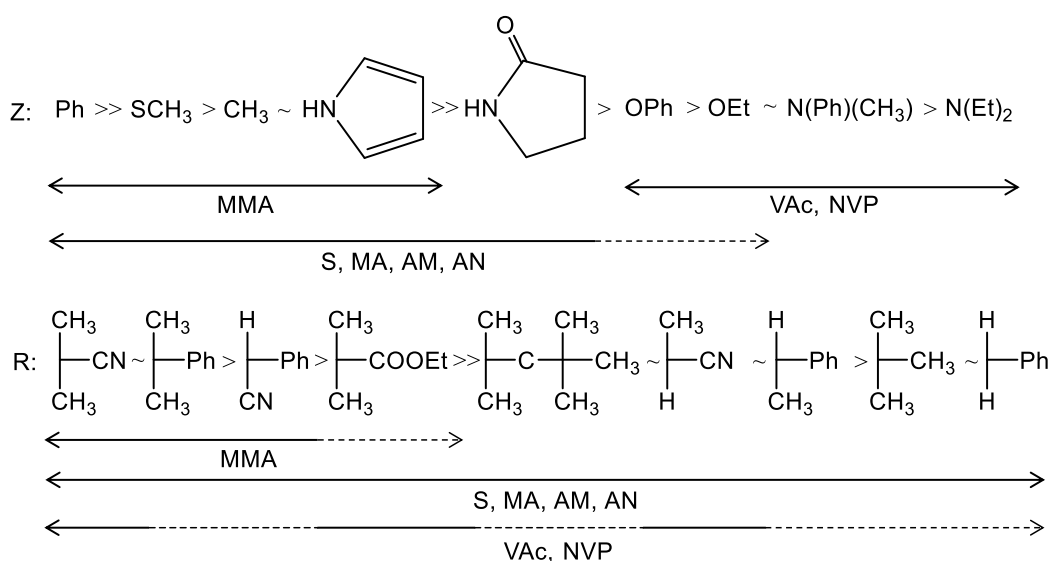
Fig. 1.8. Guidelines for the selection of the R and Z groups in the CTA for RAFT polymerisation according to Moad, Rizzardo and Thang. Solid lines indicate good control, while dashed lines indicate limited control.[21,31]

The solid lines shown in Figure 1.8 represent good RAFT control, whereas dashed lines represent poor or limited control, resulting in polymers with broad MWDs and/or retardation of the polymerisation. Less activated monomers (LAMs) possess an

electron-rich double bond and lack a radical-stabilising functional group.[32] Examples of LAMs include vinyl acetate (VAc) and *N*-vinyl pyrrolidone (NVP). Such propagating radicals are highly reactive and are relatively poor leaving groups. Consequently, they react rapidly with C=S bonds such as those found in trithiocarbonates (Z = alkylthio) and dithioesters (Z = aryl or alkyl) CTAs.[33] However, the radical intermediate (2) in Figure 1.6 is relatively stable towards fragmentation.[34] This inhibits or retards the polymerisation of LAMs.

According to the general guidelines for R and Z group selection (shown in Figure 1.8) RAFT control over the polymerisation of LAMs such as VAc can be achieved when OZ' or N'Z groups are used which are known as xanthates or dithiocarbamates respectively. Fragmentation is favoured for xanthates or dithiocarbamates as the oxygen or nitrogen atoms stabilise the intermediate radicals (2) and (4) (see Figure 1.6) to a lesser extent than the sulfur atom in trithiocarbonates or the carbon atom in dithioesters.[34] Furthermore, the reactivity of the C=S bond is reduced *via* delocalisation, lowering the rate of radical addition.[24,34,35] Thus, xanthates and dithiocarbamates can control the polymerisation of LAMs.[36–42] However, xanthates are often used preferentially owing to their convenient synthesis, often from cheap commodity chemicals.[29]

More activated monomers (MAMs) possess radical-stabilising substituents adjacent to the vinyl group. Examples of MAMs include (meth)acrylates, (meth)acrylamides and (meth)acrylnitriles. Using xanthates to polymerise such monomers leads to poor control and broad MWDs owing to their relatively low transfer constants.[43] However, MAMs can be polymerised using either dithioester (Z = aryl) or trithiocarbonate-based (Z = S-alkyl) CTAs. Such CTAs have relatively high chain transfer constants and have been shown to confer excellent control over MAMs.[27] However, trithiocarbonates are more stable than

dithioesters with respect to hydrolytic degradation and, in general, the former can be more readily synthesised.[21]

This Thesis focuses on the RAFT polymerisation of the following acrylates and acrylamides: *N,N*-dimethylacrylamide (DMAC), diacetone acrylamide (DAAM), 4-hydroxybutyl acrylate (HBA) and 2-(acryloyloxy)ethyl trimethylammonium chloride (ATAC), as shown in Figure 1.9.
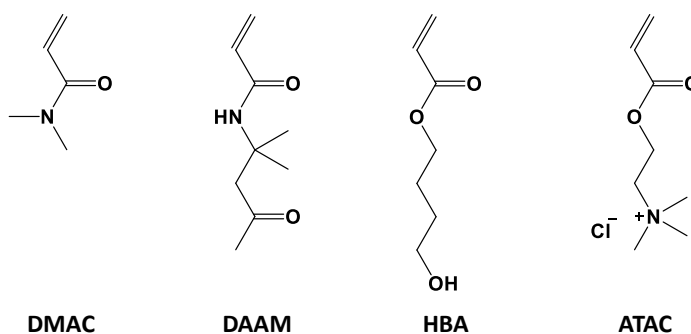
Fig. 1.9. Chemical structures of *N,N*-dimethylacrylamide (DMAC), diacetone acrylamide (DAAM), 4-hydroxybutyl acrylate (HBA) and 2-(acryloyloxy)ethyl trimethylammonium chloride (ATAC).

There are numerous literature examples of the use of 2-(dodecylthiocarbonothioylthio)-2-methylpropionic acid (DDMAT) to polymerise acrylates and acrylamides with good RAFT control (see Figure 1.10.for the chemical structure of DDMAT).[43–51]
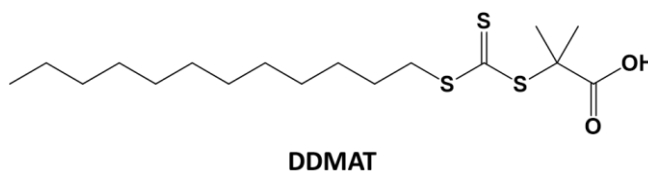
Fig. 1.10. Chemical structure of 2-(dodecylthiocarbonothioylthio)-2-methylpropionic acid (DDMAT).

For example, Lai et al. polymerised either ethyl acrylate (EA) or acrylic acid (AA) in the bulk or in solution in the presence of DDMAT.[44] In each case, excellent RAFT control was achieved for these homopolymers ($M_w/M_n = 1.07$ - 1.15). Moreover, a PAA-PEA diblock copolymer was synthesised in solution with an M_w/M_n of 1.12. Sütekin and Güven used DDMAT for the RAFT solution polymerisation of AA in an acetone/water mixture with initiation *via* gamma radiation.[43] PAA homopolymers with narrow MWDs were produced ($M_w/M_n \leq 1.37$) with DPs ≤ 600.

Very recently, Deane et al. studied the RAFT aqueous solution polymerisation of 2-(N-acryloyloxy)ethylpyrrolidone (NAEP) with DDMAT.[50] High monomer conversions and good RAFT control ($M_w/M_n < 1.20$) were reported for PNAEP DPs up to 400. Good RAFT control was also achieved for the synthesis of double hydrophilic block copolymers formed by chain extension of a PNAEP precursor with either 2-hydroxyethyl acrylate (HEA) or oligo(ethylene glycol) methyl ether acrylate ($M_w/M_n < 1.31$). DDMAT and its methylated analogue, 2-(dodecylthiocarbonothioylthio)-2-methylpropionate (Me-DDMAT) have been exclusively used as RAFT CTAs throughout this Thesis.

One drawback of RAFT polymerisation is that the sulfur-based CTAs are often coloured, malodorous and can be cytotoxic. However, a number of effective CTA removal methods have now been established. For example, Shen et al. prepared a series of polymers using four different CTAs.[52] Each polymer was exposed to excess hydrazine in either DMF or THF at room temperature. Rapid aminolysis occurred in each case, resulting in end-group removal within ≤ 5 minutes. Matioszek et al. used ozonolysis for the removal of xanthate end-groups from two low molecular weight poly(*n*-butyl acrylate) latexes.[53] Complete end-group removal was achieved in 1 hour. However, specialist apparatus was required to maintain latex stability. Jesson et al. used H_2O_2 to remove 2-cyano-2-propyl

dithiobenzoate (CPDB) end-groups from a 7.5 % w/w aqueous dispersion of worm-like poly(glycerol monomethacrylate)-poly(2-hydroxypropyl methacrylate) (PGMA-PHPMA) diblock copolymer nanoparticles.[54] More than 90 % of the CPDB end-groups were removed after 2.5 h using H_2O_2/CPBD at a molar ratio of 5 at 70 °C. Transmission electron microscopy (TEM) and rheology studies confirmed that end-group removal had minimal effect on the copolymer morphology and gelation behaviour. Essentially the same PGMA-PHPMA worms were also prepared using a trithiocarbonate-based CTA. It was found that the trithiocarbonate end-groups were significantly more difficult to remove with only 76 % end-group removal being achieved after 8 h at a H_2O_2/trithiocarbonate CTA molar ratio of 5 at 70 °C. End-group removal can also be achieved by addition of excess initiator,[55,56] thermolysis[57,58] and UV light-mediated removal.[59]

1.5.2 Choice of Initiator

The CTA guidelines provided by Moad, Rizzardo and Thang provide useful assistance in choosing a suitable CTA for a given monomer. However, other parameters such as temperature, solvent, initiator choice and [CTA]/[initiator] molar ratio usually require optimisation to achieve the best results in terms of narrow MWDs, high monomer conversion etc.

The choice of a radical source for a polymerisation is dependent on the solvent, monomer, the desired reaction temperature and properties that the initiator end-groups may confer on the final polymer. Radicals can be generated by using either heat, electromagnetic radiation or redox chemistry. In rare cases, such as for the polymerisation of styrene, auto-initiation can occur.[60]

One of the most common and extensively studied methods for generating radicals is the thermal decomposition of azo initiators by thermal decomposition. The decomposition

rate of azo initiators is largely independent of the solvent. They also tend to have low rates of hydrogen abstraction and hence produce linear polymers. Polymerisations are usually conducted at around the temperature corresponding to the 10-hour half-life ($t_{1/2}$ = 10 h) of the initiator to ensure a continuous supply of radicals during the course of the reaction. See Figure 1.11 for the chemical structures and $t_{1/2}$ = 10 h of the azo initiators used within this Thesis.

ACVA

$t_{1/2}$ = 10h = 69°C

AIBN

$t_{1/2}$ = 10h = 65°C

AIBA

$t_{1/2}$ = 10h = 56°C

VA-044

$t_{1/2}$ = 10h = 44°C
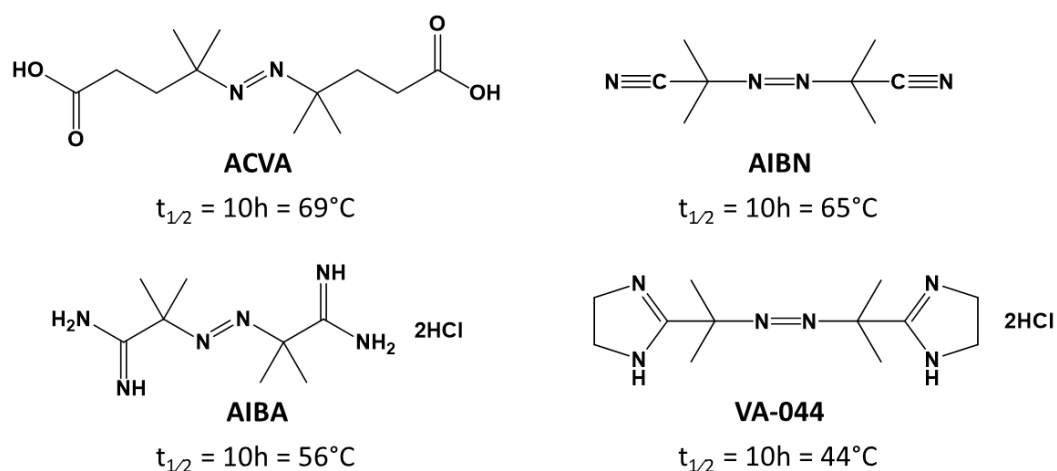
Fig. 1.11. The chemical structures and 10-hour half-life ($t_{1/2}$ = 10h) of the azo-initiators used in this Thesis: 4,4′-azobis(4-cyanovaleric acid) (ACVA), azobisisobutyronitrile (AIBN), 2,2′-azobis(2-methylpropionamidine) dihydrochloride (AIBA) and 2,2'-azobis[2-(2-imidazolin-2-yl)propane] dihydrochloride (VA-044).

Another important class of initiators are redox couples. Redox reactions involve an oxidant and a reducing agent which undergo an electron transfer process followed by bond dissociation to produce radicals. The low energy of activation required for redox initiation allows polymerisations to be carried out at around ambient temperature.[15] For example, the Destarac group polymerised NVP in water at 25 °C using a tert-butyl hydroperoxide/ascorbic acid redox initiator.[61] PNVP homopolymers with relatively narrow MWDs (M_w/M_n < 1.3) were produced. In further work, the Destarac

group polymerised NVP with a *tert*-butyl hydroperoxide/sodium sulfite redox initiator.[62] They found faster rates of NVP polymerisation with sodium sulfite compared to ascorbic acid whilst maintaining narrow MWDs. Recently, Deane et al. polymerised NAEP using a potassium persulfate/ascorbic acid (KPS/AscAc) redox couple at 30 °C with high NAEP conversions (> 99%) and good RAFT control (M_w/M_n < 1.20). A KPS/Ascorbic acid redox couple has been used for some of the RAFT polymerisations conducted in this Thesis as it allows such polymerisations to be conducted at low temperatures. This can limit the chain-transfer/branching side reactions that can occur in the polymerisation of acrylate monomers at elevated temperatures.[63]

The [CTA]/[initiator] molar ratio must be optimised to achieve good RAFT control as the number of termination reactions that occur directly corresponds to the number of radicals in the system.[64] Therefore, the livingness of the polymerisation can be maximised by using minimal initiator. However, reducing the initiator concentration can reduce monomer conversion and the polymerisation rate.

1.6 Polymerisation Methods

As previously noted, radical polymerisations can be conducted either in the bulk or a range of solvents. Many industrially relevant polymerisations are conducted in aqueous media since water is a non-toxic, non-flammable and an inexpensive solvent. Aqueous polymerisations can be conducted under various physical conditions including solution, emulsion, dispersion, precipitation and suspension. In the next section bulk, solution and dispersion polymerisations are discussed in more detail as these techniques are relevant for the work conducted in this Thesis.

1.6.1 Bulk Polymerisation

Bulk polymerisation is the simplest polymerisation method with only monomer and an initiator (or catalyst) involved. This method produces polymers with minimal contamination. However, the reaction becomes highly viscous even at low conversions, which makes heat dissipation and stirring difficult.[4]

1.6.2 Solution Polymerisation

Solution polymerisation involves the polymerisation of a soluble monomer to produce a soluble polymer. Solution polymerisation overcomes some of the disadvantages of bulk polymerisation. Conducting the polymerisation in a suitable solvent produces lower-viscosity reaction solutions, resulting in more efficient heat dissipation and easier stirring.

1.6.3 Aqueous Dispersion Polymerisation

Aqueous dispersion polymerisation involves the polymerisation of a water-soluble monomer that produces a water-insoluble polymer in the presence of a suitable stabiliser that prevents macroscopic precipitation.[65] Such polymerisations result in low viscosity, colloidally stable latexes.

The mechanism for FRP-mediated aqueous dispersion polymerisation comprises six stages, see Figure 1.12. In the first stage, all of the components are soluble in the initial aqueous solution. In the second stage, free radicals are produced by decomposition of the initiator. These radicals react with monomer to produce oligomers. Propagation continues until a critical DP is achieved when the growing polymer chains become insoluble in water resulting in the formation of nascent particles (stage 3). In stage 4, these nuclei aggregate and adsorption of the soluble polymer stabiliser occurs. New particle formation may also occur. By stage 5, all the particles are coated with sufficient stabiliser to confer

colloidal stability *via* steric or electrosteric stabilisation. In the final stage, the monomer-swollen particles act as loci for further polymerisation until, ideally, all of the monomer is consumed.[65]
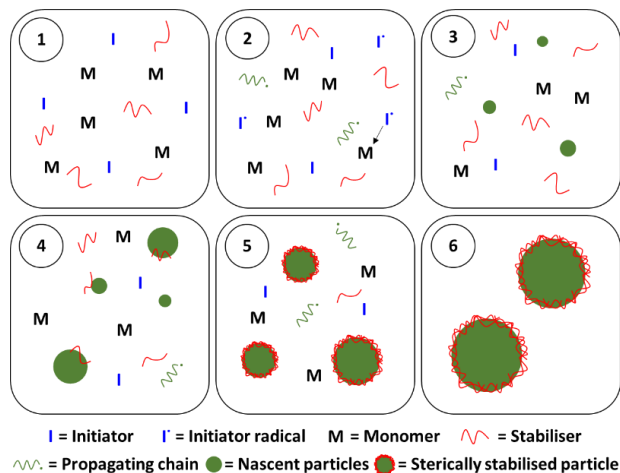
Fig. 1.12. Schematic representation of the six stages of FRP-mediated aqueous dispersion polymerisation using a suitable water-soluble polymer as a steric stabiliser.

There are relatively few literature examples of latex particles prepared by free-radical aqueous dispersion polymerisation. This is because there are relatively few suitable monomers. Armes and co-workers prepared colloidally stable polypyrrole latexes in the presence of various polymeric stabilisers including poly(vinyl alcohol) (PVA),[66] poly(VA-*co*-VAc) poly(2-vinyl pyridine-co-butyl methacrylate),[67] poly(ethylene oxide) (PEO)[67] and PNVP.[67] Moreover, they reported the first examples of (i) surfactant-stabilised polypyrrole particles prepared using sodium dodecylbenzenesulfonate[68] and (ii) polypyrrole-silica nanocomposite particles using ultrafine silica sols.[69] In 2007, Ali et al. described the preparation of PHPMA latexes using PNVP as the steric stabiliser.[70] The mean particle diameter could be varied between 350 nm and 1190 nm by systematically changing the synthesis parameters, with good control over the particle size distribution being achieved.

1.7 Hydrophobic Effect and Amphiphile Self-Assembly

Self-assembly in solution is ubiquitous throughout Nature. It is the process by which organised structures are built up from smaller, disorganised components. This includes the formation of the DNA double helix structure, the self-assembly of proteins into complex quaternary structures and the self-assembly of lipids to form membranes. One contributing factor to this spontaneous self-assembly is unfavourable interactions with water.[71]

Water is anomalous in the sense that it is a low molecular weight molecule (18 g mol^{-1}) yet it exists as a liquid at room temperature and atmospheric pressure. This is because of its extensive intermolecular hydrogen bonding. These are weak, directional bonds that cause water to adopt a tetrahedral coordination structure. All water molecules have at least one hydrogen bond so there are essentially no free water molecules throughout the liquid. Water is capable of dissolving many different ionic and polar solids as H_2O molecules are able to form favourable interactions, such as hydrogen bonds, with such substrates. In contrast, hydrophobic substrates are incapable of forming hydrogen bonds with water. When a small hydrophobic molecule is added to water, the H_2O molecules rearrange around the substrate to form a cage structure, which maximises the number of hydrogen bonds. This rearrangement is known as the hydrophobic effect.[71,72] The rearrangement of water molecules around a hydrophobic substrate can, in some cases, be enthalpically favourable.[72] However, the increase in the order of the system caused by the hydrophobic effect is entropically unfavourable. As the surface area of the hydrophobic substrate increases so does the entropic penalty, hence adding a hydrophobic substrate such as oil to water normally results in phase separation.

The hydrophobic effect is responsible for the spontaneous self-assembly of amphiphiles in water. Amphiphiles consist of a hydrophilic head group and a hydrophobic tail group. Amphiphilic substrates exist as unimers in solution until a critical micelle concentration (CMC) is reached. At the CMC, the unimers spontaneously self-assembly to form aggregates with the hydrophilic head-groups located at the surface and the hydrophobic chains buried within the cores, see Figure 1.13. This self-assembly satisfies the need for the head group to be solvated by water and for the hydrophobic tails to avoid contact with water. The CMC depends mainly on the size of the amphiphile.[71] Increasing the amphiphile concentration beyond the CMC results in an increase in the aggregation number; the concentration of unimers in solution remains relatively constant, see Figure 1.14. The aggregates are held together by weak interactions such as van der Waal interactions and electrostatic interactions. Since these weak forces are easily broken and reformed, the aggregates are fluid-like with rapid exchange of unimers between aggregates occurring under normal conditions.
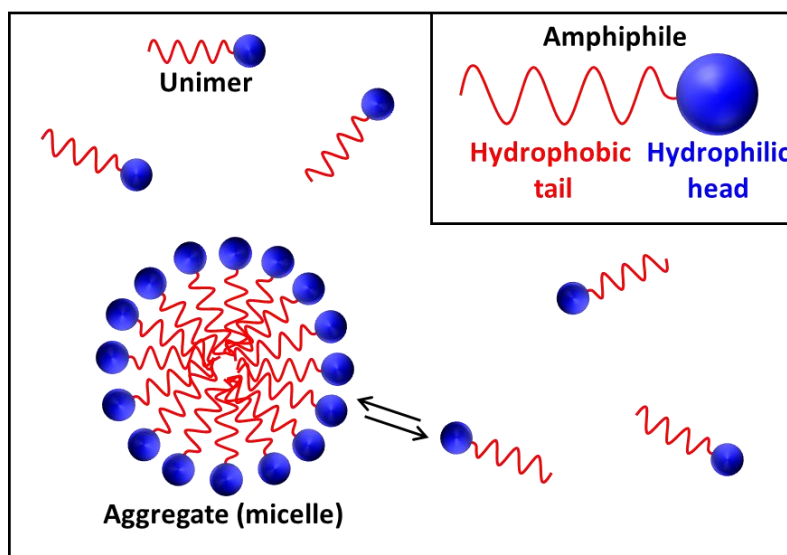
Fig.1.13. Schematic representation of an amphiphilic molecule and its self-assembly to form aggregates (micelles) from unimers in aqueous solution.
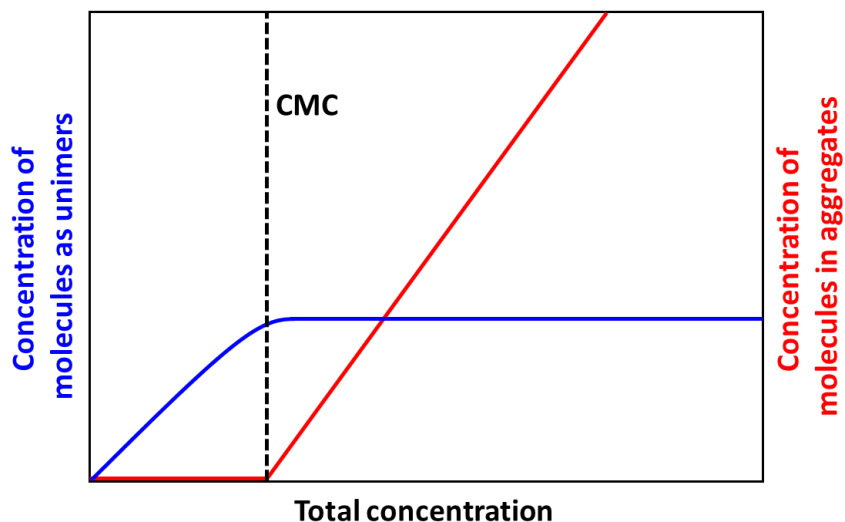
Fig. 1.14. Graphical representation of the concentration of amphiphilic molecules as unimers and the concentration of amphiphilic molecules in aggregates against the total concentration of the amphiphilic substrate. The dashed line represents the critical micelle concentration (CMC).[72]

1.8 The Packing Parameter

Only spherical micelles have been considered so far but amphiphiles such as surfactant molecules can self-assemble to form a range of dynamic structures, transforming from one to another when the solution conditions are changed.[72] Intermolecular forces, entropy and the geometry of the amphiphile govern the aggregate structure formed in aqueous solution.[73] The geometry of an amphiphile can be described in terms of the surface area occupied by the hydrophobic component (a_0), the volume occupied by the hydrophobic chains (V) and the effective length of the hydrophobic chains (l_c), see Figure 1.15. The dimensionless fractional packing parameter (P) can be defined by Equation 1.15.

$$P = \frac{V}{a_0 l_c}$$
1.15

Typical values for *P* for various morphologies are given in Figure 1.15. The packing parameter can be used to rationalise and, in some cases, predict the structure that will be formed when small molecule surfactants self-assemble in aqueous solution.[73]

$P < \frac{1}{3}$ = **Spherical micelles**

$\frac{1}{3} \leq P \leq \frac{1}{2}$ = **Non-spherical micelles**

$\frac{1}{2} < P \leq 1$ = **Vesicles or bilayers**

$P > 1$ = **Inverted structures**
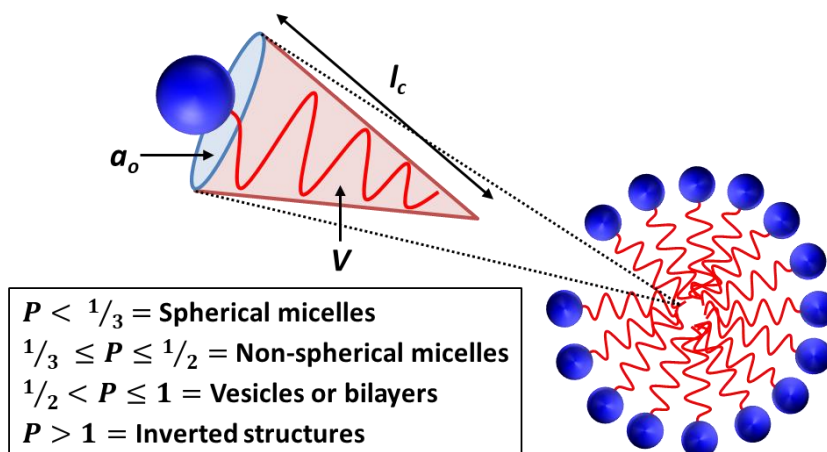
Fig. 1.15. Schematic illustration of a micelle with an expanded amphiphilic molecule showing how a_0, l_c and *V* are defined. Typical values for *P* for various micelle morphologies.[73,74]

1.9 Colloidal Stability

A stable collodial dispersion remains suspended and is resistant to aggregation or sedimentation. Two common methods used to stabilise colloidal dispersions are (i) charge stabilisation and (ii) steric stabilisation.

An electrical double layer (EDL) is formed around charged colloidal particles due to the attraction of oppositely-charged ions from bulk solvent to the charged groups present at the particle surface. Hamaker sketched potential curves as a function of particle separation to show how the dispersion stability of charged colloidal particles depends on the interplay between two counteracting forces: the attractive van der Waals force and the repulsive force arising when the particle EDLs overlap, see Figure 1.16.[75,76] Quantitative

theories of these interactions were described by Derjaguin, Landau, Verwey, and Overbeek.[77,78] Their combined work forms what is now known as the DLVO theory of colloid stability. The interaction of the EDLs for two particles on close approach represents an energy barrier that has to be overcome for aggregation to occur (ΔE). Therefore, the particles remain 'stable' unless this energy barrier can be overcome. Aggregation occurs if the particles have sufficient kinetic energy such that $k_B T > \Delta E$. The energy barrier can be lowered by changing the pH or increasing the electrolyte concentration.[72] Charge stabilisation is only effective in polar solvents such as water.
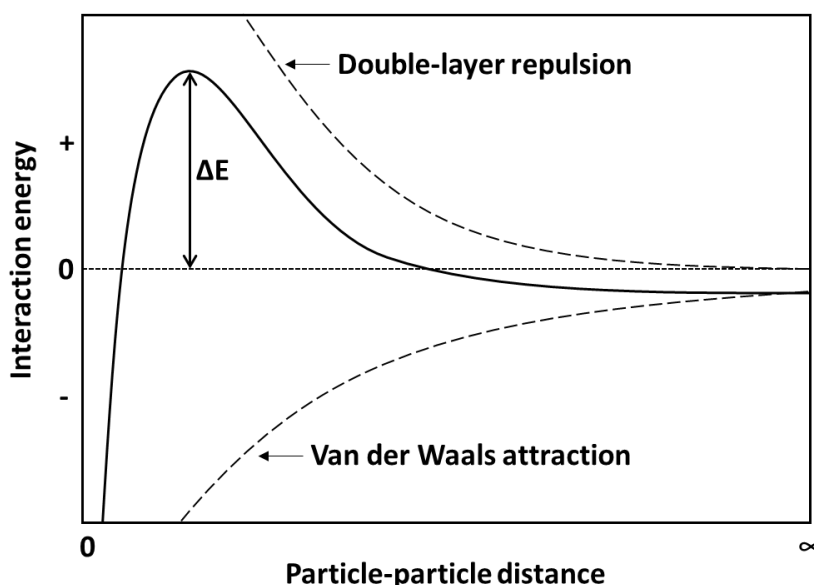
Fig. 1.16. Graphical representation of interaction energy against particle-particle distance for charge-stabilised colloidal particles.[72]

Covering the surface of colloidal particles with a suitable polymeric stabiliser confers steric stabilisation. When two polymer-coated particles approach each other and begin to overlap, they experience repulsive forces owing to the unfavourable entropy arising from the compression of polymer chains at the particle surface and the osmotic effect generated by the local increase in polymer concentration. The extent of steric stabilisation depends

on many factors, including the particle surface coverage and whether the polymer is merely physically adsorbed onto the surface or covalently bound.[72] High surface coverage and covalently-bound stabiliser chains are desirable for robust steric stabilisation. Steric stabilisation is less sensitive to the addition of electrolyte than charge stabilisation and can be used in non-polar solvents.

1.10 Self-Assembly of Diblock Copolymers

1.10.1 Self-Assembly of Diblock Copolymers in the Bulk

Self-assembly is not limited to small amphiphilic molecules. Well-defined amphiphilic block copolymers can also self-assemble either in the bulk or in a solvent which is selective for one of the blocks. Consider the case of self-assembly in the bulk for a linear AB diblock copolymer. If the two blocks are chemically different, then their enthalpic incompatibility can drive microphase separation to form various copolymer morphologies.[79]

The equation for the thermodynamics of mixing for small molecules can be applied to the microphase separation of diblock copolymers, Equation 1.16.

$$\Delta G_{mix} = \Delta H_{mix} - T\Delta S_{mix} \hspace{2cm} 1.16$$

Polymer blends tend to form non-ideal solutions where both ΔH and ΔS deviate from their ideal values. This is attributed to both the heat of mixing and the large difference in size between the polymer chains and the solvent molecules.

In 1942, Flory and Huggins independently presented a lattice model that can be used to determine ΔG_{mix} for either mixing of a polymer in solution or two distinct polymers in the solid-state using Equation 1.17.[80,81]

$$\frac{\Delta G_{mix}}{k_B T} = \left(\frac{f_A ln f_A}{N_A}\right) + \left(\frac{f_B ln f_B}{N_B}\right) + f_A f_B \chi_{AB} \qquad 1.17$$

Here f_A and f_B are the relative volume fractions of the A and B blocks respectively and N_A and N_B are their respective DPs and χ_{AB} is the Flory-Huggins parameter. The Flory-Huggins parameter specifies the degree of incompatibility between blocks A and B and can be determined using Equation 1.18.

$$\chi_{AB} = \left(\frac{z}{k_B T}\right)\left[\varepsilon_{AB} - \frac{1}{2}(\varepsilon_{AA} + \varepsilon_{BB})\right] \qquad 1.18$$

Here z is the lattice coordination number and ε_{AB}, ε_{AA} and ε_{BB} are the interaction energies between monomer units A and B.

Inspecting Equation 1.17, the entropic contribution to ΔG_{mix} depends on the volume fraction of each block and also on the DP of each block. There is usually a small entropic penalty to microphase separation as the polymer chains become stretched.[79] This is reduced as the DP is increased. The enthalpic contribution depends on the relative volume fractions of each block and also the Flory-Huggins parameter. For spontaneous microphase separation to occur, the Flory-Huggins parameter must be positive i.e. the interaction energy between A and B must be higher than between A and A and B and B. Very small differences in the structures of the two blocks in an AB diblock copolymer can result in microphase separation.[79] According to Equation 1.18, χ_{AB} is inversely proportional to temperature. Therefore, there is a critical temperature above which mixing is favoured. This is known as the order-disorder transition (ODT) temperature.

Several theories have developed to predict the morphologies formed by diblock copolymers. One of the most successful is self-consistent mean-field theory.[82–87] Matsen and Bates used this approach to produce a theoretical phase diagram obtained by varying χN (the product of the Flory-Huggins interaction parameter and the total DP) and f_A for a

given diblock copolymer, Figure 1.17.[87] This phase behaviour has been confirmed experimentally using a polyisoprene-polystyrene diblock copolymer system.[79,88]

The weak segregation limit occurs when $\chi_N < 10$. This means that disordered structures are formed. When $\chi_N \gg 10$, then microphase-separated copolymer morphologies can be formed. This is called the strong segregation limit (SSL). Above the SSL, the morphology transforms from close-packed spheres (CPS) to body-centered cubic (S) to hexagonally-packed cylinders (C) to bicontinuous gyroids (G) and finally lamellae (L) with f_A increasing from 0.0 to 0.5 at a fixed χ_N, Figure 1.17.

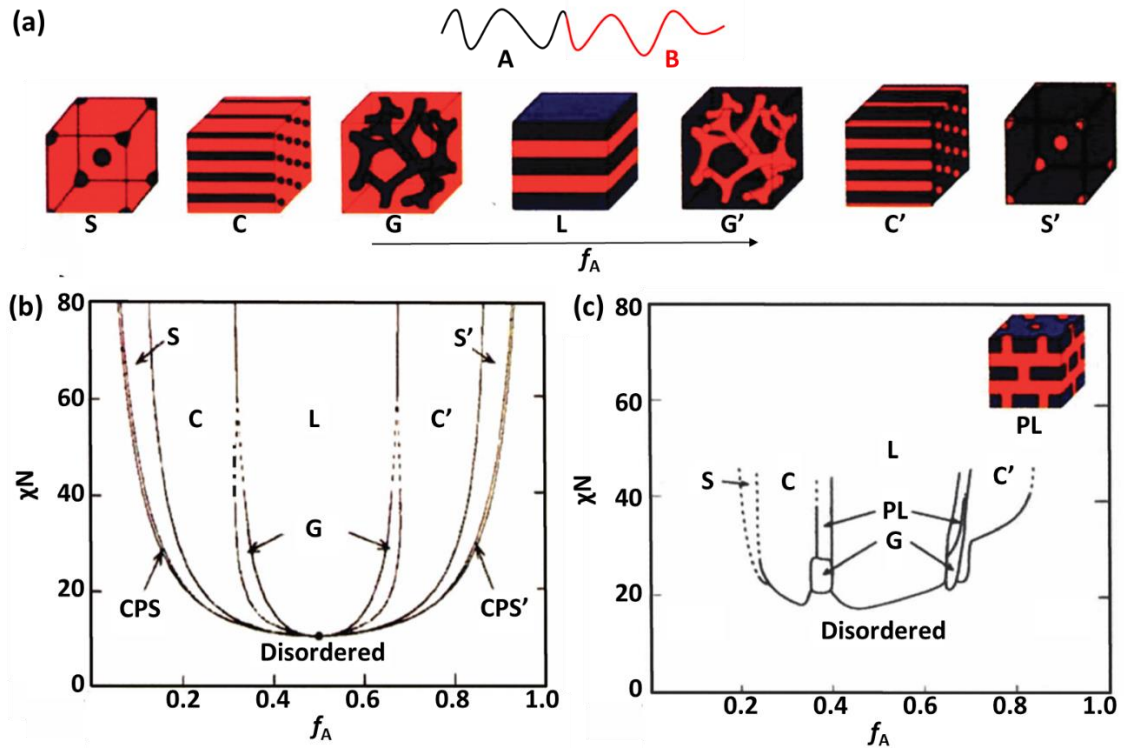Fig.1.17. (a) Schematic representation of body-centered cubic (S), hexagonally-packed cylinders (C), bicontinuous gyroid (G), lamellae (L) and the corresponding inverse structures that are formed by an AB diblock copolymer in the bulk. (b) Theoretical phase diagram for f_A against χ_N. (c) Experimental phase diagram constructed for a series of a polyisoprene-polystyrene diblock copolymers.[87,89]

1.10.2 Self-Assembly of Block Copolymers in Aqueous Solution

Diblock copolymers can be classified as amphiphilic, double-hydrophilic or double-hydrophobic depending on their aqueous solubility. In terms of self-assembly, amphiphilic diblock copolymers are the most extensively studied and are discussed exclusively in this section. Amphiphilic diblock copolymers can be considered to be analogous to the small molecule amphiphiles discussed in Section 1.7. As such, they self-assemble in water to minimise unfavourable interactions between water and the hydrophobic block.

Traditionally, block copolymer self-assembly was conducted *via* post-polymerisation processing. This was achieved by firstly dissolving the block copolymer in a good solvent for both blocks. This was followed by addition of a second solvent that is selective for only one of the blocks. For example, the Eisenberg group used a solvent switch to prepare poly(4-vinylpyridinium methyl iodide)-polystyrene diblock copolymer crew-cut micelles.[90] The diblock copolymer was first prepared in THF using anionic polymerisation. It was then dissolved in DMF followed by addition of water (a bad solvent for polystyrene) to induce self-assembly. In later work, the same group showed that rods, vesicles and lamellae could also be produced using the same post-polymerisation processing approach but by using poly(AA)-polystyrene diblock copolymers of varying DPs.[91,92]

With the development of controlled radical polymerisation techniques, many well-defined, functional diblock copolymers have now been prepared. Post-polymerisation self-assembly techniques have been used to form a wide range of morphologies.[93–109] However, the diblock copolymer nanoparticles are almost invariably prepared at rather low concentrations (< 1.0 % w/w solids).

1.11 Polymerisation-Induced Self Assembly

Over the last ten years, another route for preparing diblock copolymer nanoparticles has been developed. Polymerisation-induced self-assembly (PISA) allows diblock copolymer nanoparticles to be prepared *in situ* in the form of highly concentrated dispersions (up to 50 % w/w solids).[110–112] Typically, a soluble homopolymer precursor is chain-extended with a second monomer, which forms an insoluble polymer at a critical DP. This drives *in situ* self-assembly to produce diblock copolymer nanoparticles.[113] The PISA process is shown in Figure 1.18.
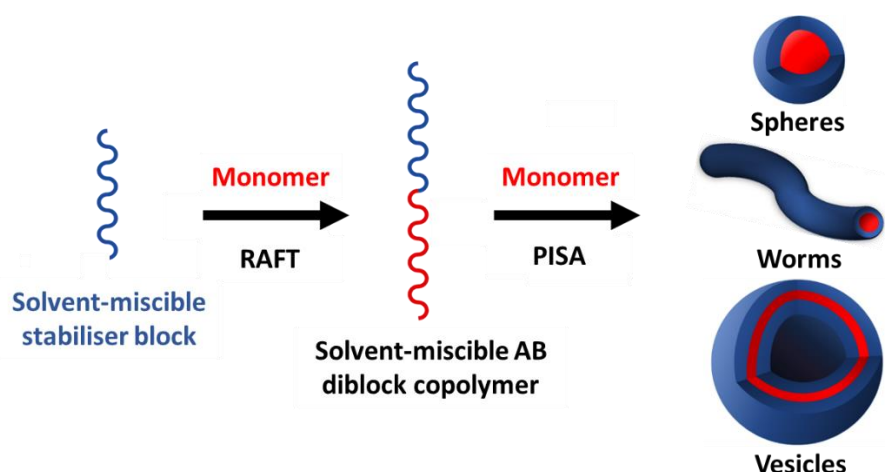
Fig.1.18. Schematic representation of the synthesis of diblock copolymer nanoparticles *via* polymerisation-induced self-assembly (PISA).

The first block is usually prepared by solution polymerisation or occasionally bulk polymerisation. The second block is prepared by either emulsion polymerisation (where the second monomer is immiscible in the chosen solvent) or dispersion polymerisation (where the second monomer is miscible in the chosen solvent). PISA can be conducted in a wide range of solvents using any living or pseudo living polymerisation method.[113-121] However, the work conducted in this Thesis focuses on PISA syntheses conducted using RAFT aqueous dispersion polymerisation.

1.12 PISA using RAFT Aqueous Dispersion Polymerisation

The first example of PISA using RAFT aqueous dispersion polymerisation was reported by Rieger et al. in 2009.[51] They chain-extended a hydrophilic PEG block with varying amounts of DMAC in order to produce a series of water-soluble PEG-PDMAC precursors of increasing chain length. These PEG-PDMAC precursors were the chain-extended with *N,N*-diethylacrylamide (DEAAM) to produce a series of thermoresponsive spherical nanoparticles *in situ*. A bisacrylamide crosslinker was required to produce stable nanoparticles at room temperature.

In 2010, Li et al. demonstrated the synthesis of vesicles *via* PISA in aqueous media through the chain extension of a $PGMA_{65}$ precursor with HPMA (target DP = 300).[122] Electron microscopy images showed that vesicles could be produced by either a two-stage synthesis or a one-pot protocol, see Figure 1.19. This was the first example of vesicles produced at high copolymer concentrations (20 % w/w solids) with high monomer conversion (> 99%).

Fig. 1.19. Representative electron microscopy images of $PGMA_{65}$-$PHPMA_{300}$ vesicles prepared by a two-stage synthesis protocol at 10 % w/w solids (left image) or a one-pot protocol at 20 % w/w solids (right image).[122]

Since this first example from Li et al., the Armes group have conducted extensive research on the PGMA-PHPMA PISA system. Blanazs et al. offered important mechanistic
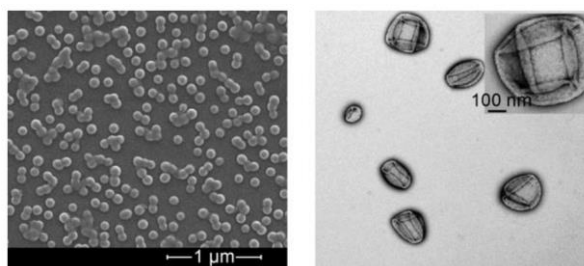
insights into the self-assembly process during RAFT aqueous dispersion polymerisation by monitoring the evolution of the copolymer morphology for the chain extension of a PGMA precursor with HPMA.[123] TEM analysis enabled various intermediate morphologies to be identified including branched worms, "octopi" and "jellyfish".

Blanzas et al. expanded on this earlier work by producing a series of post-mortem experimental phase diagrams. By systematically varying the PGMA DP, the PHPMA DP and the total copolymer concentration they were able to produce phase diagrams allowing the efficient, facile and reproducible synthesis of pure diblock copolymer spheres, worms and vesicles, see Figure 1.20.[124] The final diblock copolymer morphology was found to be dependent on the DP of both the core-forming and stabilising blocks and the total solids concentration of the aqueous dispersion reaction.

Pure sphere, worm and vesicle morphologies could be synthesised if a sufficiently short stabiliser block was used ($PGMA_{47}$ and $PGMA_{78}$). However, the phase diagrams constructed for these two PGMA precursors showed remarkable differences, see Figure 1.20. For the $PGMA_{47}$ precursor, there seemed to be no concentration dependence for the final copolymer morphology. However, for the $PGMA_{78}$ precursor, the final copolymer morphology was highly dependent on total solid concentration with only spheres being formed at 10 % w/w solids even at high PHPMA DPs. An increase in the copolymer concentration to 17 % w/w solids was required to produce pure spheres, worms and vesicles with this $PGMA_{78}$ precursor. It is clear that these morphologies represent kinetic morphologies as opposed to equilibrium morphologies since the $PGMA_{78}$-$PHPMA_{500}$ diblock copolymer can form both spheres at 10 % w/w solids and vesicles at 25 % w/w solids even though they are essentially the same diblock copolymer. The copolymer morphology concentration dependence is attributed to the steric stabilisation imposed by

the longer PGMA$_{78}$ precursor which is sufficient to prevent sphere fusion events at low copolymer concentrations.

The phase diagram constructed for PGMA$_{112}$ largely consists of spheres even at high copolymer concentrations and long PHPMA blocks. It seems that the steric stabilisation imposed by the long PGMA$_{112}$ precursor is difficult to overcome even at high solid concentrations and hence the morphology becomes kinetically trapped in the sphere phase space. They showed a monotonic increase in sphere diameter with increasing PHPMA DP for these kinetically trapped spheres produced at 10 % w/w solids as determined by TEM analysis.
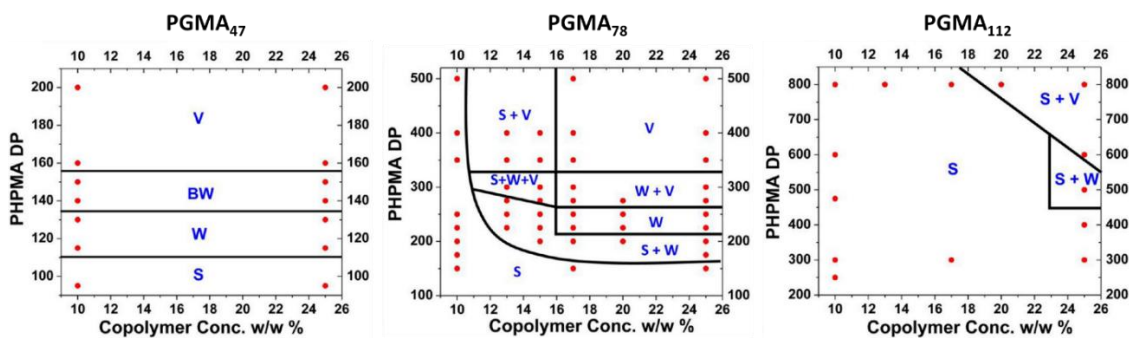
Fig. 1.20. Predictive phase diagrams for a series of PGMA-PHPMA diblock copolymers.[124]

Due to multiple inter-worm contacts, the PGMA-PHPMA worms form soft, free-standing gels at room temperature.[125] Blanazs et al. found that cooling a PGMA$_{54}$-PHPMA$_{140}$ 10 % w/w worm dispersion to 4 °C resulted in gel dissolution. This reversible physical transformation was found to be due to a worm to sphere morphology transition. Variable temperature ^{1}H NMR spectroscopy was used to probe the nature of this transition. They found that the PHPMA pendent methyl group became much more apparent on decreasing the dispersion temperature suggesting surface plasticisation of the PHPMA core chains.

This increase in hydration of the core decreases the interfacial tension between the two blocks resulting in a decrease in the core volume and an associated decrease in the packing parameter, see Figure 1.21.
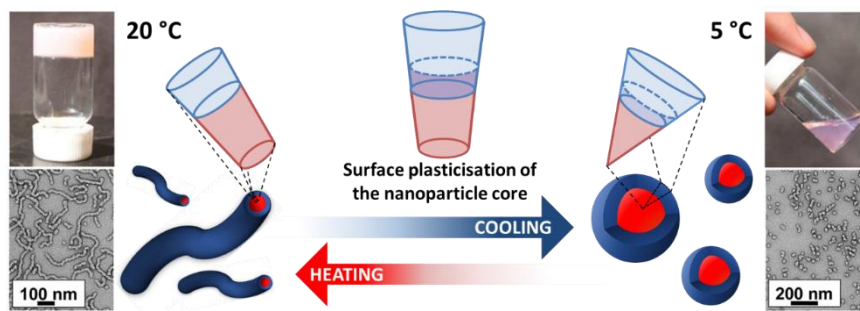
Fig. 1.21. Digital images, representative TEM images and a schematic representation of the worm to sphere transition that occurs on cooling a PGMA$_{54}$-PHPMA$_{140}$ diblock copolymer from 20 °C to 4 °C.[126]

A convenient one-pot formulation was developed by Ratcliffe et al.[127] First, the commodity monomer, glycidyl methacrylate (GlyMA) was converted to the speciality monomer GMA. GMA was then polymerised to produce a water-soluble PGMA precursor. Chain extension of the PGMA precursor with HPMA directly produced spheres, worms or vesicles in concentrated aqueous media.

Lovett et al. synthesised PGMA$_{56}$-PHPMA$_{155}$ worms at 10 % w/w solids using a carboxylic acid terminated CTA.[128] Like Blanazs et al. they found that spheres were produced on cooling the worm dispersion. However, they also found that a worm to sphere transition could be induced simply by increasing the dispersion pH from pH 3.5 to pH 6.0. This reversible morphological transition was attributed to ionisation of the terminal carboxylic acid group on the CTA which causes an increase in hydration of the PGMA block resulting in a decrease in the packing parameter. In the same work, Lovett et al. also reported the synthesis of pH-responsive PGMA$_{43}$-PHPMA$_{200}$ diblock

copolymer vesicles that formed worms on increasing the pH from pH 3.5 to pH 6.0 at ambient temperature. In a second publication, they demonstrated that an irreversible vesicle to sphere transition occurs for a $PGMA_{43}$-$PHPMA_{175}$ diblock copolymer on increasing the dispersion pH, see Figure 1.22 for a schematic diagram.[129] A critical DP was reached at DP = 225 for the PHPMA block above which no pH-responsive behaviour was seen. However, a pH switch immediately followed by cooling to 5 °C was sufficient to induce an irreversible vesicle to sphere transition for the $PGMA_{43}$-$PHPMA_{225}$ and $PGMA_{43}$-$PHPMA_{250}$ diblock copolymers.
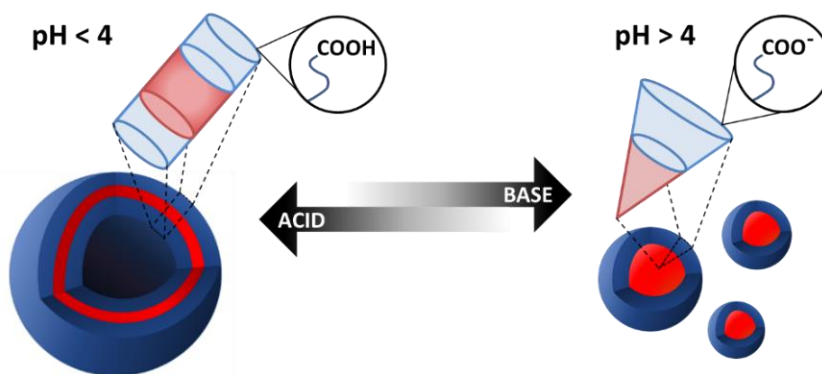
Fig. 1.22. Schematic diagram for the vesicle to worm transition on the increasing the dispersion pH from pH 3.5 to pH 6.0 for a $PGMA_{43}$-$PHPMA_{175}$ diblock copolymer.[129]

In contrast, Penfold et al. produced pH-responsive $PGMA_{50}$-$PHPMA_{140}$ diblock copolymer worms using a morpholine-functionalised CTA.[130] The worms were prepared at pH 7, subsequent acidification resulted in protonation of the end-group which induced a reversible worm to sphere transition, see Figure 1.23 for a schematic representation.
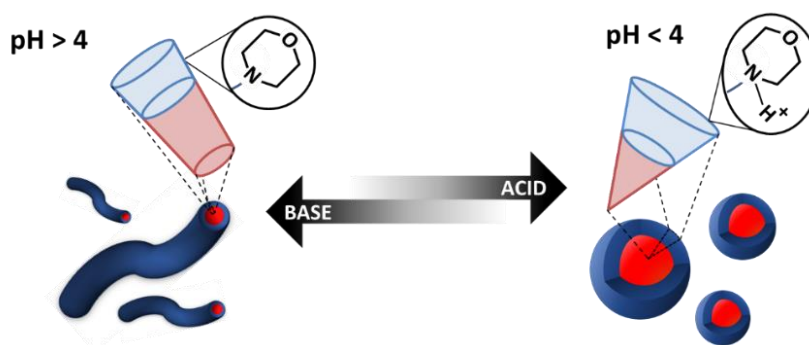
Fig. 1.23. Schematic diagram for the worm to spheres transition on decreasing the dispersion pH from pH 7.0 to pH 4.0 for a PGMA$_{50}$-PHPMA$_{140}$ diblock copolymer.[130]

In other work, PGMA-PHPMA diblock copolymer spheres and worms have been used as Pickering emulsion stabilisers.[131,132] The PGMA-PHPMA worm gels are biocompatible and can be used for stem cell storage[133] and silica and bovine serum albumin have been encapsulated in PGMA-PHPMA diblock copolymer vesicles.[134,135]

The Armes group have also investigated a range of other water-soluble precursors for the polymerisation of HPMA including poly(2-(methacryloyloxy)ethylphosphorylcholine) (PMPC),[136] PEG,[137,138] poly(*N*-(2-methacryloyloxy)ethyl pyrrolidone) (PNMEP),[139] poly(L-cysteine-based methacrylate),[140] poly((2-methacryloyloxy)ethyl dimethyl-(3-sulfopropyl) ammonium hydroxide),[141] poly(potassium 3-sulfopropyl methacrylate) (PKSPMA),[142] and poly([2-(methacryloyloxy)ethyl]trimethylammonium chloride) (PMATAC).[143–145]

PISA conducted using a charged stabiliser block generally results in the formation of spherical nanoparticles.[142–145] This due to the high charge densities on the nanoparticles which prevent sphere-sphere fusion events. Sphere-sphere fusion is thought to be the mechanism by which worms are formed during PISA and is therefore a requirement for morphological evolution.[123]

In order to obtain worms and vesicles using a charged stabiliser block it is necessary to reduce the charge density. This can be achieved by: (1) adding salt to screen the charge (2) copolymerisation of charged and neutral monomers to form a copolymer stabiliser block or (3) simultaneous chain extension of a binary mixture of charged and neutral stabiliser blocks. Semsarilar et al. studied a PISA system composed of a PHPMA core stabilised by either a PKSPMA stabiliser block, a PKSPMA-PGMA copolymer stabiliser block or a binary mixture of PKSPMA and PGMA.[142] The PISA syntheses were conducted in the presence of a low concentration of background salt to aid nanoparticle formation (0.1 - 0.3 M NaCl). They found that higher-order morphologies, in this case vesicles, could only be produced by simultaneous chain extension of a binary mixture of PGMA and PKSPMA homopolymers with HPMA. Building on this previous work, Semsarilar et al. produced cationic spheres, worms and vesicles by chain extension of a binary mixture of PMATAC and PGMA with HPMA in the presence of a low concentration of background salt (0.1 – 0.3 M NaCl).[145] Williams et al. conducted a more extensive study using PMATAC, PGMA and HPMA.[143] They constructed a post-mortem phase diagram to allow reproducible synthesis of spheres, worm and vesicles using a binary mixture of PGMA and PMATAC, see Figure 1.24. The phase diagram was constructed by varying the mole fraction of the cationic MATAC homopolymer and the DP of the core-forming PHPMA block at a fixed concentration of 20 % w/w solids. Penfold et al. chain extended a binary mixture of PEG and PGMA with HPMA using a cationic CTA to form cationic spheres and worms.[144] Interestingly, vesicles could not be formed using this system.
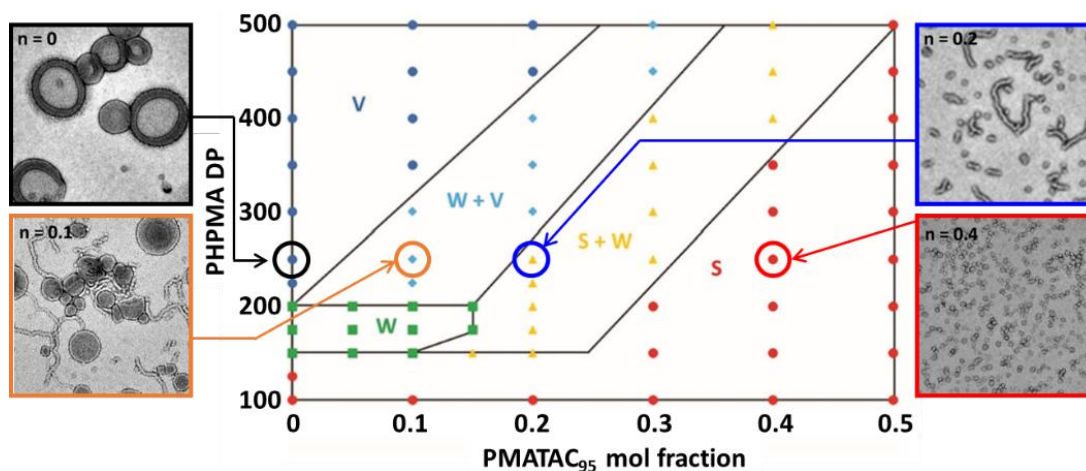
Fig. 1.24. Post-mortem experimental phase diagram and representative TEM images for ([1−n] PGMA$_{62}$ +[n] PMATAC$_{95}$) − PHPMA$_x$ diblock copolymer nanoparticles where *n* is the mole fraction of PMATAC in the stabiliser.[143]

There are relatively few examples of work published by other groups in which PISA is conducted in entirely aqueous media using RAFT dispersion polymerisation. Most of the work which has been conducted focuses on acrylate and acrylamide monomers. Recently, DAAM has been explored in the context of PISA using RAFT aqueous dispersion polymerisation.[146–155] For example, the Cia group chain extended a poly(2-hydroxypropylmethacrylamide) (PHPMAC) stabiliser block with DAAM and a minimal amount of 2-aminoethylacrylamide hydrochloride (AEAM) as a comonomer to produce PHPMAC-P(DAAM$_{176}$-AEAM$_{15}$) diblock copolymer nanoparticles with NH$_3^+$ decorated core–shell interfaces.[148] In the same year, they prepared PHPMAC-PAEAM diblock copolymer nanoparticles using poly(sodium 2-acrylamido-2-methylpropanesulfonate) (PAMPS) as a polyion complexation template.[156] PAEAM forms a water-soluble homopolymer, however its complexation to PAMPS drives self-assembly. In other work, they synthesised PHPMAC-PDAAM nano-objects using

visible-light mediated RAFT aqueous dispersion polymerisation.[150] They reported unusual silk/film, flexible/curled/interlocked ribbon and interlinked vesicle morphologies. This was attributed to the formation of these unusual higher-order nano-objects to hydrogen bonding.

An and co-workers reported the formation of well-defined spherical and vesicular nano-objects using a PDMAC stabiliser block.[147] Both the PDMAC-PDAAM spheres and vesicles could be fluorescently labelled using fluorescein-5-thiosemicarbazide *via* the ketone moiety in the DAAM residues. The same team prepared vesicles *via* the RAFT aqueous dispersion copolymerisation of DAAM with allyl acrylamide using a PDMAC stabiliser block. Comparable acrylamide comonomer reactivities enabled vesicle formation *via* PISA, followed by latent cross-linking within the vesicle membranes *via* the less reactive pendent allyl groups.[149]

Poly(*N*-isopropylacrylamide) (PNIPAM) can also act as a suitable core-forming block in PISA formulations. PNIPAM exhibits a lower critical solution temperature (LCST) at 32 °C.[157–159] Hence, for nanoparticles to be formed during the polymerisation then the reaction must be conducted above this temperature. Moreover, for the nanoparticles to remain intact on cooling to room temperature, a suitable crosslinking mechanism is required. In 2015, the Sumerlin group presented polymerisation-induced thermal self-assembly (PITSA) in which judicious choice of the reaction temperature allows nanoparticles to be produced *in-situ* using a second block that displays LCST or upper critical solution temperature (UCST) behaviour.[160] They showed that chain extension of a PDMAC/PAA precursor with NIPAM at 70 °C produced spheres, worms and vesicles, see Figure 1.25. Crosslinking of the acid groups in the PAA was required prior to cooling the dispersions to room temperature in order for the nanoparticles to remain intact.
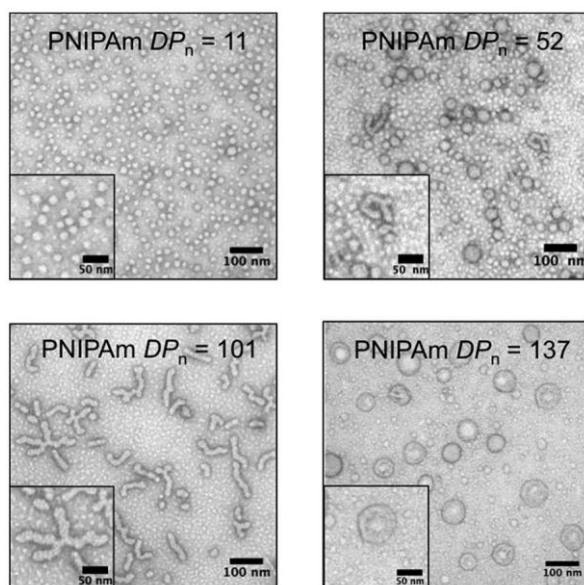
Fig. 1.25. TEM images of spheres, worms and vesicles formed from the chain extension of a PDMAC$_{34}$-*b*-P(DMAC$_{14}$-co-AA$_6$) precursor with PNIPAM. The nanoparticles were crosslinked with ethylenediamine to allow imaging at ambient temperature.[160]

In a recent publication, the O'Reilly group presented a method for predicting suitable core-forming monomers for PISA in water.[161] They evaluated the variance in polymer hydrophobicity with increasing chain length for various monomers which they predicted to be a key feature. First, they determined a general trend for monomers that have previously been used as core-forming blocks in PISA. From this trend, they identified several new suitable monomers. They conducted experiments on the newly identified monomers to prove that they could indeed be used for the core-forming block in PISA systems. Such *in silico* methods could prove useful for identifying suitable monomers for PISA in the future. However, at the current time *in lab* experiments are still required to evaluate monomers for PISA and to assess their stimulus-responsive behaviour.

1.13 Thesis Aims and Outline

The overall aims of this Thesis are: (i) to identify new combinations of acrylate/acrylamide monomers that enable the synthesis of diblock copolymer nano-objects using RAFT aqueous dispersion polymerisation and (ii) to evaluate their stimulus-responsive behaviour in aqueous solution. DAAM and HBA monomers are examined in turn for producing the hydrophobic, core-forming block, while a cationic acrylate monomer, ATAC, is explored as a potential hydrophilic stabiliser block. Chapter 2 reports the use of DAAM for the chain extension of a series of PDMAC homopolymers using aqueous PISA. An experimental phase diagram is constructed with the aim of identifying the elusive worm phase, which had not been previously reported for this PISA system. In addition, a potentially facile nanoparticle crosslinking mechanism is explored using ADH as a water-soluble crosslinker. In Chapter 3, a highly convenient one-pot protocol is developed for the synthesis of PDMAC-PHBA and PDMAC-P(HBA-DAAM) diblock copolymer nanoparticles at either pH 3 or pH 7. Their remarkable thermoresponsive character is investigated in detail. The ability of (n PATAC + (1-n) PDMAC)-PDAAM diblock copolymer nano-objects to withstand aggregation on dilution into concentrated aqueous solutions of either KCl or ammonium sulfate is explored in Chapter 4. One objective here was to identify the maximum salt concentration at which colloid stability is retained for spheres, worms and vesicles. In Chapter 5, high molecular weight PATAC-PDMAC diblock copolymer nanoparticles are synthesised in highly salty aqueous media. In this case, the aims were (i) to identify the maximum PDMAC DP that can be achieved while maintaining high monomer conversion and (ii) to establish the maximum copolymer concentration at which such PISA syntheses could be performed.

References

(1)   Staudinger, H. Über Polymerisation. *Berichte der Dtsch. Chem. Gesellschaft* **1920**, *53*, 1073–1085.

(2)   Cowie, J. *Polymers: Chemistry & Physics of Modern Materials*, Second Edi.; Nelson Thornes: Cheltenham, 1991.

(3)   Carothers, W. H. Studies on Polymerization and Ring Formation. I. An Introduction to the General Theory of Condensation Polymers. *J. Am. Chem. Soc.* **1929**, *51*, 2548–2559.

(4)   Odian, G. *Principles of Polymerization*, Fourth Edi.; John Wiley & Sons, Inc.: Hoboken, 2004.

(5)   Flory, P. *Principles of Polymer Chemistry*, First Edi.; Cornell University Press: London, 1953.

(6)   Szwarc, M. "Living" Polymers. *Nature* **1956**, *178*, 1168–1169.

(7)   Szwarc, M.; Levy, M.; Milkovich, R. Polymerisation Initiated by Electron Transfer to Monomer. A New Method of Formation of Block Polymers. *J. Am. Chem. Soc.* **1956**, *78*, 2656–2657.

(8)   Zilliox, J. G.; Hoovers, J. E. L.; Bywater, S. Preparation and Properties of Polydimethylsiloxane and Its Block Copolymers with Styrene. *Macromolecules* **1975**, *8*, 573–578.

(9)   Wang, Y.; Kausch, C. M.; Chun, M.; Quirk, R. P.; Mattice, W. L. Exchange of Chains between Micelles of Labeled Polystyrene-Block-Poly(Oxyethylene) as Monitored by Nonradiative Singlet Energy Transfer. *Macromolecules* **1995**, *28*, 904–911.

(10)   Waack, R.; Rembaum, A.; Coombes, J. D.; Szwarc, M. Molecular Weight of "Living" Polymers. *J. Am. Chem. Soc.* **1957**, *79*, 2026–2027.

(11)   Ishizone, T.; Goseki, R. *Living Anionic Addition Polymerization*, Living Edi.; Kobayashi, S., Müllen, K., Eds.; Springer: Heidelberg, 2014.

(12)   Braunecker, W. A.; Matyjaszewski, K. Controlled/Living Radical Polymerization: Features, Developments, and Perspectives. *Prog. Polym. Sci.* **2007**, *32*, 93–146.

(13)   Matyjaszewski, K.; Gnanou, Y.; Leibler, L. *Macromolecular Engineering. Precise Synthesis, Materials, Properties, Applications*; Wiley-VCH: Weinheim, 2007.

(14)   Moad, G.; Solomon, D. *The Chemistry of Free Radical Polymerization*, First Edi.; Elsevier Science Ltd: Oxford, 1995.

(15)   Misra, G. S.; Bajpai, U. D. N. Redox Polymerization. *Prog. Polym. Sci.* **1982**, *8*, 61–131.

(16)   Gridnev, A. A.; Ittel, S. D. Dependence of Free-Radical Propagation Rate Constants on the Degree of Polymerization. *Macromolecules* **1996**, *29*, 5864–5874.

(17)   Matyjaszewski, K. Atom Transfer Radical Polymerization (ATRP): Current Status

and Future Perspectives. *Macromolecules* **2012**, *45*, 4015–4039.

(18) Otsu, T.; Yoshida, M.; Tazaki, T. A Model for Living Radical Polymerisation. *Macromol. Rapid Commun.* **1982**, *3*, 133–140.

(19) Tsarevsky, N. V; Matyjaszewski, K. "Green" Atom Transfer Radical Polymerization: From Process Design to Preparation of Well-Defined Environmentally Friendly Polymeric Materials. *Chem. Rev.* **2007**, *107*, 2270–2299.

(20) Matyjaszewski, K.; Xia, J. Atom Transfer Radical Polymerization. *Chem. Rev.* **2001**, *101*, 2921–2990.

(21) Moad, G.; Rizzardo, E.; Thang, S. H. Radical Addition-Fragmentation Chemistry in Polymer Synthesis. *Polymer* **2008**, *49*, 1079–1131.

(22) Sciannamea, V.; Jérôme, R.; Detrembleur, C. In-Situ Nitroxide-Mediated Radical Polymerization (NMP) Processes: Their Understanding and Optimization. *Chem. Rev.* **2008**, *108*, 1104–1126.

(23) Coote, M. L.; Krenske, E. H.; Izgorodina, E. I. Quantum-Chemical Studies of RAFT Polymerization: Methodology, Structure-Reactivity Correlations and Kinetic Implications. In *Handbook of RAFT Polymerisation*; Barner-kowollik, C., Ed.; Wiley-VCH: Weinheim, 2008; pp 5–49.

(24) Chiefari, J.; Chong, Y. K. B.; Ercole, F.; Krstina, J.; Jeffery, J.; Le, T. P. T.; Mayadunne, R. T. A.; Meijs, G. F.; Moad, C. L.; Moad, G.; et al. Living Free-Radical Polymerization by Reversible Addition - Fragmentation Chain Transfer : The RAFT Process. *Macromolecules* **1998**, *31*, 5559–5562.

(25) Delduc, P.; Tailhan, C.; Zard, S. A Convenient Source of Alkyl and Acyl Radicals. *J. Chem. Soc. Chem. Commun.* **1988**, No. 4, 308–310.

(26) Corpart, P.; Charmot, D.; Zard, S. Z.; Biadatti, Thibaud Michelet, D. Method for Block Polymer Synthesis by Controlled Radical Polymerisation. WO98/58974, 2000.

(27) Moad, G.; Rizzardo, E.; Thang, S. H. Living Radical Polymerization by the RAFT Process-A Second Update. *Aust. J. Chem.* **2009**, *62*, 1402–1472.

(28) Schilli, C. M.; Zhang, M.; Rizzardo, E.; Thang, S. H.; Chong, Y. K.; Edwards, K.; Karlsson, G.; Müller, A. H. E. A New Double-Responsive Block Copolymer Synthesized via RAFT Polymerization: Poly(N-Isopropylacrylamide)-Block-Poly(Acrylic Acid). *Macromolecules* **2004**, *37*, 7861–7866.

(29) Taton, D.; Destarac, M.; Zard, S. Z. Macromolecular Design by Interchange of Xanthates: Background, Design, Scope and Applications. In *Handbook of RAFT Polymerisation*; Barner-kowollik, C., Ed.; Wiley-VCH: Weinheim, 2008; pp 373–414.

(30) Chiefari, J.; Mayadunne, R. T. A.; Moad, C. L.; Moad, G.; Rizzardo, E.; Postma, A.; Skidmore, M. A.; Thang, S. H. Thiocarbonylthio Compounds (S=C(Z)S-R) in Free Radical Polymerization with Reversible Addition-Fragmentation Chain Transfer (RAFT Polymerization). Effect of the Activating Group Z. *Macromolecules* **2003**, *36*, 2273–2283.

(31) Keddie, D. J.; Moad, G.; Rizzardo, E.; Thang, S. H. RAFT Agent Design and Synthesis. *Macromolecules* **2012**, *45*, 5321–5342.

(32) Sugihara, S.; Kawamoto, Y.; Maeda, Y. Direct Radical Polymerization of Vinyl Ethers: Reversible Addition–Fragmentation Chain Transfer Polymerization of Hydroxy-Functional Vinyl Ethers. *Macromolecules* **2016**, *49*, 1563–1574.

(33) Góis, J. R.; Costa, J. R. C.; Popov, A. V.; Serra, A. C.; Coelho, J. F. J. Synthesis of Well-Defined Alkyne Terminated Poly(N-Vinyl Caprolactam) with Stringent Control over the LCST by RAFT. *RSC Adv.* **2016**, *6*, 16996–17007.

(34) Stenzel, M. H.; Cummins, L.; Roberts, G. E.; Davis, T. P.; Vana, P.; Barner-kowollik, C. Xanthate Mediated Living Polymerization of Vinyl Acetate : A Systematic Variation in MADIX/RAFT Agent Structure. *Macromol. Chem. Phys.* **2003**, *204*, 1160–1168.

(35) Perrier, S.; Takolpuckdee, P. Macromolecular Design via Reversible Addition-Fragmentation Chain Transfer (RAFT)/Xanthates (MADIX) Polymerization. *J. Polym. Sci. Part A Polym. Chem.* **2005**, *43*, 5347–5393.

(36) Roy, D.; Sumerlin, B. S. Block Copolymerization of Vinyl Ester Monomers via RAFT/MADIX under Microwave Irradiation. *Polymer* **2011**, *52*, 3038–3045.

(37) Binauld, S.; Delafresnaye, L.; Charleux, B.; D'agosto, F.; Lansalot, M. Emulsion Polymerization of Vinyl Acetate in the Presence of Different Hydrophilic Polymers Obtained by RAFT/MADIX. *Macromolecules* **2014**, *47*, 3461–3472.

(38) Giliomee, J.; Pfukwa, R.; Gule, N. P.; Klumperman, B. Smart Block Copolymers of PVP and an Alkylated PVP Derivative: Synthesis, Characterization, Thermoresponsive Behaviour and Self-Assembly. *Polym. Chem.* **2016**, *7*, 1138–1146.

(39) Hu, N.; Ji, W.; Tong, Y.-Y.; Li, Z.; Chen, E. Synthesis of Diblock Copolymers Containing Poly(N-Vinylcarbazole) by Reversible Addition-Fragmentation Chain Transfer Polymerisation. *J. Polym. Sci.* **2010**, *48*, 4621–4626.

(40) Patel, V. K.; Mishra, A. K.; Vishwakarma, N. K.; Biswas, C. S.; Ray, B. (S)-2-(Ethyl Propionate)-(O-Ethyl Xanthate) and (S)-2-(Ethyl Isobutyrate)-(O-Ethyl Xanthate)-Mediated RAFT Polymerization of N-Vinylpyrrolidone. *Polym. Bull.* **2010**, *65*, 97–110.

(41) Tong, Y. Y.; Dong, Y. Q.; Du, F. S.; Li, Z. C. Synthesis of Well-Defined Poly(Vinyl Acetate)-b-Polystyrene by Combination of ATRP and RAFT Polymerization. *Macromolecules* **2008**, *41*, 7339–7346.

(42) Shanmugam, S.; Xu, J.; Boyer, C. Photoinduced Electron Transfer − Reversible Addition − Fragmentation Chain Transfer (PET-RAFT) Polymerization of Vinyl Acetate and N - Vinylpyrrolidinone: Kinetic and Oxygen Tolerance Study. *Macromolecules* **2014**, *47*, 4930–4942.

(43) Sütekin, S. D.; Güven, O. Radiation-Induced Controlled Polymerization of Acrylic Acid by RAFT and RAFT-MADIX Methods in Protic Solvents. *Radiat. Phys. Chem.* **2018**, *142*, 82–87.

(44) Lai, J. T.; Filla, D.; Shea, R. Functional Polymers from Novel Carboxyl-

Terminated Trithiocarbonates as Highly Efficient RAFT Agents. *Am. Chem. Soc. Polym. Prepr. Div. Polym. Chem.* **2002**, *35*, 6754–6756.

(45) Lu, L.; Yang, N.; Cai, Y. Well-Controlled Reversible Addition-Fragmentation Chain Transfer Radical Polymerisation under Ultraviolet Radiation at Ambient Temperature. *Chem. Commun.* **2005**, No. 42, 5287–5288.

(46) Oyeneye, O. O.; Xu, W. Z.; Charpentier, P. A. Adhesive RAFT Agents for Controlled Polymerization of Acrylamide: Effect of Catechol-End R Groups. *RSC Adv.* **2015**, *5*, 76919–76926.

(47) Ratcliffe, L. P. D.; McKenzie, B. E.; Le Bouëdec, G. M. D.; Williams, C. N.; Brown, S. L.; Armes, S. P.; Le Bouëdec, G. M. D.; Williams, C. N.; Brown, S. L.; Armes, S. P. Polymerization-Induced Self-Assembly of All-Acrylic Diblock Copolymers via RAFT Dispersion Polymerization in Alkanes. *Macromolecules* **2015**, *48*, 8594–8607.

(48) Chalmers, B. A.; Magee, C.; Cheung, D. L.; Zetterlund, P. B.; Aldabbagh, F. CO2-Responsive Polyacrylamide Copolymer Vesicles with Acid-Sensitive Morpholine Moieties and Large Hydrophobic RAFT End-Group. *Eur. Polym. J.* **2017**, *97*, 129–137.

(49) Liao, X.; Walden, G.; Falcon, N. D.; Donell, S.; Raxworthy, M. J.; Wormstone, M.; Riley, G. P.; Saeed, A. A Direct Comparison of Linear and Star-Shaped Poly(Dimethylaminoethyl Acrylate) Polymers for Polyplexation with DNA and Cytotoxicity in Cultured Cell Lines. *Eur. Polym. J.* **2017**, *87*, 458–467.

(50) Deane, O. J.; Lovett, J. R.; Musa, O. M.; Fernyhough, A.; Armes, S. P. Synthesis of Well-Defined Pyrrolidone-Based Homopolymers and Stimulus-Responsive Diblock Copolymers via RAFT Aqueous Solution Polymerization of 2-(N-Acryloyloxy)Ethylpyrrolidone. *Macromolecules* **2018**, *51*, 7756–7766.

(51) Rieger, J.; Grazon, C.; Charleux, B.; Alaimo, D.; Jérôme, C. Pegylated Thermally Responsive Block Copolymer Micelles and Nanogels via In Situ RAFT Aqueous Dispersion Polymerization. *J. Polym. Sci. Part A Polym. Chem.* **2009**, *47*, 2373–2390.

(52) Shen, W.; Qiu, Q.; Wang, Y.; Miao, M.; Li, B.; Zhang, T.; Cao, A.; An, Z. Hydrazine as a Nucleophile and Antioxidant for Fast Aminolysis of RAFT Polymers in Air. *Macromol. Rapid Commun.* **2010**, *31*, 1444–1448.

(53) Matioszek, D.; Dufils, P. E.; Vinas, J.; Destarac, M. Selective and Quantitative Oxidation of Xanthate End-Groups of RAFT Poly(n-Butyl Acrylate) Latexes by Ozonolysis. *Macromol. Rapid Commun.* **2015**, *36*, 1354–1361.

(54) Jesson, C. P.; Pearce, C. M.; Simon, H.; Werner, A.; Cunningham, V. J.; Lovett, J. R.; Smallridge, M. J.; Warren, N. J.; Armes, S. P. H2O2 Enables Convenient Removal of RAFT End-Groups from Block Copolymer Nano-Objects Prepared via Polymerization-Induced Self- Assembly in Water. *Macromolecules* **2017**, *50*, 182–191.

(55) Perrier, S.; Takolpuckdee, P.; Mars, C. A. Reversible Addition-Fragmentation Chain Transfer Polymerization: End Group Modification for Functionalized Polymers and Chain Transfer Agent Recovery. *Macromolecules* **2005**, *38*, 2033–

2036.

(56) Chong, Y. K.; Moad, G.; Rizzardo, E.; Thang, S. H. Thiocarbonylthio End Group Removal from RAFT-Synthesized Polymers by Radical-Induced Reduction. *Macromolecules* **2007**, *40*, 4446–4455.

(57) Legge, T. M.; Slark, A. T.; Perrier, S. Thermal Stability of Reversible Addition– Fragmentation Chain Transfer/Macromolecular Architecture Design by Interchange of Xanthates Chain-Transfer Agents. *J. Polym. Sci. Part A - Polym. Chem.* **2006**, *44*, 6980–6987.

(58) Postma, A.; Davis, T. P.; Moad, G.; O'Shea, M. S. Thermolysis of RAFT-Synthesized Polymers. A Convenient Method for Trithiocarbonate Group Elimination. *Macromolecules* **2005**, *38*, 5371–5374.

(59) Mattson, K. M.; Pester, C. W.; Gutekunst, W. R.; Hsueh, A. T.; Discekici, E. H.; Luo, Y.; Schmidt, B. V. K. J.; McGrath, A. J.; Clark, P. G.; Hawker, C. J. Metal-Free Removal of Polymer Chain Ends Using Light. *Macromolecules* **2016**, *49*, 8162–8166.

(60) Chong, Y. K.; Rizzardo, E.; Solomon, D. H. Confirmation of the Mayo Mechanism for the Initiation of the Thermal Polymerization of Styrene. *J. Am. Chem. Soc.* **1983**, *105*, 7761–7762.

(61) Guinaudeau, A.; Mazières, S.; Wilson, D. J.; Destarac, M. Aqueous RAFT/MADIX Polymerisation of N-Vinyl Pyrrolidone at Ambient Temperature. *Polym. Chem.* **2012**, *3*, 81.

(62) Guinaudeau, A.; Coutelier, O.; Sandeau, A. A.; Mazieres, S.; Nguyen Thi, H. D.; Le Drogo, V.; Wilson, D. J.; Destarac, M.; Mazières, S.; Nguyen Thi, H. D.; et al. Facile Access to Poly(N-Vinylpyrrolidone)-Based Double Hydrophilic Block Copolymers by Aqueous Ambient RAFT/MADIX Polymerization. *Macromolecules* **2014**, *47*, 41–50.

(63) Martin, L.; Gody, G.; Perrier, S. Preparation of Complex Multiblock Copolymers via Aqueous RAFT Polymerization at Room Temperature. *Polym. Chem.* **2015**, *6*, 4875–4886.

(64) Perrier, S. 50th Anniversary Perspective: RAFT Polymerization - A User Guide. *Macromolecules* **2017**, *50*, 7433–7447.

(65) Monterio, M.; Van Herk, A. M. Heterogeneous Systems. In *Handbook of Radical Polymerization*; Matyjaszewski, K., Davis, T. P., Eds.; John Wiley & Sons, Inc., 2002; pp 301–331.

(66) Armes, S. P.; Vincent, B. Dispersions of Electrically Conducting Polypyrrole Particles in Aqueous Media. *J. Chem. Soc. Chem. Commun.* **1987**, No. 4, 288–290.

(67) Armes, S. P.; Aldissi, M.; Idzorek, G. C.; Keaton, P. W.; Rowton, L. J.; Stradling, G. L.; Collopy, M. T.; McColl, D. B. Particle Size Distributions of Polypyrrole Colloids. *J. Colloid Interface Sci.* **1991**, *141*, 119–126.

(68) DeArmitt, C.; Armes, S. P. Colloidal Dispersions of Surfactant-Stabilized Polypyrrole Particles. *Langmuir* **1993**, *9*, 652–654.

(69)   Maeda, S.; Armes, S. P. Preparation and Characterisation of Novel Polypyrrole-Silica Colloidal Nanocomposites. *J. Mater. Chem.* **1994**, *4*, 935–942.

(70)   Ali, A. M. I.; Pareek, P.; Sewell, L.; Schmid, A.; Fujii, S.; Armes, S. P.; Shirley, I. M. Synthesis of Poly(2-Hydroxypropyl Methacrylate) Latex Particles via Aqueous Dispersion Polymerization. *Soft Matter* **2007**, *3*, 1003–1013.

(71)   Tanford, C. The Hydrophobic Effect and the Organization of Living Matter Charles Tanford. *Science* **1978**, *200*, 1012–1018.

(72)   Israelachvili, J. N. *Intermolecular and Surface Forces*, Third Edi.; Academic Press: London, 2011.

(73)   Israelachvili, J. N.; Mitchell, D. J.; Ninham, B. W.; Israelachvil, J. N.; Mitchell, D. J.; Ninham, B. W. Theory of Self-Assembly of Hydrocarbon Amphiphiles into Micelles and Bilayers. *J. Chem. Soc., Faraday Trans. 2* **1976**, *72*, 1525–1568.

(74)   Nagarajan, R. Molecular Packing Parameter and Surfactant Self-Assembly: The Neglected Role of the Surfactant Tail. *Langmuir* **2002**, *18*, 31–38.

(75)   Hamaker, H. A General Theory of Lyophobic Colloids I. *Recl. des Trav. Chim. des Pays-Bas* **1936**, *56*, 727.

(76)   Hamaker, H. A General Theory of Lyophobic Colloids. II. *Recl. des Trav. Chim. des Pays-Bas* **1937**, *56*, 727.

(77)   Derjaguin, B.; Landau, L. Theory of the Stability of Strongly Charged Lyophobic Sols and of the Adhesion of Strongly Charged Particles in Solution of Electrolytes. *Acta Physicochim. U.R.S.S* **1941**, *14*, 633–662.

(78)   Verwey, E.; Overbeek, Jt. *Theory of the Stability of Lyophobic Colloids*; Elsevier: Amsterdam, 1948.

(79)   Bates, F. S.; Fredrickson, G. H. Block Copolymers-Designer Soft Materials. *Phys. Today* **1999**, *52*, 32–38.

(80)   Huggins, M. L. Theory of Solutions of High Polymers. *J. Am. Chem. Soc.* **1942**, *64*, 1712–1719.

(81)   Flory, P. J. Thermodynamics of High Polymer Solutions. *J. Chem. Phys.* **1943**, *10*, 51–61.

(82)   Helfand, E.; Wasserman, Z. R. Block Copolymer Theory. 4. Narrow Interphase Approximation. *Macromolecules* **1976**, *9*, 879–888.

(83)   Helf, E.; Wasserman, Z. R. Block Copolymer Theory. 5. Spherical Domains. *Macromolecules* **1978**, *11*, 960–966.

(84)   Helfand, E.; Wasserman, Z. R. Block Copolymer Theory. 6. Cylindrical Domains. *Macromolecules* **1980**, *13*, 994–998.

(85)   Leibler, L. Theory of Microphase Separation in Block Copolymers. *Macromolecules* **1980**, *13*, 1602–1617.

(86)   Matsen, M. W.; Schick, M. Stable and Unstable Phases of a Diblock Copolymer Melt. *Phys. Rev. Lett.* **1994**, *72*, 2660–2663.

(87)   Matsen, M. W.; Bates, F. S. Unifying Weak- and Strong-Segregation Block Copolymer Theories. *Macromolecules* **1996**, *29*, 1091–1098.

(88)   Khandpur, A. K.; Förster, S.; Bates, F. S.; Hamley, I. W.; Ryan, A. J.; Bras, W.; Almdal, K.; Mortensen, K. Polyisoprene-Polystyrene Diblock Copolymer Phase Diagram near the Order-Disorder Transition. *Macromolecules* **1995**, *28*, 8796–8806.

(89)   Swann, J. M. G.; Topham, P. D. Design and Application of Nanoscale Actuators Using Block-Copolymers. *Polymers* **2010**, *2*, 454–469.

(90)   Gao, Z.; Varshney, S. K.; Wong, S.; Eisenberg, A. Block Copolymer "Crew-Cut" Micelles in Water. *Macromolecules* **1994**, *27*, 7923–7927.

(91)   Zhang, L.; Eisenberg, A. Multiple Morphologies of "Crew-Cut" Aggregates of Polystyrene-b-Poly(Acrylic Acid) Block Copolymers. *Science* **1995**, *268*, 1728–1731.

(92)   Zhang, L.; Eisenberg, A. Multiple Morphologies and Characteristics of "Crew-Cut" Aggregates of Polystyrene-b-Poly(Acrylic Acid) Diblock Copolymers in Aqueous Solutions. *J. Am. Chem. Soc.* **1996**, *118*, 3168–3181.

(93)   Won, Y.-Y.; Davis, H. T.; Bates, F. S. Giant Wormlike Rubber Micelles. *Science* **1999**, *283*, 960–963.

(94)   Dalhaimer, P.; Engler, A. J.; Parthasarathy, R.; Discher, D. E. Targeted Worm Micelles. *Biomacromolecules* **2004**, *5*, 1714–1719.

(95)   Rodríguez-Hernández, J.; Lecommandoux, S. Reversible Inside-out Micellization of PH-Responsive and Water-Soluble Vesicles Based on Polypeptide Diblock Copolymers. *J. Am. Chem. Soc.* **2005**, *127*, 2026–2027.

(96)   Mortensen, K.; Brown, W. Poly(Ethylene Oxide)—Poly(Propylene Oxide)—Poly(Ethylene Oxide) Triblock Copolymers in Aqueous Solution. The Influence of Relative Block Size. *Macromolecules* **1993**, *26*, 4128–4135.

(97)   Madsen, J.; Armes, S. P. (Meth)Acrylic Stimulus-Responsive Block Copolymer Hydrogels. *Soft Matter* **2012**, *8*, 592–605.

(98)   Zhou, C.; Hillmyer, M. A.; Lodge, T. P. Efficient Formation of Multicompartment Hydrogels by Stepwise Self-Assembly of Thermoresponsive ABC Triblock Terpolymers. *J. Am. Chem. Soc.* **2012**, *134*, 10365–10368.

(99)   Wang, X.; Guerin, G.; Wang, H.; Wang, Y.; Manners, I.; Winnik, M. A. Cylindrical Block Copolymer Micelles and Co-Micelles of Controlled Length and Architecture. *Science* **2007**, *317*, 644–647.

(100) Erhardt, R.; Zhang, M.; Böker, A.; Zettl, H.; Abetz, C.; Frederik, P.; Krausch, G.; Abetz, V.; Müller, A. H. E. Amphiphilic Janus Micelles with Polystyrene and Poly(Methacrylic Acid) Hemispheres. *J. Am. Chem. Soc.* **2003**, *125*, 3260–3267.

(101) Christian, D. A.; Tian, A.; Ellenbroek, W. G.; Levental, I.; Rajagopal, K.; Janmey, P. A.; Liu, A. J.; Baumgart, T.; Discher, D. E. Spotted Vesicles, Striped Micelles and Janus Assemblies Induced by Ligand Binding. *Nat. Mater.* **2009**, *8*, 843–849.

(102) Geng, Y.; Discher, D. E. Hydrolytic Degradation of Poly(Ethylene Oxide)-Block-

Polycaprolactone Worm Micelles. *J. Am. Chem. Soc.* **2005**, *127*, 12780–12781.

(103) Discher, B. M.; Won, Y.; Ege, D. S.; Lee, J. C.-M.; Bates, F. S.; Discher, D. E.; Hammer, D. A. Polymersomes: Tough Vesicles Made from Diblock Copolymers. *Science* **1999**, *284*, 1143–1146.

(104) Discher, D. E.; Eisenberg, A. Polymer Vesicles. *Science* **2002**, *297*, 967–973.

(105) Thurmond, K. B.; Kowalewski, T.; Wooley, K. L. Water-Soluble Knedel-like Structures: The Preparation of Shell-Cross-Linked Small Particles. *J. Am. Chem. Soc.* **1996**, *118*, 7239–7240.

(106) Read, E. S.; Armes, S. P. Recent Advances in Shell Cross-Linked Micelles. *Chem. Commun.* **2007**, No. 29, 3021–3035.

(107) Pochan, D. J.; Chen, Z.; Cui, H.; Hales, K.; Qi, K.; Wooley, K. L. Toroidal Triblock Copolymer Assemblies. *Science* **2004**, *306*, 94–97.

(108) Bütün, V.; Liu, S.; Weaver, J. V. M.; Bories-Azeau, X.; Cai, Y.; Armes, S. P. A Brief Review of "schizophrenic" Block Copolymers. *React. Funct. Polym.* **2006**, *66*, 157–165.

(109) Arotçaréna, M.; Heise, B.; Ishaya, S.; Laschewsky, A. Switching the inside and the Outside of Aggregates of Water-Soluble Block Copolymers with Double Thermoresponsivity. *J. Am. Chem. Soc.* **2002**, *124*, 3787–3793.

(110) Derry, M. J.; Fielding, L. A.; Armes, S. P. Industrially-Relevant Polymerization-Induced Self-Assembly Formulations in Non-Polar Solvents: RAFT Dispersion Polymerization of Benzyl Methacrylate. *Polym. Chem.* **2015**, *6*, 3054–3062.

(111) Cunningham, V. J.; Alswieleh, A. M.; Thompson, K. L.; Williams, M.; Leggett, G. J.; Armes, S. P.; Musa, O. M. Poly(Glycerol Monomethacrylate)-Poly(Benzyl Methacrylate) Diblock Copolymer Nanoparticles via RAFT Emulsion Polymerization: Synthesis, Characterization, and Interfacial Activity. *Macromolecules* **2014**, *47*, 5613–5623.

(112) Liu, G.; Qiu, Q.; Shen, W.; An, Z. Aqueous Dispersion Polymerization of 2-Methoxyethyl Acrylate for the Synthesis of Biocompatible Nanoparticles Using a Hydrophilic RAFT Polymer and a Redox Initiator. *Macromolecules* **2011**, *44*, 5237–5245.

(113) Canning, S. L.; Smith, G. N.; Armes, S. P. A Critical Appraisal of RAFT-Mediated Polymerization-Induced Self-Assembly. *Macromolecules* **2016**, *49*, 1985–2001.

(114) Charleux, B.; Delaittre, G.; Rieger, J.; D'Agosto, F. Polymerization-Induced Self-Assembly: From Soluble Macromolecules to Block Copolymer Nano-Objects in One Step. *Macromolecules* **2012**, *45*, 6753–6765.

(115) Derry, M. J.; Fielding, L. A.; Armes, S. P. Polymerization-Induced Self-Assembly of Block Copolymer Nanoparticles via RAFT Non-Aqueous Dispersion Polymerization. *Prog. Polym. Sci.* **2016**, *52*, 1–18.

(116) Delaittre, G.; Nicolas, J.; Lefay, C.; Save, M.; Charleux, B. Surfactant-Free Synthesis of Amphiphilic Diblock Copolymer Nanoparticles via Nitroxide-Mediated Emulsion Polymerization. *Chem. Commun.* **2005**, *1*, 614–616.

(117) Brusseau, S.; Dagosto, F.; Magnet, S.; Couvreur, L.; Chamignon, C.; Charleux, B. Nitroxide-Mediated Copolymerization of Methacrylic Acid and Sodium 4-Styrenesulfonate in Water Solution and One-Pot Synthesis of Amphiphilic Block Copolymer Nanoparticles. *Macromolecules* **2011**, *44*, 5590–5598.

(118) Groison, E.; Brusseau, S.; D'Agosto, F.; Magnet, S.; Inoubli, R.; Couvreur, L.; Charleux, B. Well-Defined Amphiphilic Block Copolymer Nanoobjects via Nitroxide-Mediated Emulsion Polymerization. *ACS Macro Lett.* **2012**, *1*, 47–51.

(119) Kim, K. H.; Kim, J.; Jo, W. H. Preparation of Hydrogel Nanoparticles by Atom Transfer Radical Polymerization of N-Isopropylacrylamide in Aqueous Media Using PEG Macro-Initiator. *Polymer* **2005**, *46*, 2836–2840.

(120) Sugihara, S.; Sugihara, K.; Armes, S. P.; Ahmad, H.; Lewis, A. L. Synthesis of Biomimetic Poly(2-(Methacryloyloxy)Ethyl Phosphorylcholine) Nanolatexes via Atom Transfer Radical Dispersion Polymerization in Alcohol/Water Mixtures. *Macromolecules* **2010**, *43*, 6321–6329.

(121) Sugihara, S.; Armes, S. P.; Lewis, A. L. One-Pot Synthesis of Biomimetic Shell Cross-Linked Micelles and Nanocages by ATRP in Alcohol/Water Mixtures. *Angew. Chem. Int. Ed.* **2010**, *49*, 3500–3503.

(122) Li, Y.; Armes, S. P. RAFT Synthesis of Sterically Stabilized Methacrylic Nanolatexes and Vesicles by Aqueous Dispersion Polymerization. *Angew. Chem. Int. Ed.* **2010**, *49*, 4042–4046.

(123) Blanazs, A.; Madsen, J.; Battaglia, G.; Ryan, A. J.; Armes, S. P. Mechanistic Insights for Block Copolymer Morphologies: How Do Worms Form Vesicles? *J. Am. Chem. Soc.* **2011**, *133*, 16581–16587.

(124) Blanazs, A.; Ryan, A. J.; Armes, S. P. Predictive Phase Diagrams for RAFT Aqueous Dispersion Polymerization: Effect of Block Copolymer Composition, Molecular Weight, and Copolymer Concentration. *Macromolecules* **2012**, *45*, 5099–5107.

(125) Lovett, J. R.; Derry, M. J.; Yang, P.; Hatton, F. L.; Warren, N. J.; Fowler, P. W.; Armes, S. P. Can Percolation Theory Explain the Gelation Behavior of Diblock Copolymer Worms? *Chem. Sci.* **2018**, *9*, 7138–7144.

(126) Blanazs, A.; Verber, R.; Mykhaylyk, O. O.; Ryan, A. J.; Heath, J. Z.; Douglas, C. W. I.; Armes, S. P. Sterilizable Gels from Thermoresponsive Block Copolymer Worms. *J. Am. Chem. Soc.* **2012**, *134*, 9741–9748.

(127) Ratcliffe, L. P. D.; Ryan, A. J.; Armes, S. P. From a Water-Immiscible Monomer to Block Copolymer Nano-Objects via a One-Pot RAFT Aqueous Dispersion Polymerization Formulation. *Macromolecules* **2013**, *46*, 769–777.

(128) Lovett, J. R.; Warren, N. J.; Ratcliffe, L. P. D.; Kocik, M. K.; Armes, S. P. PH-Responsive Non-Ionic Diblock Copolymers : Ionization of Carboxylic Acid End-Groups Induces an Order-Order Morphological Transition. *Angew. Chem. Int. Ed.* **2015**, *54*, 1279–1283.

(129) Lovett, J. R.; Warren, N. J.; Armes, S. P.; Smallridge, M. J.; Cracknell, R. B. Order-Order Morphological Transitions for Dual Stimulus Responsive Diblock

Copolymer Vesicles. *Macromolecules* **2016**, *49*, 1016–1025.

(130) Penfold, N. J. W.; Lovett, J. R.; Warren, N. J.; Verstraete, P.; Smets, J.; Armes, S. P. PH-Responsive Non-Ionic Diblock Copolymers: Protonation of a Morpholine End-Group Induces an Order–Order Transition. *Polym. Chem.* **2016**, *7*, 79–88.

(131) Hunter, S. J.; Thompson, K. L.; Lovett, J. R.; Hatton, F. L.; Derry, M. J.; Lindsay, C.; Taylor, P.; Armes, S. P. Synthesis, Characterization, and Pickering Emulsifier Performance of Anisotropic Cross-Linked Block Copolymer Worms: Effect of Aspect Ratio on Emulsion Stability in the Presence of Surfactant. *Langmuir* **2019**, *35*, 254–265.

(132) Thompson, K. L.; Mable, C. J.; Cockram, A.; Warren, N. J.; Cunningham, V. J.; Jones, E. R.; Verber, R.; Armes, S. P. Are Block Copolymer Worms More Effective Pickering Emulsifiers than Block Copolymer Spheres? *Soft Matter* **2014**, *10*, 8615–8626.

(133) Canton, I.; Warren, N. J.; Chahal, A.; Amps, K.; Wood, A.; Weightman, R.; Wang, E.; Moore, H.; Armes, S. P. Mucin-Inspired Thermoresponsive Synthetic Hydrogels Induce Stasis in Human Pluripotent Stem Cells and Human Embryos. *ACS Cent. Sci.* **2016**, *2*, 65–74.

(134) Mable, C. J.; Gibson, R. R.; Prevost, S.; McKenzie, B. E.; Mykhaylyk, O. O.; Armes, S. P. Loading of Silica Nanoparticles in Block Copolymer Vesicles during Polymerization-Induced Self-Assembly: Encapsulation Efficiency and Thermally Triggered Release. *J. Am. Chem. Soc.* **2015**, *137*, 16098–16108.

(135) Mable, C. J.; Derry, M. J.; Thompson, K. L.; Fielding, L. A.; Mykhaylyk, O. O.; Armes, S. P. Time-Resolved SAXS Studies of the Kinetics of Thermally Triggered Release of Encapsulated Silica Nanoparticles from Block Copolymer Vesicles. *Macromolecules* **2017**, *50*, 4465–4473.

(136) Sugihara, S.; Blanazs, A.; Armes, S. P.; Ryan, A. J.; Lewis, A. L. Aqueous Dispersion Polymerization: A New Paradigm for In Situ Block Copolymer Self-Assembly in Concentrated Solution. *J. Am. Chem. Soc.* **2011**, *133*, 15707–15713.

(137) Warren, N. J.; Mykhaylyk, O. O.; Mahmood, D.; Ryan, A. J.; Armes, S. P. RAFT Aqueous Dispersion Polymerization Yields Poly(Ethylene Glycol)-Based Diblock Copolymer Nano-Objects with Predictable Single Phase Morphologies. *J. Am. Chem. Soc.* **2014**, *136*, 1023–1033.

(138) Penfold, N. J. W.; Whatley, J. R.; Armes, S. P. Thermoreversible Block Copolymer Worm Gels Using Binary Mixtures of PEG Stabilizer Blocks. *Macromolecules* **2019**, *52*, 1653–1662.

(139) Gibson, R. R.; Armes, S. P.; Musa, O. M.; Fernyhough, A. End-Group Ionisation Enables the Use of Poly(N-(2-Methacryloyloxy)Ethyl Pyrrolidone) as an Electrosteric Stabiliser Block for Polymerisation-Induced Self-Assembly in Aqueous Media. *Polym. Chem.* **2019**, *10*, 1312–1323.

(140) Ladmiral, V.; Charlot, A.; Semsarilar, M.; Armes, S. P. Synthesis and Characterization of Poly(Amino Acid Methacrylate)-Stabilized Diblock Copolymer Nano-Objects. *Polym. Chem.* **2015**, *6*, 1805–1816.

(141) Doncom, K. E. B.; Warren, N. J.; Armes, S. P. Polysulfobetaine-Based Diblock Copolymer Nano-Objects via Polymerization-Induced Self-Assembly. *Polym. Chem.* **2015**, *6*, 7264–7273.

(142) Semsarilar, M.; Ladmiral, V.; Blanazs, A.; Armes, S. P. Anionic Polyelectrolyte-Stabilized Nanoparticles via RAFT Aqueous Dispersion Polymerization. *Langmuir* **2012**, *28*, 914–922.

(143) Williams, M.; Penfold, N. J. W.; Lovett, J. R.; Warren, N. J.; Douglas, C. W. I.; Doroshenko, N.; Verstraete, P.; Smets, J.; Armes, S. P. Bespoke Cationic Nano-Objects via RAFT Aqueous Dispersion Polymerisation. *Polym. Chem.* **2016**, *7*, 3864–3873.

(144) Penfold, N.; Ning, Y.; Verstraete, P.; Smets, J.; Armes, S. P. Cross-Linked Cationic Diblock Copolymer Worms Are Superflocculants for Micrometer-Sized Silica Particles. *Chem. Sci.* **2016**, *7*, 6894–6904.

(145) Semsarilar, M.; Ladmiral, V.; Blanazs, A.; Armes, S. P. Cationic Polyelectrolyte-Stabilized Nanoparticles via RAFT Aqueous Dispersion Polymerization. *Langmuir* **2013**, *29*, 7416–7424.

(146) Figg, C. A.; Carmean, R. N.; Bentz, K. C.; Mukherjee, S.; Savin, D. A.; Sumerlin, B. S. Tuning Hydrophobicity To Program Block Copolymer Assemblies from the Inside Out. *Macromolecules* **2017**, *50*, 935–943.

(147) Zhou, W.; Qu, Q.; Xu, Y.; An, Z. Aqueous Polymerization-Induced Self-Assembly for the Synthesis of Ketone-Functionalized Nano-Objects with Low Polydispersity. *ACS Macro Lett.* **2015**, *4*, 495–499.

(148) Jiang, Y.; Xu, N.; Han, J.; Yu, Q.; Guo, L.; Gao, P.; Lu, X.; Cai, Y. The Direct Synthesis of Interface-Decorated Reactive Block Copolymer Nanoparticles via Polymerisation-Induced Self-Assembly. *Polym. Chem.* **2015**, *6*, 4955–4965.

(149) Qu, Q.; Liu, G.; Lv, X.; Zhang, B.; An, Z. In Situ Cross-Linking of Vesicles in Polymerization-Induced Self-Assembly. *ACS Macro Lett.* **2016**, *5*, 316–320.

(150) Gao, P.; Cao, H.; Ding, Y.; Cai, M.; Cui, Z.; Lu, X.; Cai, Y. Synthesis of Hydrogen-Bonded Pore-Switchable Cylindrical Vesicles via Visible-Light-Mediated RAFT Room-Temperature Aqueous Dispersion Polymerization. *ACS Macro Lett.* **2016**, *5*, 1327–1331.

(151) Wang, X.; Figg, C. A.; Lv, X.; Yang, Y.; Sumerlin, B. S.; An, Z. Star Architecture Promoting Morphological Transitions during Polymerization-Induced Self-Assembly. *ACS Macro Lett.* **2017**, *6*, 337–342.

(152) Wang, X.; Zhou, J.; Lv, X.; Zhang, B.; An, Z. Temperature-Induced Morphological Transitions of Poly(Dimethylacrylamide)-Poly(Diacetone Acrylamide) Block Copolymer Lamellae Synthesized via Aqueous Polymerization-Induced Self-Assembly. *Macromolecules* **2017**, *50*, 7222–7232.

(153) Biais, P.; Beaunier, P.; Stoffelbach, F.; Rieger, J. Loop-Stabilized BAB Triblock Copolymer Morphologies by PISA in Water. *Polym. Chem.* **2018**, *9*, 4483–4491.

(154) Mellot, G.; Beaunier, P.; Guigner, J. M.; Bouteiller, L.; Rieger, J.; Stoffelbach, F. Beyond Simple AB Diblock Copolymers: Application of Bifunctional and

Trifunctional RAFT Agents to PISA in Water. *Macromol. Rapid Commun.* **2019**, *40*, 1–7.

(155) Ma, Y.; Gao, P.; Ding, Y.; Huang, L.; Wang, L.; Lu, X.; Cai, Y. Visible Light Initiated Thermoresponsive Aqueous Dispersion Polymerization-Induced Self-Assembly. *Macromolecules* **2019**, *52*, 1033–1041.

(156) Yu, Q.; Ding, Y.; Cao, H.; Lu, X.; Cai, Y. Use of Polyion Complexation for Polymerization-Induced Self-Assembly in Water under Visible Light Irradiation at 25 °C. *ACS Macro Lett.* **2015**, *4*, 1293–1296.

(157) Scarpa, J. S.; Mueller, D. D.; Klotz, I. M. Slow Hydrogen-Deuterium Exchange in a Non-α-Helical Polyamide. *J. Am. Chem. Soc.* **1967**, *89*, 6024–6030.

(158) Heskins, M.; Guillet, J. E. Solution Properties of Poly(N-Isopropylacrylamide). *J. Macromol. Sci.* **1968**, *2*, 1441–1455.

(159) Schild, H. G. Poly(N-Isopropylacrylamide): Experiment, Theory and Application. *Prog. Polym. Sci.* **2003**, *17*, 163–249.

(160) Figg, C. A.; Simula, A.; Gebre, K. A.; Tucker, B. S.; Haddleton, D. M.; Sumerlin, B. S. Polymerization-Induced Thermal Self-Assembly (PITSA). *Chem. Sci.* **2015**, *6*, 1230–1236.

(161) Foster, J. C.; Varlas, S.; Couturaud, B.; Jones, J. R.; Keogh, R.; Mathers, R. T.; O'Reilly, R. K. Predicting Monomers for Use in Polymerization-Induced Self-Assembly. *Angew. Chem. Int. Ed.* **2018**, *57*, 15733–15737.

Chapter 2

Preparation and Cross-linking of All-Acrylamide Diblock Copolymer Nano-objects

2.1 Introduction

The RAFT aqueous dispersion polymerisation of DAAM to prepare spheres and vesicles *via* PISA has been reviewed in Chapter 1. However, when the work presented in this present Chapter was conducted in 2017, there were no reports of PDAAM-based block copolymer *worms*. This omission was perhaps not too surprising given that numerous PISA studies have shown that worms typically occupy a relatively narrow phase space.[1–3] However, it is this narrow phase space that makes these nanoparticles interesting for stimulus-responsive studies since a small perturbation in the nanoparticle core-hydration or stabiliser volume can result in a stimulus-induced morphological transition.[4]

When Blanazs et al. monitored the evolution of copolymer morphology during the PISA synthesis of PGMA$_{47}$-PHPMA$_{200}$ diblock copolymer nano-objects using TEM the worm phase was shown to be one of several intermediate states between spheres and vesicles.[5] Similar findings have been reported for other PISA formulations, suggesting that this is generic behaviour.[1,6,7] Thus, if both spheres and vesicles can be produced using a PDMAC-PDAAM PISA formulation, worms should also be accessible if appropriate conditions can be identified.

Since the publication of this work, a number of research groups have now reported the formation of pure worm-like nanoparticles using DAAM as the core-forming block. Firstly, Figg et al. copolymerised DMAC and DAAM from a PDMAC$_{67}$ stabiliser block under aqueous dispersion conditions at 70 °C.[8] They found a surprisingly large worm phase space (total core DP = 110 – 176) when a 75:25 DAAM/DMAC molar ratio was used for the second block. Furthermore, worms were also synthesised when an 80:20 DAAM/DMAC molar ratio was used when the PDAAM/PDMAC DP = 87. Interestingly, only spheres were produced when pure DAAM was used as the core-forming block.

Wang et al. used a bifunctional PEG_{113} stabiliser block which was chain extended with DAAM (total PDAAM DP = 140) under aqueous dispersion conditions at 70 °C to produce ABA triblock copolymer worms.[9] Biais et al. used a PDMAC bifunctional trithiocarbonate stabiliser block which was chain extended with DAAM (target DP = 181) at pH 4.2 to produce ABA triblock copolymer worms stabilised by PDMAC loops.[10] Moreover, Ma et al. used PITSA to chain extend a $PHPMAC_{38}$ stabiliser block with DAAM (target DP = 100).[11] Vesicles were formed at the reaction temperature (70 °C) however, on cooling to 25 °C for two days a vesicle to worm transition took place, as determined by cryo-TEM.

Until the work in this Chapter was conducted, the ketone moiety within the DAAM residues had not yet been exploited for covalent stabilisation of diblock copolymer nano-objects. Typically, cross-linking is achieved *via* the addition of a bifunctional vinyl monomer such as ethylene glycol dimethacrylate to form a third, hydrophobic block.[12–16] This approach works well for spheres and vesicles, but can be problematic for worms.[12] This is because even minor perturbations to the copolymer composition can lead to the formation of mixed phases (e.g. worms plus spheres or worms plus vesicles). However, reaction of the pendent ketone groups within the PDAAM block with a suitable bifunctional hydrazide could offer a simple crosslinking mechanism for PDAAM core nano-objects.

In this Chapter, RAFT aqueous dispersion polymerisation has been used to prepare PDMAC-PDAAM diblock copolymer spheres, worms and vesicles *via* PISA and a morphology phase diagram has been constructed to facilitate reproducible syntheses of such pure phases. Additionally, the stimuli response of the PDMAC-PDAAM nano-objects has been investigated. Finally, the cross-linking of such nano-objects *via* the

ketone group in the DAAM moiety was explored by post-polymerisation modification using a commercial water-soluble adipic acid dihydrazide (ADH) reagent at ambient temperature.

2.2 Results and Discussion

2.2.1 Homopolymerisation of DMAC

The RAFT solution polymerisation of DMAC was performed in dioxane at 70 °C using DDMAT as the CTA is outlined in Figure 2.1. A ^{1}H NMR spectrum of DDMAT is provided in Figure 2.2.
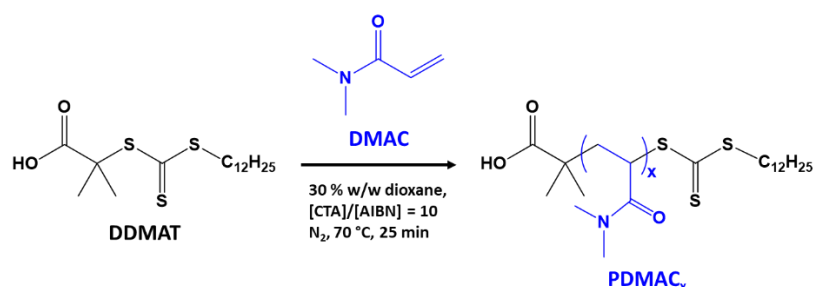

Fig. 2.1. Reaction scheme for the synthesis of the PDMAC homopolymer precursors by RAFT solution polymerisation of DMAC using a DDMAT CTA.
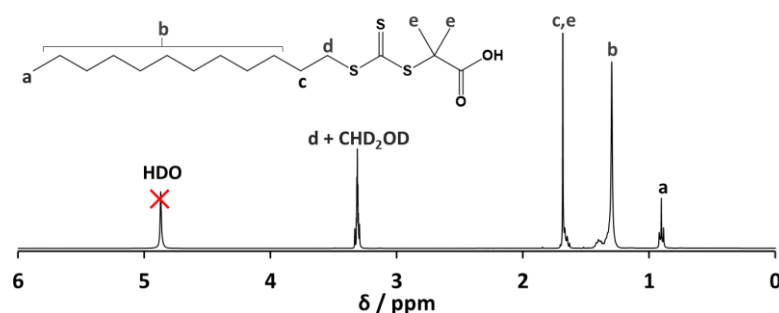

Fig. 2.2. ^{1}H NMR spectrum recorded for DDMAT in CD$_3$OD.

A kinetic study of the synthesis of PDMAC$_{100}$ showed that the DMAC polymerisation proceeded to ~98 % conversion within 90 minutes (see Figure 2.3).

Monomer conversions were calculated from ^{1}H NMR spectra by comparing the integrated DMAC vinyl signals between 5.5 and 7.0 ppm to the combined polymer/monomer signals in the region from 2.3 to 3.25 ppm (Figure 2.4). A linear semi-logarithmic plot indicated pseudo first-order kinetics with respect to DMAC as determined using ^{1}H NMR spectroscopy (see Figure 2.3). The linear evolution of M_n with conversion was accompanied by low dispersities throughout ($M_w/M_n \leq 1.12$), which indicates a well-controlled RAFT polymerisation.[17–19]
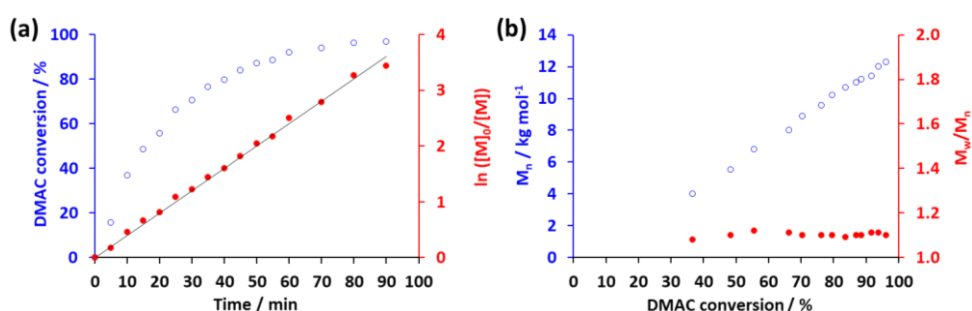
Fig. 2.3. (a) DMAC conversion vs. time plot and corresponding semi-logarithmic plot and (b) evolution of M_n and M_w/M_n vs. DMAC conversion for the RAFT solution polymerisation of DMAC using DDMAT at 30 % w/w in dioxane at 70 °C. DMAC target DP = 100. GPC analyses were performed in DMF eluent using a series of near-monodisperse poly(methyl methacrylate) calibration standards.
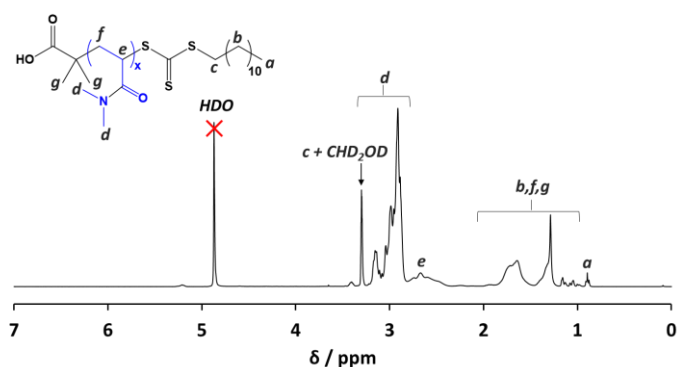
Fig. 2.4. ^{1}H NMR spectrum recorded in CD$_3$OD for PDMAC$_{40}$ stabiliser block (see entry 1 in Table 2.1).

Subsequently, a range of PDMAC precursors were prepared with number-average mean DPs of 40, 46 58, 68 or 77, as determined by end-group analysis using UV spectroscopy (see Figure 2.5 for a Beer-Lambert plot obtained for DDMAT at its absorption maximum of 311 nm). GPC analysis indicated low dispersities (M_w/M_n = 1.09 – 1.12) for all five PDMAC stabiliser blocks used in this work (see Figure 2.6). Characterisation data for these stabiliser blocks are summarised in Table 2.1.
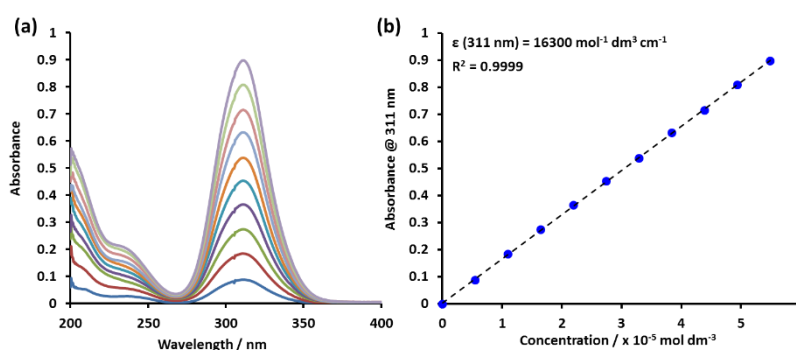
Fig 2.5. (a) UV/visible absorption spectra recorded in methanol for DDMAT at concentrations ranging from 5.5 µmol dm^{-3} to 54.9 µmol dm^{-3}. (b) Beer-Lambert calibration plot constructed for DDMAT to calculate the molar extinction coefficient (ε) at the absorption maximum at 311 nm.
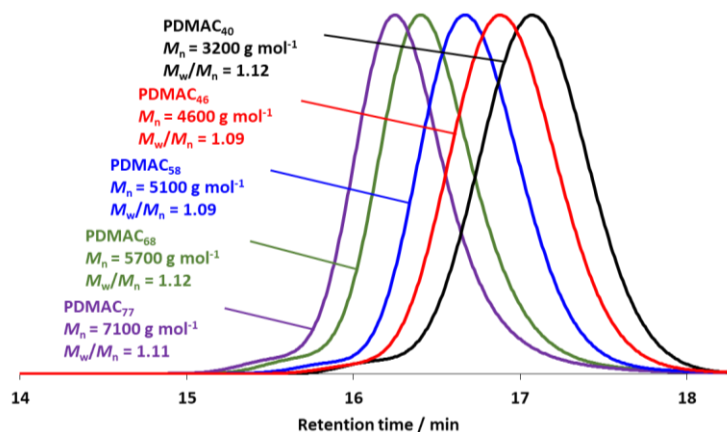
Figure 2.6. DMF GPC chromatograms for a series of PDMAC$_x$ homopolymers where x = 40 to 77.

Table 2.1. Summary of conversion and molecular weight data obtained for PDMAC homopolymers prepared *via* RAFT solution polymerisation of DMAC at 30 % w/w in dioxane at 70 °C.

Entry	PDMAC homopolymer	DMAC Target DP	DMAC conv.[a] / %	Actual DP[b]	$M_{n,GPC}$[c] / g mol^{-1}	M_w/M_n[c]
1	PDMAC$_{40}$	60	60	40	3200	1.12
2	PDMAC$_{46}$	55	87	46	4600	1.09
3	PDMAC$_{58}$	50	96	58	5100	1.09
4	PDMAC$_{68}$	60	95	68	5700	1.12
5	PDMAC$_{77}$	70	93	77	7100	1.11

[a] Determined using ^{1}H NMR spectroscopy in CD$_3$OD, [b] UV spectroscopy analysis in methanol [c] $M_{n,th} = \left(([DMAC]_0/[DDMAT]_0) \times DMAC\ conversion \times M_{DMAC}\right) + M_{DDMAT}$, [d] Determined by DMF GPC using a series of near-monodisperse poly(methyl methacrylate) calibration standards.

2.2.2 RAFT Aqueous Dispersion Polymerisation of DAAM

The PDMAC precursors were chain extended with DAAM using RAFT aqueous dispersion polymerisation at 70 °C and 20 % w/w solids (see Figure 2.7).
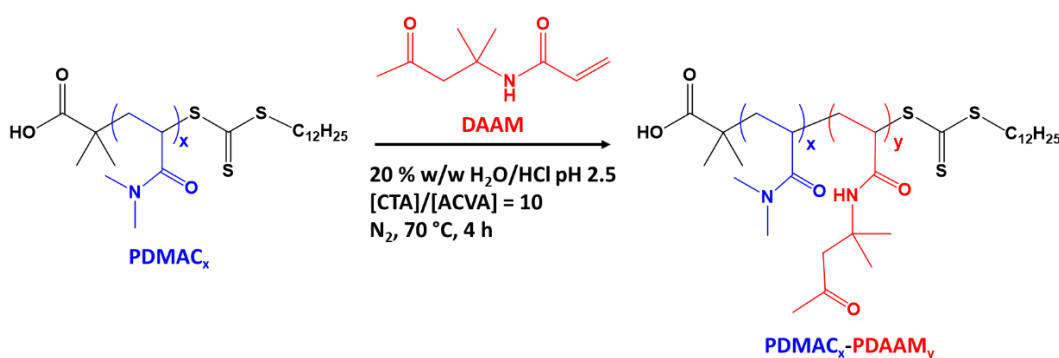
Fig. 2.7. Chain extension of the PDMAC$_x$ precursor with DAAM using RAFT aqueous dispersion polymerisation at pH 2.5 to produce PDMAC$_x$-PDAAM$_y$ diblock copolymer nano-objects.

Recently, Lovett and co-workers have shown that ionisation of CTA-derived carboxylic acid end-groups can influence the morphology of diblock copolymer nano-objects

prepared *via* PISA.[20,21] Thus HCl was used to lower the solution pH to pH 2.5 so as to ensure that the terminal carboxylic acid groups located on the PDMAC stabiliser chains remained in their neutral acid form during the PISA synthesis.

A kinetic study of the chain extension of PDMAC$_{58}$ with DAAM when targeting a DP of 120 for the core-forming block confirmed that ~99 % conversion occurred within 90 minutes (see Figure 2.8a). DAAM conversions were determined by comparison of the residual vinyl signals at 5.4 - 6.4 ppm to the PDAAM methyl signal labelled '*l*' in Figure 2.9. The semi-logarithmic plot (Figure 2.8a) indicated more than a five-fold increase in the rate of polymerisation after approximately 25 minutes, which coincided with the reaction solution becoming distinctly turbid. This indicates the onset of micellar nucleation, with the immediate formation of monomer-swollen particles resulting in a relatively high local DAAM concentration.[5,22] A linear evolution of M_n with DAAM conversion was observed (see Figure 2.8b), which is consistent with a controlled radical polymerisation. However, there was also a modest increase in the M_w/M_n with conversion, resulting in a final M_w/M_n of 1.33.
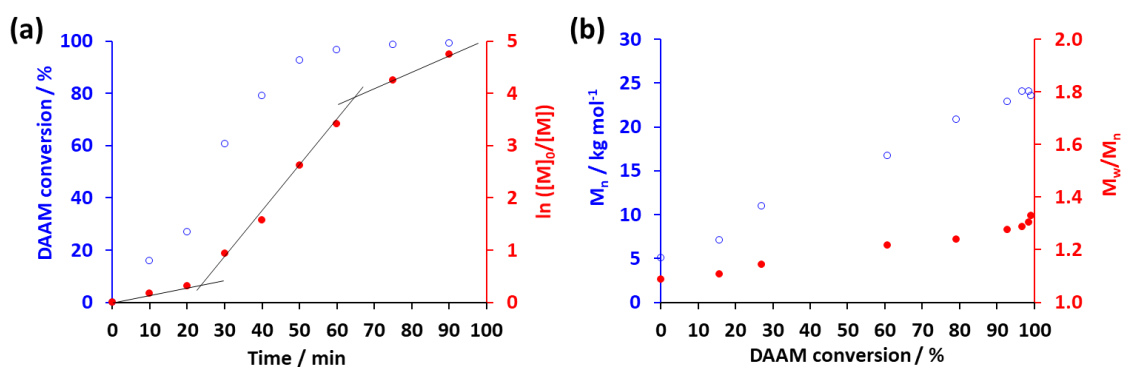
Fig. 2.8. (a) Monomer conversion vs. time curve and corresponding $\ln[M]_0/[M]$ plot and (b) evolution of M_n and M_w/M_n with DAAM conversion for the RAFT aqueous dispersion polymerisation of DAAM at 70 °C and pH 2.5 using a PDMAC$_{58}$ stabiliser block targeting a PDMAC$_{58}$-PDAAM$_{120}$ diblock copolymer.
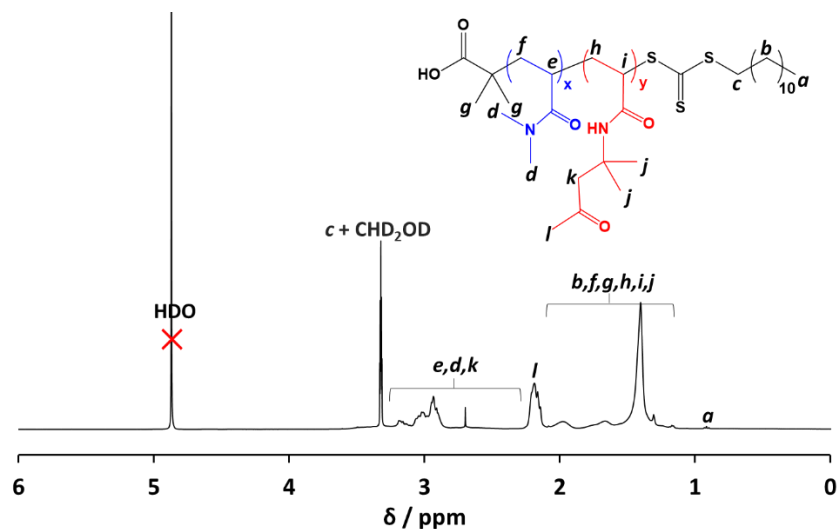
Fig. 2.9. ^{1}H NMR spectrum recorded in CD$_3$OD for the PDMAC$_{40}$-PDAAM$_{85}$ diblock copolymer (see entry 3 in Table 2.2).

Following this kinetic study, a series of PDMAC$_x$-PDAAM$_y$ diblock copolymers was prepared by systematically varying the target PDAAM DP (y), for each of the five PDMAC$_x$ precursors (where x = 40, 46, 58, 68 or 77). Monomer conversions exceeding 98 % were achieved for all such PISA syntheses within 4 h at 70 °C (Table 2.2). All GPC chromatograms were unimodal. A series of representative GPC chromatograms obtained for the PDMAC$_{77}$-PDAAM$_y$ diblock copolymers are provided in Figure 2.10.

Fig. 2.10. DMF GPC chromatograms recorded for a series of PDMAC$_{77}$-PDAAM$_y$ diblock copolymers where y = 100 to 600.

Table 2.2. Characterisation data for all of the PDMAC$_x$-PDAAM$_y$ compositions.

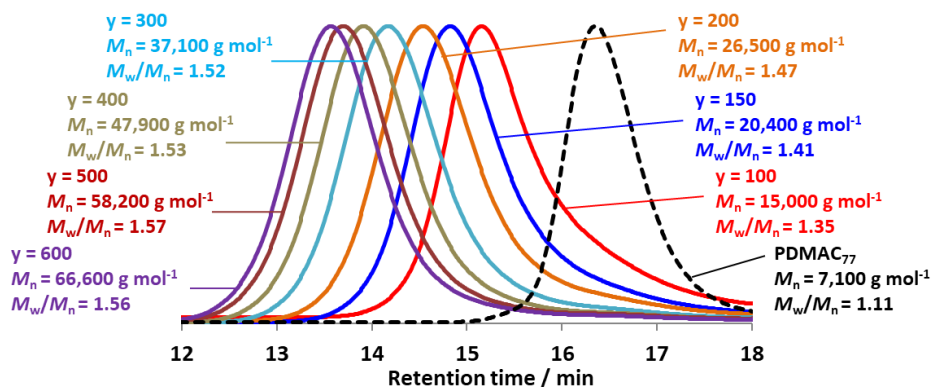| Entry	PDMAC DP	Target DAAM DP	Conv.^{a} / %	Actual DAAM DP	GPC M$_n$^{b}	M$_w$/M$_n$^{b}	DLS Diameter / nm (PDI)^c	Assigned morphology^d
1	40	50	100	50	8900	1.13	144 (0.62)	S+W
2	40	70	100	70	10800	1.24	125 (0.56)	S+W
3	40	85	100	85	12700	1.20	352 (0.55)	S+W
4	40	90	100	90	14800	1.27	-	S+W
5	40	95	100	95	14900	1.25	-	S+W
6	40	100	99	99	14000	1.28	403 (0.45)	W
7	40	105	100	105	16200	1.26	-	W+V
8	40	110	100	110	16900	1.30	-	W+V
9	40	115	100	115	17000	1.30	-	W+V
10	40	120	100	120	16300	1.22	432 (0.27)	W+V
11	40	140	100	140	18600	1.20	467 (0.23)	V
12	40	150	100	150	18200	1.38	560 (0.25)	V
13	40	200	99	198	23700	1.43	559 (0.16)	V
14	46	54	100	54	10600	1.14	41 (0.23)	S+W
15	46	65	100	65	11800	1.15	49 (0.16)	S+W
16	46	76	100	76	13000	1.16	95 (0.19)	S+W
17	46	87	100	87	14100	1.27	127 (0.40)	S+W
18	46	98	100	98	15200	1.20	188 (0.37)	W+V
19	46	109	100	109	16400	1.20	168 (0.19)	W+V
20	46	131	100	131	19100	1.22	332 (0.20)	W+V
21	46	176	98	172	23100	1.27	452 (0.17)	V
22	46	218	99	216	28900	1.27	453 (0.16)	V
23	58	57	100	57	9700	1.27	31 (0.04)	S+W
24	58	69	100	69	10900	1.28	37 (0.05)	S+W
25	58	80	100	80	12000	1.30	48 (0.08)	S+W
26	58	92	99	91	14600	1.28	75 (0.16)	S+W
27	58	92	100	92	13400	1.33	49 (0.06)	S+W
28	58	103	100	103	14500	1.34	58 (0.09)	S+W
29	58	109	98	107	17200	1.22	95 (0.09)	W+V
30	58	126	100	126	18700	1.30	81 (0.09)	W+V
31	58	138	100	138	20000	1.29	96 (0.05)	W+V
32	58	144	99	143	18000	1.31	96 (0.08)	W+V
33	58	149	100	149	21000	1.30	117 (0.07)	V
34	58	161	100	161	22200	1.33	128 (0.08)	V
35	58	172	99	170	23600	1.39	397 (0.17)	V
36	58	172	100	172	22200	1.33	157 (0.11)	V
37	58	201	100	201	24500	1.38	279 (0.28)	V
38	58	207	100	207	26300	1.38	248 (0.19)	V
39	58	218	100	218	27300	1.37	337 (0.13)	V
40	58	230	98	225	27100	1.54	412 (0.11)	V
41	58	230	99	228	25900	1.37	360 (0.15)	V
42	58	230	100	230	28500	1.37	373 (0.13)	V
43	58	230	100	230	31100	1.39	402 (0.19)	V
44	58	345	99	342	34600	1.44	410 (0.12)	V
45	68	78	100	78	14400	1.21	40 (0.09)	S
46	68	104	100	104	17400	1.24	47 (0.08)	S
47	68	157	100	157	23400	1.32	53 (0.09)	S
48	68	209	99	207	26300	1.56	65 (0.05)	S
49	68	417	99	413	46400	1.68	-	S
50	68	626	99	620	60300	1.80	150 (0.03)	S
51	77	75	100	75	14700	1.21	38 (0.05)	S
52	77	100	100	100	17400	1.25	46 (0.14)	S
53	77	150	99	149	20400	1.41	53 (0.06)	S
54	77	200	99	198	26500	1.47	60 (0.05)	S
55	77	300	99	297	37100	1.52	75 (0.02)	S
56	77	400	99	396	47900	1.53	87 (0.03)	S
57	77	500	99	495	58200	1.57	100 (0.03)	S
58	77	600	98	588	66600	1.56	113 (0.03)	S

^{a} Determined by ^{1}H NMR spectroscopy in CD$_3$OD,^{b} Determined by DMF GPC vs. PMMA standards ^{c} Determined by dynamic light scattering on 0.1 % w/v dispersions in pH 2.5 water ^{d} Determined by TEM studies of 0.1 % w/v aqueous dispersions at pH 2.5. S = pure spheres, S+W = mixed phase of spherical micelles and worms, W = pure worms, W+V = mixed phase of worms and vesicles and V = pure vesicles.

2.2.3 PDMAC-PDAAM Nano-object Characterisation

The resulting PDMAC-PDAAM diblock copolymer nano-objects were characterised using TEM. The assigned morphologies were used to construct a phase diagram at a fixed copolymer concentration of 20 % w/w solids. This is shown in Figure 2.11, along with representative TEM images of the pure spheres, worms and vesicles.
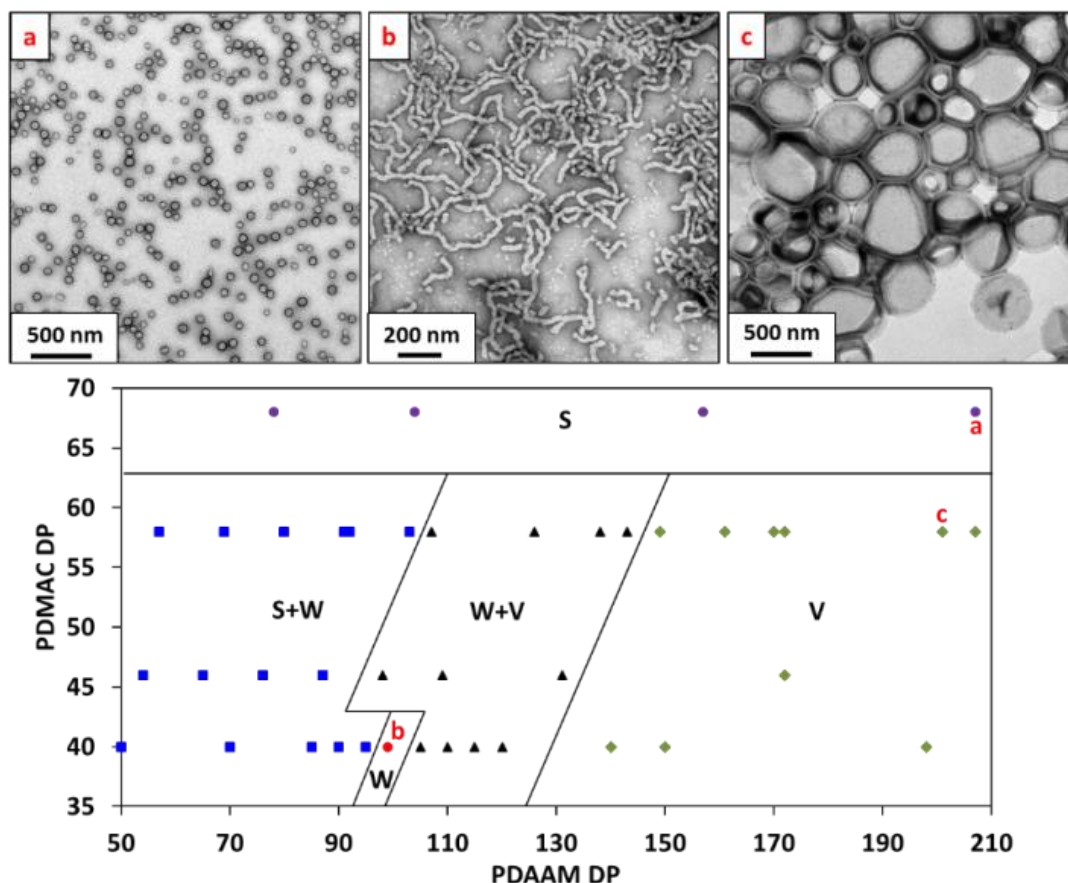
Fig. 2.11. Representative TEM images showing pure sphere, worm and vesicle morphologies obtained for 0.1 % w/w aqueous dispersions of $PDMAC_x$-$PDAAM_y$ diblock copolymer nano-objects at pH 2.5: (a) $PDMAC_{68}$-$PDAAM_{207}$; (b) $PDMAC_{40}$-$PDAAM_{99}$; (c) $PDMAC_{58}$-$PDAAM_{201}$. Phase diagram constructed for a series of $PDMAC_x$−$PDAAM_y$ diblock copolymer nano-objects. S = spheres, S+W = mixed spheres and worms, W = worms, W+V = mixed worms and vesicles and V = vesicles.

Only spheres could be accessed when using a relatively long PDMAC stabiliser block (DP $\geq$ 68), because such formulations favour elastic collisions between nascent spheres rather than the stochastic 1D sphere-sphere fusion events that lead to the formation of worms. Hence spheres represent a kinetically-trapped phase when targeting highly asymmetric diblock compositions.[2] For example, increasing the PDAAM DP from 78 to 620 when using a PDMAC$_{68}$ stabiliser block only resulted in a monotonic increase in mean sphere diameter from 40 to 150 nm, as determined by dynamic light scattering (DLS) analysis. In contrast, worms and vesicles could be accessed when using shorter PDMAC stabiliser blocks (DP $\leq$ 58). For example, targeting PDMAC$_x$-PDAAM$_y$ where x = 40, 46 and 58 and y $\geq$ 150 gave pure vesicles. The phase space for pure worms was extremely narrow and was bounded by sphere/worm and worm/vesicle mixed phases. Similar observations have been reported by Blanazs et al. for an alternative RAFT aqueous dispersion polymerisation formulation.[2] Indeed, pure worms were only attained for PDMAC$_{40}$-PDAAM$_{99}$. This composition resulted in a free-standing gel, most likely as a result of multiple inter-worm contacts.[23,24] Nevertheless, the phase diagram shown in Figure 2.11 enables the pure worm phase to be reproducibly targeted.

Lovett et al. reported that PGMA−PHPMA diblock copolymer nano-objects prepared by RAFT aqueous dispersion polymerisation using a carboxylic acid-functionalised CTA exhibit pH-responsive behaviour.[20,21] More specifically, worm-to-sphere and vesicle-to-worm transitions were observed on increasing the solution pH from 3.5 to 6.0. Such morphological transitions were attributed to ionisation of the carboxylic acid end-groups on the PGMA chains, which increases the effective volume fraction of this hydrophilic stabiliser block. In the present study, the PDMAC stabiliser blocks also contain a terminal carboxylic acid group, so similar pH-responsive behaviour was anticipated. To examine this hypothesis, DLS and aqueous electrophoresis measurements were recorded for a

series of 0.1 % w/w PDMAC-PDAAM aqueous dispersions as a function of solution pH

(see Figure 2.12).
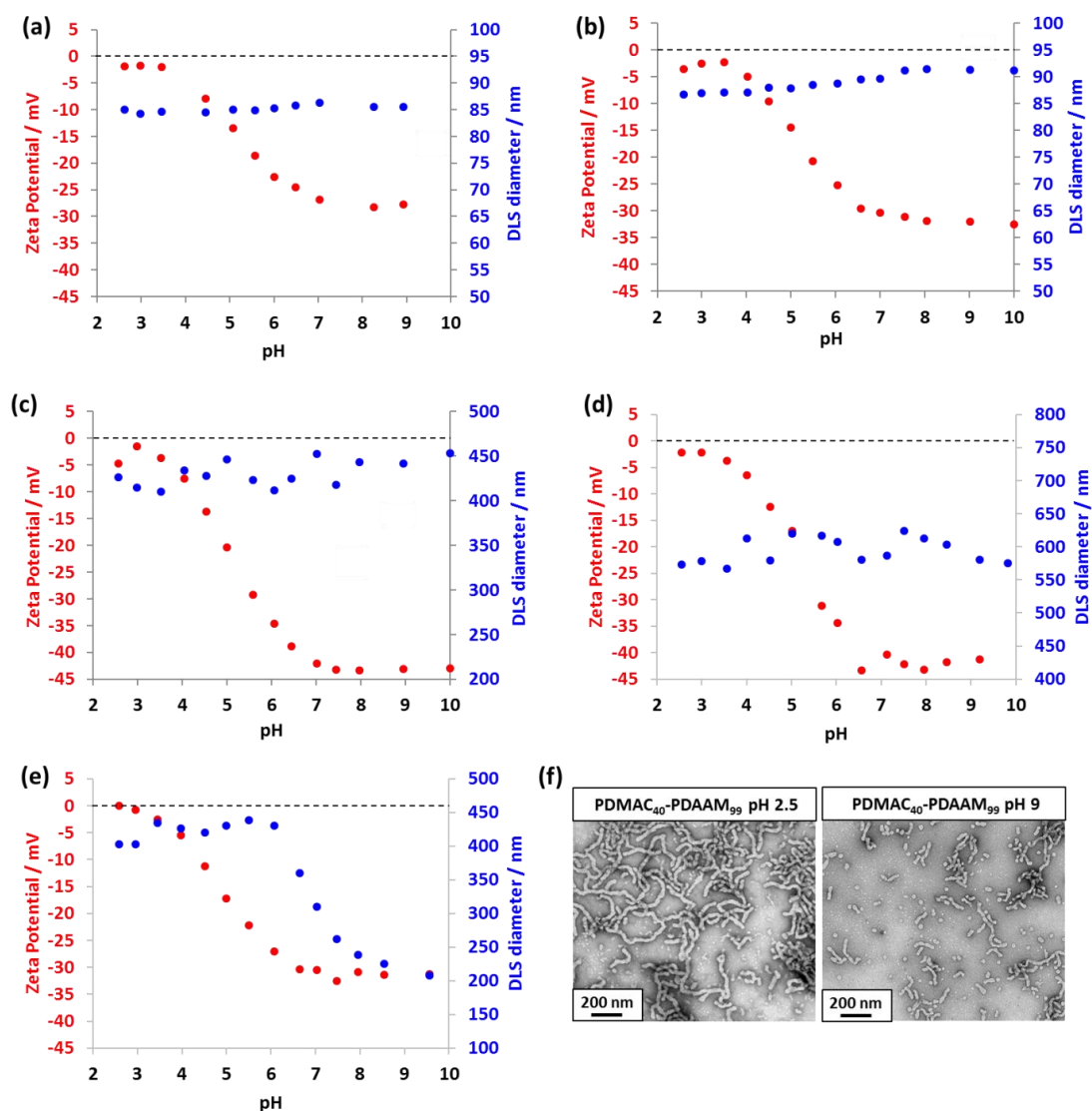
Fig. 2.12. Variation of intensity-average hydrodynamic particle diameter (measured by DLS) and zeta potential with pH recorded at 25 °C for 0.1 % w/w aqueous dispersions of (a) a PDMAC$_{58}$-PDAAM$_{91}$ worm/sphere mixed phase (b) a PDMAC$_{58}$-PDAAM$_{107}$ worm/vesicle mixed phase (c) PDMAC$_{58}$-PDAAM$_{170}$ vesicles (d) PDMAC$_{40}$-PDAAM$_{140}$ vesicles and (e) PDMAC$_{40}$-PDAAM$_{99}$ worms. (f) TEM images obtained for a 0.1 % w/w aqueous PDMAC$_{40}$-PDAAM$_{99}$ dispersion at pH 2.5 and pH 9.

In each case, the zeta potential became more negative at higher pH as a result of deprotonation of the carboxylic acid end-groups on the PDMAC chains originating from the DDMAT CTA. However, the original sphere-equivalent particle diameter remained essentially unchanged over the entire pH range studied for PDMA-PDAAM nano-objects synthesised using a relatively long PDMAC stabiliser block (DP $\geq$ 58) or containing a PDAAM block with a mean DP of at least 140 (see Figure 2.12). Clearly, end-group ionisation is insufficient to induce a morphology transition for such copolymers. In contrast, $PDMAC_{40}$-$PDAAM_{99}$ worms proved to be weakly pH-responsive: their sphere-equivalent particle diameter was reduced from 403 nm at pH 2.6 to 208 nm at pH 9.6 (see Figure 2.12e). TEM studies indicated that this is the result of a transition from pure worms to a mixed phase comprising relatively short worms and spheres (Figure 2.12f).

There are numerous literature examples of thermoresponsive diblock copolymer nano-objects prepared by RAFT aqueous dispersion polymerisation. Such behaviour has been reported for relatively weakly hydrophobic core-forming blocks such as PHPMA, PNIPAM and poly(2-methoxyethyl acrylate) (PMEA).[4,16,20,25,26] Given that the DAAM monomer is fully miscible with water, the corresponding PDAAM block might be expected to be weakly hydrophobic and partially hydrated, as previously reported for PHPMA.[4] For $PDMAC_{58}$-$PDAAM_y$ nano-objects, no change in either solution viscosity or turbidity was observed when cooling 20 % w/w aqueous dispersions of spheres, worms or vesicles to below 5 °C, or on heating up to 50 °C. DLS studies confirmed that no discernible change in hydrodynamic diameter occurred on either heating or cooling a 0.1 % w/w aqueous dispersion of $PDMAC_{58}$-$PDAAM_{170}$ vesicles at pH 2.5 (Figure 2.13a). In contrast, a modest reduction in the sphere-equivalent particle diameter from approximately 360 nm to around 300 nm was observed for a 0.1 % w/w aqueous dispersion of $PDMAC_{40}$-$PDAAM_{99}$ worms on heating from 20 °C to 50 °C (see Figure

2.13b). TEM studies indicate that this is due to a morphological transition from worms to

a mixture of short worms and vesicles (see Figure 2.13c). This transition is believed to be

related to the relatively narrow phase space occupied by these pure worms.
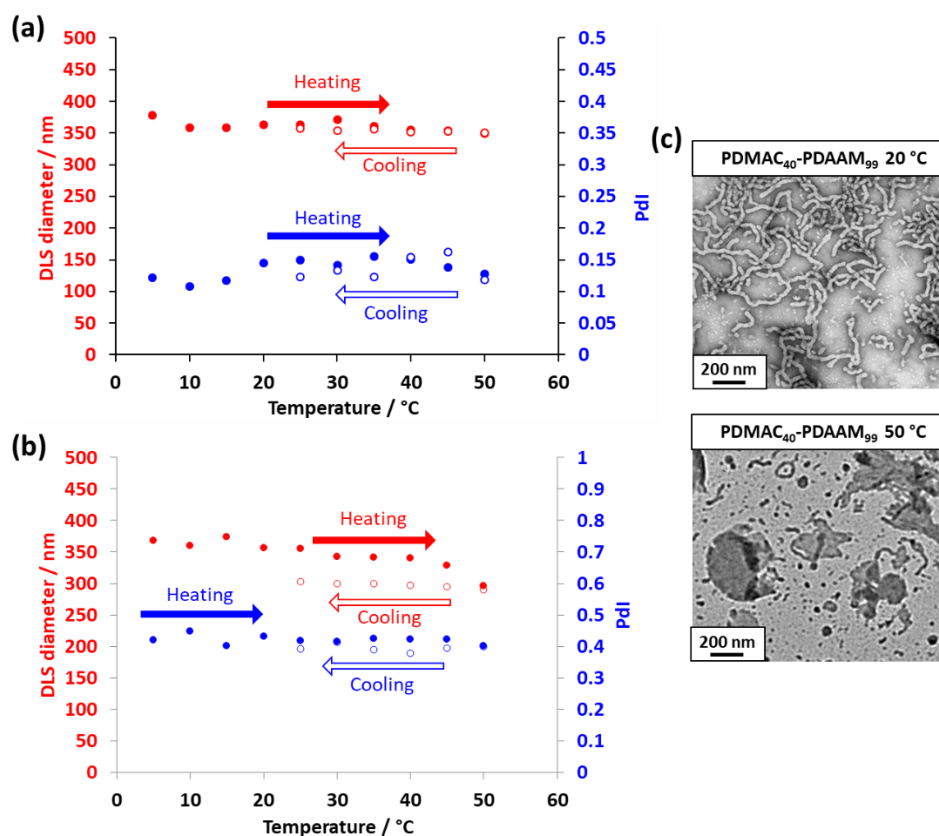

Fig. 2.13. Variation of intensity-average hydrodynamic particle diameter and polydispersity (determined by DLS) with temperature on heating a 0.1% w/w aqueous dispersion of (a) $PDMAC_{58}$-$PDAAM_{170}$ vesicles and (b) $PDMAC_{40}$-$PDAAM_{99}$ worms from 5 °C to 50 °C followed by cooling from 50 °C to 25 °C at 5 °C intervals, allowing 15 min for thermal equilibrium at each temperature. (c) TEM images obtained for a 0.1 % w/w aqueous $PDMAC_{40}$-$PDAAM_{99}$ dispersion at 20 °C and 50 °C.

In summary, $PDMAC_x$-$PDAAM_y$ diblock copolymer nano-objects with $x \geq 58$ or $y \geq 140$ prepared herein proved to be neither pH-responsive on raising the solution pH to pH 10 nor thermoresponsive on lowering the solution temperature to 5 °C or heating to 50 °C.

In contrast, $PDMAC_{40}$-$PDAAM_{99}$ worms proved to be weakly responsive with respect to changes to either solution pH or temperature. However, it is perhaps noteworthy that, unlike the observations made by Lovett and co-workers,[21] no *additional* change in copolymer morphology was observed when subjecting these $PDMAC_{40}$-$PDAAM_{99}$ worms to a *dual* stimulus-response (i.e. switching the solution pH to pH 9 while simultaneously cooling to 5 °C, or heating to 50 °C).

Since this work was conducted in 2017, there are now reports of thermoresponsive nano-objects being prepared using PDAAM as the core-forming block. For example, the An group have reported the synthesis of $PDMAC_{30}$-$PDAAM_x$ lamellae (where x = 60 - 90).[27] It was found that these lamellae underwent a lamella to sphere/worm morphological transition on cooling. The Cai group prepared thermoresponsive $PDMAC_{38}$-$PDAAM_{90}$ and $PDMAC_{38}$-$PDAAM_{100}$ vesicles.[11] They found that on cooling these vesicle dispersions from the reaction temperature (70 °C) to 25 °C for two days a reversible vesicle to lamellae or a vesicle to worm transition occurred for the $PDMAC_{38}$-$PDAAM_{90}$ and $PDMAC_{38}$-$PDAAM_{100}$ vesicles respectively. It is still unclear why the nano-objects produced in this work were not particularly thermoresponsive.

2.2.4 Covalent Stabilisation of PDMAC-PDAAM Diblock Copolymer Nano-objects

All PDMAC-PDAAM syntheses were conducted at an initial solution pH of 2.5. However, for the 20 % w/w formulations reported herein, the solution pH had risen in each case to approximately pH 4.0 after DAAM polymerisation. Fortuitously, this is the optimum pH for subsequent cross-linking using ADH, as reported by Kessel et al.[28] The hydrazide groups present on ADH can react with the pendent ketone groups on the PDAAM chains *via* nucleophilic substitution to form hydrazone linkages (Figure 2.14).

In principle, this should result in covalent stabilisation of these nano-objects. All such cross-linking reactions were conducted at 25 °C using various ADH/DAAM molar ratios.
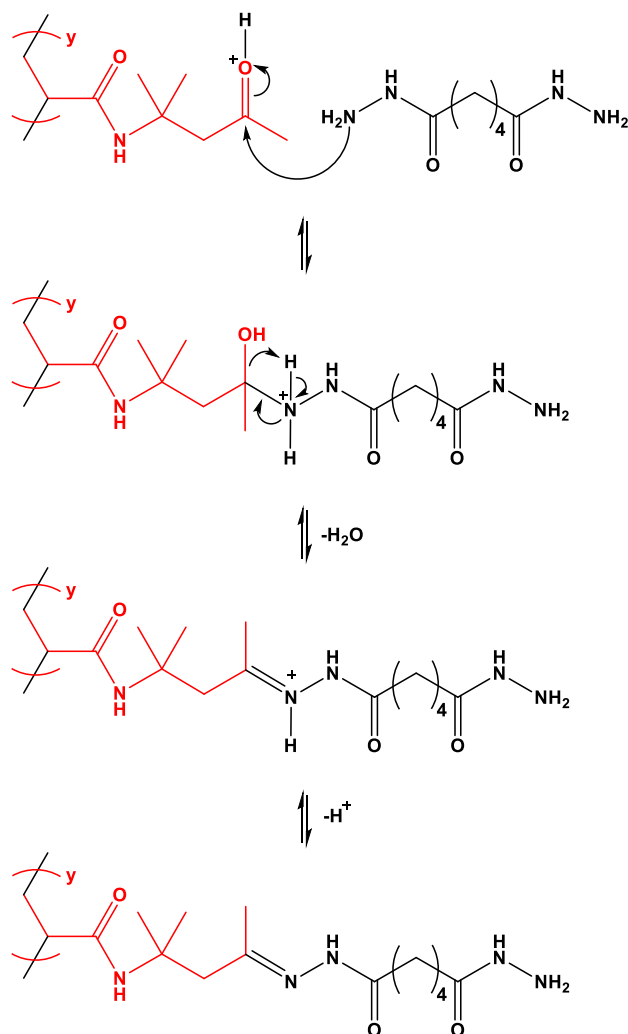
Fig. 2.14. Reaction scheme illustrating the acid catalysed nucleophilic attack of PDAAM pendent ketone groups by ADH. If the pendent hydrazine group then reacts with a ketone group on a second PDAAM chain, this leads to cross-linking.

Spectroscopic evidence for the proposed cross-linking reaction was obtained from Fourier-transform infrared spectroscopy (FT-IR) studies. First, a model reaction was conducted whereby a stirred 20 % w/w aqueous solution of DAAM monomer was reacted with ADH using an ADH/DAAM molar ratio of 0.50 at 25 °C. This reaction mixture

gradually became turbid and after 6 h the crude product was isolated by freeze-drying overnight. FT-IR spectra recorded for ADH alone, the DAAM monomer and the freeze-dried crude product are shown in Figure 2.15.
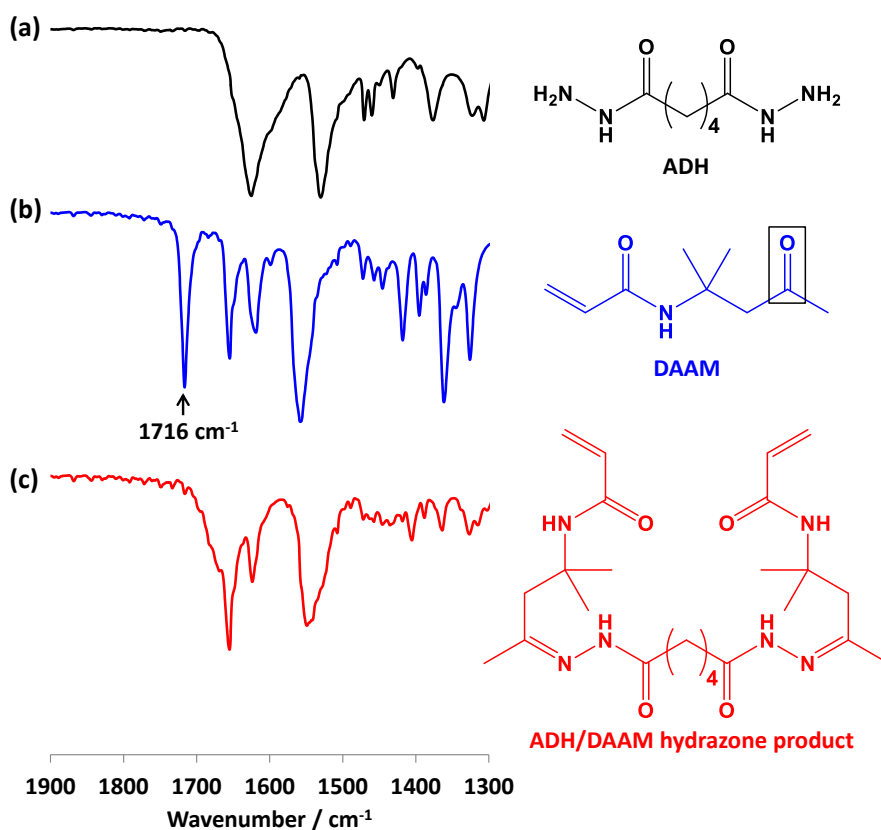
Fig. 2.15. FT-IR spectra recorded for (a) ADH, (b) DAAM and (c) the freeze-dried product obtained from the reaction of ADH with DAAM at 25 °C for 6 h using an ADH/DAAM molar ratio of 0.50. Conditions: 20 % w/w solution, pH 2.5.

The DAAM monomer spectrum has a strong ketone band at 1716 cm^{-1}. This characteristic feature is absent in the product, indicating loss of the ketone moiety. Complete attenuation of this ketone band indicates efficient reaction of the ADH with DAAM monomer within 6 h at 25 °C.

Following this successful model reaction, an FT-IR study of the addition of ADH to an aqueous dispersion of PDMAC$_{58}$-PDAAM$_{230}$ vesicles was undertaken, see Figure 2.16.

Fig. 2.16. FT-IR spectra recorded for: (a) ADH, (b) a freeze-dried 20 % w/w aqueous dispersion of PDMAC$_{58}$-PDAAM$_{230}$ vesicles; (c) the freeze-dried 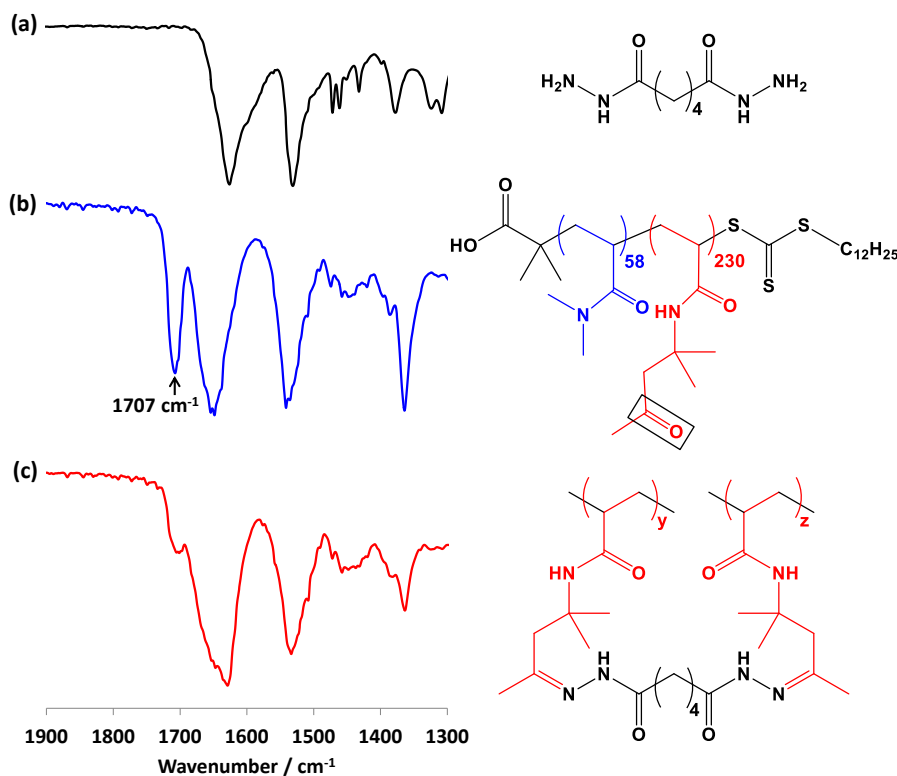product of the reaction of a 20 % w/w aqueous dispersion of PDMAC$_{58}$-PDAAM$_{230}$ vesicles with ADH. Conditions: ADH/DAAM molar ratio = 0.50, 6 h, 25 °C, pH 4.

The pendent ketone groups in the PDAAM chains exhibit a characteristic band at 1707 cm^{-1}, which is close to that observed for DAAM monomer (1716 cm^{-1}). After cross-linking with ADH for 6 h at 25 °C, this spectral feature became substantially attenuated relative to the other IR bands. The remaining shoulder observed for the cross-linked PDMAC-PDAAM vesicles suggests that cross-linking remained incomplete after 6 h. It is also worth emphasising that reaction of the ADH with the pendent ketone groups on the PDAAM chains does not necessarily guarantee that an intermolecular crosslink is obtained. It is likely that at least some of the ADH is consumed in the formation of intramolecular cycles *via* reaction with two ketones located on the same PDAAM

chain.[29–31] Moreover, it is also possible that the ADH might only react once, with its second hydrazide group being unable to react with another ketone group because of steric congestion. This latter problem is more likely to occur at higher degrees of cross-linking as the PDAAM cores become more solid-like.

FT-IR spectra recorded when cross-linking $PDMAC_{58}$-$PDAAM_{230}$ vesicles using ADH/DAAM molar ratios of 1.00, 0.50, 0.25 or 0.10 indicated that greater attenuation of the ketone band occurred at higher ADH concentrations, see Figure 2.17.
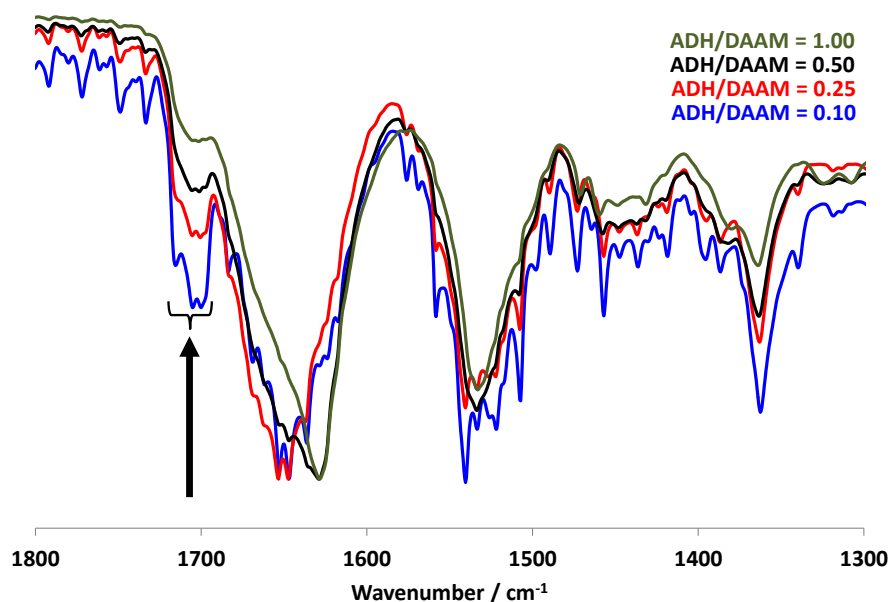
Fig. 2.17. FT-IR spectra recorded for the freeze-dried copolymer products arising from the reaction of a 20 % w/w aqueous dispersion of $PDMAC_{58}$-$PDAAM_{230}$ vesicles with ADH at 25 °C for 6 h using ADH/DAAM molar ratios of 1.00, 0.50, 0.25 or 0.10. The arrow indicates the carbonyl band assigned to the DAAM residues.

The effect of varying the ADH concentration on the extent of cross-linking (and hence the degree of covalent stabilisation of the nano-objects) was studied using DLS. Accordingly, ADH was added to a 20 % w/w aqueous dispersion of

$PDMAC_{58}$-$PDAAM_{230}$ vesicles at ADH/DAAM molar ratios of 0.010, 0.025, 0.050, 0.075, 0.100, 0.150 or 0.200 and allowed to react at 25 °C with continuous stirring for 24 h. Aliquots taken at various time intervals were diluted to 0.1 % w/v in methanol, which is a good solvent for both PDMAC and PDAAM. Thus, if no cross-linking had occurred, then molecular dissolution would be expected in this solvent. All these dilute methanolic dispersions were analysed by DLS to establish the minimum time required for sufficient covalent stabilisation to preserve the original nano-objects. As ADH cross-linking progressed, the vesicles became gradually more resistant to methanol dissolution. For each ADH concentration, the scattered light intensity (or derived count rate) and the sphere-equivalent particle diameter were monitored as a function of time, see Figure 2.18. The former parameter increased up to approximately 6 h, after which plateau values were observed (Figure 2.18a). This suggests that cross-linking is close to completion on this time scale. Moreover, maximum covalent stabilisation is achieved for ADH/DAAM molar ratios ≥ 0.075.

The DLS diameter for a dilute aqueous dispersion of $PDMAC_{58}$-$PDAAM_{230}$ vesicles (0.1 % w/w at pH 2.5) prior to cross-linking was 402 nm. Figure 2.18b indicates that larger particle diameters were observed for all ADH concentrations after 24 hours as a result of swelling of the cross-linked vesicles when diluted in methanol. Substantial swelling was observed for the lightly cross-linked vesicles in the presence of methanol. In contrast, much less swelling occurred for ADH/DAAM molar ratios ≥ 0.050, because more extensive cross-linking was obtained under these conditions. TEM studies of the linear $PDMAC_{58}$-$PDAAM_{230}$ vesicles and a series of vesicles cross-linked by reaction with various ADH/DAAM molar ratios for 24 h are shown in Figure 2.19. Retention of the copolymer morphology after dilution in methanol confirms covalent stabilisation of the original vesicle morphology.

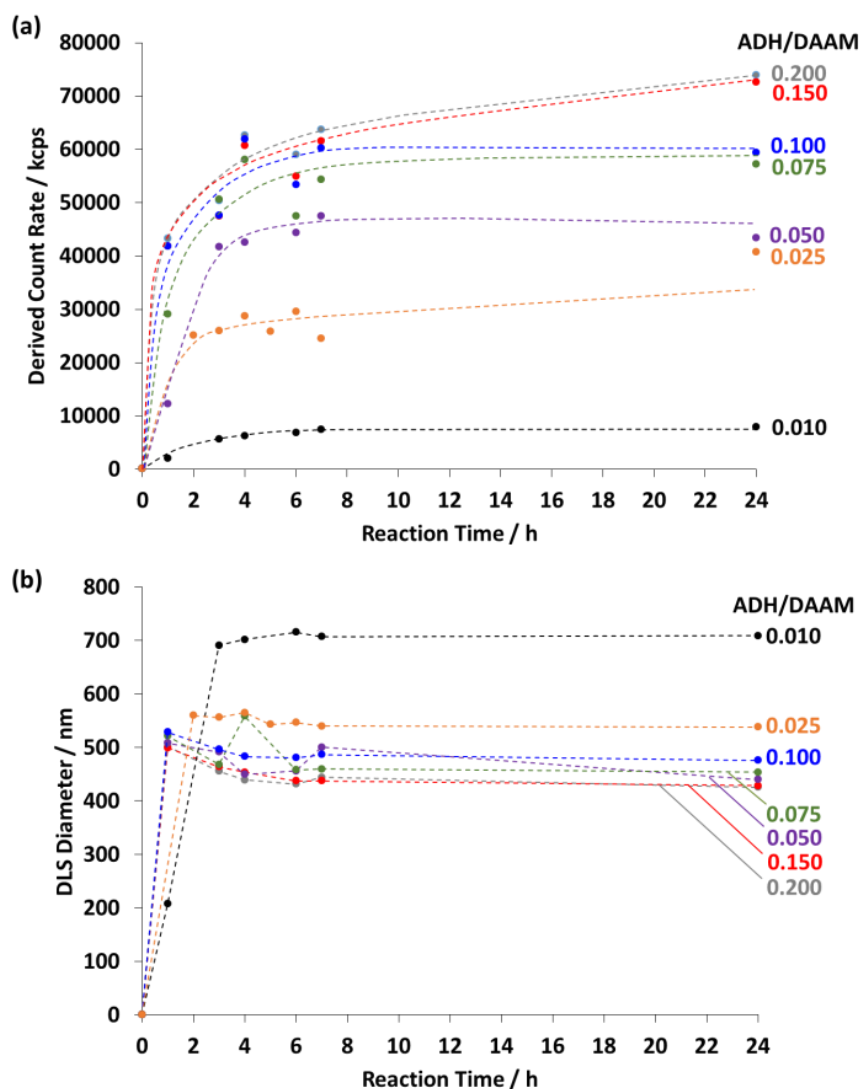Fig. 2.18. Time dependence for (a) scattered light intensity count rate and (b) DLS diameter when cross-linking a 20 % w/w aqueous dispersion of $PDMAC_{58}$-$PDAAM_{230}$ vesicles at pH 4 using ADH at ADH/DAAM molar ratios of 0.200, 0.150, 0.100, 0.075, 0.050, 0.025 or 0.010 at 25 °C. Aliquots were extracted from the reaction solution at regular time intervals prior to quenching *via* dilution to 0.1 % w/v solids using methanol.
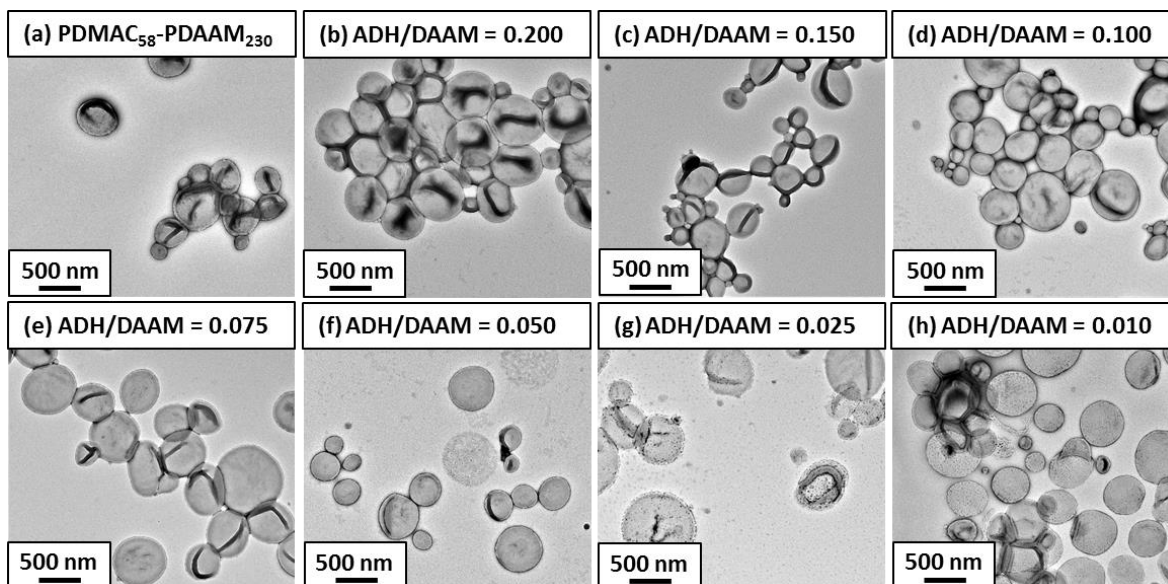
Fig. 2.19. TEM images obtained for (a) a 0.1 % w/w *aqueous* dispersion of linear PDMAC$_{58}$-PDAAM$_{230}$ vesicles at pH 2.5 and (b-h) a series of 0.1 % w/w *methanolic* dispersions of PDMAC$_{58}$-PDAAM$_{230}$ vesicles crosslinked using ADH/DAAM molar ratios of 0.200, 0.150, 0.100, 0.075, 0.050, 0.250 or 0.010, respectively, reaction conditions: 20 % w/w solids, 24 h.

Cross-linking was also conducted on aqueous dispersions of PDMAC$_{68}$-PDAAM$_{207}$ spheres and PDMAC$_{40}$-PDAAM$_{99}$ worms, respectively (ADH/DAAM molar ratio = 0.100; 6 h at 25 °C). In both cases, the original copolymer morphology was retained on exposure to methanol as determined by TEM analysis (Figure 2.20). Swelling of the cross-linked PDMAC$_{68}$-PDAAM$_{207}$ spheres in methanol resulted in a larger DLS diameter of 77 nm (compared to 65 nm measured at pH 2.5 prior to cross-linking). Conversely, the sphere-equivalent diameter obtained for the cross-linked PDMAC$_{40}$-PDAAM$_{99}$ worms was *lower* than that determined prior to cross-linking (317 nm vs. 403 nm). Given that the TEM images shown in Figure 2.20 confirm retention of the worm morphology, one possible explanation for these DLS observations is that

insufficient worm crosslinking may result in partial worm fragmentation on exposure to methanol.
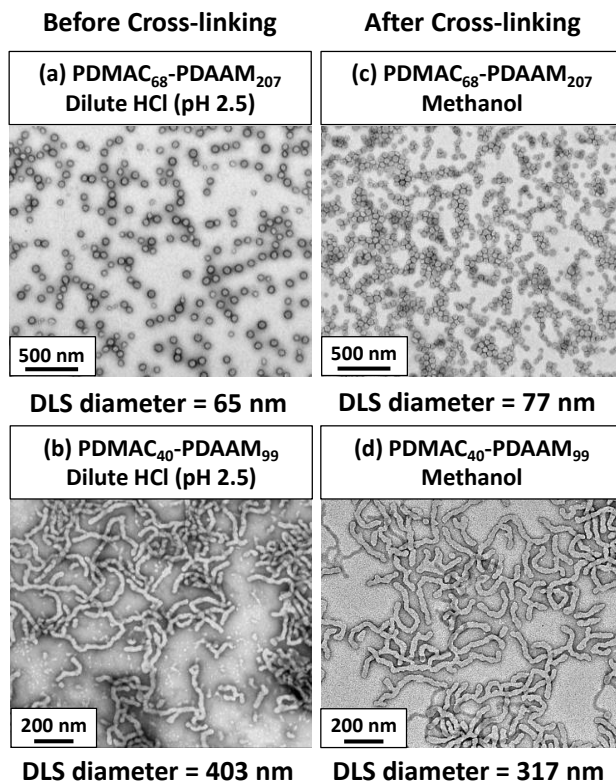
Fig. 2.20. TEM images and DLS measurements recorded for 0.1% *aqueous* dispersions of (a) linear PDMAC$_{68}$-PDAAM$_{207}$ spheres and (b) linear PDMAC$_{40}$-PDAAM$_{99}$ worms at pH 2.5; 0.1% *methanolic* dispersions of (c) cross-linked PDMAC$_{68}$-PDAAM$_{207}$ spheres and (d) cross-linked PDMAC$_{40}$-PDAAM$_{99}$ worms after reacting with ADH at an ADH/DAAM molar ratio of 0.10 for 6 h at 25 °C.

2.2.5 Rheological Studies

The storage modulus, G′, of a 20 % w/w PDMAC$_{40}$-PDAAM$_{99}$ worm gel was determined by oscillatory rheology before and after ADH cross-linking for 6 h at 25 °C using an ADH/DAAM molar ratio of 0.10. At a fixed angular frequency of 1.0 rad s^{-1} and a constant strain of 1.0 %, G′ increased from 2370 Pa to 10330 Pa at 25 °C (see Figure 2.21). Similar enhancements in gel strength after cross-linking were also reported

by both Lovett et al.[32] and Won et al..[33] This has been attributed to worm stiffening, which leads to an increase in the worm mean persistence length.
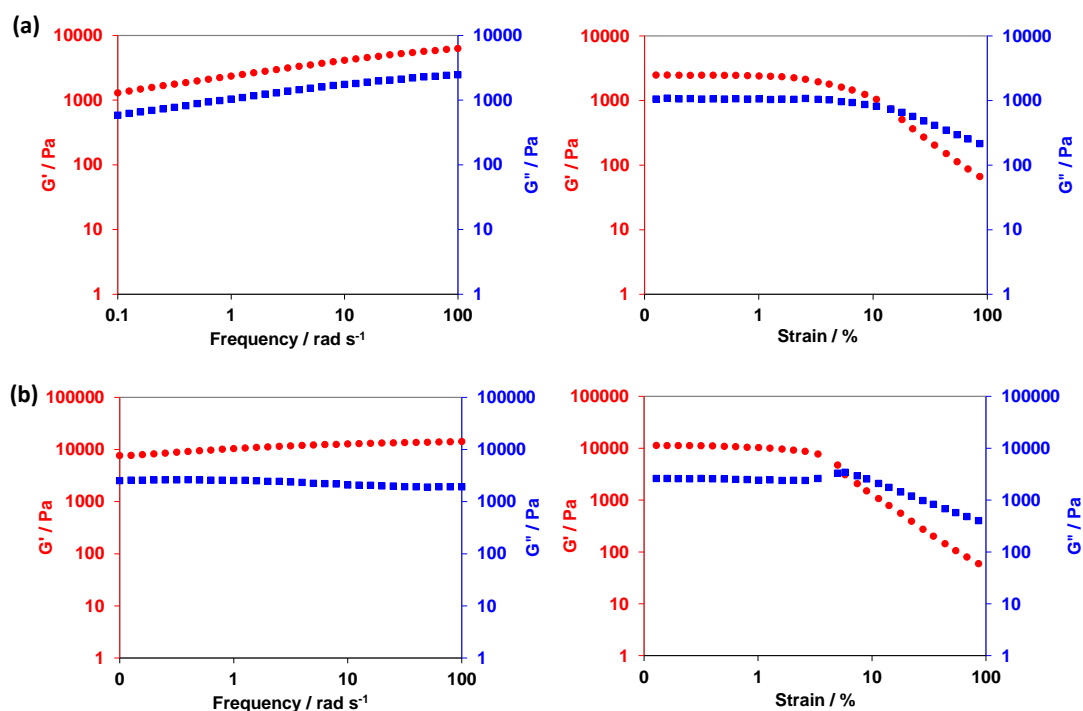
Fig. 2.21. Variation of gel moduli (G′, red circles and G″, blue squares) with frequency at an applied strain of 1.0 % and variation of gel moduli (G′, red circles and G″, blue squares) with strain at an applied frequency of 1 rad s^{-1} for (a) linear PDMAC$_{40}$-PDAAM$_{99}$ diblock copolymer prepared at 20 % w/w solids in water at pH 2.5 and (b) cross-linked PDMAC$_{40}$-PDAAM$_{99}$ diblock copolymer prepared at 20 % w/w solids in water at pH 2.5 with subsequent cross-linking at 25 °C for 6 h (ADH/DAAM molar ratio = 0.10).

The linear and crosslinked PDMAC$_{40}$-PDAAM$_{99}$ worm gels were also analysed by shear-induced polarised light imaging (SIPLI).[34,35] SIPLI combines rotational rheology with a reflection polariscope in order to study the birefringence from an aligned sample. In the SIPLI technique polarised light is passed through a sample, it is then reflected from the polished steel top plate of the rheometer towards the detector. If the particles within the sample are aligned the sample will act as a grating and will change the orientation of

the polarised light allowing it to pass through the analyser which is orthogonal to the axis of polarised light. This results in a characteristic Maltese cross pattern.

As expected, the SIPLI images obtained at a shear rate of 10 s^{-1} for both the linear and crosslinked PDMAC$_{40}$-PDAAM$_{99}$ worm gels show the characteristic Maltese cross pattern associated with alignment, see Figure 2.22. However, the Maltese cross for the crosslinked worm gel appears more pronounced than the linear worm gel which could be a result of the increase in the worm mean persistence length allowing for easier worm orientation.
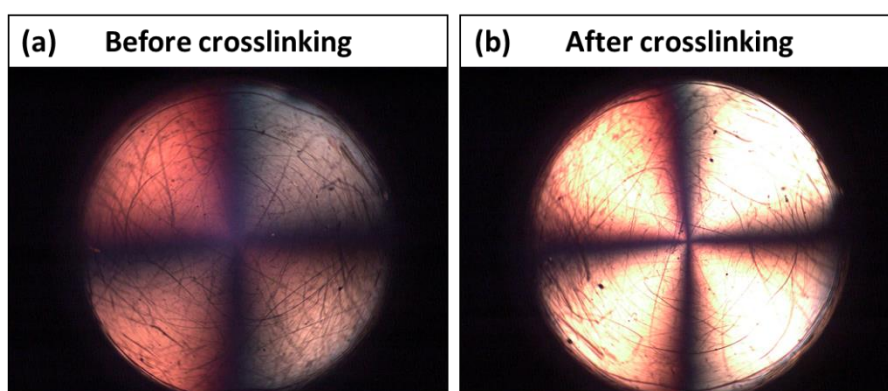
Fig. 2.22. Shear-induced polarised light images obtained at a constant shear rate of 10 s^{-1} at 20 °C for (a) linear PDMAC$_{40}$-PDAAM$_{99}$ diblock copolymer prepared at 20 % w/w solids in water at pH 2.5 and (b) cross-linked PDMAC$_{40}$-PDAAM$_{99}$ diblock copolymer prepared at 20 % w/w solids in water at pH 2.5 with subsequent cross-linking at 25 °C for 6 h (ADH/DAAM molar ratio = 0.10).

2.3 Conclusions

In summary, a series of well-defined hydrophilic PDMAC homopolymer precursors (mean DPs = 40, 46, 58, 68 or 77) were prepared using DDMAT and subsequently chain extended with DAAM using a RAFT aqueous dispersion polymerisation formulation. The resulting amphiphilic diblock copolymers formed a range of nano-objects *via* PISA. A

phase diagram was constructed for various diblock copolymer compositions at 20 % w/w solids. Pure spheres, worms and vesicles were identified by TEM studies. The worm phase space was extremely narrow, which no doubt explains why this copolymer morphology had not been previously identified for this particular PISA formulation.[36]

Remarkably, most of these PDMAC-PDAAM nano-objects reported herein proved to be insensitive to changes in both solution temperature and pH. This behaviour is atypical compared to other RAFT aqueous dispersion polymerisation formulations based on HPMA, NIPAM or MEA,[4,16,20,25] where such water-miscible monomers normally produce rather weakly hydrophobic structure-directing blocks with significant degrees of plasticisation.[37] However, the $PDMAC_{40}$-$PDAAM_{99}$ worms did prove to be both weakly pH-responsive and thermosensitive: this is attributed to the extremely narrow phase space occupied by the worm phase, and perhaps also the relatively low mean DP for each block.

Concentrated aqueous dispersions of covalently-stabilised diblock copolymer nano-objects could be prepared at ambient temperature using ADH, which reacts selectively with the pendent ketone groups on the hydrophobic PDAAM chains to form hydrazone moieties. FT-IR studies provided direct spectroscopic evidence for this cross-linking chemistry, while DLS measurements performed in methanol (a good solvent for the PDMAC and PDAAM blocks) confirmed that covalent stabilisation could be achieved within 6 h at 25 °C using ADH/DAAM molar ratios as low as 0.075. Finally, rheological studies indicated a four-fold increase in worm gel strength when using a DAAM/ADH molar ratio of 0.10, presumably because cross-linking leads to an increase in the worm persistence length.

2.4. Experimental

2.4.1 Materials

DDMAT (98 %) and DMAC (≥ 98.5 %) were purchased from Sigma-Aldrich. AIBN (98 %) was purchased from Molekula. DAAM 99 %), ADH (≥ 98 %) and ACVA (98 %) were purchased from Alfa Aesar. All chemicals were used as received Deuterated methanol (99 %) was purchased from Cambridge Isotope Laboratories. Dioxane was purchased from Sigma-Aldrich UK and diethyl ether was purchased from Fisher Scientific. All solvents were HPLC-grade.

2.4.2 Synthesis of PDMAC Homopolymers *via* RAFT Solution Polymerisation

A typical protocol for the synthesis of a PDMAC$_{68}$ stabiliser block was conducted as follows. DDMAT (0.613 g, 1.68 mmol), AIBN (27.0 mg 0.17 mmol, CTA/AIBN molar ratio = 10.0) and DMAC (10.0 g, 0.101 mol) were weighed into a 100 mL round-bottomed flask. Dioxane (24.8 mL) was added to produce a 30 % w/w solution, which was purged with nitrogen for 30 min. The sealed flask was immersed into an oil bath set at 70 °C for 25 min (final DMAC conversion = 89 %, as judged by ^{1}H NMR spectroscopy) and the polymerisation was subsequently quenched by immersing the flask in ice, followed by exposure to air. Dioxane (50 mL) was added to the reaction solution, followed by precipitation from a ten-fold excess of diethyl ether (1 L). The precipitate was redissolved in dioxane and precipitated once more from excess diethyl ether. The crude stabiliser block was dissolved in deionized water, any residual diethyl ether/dioxane was removed under reduced pressure, and the resulting aqueous solution was freeze-dried for 48 h. The purified PDMAC homopolymer was obtained as a yellow solid. End-group analysis using UV spectroscopy indicated a mean degree of polymerisation of 68 and the M_n and M_w/M_n were 5700 g mol^{-1} and 1.12, respectively, as determined by DMF GPC. The same protocol was used to synthesise a PDMAC$_{40}$ stabiliser block, which had an M_n of

3200 g mol^{-1} and an M_w/M_n of 1.12, a PDMAC$_{46}$ stabiliser block with an M_n of 4600 g mol^{-1} and an M_w/M_n of 1.09, a PDMAC$_{58}$ stabiliser block with an M_n of 5100 g mol^{-1} and an M_w/M_n of 1.09 and a PDMAC$_{77}$ stabiliser block with an M_n of 7100 g mol^{-1} and M_w/M_n of 1.11.

2.4.3 Synthesis of PDMAC$_{58}$-PDAAM$_{230}$ Diblock Copolymer Vesicles by RAFT Aqueous Dispersion Polymerisation at pH 2.5

The typical protocol for the synthesis of PDMAC$_{58}$-PDAAM$_{230}$ vesicles at 20 % w/w solids was as follows. PDMAC$_{58}$ precursor (0.136 g, 0.022 mmol), ACVA (0.6 mg, 0.002 mmol, CTA/ACVA molar ratio = 10), and DAAM monomer (0.864 g, 5.1 mmol; target DP = 230) were weighed into a 14 mL vial. Deionized water adjusted to pH 2.5 with HCl (4.0 mL) was then added to give a 20 % w/w aqueous solution, which was degassed for 15 min at 4 °C prior to immersion in an oil bath set at 70 °C. This reaction solution was stirred for 4 h and then quenched by exposure to air. The DAAM monomer conversion was greater than 98 % as judged by ^{1}H NMR spectroscopy, while the M_n and M_w/M_n were 27100 g mol^{-1} and 1.54, respectively, as judged by DMF GPC. All other PISA syntheses were conducted at the same initial volume (5.0 mL) at 20 % w/w solids.

2.4.4 Post-polymerisation Cross-linking Using ADH

A typical protocol for cross-linking PDMAC$_{58}$-PDAAM$_{230}$ vesicles is as follows. A 20 % w/w dispersion of PDMAC$_{58}$-PDAAM$_{230}$ vesicles (2.5 g) prepared using the previously stated protocol and ADH (ADH; 0.045 g, 0.26 mmol, DAAM/ADH molar ratio = 10.0) were added to a 14 mL vial. The reaction solution was stirred at 25 °C for 6 h.

2.4.5 Polymer Characterisation

^{1}H NMR spectroscopy

^{1}H NMR spectra were recorded using a 400 MHz Bruker Avance III HD 400 spectrometer in deuterated methanol at 25 °C (64 scans were averaged to ensure high-quality spectra) and were analysed using MestraNova software.

UV-visible absorption spectroscopy

UV/visible absorption spectra were recorded between 200 and 800 nm using a PC-controlled UV-1800 spectrophotometer at 25 °C using a 1 cm path length quartz cell. A Beer-Lambert curve was constructed using a series of ten DDMAT solutions in methanol. The absorption maximum at 311 nm assigned to the trithiocarbonate group[38] was used for this calibration plot and DDMAT concentrations were selected such that the absorbance always remained below unity. The mean DP for each of the five PDMAC homopolymers was determined using the molar extinction coefficient of 16 300 ± 160 mol^{-1} dm^3 cm^{-1} determined for the DDMAT.

Gel permeation chromatography (GPC)

Copolymer MWDs determined using DMF GPC. The set-up comprising two Agilent PL gel 5 μm Mixed-C columns and a PL-gel guard column connected in series to a Agilent 1260 Infinity GPC system equipped with both refractive index and UV-visible detectors (only the refractive index detector was used) operating at 60 °C. The GPC eluent was HPLC-grade DMF containing 10 mM LiBr at a flow rate of 1.0 mL min^{-1}. DMSO was used as a flow-rate marker. Calibration was achieved using a series of ten near-monodisperse poly(methyl methacrylate) standards (ranging in M_p from 625 to 618 000 g mol^{-1}). Chromatograms were analysed using Agilent GPC/SEC software.

Dynamic Light Scattering (DLS)

The intensity-average sphere-equivalent diameters of the diblock copolymer nano-objects were determined at 25 °C by DLS using a Malvern Zetasizer NanoZS instrument *via* the Stokes-Einstein equation, which assumes perfectly monodisperse, non-interacting spheres. All measurements were made on 0.1 % w/w copolymer dispersions in either acidic aqueous solution (pH 2.5) or methanol using disposable plastic cuvettes. Data were averaged over three consecutive runs consisting of 10 sub-runs. For variable temperature DLS studies, 0.1 % w/w aqueous copolymer dispersions were heated from 5 °C to 50 °C, followed by cooling to 25 °C, at 5 °C intervals with 15 min thermal equilibriation at each temperature. In this case, copolymer dispersions were analysed using a glass cuvette, and data was averaged over three consecutive runs at each temperature.

Aqueous Electrophoresis

Zeta potential measurements were performed using a Malvern Zetasizer Nano ZS instrument on 0.1 % w/w aqueous copolymer dispersions at 25 °C in the presence of 1 mM KCl. The initial copolymer dispersion was acidic (pH 2.5) with the solution pH being adjusted by addition of dilute NaOH with 5 min equilibriation at each pH. Zeta potentials were calculated from the Henry equation using the Smoluchowski approximation. Hydrodynamic DLS diameters were also recorded during these pH experiments. All data were averaged over three consecutive runs.

Transmission Electron Microscopy (TEM)

Copper/palladium TEM grids (Agar Scientific, UK) were coated in-house with a thin film of amorphous carbon. The grids were then subjected to a glow discharge for 30 s. Individual 10.0 μL droplets of 0.1 % w/w aqueous copolymer dispersions were placed on freshly-treated grids for 1 min and then carefully blotted with filter paper to remove

excess solution. To ensure sufficient electron contrast, uranyl formate (9.0 μL of a 0.75%

w/w solution) was absorbed onto the sample-loaded grid for 20 s and then carefully

blotted to remove excess stain. Each grid was then dried using a vacuum hose. Imaging

was performed using a FEI Tecnai Spirit 2 microscope fitted with an Orius SC1000B

camera operating at 80 kV.

Rheology

An AR-G2 rheometer equipped with a variable temperature Peltier plate and a 40 ml 2°

aluminium cone was used for all experiments. Percentage strain sweeps were conducted

at 25 °C using a fixed angular frequency of 1.0 rad s^{-1}. Angular frequency sweeps were

conducted at 25 °C using a constant percentage strain of 1.0 %.

FT-IR spectroscopy

FT-IR spectra were recorded for solid samples using a Thermo Scientific Nicolet iS10

FT-IR spectrometer fitted with a Golden Gate Diamond ATR accessory. Each spectrum

was averaged over 500 scans at a resolution of 4 cm^{-1}.

Shear-Induced Polarised Light Imaging (SIPLI)

SIPLI experiments were conducted using a mechano-optical rheometer (Anton Paar

Physica MCR301 with SIPLI attachment). Measurements were performed using a

plate-plate geometry composed of a 25 mm polished steel plate and a fused quartz plate

connected to a variable temperature Peltier system. The gap between plates was set at

0.5 mm for all experiments. An additional Peltier hood was used to ensure good control

of the sample temperature. Sample illumination was achieved using an Edmund Optics

150 W MI-150 high-intensity fiber- optic white light source with a constant light intensity

maintained for all measurements. The polariser and analyser axes were crossed at 90° in

order to obtain polarised light images (PLIs), which were recorded using a colour CCD

camera (Lumenera Lu165c).

References

(1)   Lopez-Oliva, A. P.; Warren, N. J.; Rajkumar, A.; Mykhaylyk, O. O.; Derry, M. J.; Doncom, K. E. B.; Rymaruk, M. J.; Armes, S. P. Polydimethylsiloxane-Based Diblock Copolymer Nano-Objects Prepared in Nonpolar Media via RAFT-Mediated Polymerization-Induced Self-Assembly. *Macromolecules* **2015**, *48*, 3547–3555.

(2)   Blanazs, A.; Ryan, A. J.; Armes, S. P. Predictive Phase Diagrams for RAFT Aqueous Dispersion Polymerization: Effect of Block Copolymer Composition, Molecular Weight, and Copolymer Concentration. *Macromolecules* **2012**, *45*, 5099–5107.

(3)   Semsarilar, M.; Penfold, N. J. W.; Jones, E. R.; Armes, S. P. Semi-Crystalline Diblock Copolymer Nano-Objects Prepared via RAFT Alcoholic Dispersion Polymerization of Stearyl Methacrylate. *Polym. Chem.* **2015**, *6*, 1751–1757.

(4)   Blanazs, A.; Verber, R.; Mykhaylyk, O. O.; Ryan, A. J.; Heath, J. Z.; Douglas, C. W. I.; Armes, S. P. Sterilizable Gels from Thermoresponsive Block Copolymer Worms. *J. Am. Chem. Soc.* **2012**, *134*, 9741–9748.

(5)   Blanazs, A.; Madsen, J.; Battaglia, G.; Ryan, A. J.; Armes, S. P. Mechanistic Insights for Block Copolymer Morphologies: How Do Worms Form Vesicles? *J. Am. Chem. Soc.* **2011**, *133*, 16581–16587.

(6)   Sugihara, S.; Blanazs, A.; Armes, S. P.; Ryan, A. J.; Lewis, A. L. Aqueous Dispersion Polymerization: A New Paradigm for In Situ Block Copolymer Self-Assembly in Concentrated Solution. *J. Am. Chem. Soc.* **2011**, *133*, 15707–15713.

(7)   Derry, M. J.; Fielding, L. a.; Warren, N. J.; Mable, C. J.; Smith, A. J.; Mykhaylyk, O. O.; Armes, S. P. In Situ Small-Angle X-Ray Scattering Studies of Sterically-Stabilized Diblock Copolymer Nanoparticles Formed During Polymerization-Induced Self-Assembly in Non-Polar Media. *Chem. Sci.* **2016**, *7*, 5078–5090.

(8)   Figg, C. A.; Carmean, R. N.; Bentz, K. C.; Mukherjee, S.; Savin, D. A.; Sumerlin, B. S. Tuning Hydrophobicity To Program Block Copolymer Assemblies from the Inside Out. *Macromolecules* **2017**, *50*, 935–943.

(9)   Wang, X.; Figg, C. A.; Lv, X.; Yang, Y.; Sumerlin, B. S.; An, Z. Star Architecture Promoting Morphological Transitions during Polymerization-Induced Self-Assembly. *ACS Macro Lett.* **2017**, *6*, 337–342.

(10)   Biais, P.; Beaunier, P.; Stoffelbach, F.; Rieger, J. Loop-Stabilized BAB Triblock Copolymer Morphologies by PISA in Water. *Polym. Chem.* **2018**, *9*, 4483–4491.

(11)   Ma, Y.; Gao, P.; Ding, Y.; Huang, L.; Wang, L.; Lu, X.; Cai, Y. Visible Light Initiated Thermoresponsive Aqueous Dispersion Polymerization-Induced Self-Assembly. *Macromolecules* **2019**, *52*, 1033–1041.

(12)   Thompson, K. L.; Mable, C. J.; Cockram, A.; Warren, N. J.; Cunningham, V. J.; Jones, E. R.; Verber, R.; Armes, S. P. Are Block Copolymer Worms More Effective Pickering Emulsifiers than Block Copolymer Spheres? *Soft Matter* **2014**, *10*, 8615–8626.

(13)   Thompson, K. L.; Chambon, P.; Verber, R.; Armes, S. P. Can Polymersomes Form Colloidosomes? *J. Am. Chem. Soc.* **2012**, *134*, 12450–12453.

(14)   Chambon, P.; Blanazs, A.; Battaglia, G.; Armes, S. P. Facile Synthesis of Methacrylic ABC Triblock Copolymer Vesicles by RAFT Aqueous Dispersion Polymerization. *Macromolecules* **2012**, *45*, 5081–5090.

(15)   Sugihara, S.; Armes, S. P.; Blanazs, A.; Lewis, A. L. Non-Spherical Morphologies from Cross-Linked Biomimetic Diblock Copolymers Using RAFT Aqueous Dispersion Polymerization. *Soft Matter* **2011**, *7*, 10787–10793.

(16)   An, Z.; Shi, Q.; Tang, W.; Tsung, C. K.; Hawker, C. J.; Stucky, G. D. Facile RAFT Precipitation Polymerization for the Microwave-Assisted Synthesis of Well-Defined, Double Hydrophilic Block Copolymers and Nanostructured Hydrogels. *J. Am. Chem. Soc.* **2007**, *129*, 14493–14499.

(17)   Chiefari, J.; Chong, Y. K. B.; Ercole, F.; Krstina, J.; Jeffery, J.; Le, T. P. T.; Mayadunne, R. T. A.; Meijs, G. F.; Moad, C. L.; Moad, G.; et al. Living Free-Radical Polymerization by Reversible Addition-Fragmentation Chain Transfer: The RAFT Process. *Macromolecules* **1998**, *31*, 5559–5562.

(18)   Moad, G.; Rizzardo, E.; Thang, S. H. Living Radical Polymerization by the RAFT Process-A Second Update. *Aust. J. Chem.* **2009**, *62*, 1402–1472.

(19)   Moad, G.; Rizzardo, E.; Thang, S. H. Radical Addition-Fragmentation Chemistry in Polymer Synthesis. *Polymer* **2008**, *49*, 1079–1131.

(20)   Lovett, J. R.; Warren, N. J.; Armes, S. P.; Smallridge, M. J.; Cracknell, R. B. Order-Order Morphological Transitions for Dual Stimulus Responsive Diblock Copolymer Vesicles. *Macromolecules* **2016**, *49*, 1016–1025.

(21)   Lovett, J. R.; Warren, N. J.; Ratcliffe, L. P. D.; Kocik, M. K.; Armes, S. P. PH-Responsive Non-Ionic Diblock Copolymers : Ionization of Carboxylic Acid End-Groups Induces an Order-Order Morphological Transition. *Angew. Chem. Int. Ed.* **2015**, *54*, 1279–1283.

(22)   Warren, N. J.; Mykhaylyk, O. O.; Mahmood, D.; Ryan, A. J.; Armes, S. P. RAFT Aqueous Dispersion Polymerization Yields Poly(Ethylene Glycol)-Based Diblock Copolymer Nano-Objects with Predictable Single Phase Morphologies. *J. Am. Chem. Soc.* **2014**, *136*, 1023–1033.

(23)   Verber, R.; Blanazs, A.; Armes, S. P. Rheological Studies of Thermo-Responsive Diblock Copolymer Worm Gels. *Soft Matter* **2012**, *8*, 9915–9922.

(24)   Lovett, J. R.; Derry, M. J.; Yang, P.; Hatton, F. L.; Warren, N. J.; Fowler, P. W.; Armes, S. P. Can Percolation Theory Explain the Gelation Behavior of Diblock Copolymer Worms? *Chem. Sci.* **2018**, *9*, 7138–7144.

(25)   Liu, G.; Qiu, Q.; An, Z. Development of Thermosensitive Copolymers of Poly(2-Methoxyethyl Acrylate-Co-Poly(Ethylene Glycol) Methyl Ether Acrylate) and Their Nanogels Synthesized by RAFT Dispersion Polymerization in Water. *Polym. Chem.* **2012**, *3*, 504–513.

(26)   Vogt, A. P.; Sumerlin, B. S. Temperature and Redox Responsive Hydrogels from ABA Triblock Copolymers Prepared by RAFT Polymerization. *Soft Matter* **2009**,

5, 2347–2351.

(27)   Wang, X.; Zhou, J.; Lv, X.; Zhang, B.; An, Z. Temperature-Induced Morphological Transitions of Poly(Dimethylacrylamide)-Poly(Diacetone Acrylamide) Block Copolymer Lamellae Synthesized via Aqueous Polymerization-Induced Self-Assembly. *Macromolecules* **2017**, *50*, 7222–7232.

(28)   Kessel, N.; Illsley, D. R.; Keddie, J. L. The Diacetone Acrylamide Crosslinking Reaction and Its Influence on the Film Formation of an Acrylic Latex. *J. Coatings Technol. Res.* **2008**, *5*, 285–297.

(29)   Li, Y.; Armes, S. P. Synthesis of Model Primary Amine-Based Branched Copolymers by Pseudo-Living Radical Copolymerization and Post-Polymerization Coupling of Homopolymers. *Macromolecules* **2009**, *42*, 939–945.

(30)   Li, Y.; Ryan, A. J.; Armes, S. P. Synthesis of Well-Defined Branched Copolymers by Quaternization of Near-Monodisperse Homopolymers. *Macromolecules* **2008**, *41*, 5577–5581.

(31)   Rosselgong, J.; Armes, S. P. Quantification of Intramolecular Cyclization in Branched Copolymers by 1H NMR Spectroscopy. *Macromolecules* **2012**, *45*, 2731–2737.

(32)   Lovett, J. R.; Ratcliffe, L. P. D.; Warren, N. J.; Armes, S. P.; Smallridge, M. J.; Cracknell, R. B.; Saunders, B. R. A Robust Cross-Linking Strategy for Block Copolymer Worms Prepared via Polymerization-Induced Self-Assembly. *Macromolecules* **2016**, *49*, 2928–2941.

(33)   Won, Y.-Y.; Davis, H. T.; Bates, F. S. Giant Wormlike Rubber Micelles. *Science* **1999**, *283*, 960–963.

(34)   Mykhaylyk, O. O.; Warren, N. J.; Parnell, A. J.; Pfeifer, G.; Laeuger, J. Applications of Shear-Induced Polarized Light Imaging (SIPLI) Technique for Mechano-Optical Rheology of Polymers and Soft Matter Materials. *J. Polym. Sci. Part B Polym. Phys.* **2016**, *54*, 2151–2170.

(35)   Mykhaylyk, O. O. Time-Resolved Polarized Light Imaging of Sheared Materials: Application to Polymer Crystallization. *Soft Matter* **2010**, *6*, 4430–4440.

(36)   Zhou, W.; Qu, Q.; Xu, Y.; An, Z. Aqueous Polymerization-Induced Self-Assembly for the Synthesis of Ketone-Functionalized Nano-Objects with Low Polydispersity. *ACS Macro Lett.* **2015**, *4*, 495–499.

(37)   Warren, N. J.; Armes, S. P. Polymerization-Induced Self-Assembly of Block Copolymer Nano-Objects via RAFT Aqueous Dispersion Polymerization. *J. Am. Chem. Soc.* **2014**, *136*, 10174–10185.

(38)   Skrabania, K.; Miasnikova, A.; Bivigou-Koumba, A. M.; Zehm, D.; Laschewsky, A. Examining the UV-Vis Absorption of RAFT Chain Transfer Agents and Their Use for Polymer Analysis. *Polym. Chem.* **2011**, *2*, 2074–2083.

Chapter 3

Aqueous Self-assembly Behaviour of a Thermoresponsive Diblock Copolymer

3.1 Introduction

In recent years there has been a growing interest in stimulus-responsive polymers or 'smart polymers' i.e. those polymers which undergo a chemical or physical change due to an applied stimulus. For aqueous systems, temperature is one of the most extensively explored stimuli for various applications, for example, ultrafiltration,[1] cell storage mediums,[2] bioseparation and drug delivery mechanisms.[3]

One of the most widely studied monomers for the preparation of thermo-responsive polymers is NIPAM. PNIPAM exhibits LCST at 32°C.[4–6] At this temperature, phase separation occurs due to entropic effects which makes mixing unfavourable. This causes a transition from a coil structure to a globular structure. The LCST of PNIPAM is close to human physiological conditions and can be tuned by functionalisation or copolymerization with other monomers.[7–9] Other polymers that exhibit LCST behaviour include derivatives of poly(2-oxazoline),[10–14] natural polymers synthesised from cellulose derivatives,[15] PDEAAM,[16] poly(methyl vinyl ether),[17] poly(*N*-vinylcaprolactam),[18] PEG[19,20] and poly(*N*-ethylacrylamide).[21]

There are far fewer examples of homopolymers that exhibit sharp UCSTs in aqueous media i.e at low temperatures the polymers are phase-separated and once a critical temperature is reached the polymer dissolves.[22] One UCST polymer is poly(*N*-acryloylglycinamide) (PNAGA). Glatzel *et al.* synthesised a series of PNAGA homopolymers with protein-like gelation behaviour. The homopolymers were prepared by RAFT polymerisation with target DPs from 100 to 500. They found that the longest homopolymer had a gel-sol transition at 27 °C however, no precise UCST temperature was reported.[23] Seuring *et al.* conducted a more in-depth study into PNAGA.[24] They synthesised a PNAGA homopolymer by FRP. The phase transition temperature of a

1 % w/w PNAGA solution in pure water was determined to be 22°C - 23°C on heating. However, significant hysteresis was seen on cooling. Moreover, rigorous purification of the monomer and judicious choice of the reaction conditions was required to limit ionic groups which prevent globule formation.

The incorporation of polymers that exhibit LCST or UCST behaviour into PISA formulations is not trivial. A careful choice of the reaction temperature is required to ensure particle formation during the reaction and an efficient particle stabilised technique, such as covalent cross-linking, must be used in order for the nanoparticles to be stable below the LCST or above the UCST.

In order to avoid this drawback, recent research has been focused on hydrophobic thermoresponsive polymers which possess LCST-like or UCST-like behaviour. Rather than precipitating at a critical temperature, subtle changes in the polymer hydration occur on heating or cooling. These changes in hydration are significant enough to cause nanoparticle morphological transitions. The Armes group first reported this phenomenon when they prepared a thermoresponsive $PGMA_{54}$-$PHPMA_{140}$ diblock copolymer worm-gel which, on cooling to 5°C, formed spheres with concomitant degelation.[1] The change in morphology was rationalised in terms of surface plasticisation of the PHPMA core by water on cooling.[25–27] Such behaviour could be described as 'LCST-like' since the PHPMA core becomes more soluble on cooling.

In recent work, the Cai group reported the thermoresponsive behaviour of PHPMAC-PDAAM diblock copolymer nanoparticles prepared *via* photo-PISA at 70 °C in water.[28] They reported vesicle to worm and vesicle to lamellae transitions on cooling $PHPMAC_{38}$−$PDAAM_{100}$ and $PHPMAC_{38}$−$PDAAM_{90}$ diblock copolymer nanoparticles

from 70 °C to 25 °C respectively. They found that the morphological transitions were reversible in concentrated dispersions but the transitions were slow (2 days).

The Armes group have also prepared dual stimuli-responsive diblock copolymer nano-objects. Lovett *et al.* prepared PGMA$_{43}$-PHPMA$_{175}$ diblock copolymer vesicles by RAFT aqueous dispersion polymerisation using a carboxylic acid terminated CTA.[29] They demonstrated that upon cooling the turbid, free-flowing vesicle dispersion from 25 °C to 5 °C a free-standing worm gel was formed. A vesicle to sphere transition could also be induced by switching the dispersion pH from pH 3 to pH 6.[29] This morphology transition was attributed to the ionisation of the single, terminal carboxylic acid group on the PGMA stabiliser block. This ionisation increases the hydrophilic character of the PGMA block which lowers the packing parameter for the copolymer chains.

Kim *et al*. also demonstrated a dual response diblock copolymer namely, monomethoxy-poly(ethylene glycol)-*b*-poly(trimethylene carbonate).[30] This diblock copolymer can undergo either a sphere to worm transition on heating in water or a vesicle to sphere transition on increasing the copolymer concentration. However, this diblock copolymer was prepared *via* ring-opening polymerisation in toluene rather than PISA.

There is only one report of a diblock copolymer that can cross two major phase boundaries simply by varying the temperature.[31] The Lodge group prepared a poly(styrene-*b*-dimethylsiloxane) diblock copolymer by anionic polymerisation.[30] They observed a vesicle to worm to sphere transition on heating the dilute dispersion in diethyl phthalate from ambient temperature to 180 °C.

So far there have been no reports of a *single* (i.e. fixed composition) diblock copolymer in any solvent that is capable of crossing three phase boundaries to form either spheres, worms, vesicles or lamellae by simply varying the dispersion temperature. Moreover,

there are no reports of a thermoresponsive diblock copolymer that can undergo morphological transitions reversibly at low copolymer concentrations ($\leq$ 0.1 % w/w solids).

In this chapter, 4-hydroxybutyl acrylate (HBA) has been investigated as a thermo-responsive core-forming block. Given that HBA is isomeric with HPMA it was expected to have interesting thermoresponsive properties. A series of new PDMAC-PHBA and PDMAC-P(HBA-*stat*-DAAM) amphiphilic diblock copolymers were prepared by a one-pot PISA protocol in aqueous solution at pH 3 using a carboxylic acid terminated CTA. The unprecedented thermo-responsive nature of these diblock copolymers has been examined. Moreover, the pH-responsive nature of these copolymers is demonstrated. Finally, a thermoresponsive PDMAC-P(HBA-*stat*-DAAM) diblock copolymer has been prepared using a neutral CTA at pH 7.

3.2 Results and Discussion

3.2.1 PDMAC-PHBA Synthesis

All of the diblock copolymers used in this study were prepared *via* PISA using a highly convenient one-pot RAFT aqueous dispersion polymerisation formulations. Initially, three PDMAC-PHBA diblock copolymers were synthesised at pH 3, the reaction scheme is given in Figure 3.1. First, DMAC was polymerised in an 80 % w/w aqueous solution at 30 °C using a trithiocarbonate-based CTA combined with a low-temperature redox initiator. The initial highly concentrated aqueous solution was required to ensure the solubility of the DDMAT CTA. After 30 min, the reaction mixture was diluted to 20 % w/w to lower the solution viscosity. After 4 h, a small aliquot of the resulting water-soluble PDMAC precursor was removed for analysis. This one-pot synthesis was conducted three times to produce three PDMAC precursors. ^{1}H NMR spectroscopy studies confirmed that more than 99 % DMAC conversion had been achieved for each PDMAC synthesis by comparison of the integrals of the residual DMAC vinyl signals in the 5.0 – 7.0 ppm region to the polymer signal at 3.0 ppm, see Figure 3.2. DMF GPC analysis demonstrated the reproducibility of the precursor synthesis, Figure 3.3a. For each of the three PDMAC precursors, the DP was determined to be 54 by end-group analysis using UV spectroscopy, Figure 3.3b.
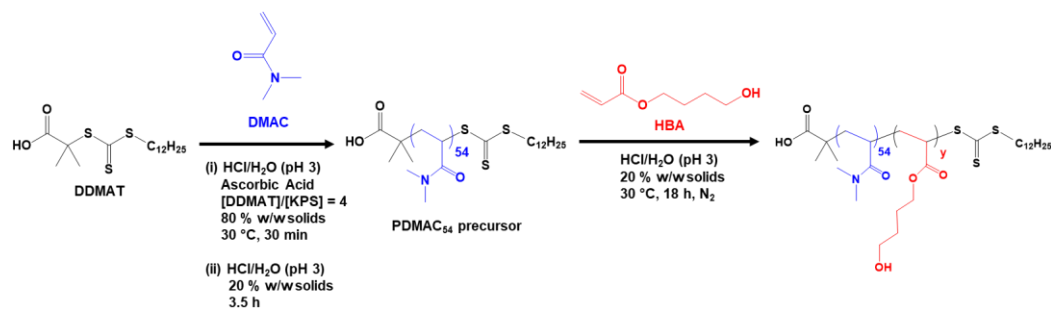
Fig. 3.1. Reaction scheme for the synthesis of the PDMAC$_{54}$ precursors *via* RAFT solution polymerisation of DMAC at 30°C using a DDMAT CTA and a redox initiator, KPS plus AscAc. Subsequent PDMAC$_{54}$ chain extension with HBA via RAFT aqueous dispersion polymerisation at pH 3 produced PDMAC$_{54}$−PHBA$_y$ diblock copolymers.
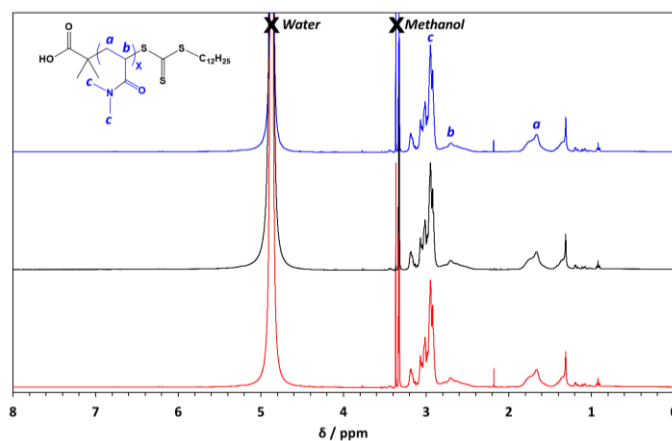

Fig. 3.2. ^{1}H NMR spectra recorded in CD$_3$OD for the three PDMAC$_{54}$ precursors prepared using the synthesis method outlined in Figure 3.1.
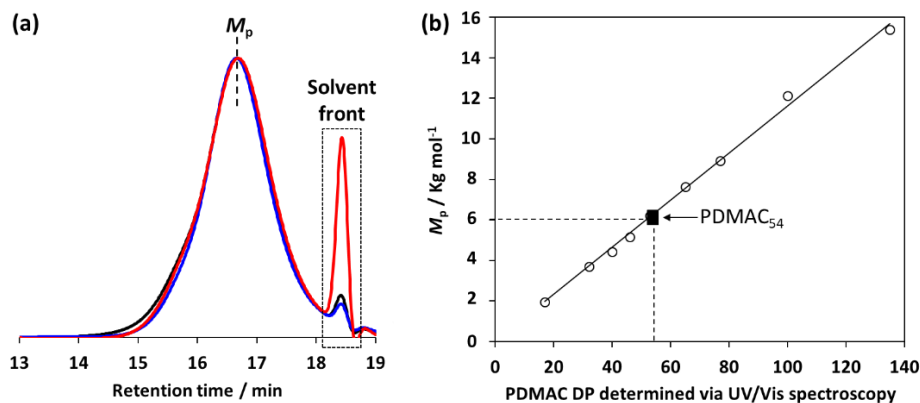
Fig. 3.3. (a) DMF GPC chromatograms recorded for the PDMAC$_{54}$ precursors prepared using the one-pot protocol outlined in Figure 3.1. (b) Calibration plot for determining the mean DP of the PDMAC precursors. M_p (determined by DMF GPC analysis using a refractive index detector) vs. PDMAC DP (determined by UV/visible spectroscopy using the Beer-Lambert calibration plot constructed for DDMAT in Chapter 2) for a series of PDMAC homopolymers synthesised by RAFT solution polymerisation of DMAC in dioxane using DDMAT and purified by precipitation (open black circles). Black squares: M_p for the PDMAC$_{54}$ precursors synthesised by RAFT solution polymerisation of DMAC in pH 3 water using DDMAT at 30°C *via* the one-pot protocol given in Figure 3.1.

These three PDMAC$_{54}$ precursors were then chain-extended with HBA at 20 % w/w solids to produce PDMAC$_{54}$-PHBA$_y$ diblock copolymers, where the subscript y refers to the mean DP of the PHBA block. ^{1}H NMR spectroscopy studies confirmed essentially full conversion for the HBA monomer by comparison of the HBA vinyl signals in the 5.0 - 7.0 ppm region to the polymer signal at 2.3 ppm, Figure 3.4. The final PHBA DPs (y) were determined by ^{1}H NMR spectroscopy to be 218, 244 and 269. DMF GPC analysis indicated high blocking efficiencies and a relatively narrow MWDs ($M_w/M_n \leq 1.29$) for the final diblock copolymers (see Figure 3.5).
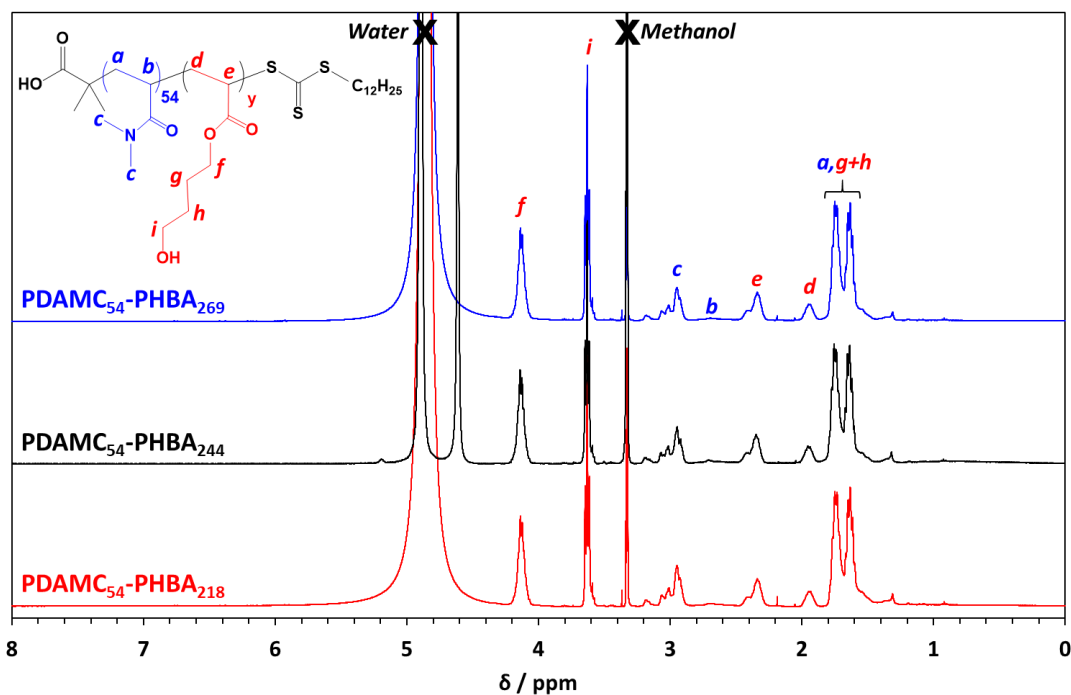
Fig. 3.4. Assigned ^{1}H NMR spectra recorded in CD$_3$OD for the PDMAC$_{54}$-PHBA$_{218}$ diblock copolymer (red data), the PDMAC$_{54}$-PHBA$_{244}$ diblock copolymer (black data) and the PDMAC$_{54}$-PHBA$_{269}$ diblock copolymer (blue data) prepared using the one-pot protocol shown in Figure 3.1.

Fig. 3.5. DMF GPC chromatograms recorded for the PDMAC$_{54}$-PHBA$_{218}$ diblock copolymer (red data), the PDMAC$_{54}$-PHBA$_{244}$ diblock copolymer (black data) and the PDMAC$_{54}$-PHBA$_{269}$ diblock copolymer (blue data) prepared by the one-pot protocol shown in Figure 3.1.

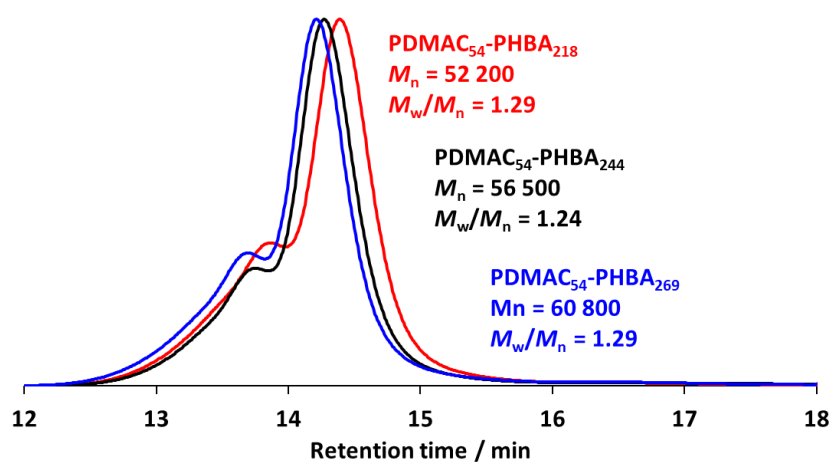## 3.2.2 PDMAC-PHBA Nanoparticle Characterisation

Rheology studies were conducted on the 20 % w/w aqueous dispersions of PDMAC$_{54}$-PHBA$_y$ nano-objects as a function of temperature (Figure 3.6 and Figure 3.7). For each dispersion, low-viscosity fluids were formed at 1 °C. Warming to ambient temperature caused an increase in dispersion viscosity with the maximum viscosity obtained at 25 °C, 21 °C and 17 °C for y = 218, 244 and 269, respectively. Further heating led to firstly, a significant reduction in dispersion viscosity followed by a second increase in viscosity at 48 °C, 46 °C and 42 °C for y = 218, 244 and 269 respectively.

Fig. 3.6. Temperature-dependent rheological studies for 20 % w/w aqueous dispersions of PDMAC$_{54}$-PHBA$_y$ nano-objects at an applied strain of 1.0 % and an angular frequency of 1.0 rad s^{-1}. The dispersions were equilibrated at 1 °C for 15 minutes prior to a thermal cycle from 1 °C to 50 °C to 1 °C at 1 °C min^{-1}. Complex viscosity ($|\eta^*|$) vs. temperature data for (a) the PDMAC$_{54}$-PHBA$_{218}$ dispersion (b) the PDMAC$_{54}$-PHBA$_{244}$ dispersion and (c) the PDMAC$_{54}$-PHBA$_{269}$ dispersion.
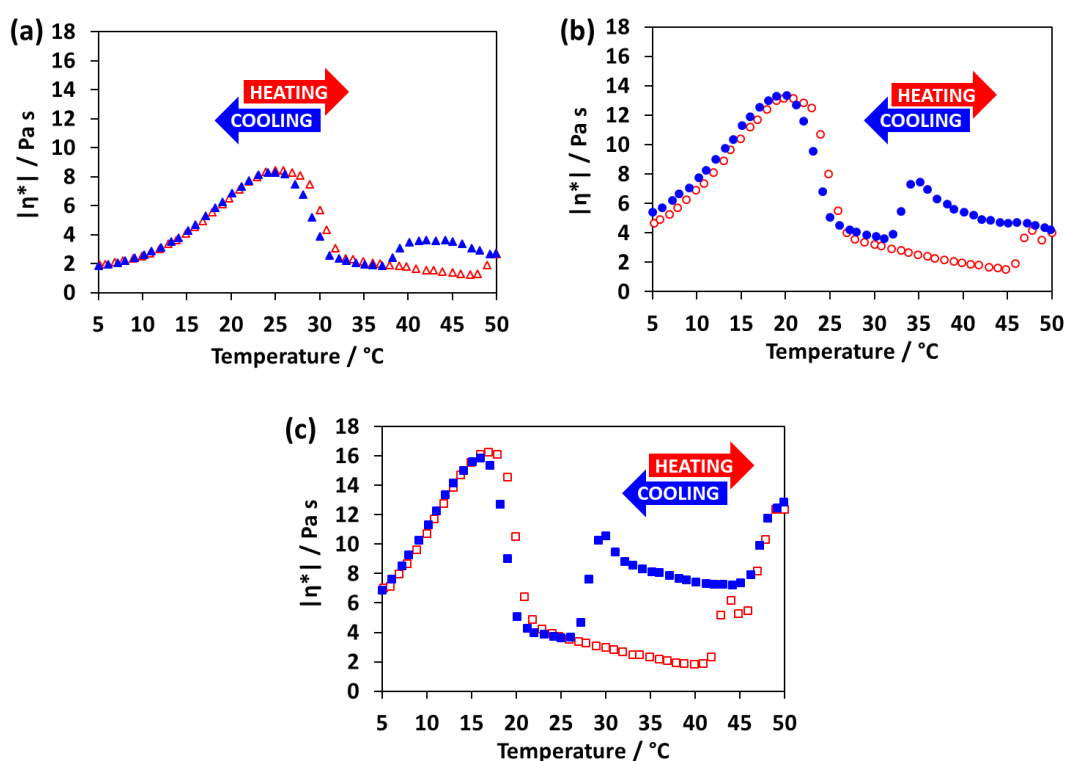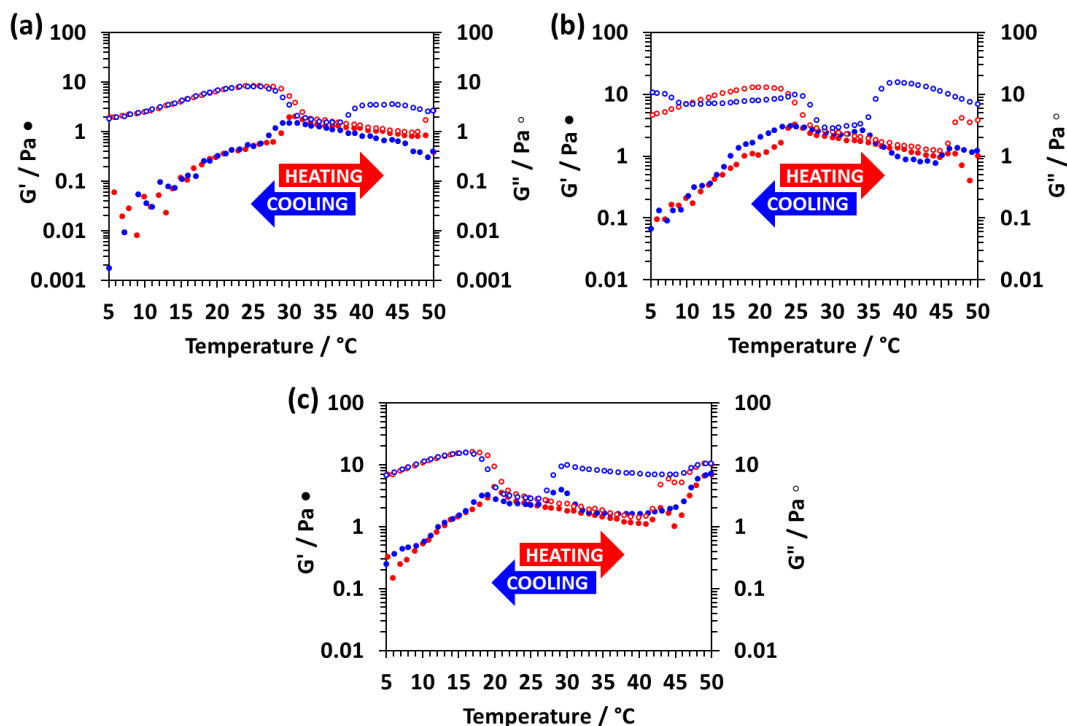
Fig. 3.7. Temperature-dependent rheological studies for 20 % w/w aqueous dispersions of $PDMAC_{54}$-$PHBA_y$ nano-objects at an applied strain of 1.0 % and an angular frequency of 1.0 rad s^{-1}. The dispersions were equilibrated at 1 °C for 15 min prior to a thermal cycle from 1 °C to 50 °C to 1 °C at 1 °C min^{-1}. G' and G" vs. temperature for (a) the $PDMAC_{54}$-$PHBA_{218}$ dispersion (b) the $PDMAC_{54}$-$PHBA_{244}$ dispersion and (c) the $PDMAC_{54}$-$PHBA_{269}$ dispersion.

The transitions seen during heating proved to be remarkably reversible on cooling, with relatively little hysteresis being observed at heating/cooling rates of 1 °C min^{-1}. Moreover, the temperature at which the transitions occur is dependent on the PHBA DP.

Unfortunately, the nature of these transitions could not be investigated using conventional TEM imaging due to the relatively low glass transition temperature of the PHBA block. Cryo-TEM was attempted on these dispersions but proved inconclusive. In order to overcome this drawback a third, crosslinkable monomer, namely DAAM, was copolymerised with HBA within the nano-object core.

3.2.3 Synthesis of PDMAC-P(HBA-*stat*-DAAM) diblock copolymers at pH 3

A PDMAC-P(HBA-*stat*-DAAM) diblock copolymer was prepared by the one-pot RAFT aqueous dispersion polymerisation protocol shown in Figure 3.8. As before, DMAC was polymerised in an 80 % w/w aqueous solution at 30 °C using DDMAT with a KPS/AscAc redox initiator. After 30 min, the reaction mixture was diluted to 20 % w/w to lower the solution viscosity. After 4 h, a small aliquot of the resulting water-soluble PDMAC precursor was removed for analysis. ^{1}H NMR spectroscopy studies confirmed that more than 99 % DMAC conversion had been achieved (Figure 3.9). DMF GPC analysis indicated a relatively narrow MWD (M_w/M_n = 1.23, see Figure 3.10a). The PDMAC precursor DP was determined to be 56 by end-group analysis using UV spectroscopy (see Figure 3.10b).

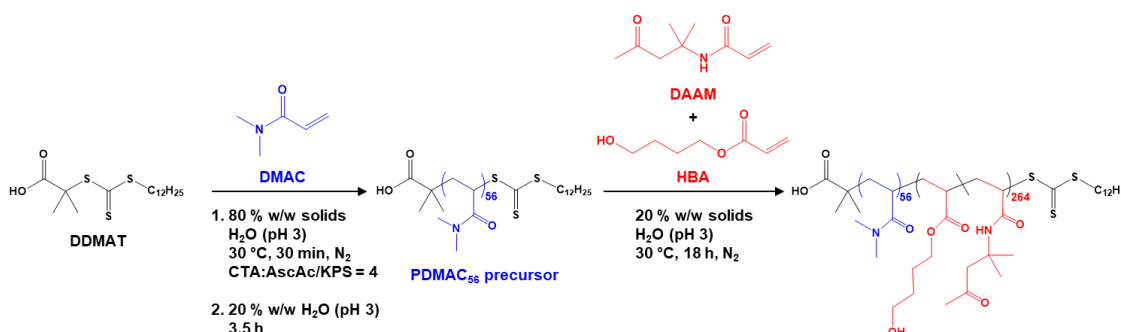Fig. 3.8. Reaction scheme for the synthesis of a PDMAC$_{56}$ precursor *via* RAFT solution polymerisation of DMAC at 30°C using a DDMAT CTA and a redox initiator, KPS/AscAc. Subsequent PDMAC$_{56}$ chain extension with a binary mixture of HBA (80 mol%) and DAAM (20 mol%) *via* RAFT aqueous dispersion copolymerisation at pH 3 produced a PDMAC$_{56}$−P(HBA-*stat*-DAAM)$_{264}$ diblock copolymer.

This PDMAC$_{56}$ precursor was then chain-extended by statistical copolymerisation of a mixture of HBA (80 mol%) and DAAM (20 mol%) at 20 % w/w solids to produce a PDMAC$_{56}$-P(HBA-*stat*-DAAM)$_{264}$ diblock copolymer. ^{1}H NMR spectroscopy studies confirmed essentially full conversion for the HBA and DAAM comonomers (> 99%; see Figure 3.9) and the expected core-forming block composition (78 ± 2 mol % HBA) was obtained within experimental error. DMF GPC analysis indicated a high blocking efficiency and a relatively narrow MWD ($M_w/M_n < 1.20$) for the final diblock copolymer (see Figure 3.10).
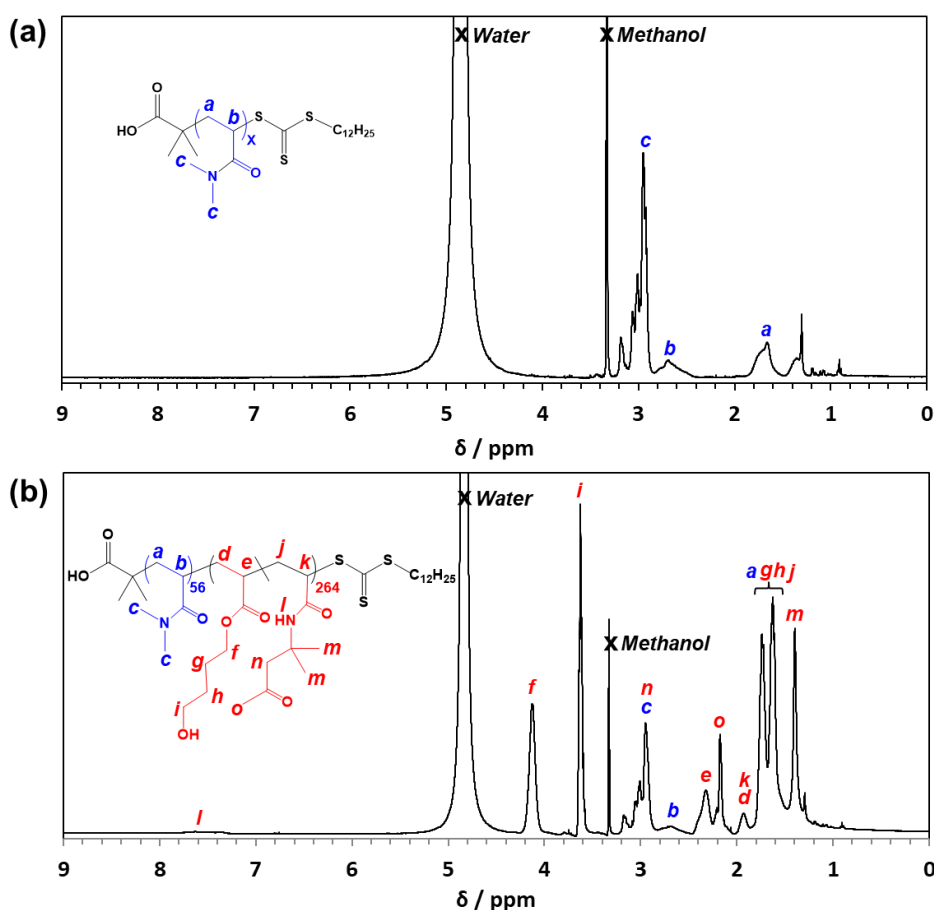

Fig. 3.9. Assigned ^{1}H NMR spectra recorded in CD$_3$OD for (a) the PDMAC$_{56}$ precursor and (b) the PDMAC$_{56}$−P(HBA-*stat*-DAAM)$_{264}$ diblock copolymer prepared in the one-pot protocol outlined in Figure 3.8.
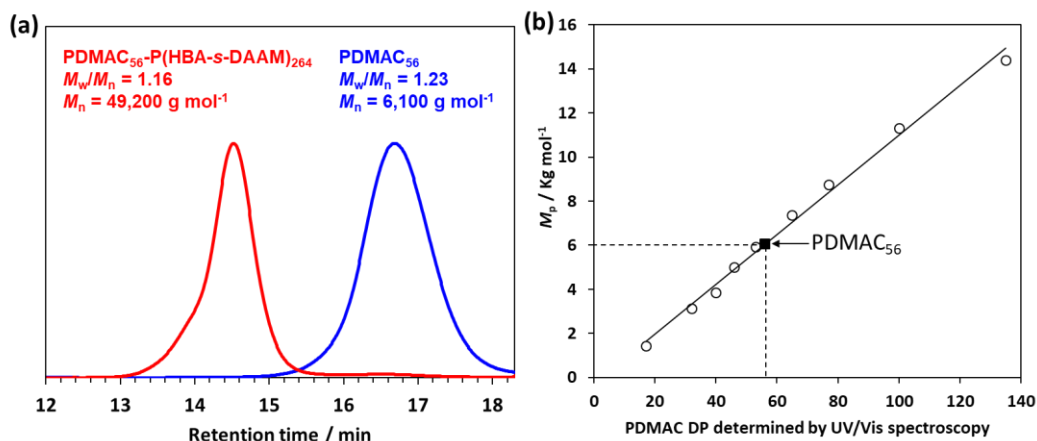
Fig. 3.10. (a) DMF GPC chromatograms recorded for the PDMAC$_{56}$ precursor (blue trace) and the final PDMAC$_{56}$-P(HBA-*stat*-DAAM)$_{264}$ diblock copolymer (red trace) prepared in the protocol outlined in Figure 3.8. (b) Calibration plot for determining the mean DP of the PDMAC precursor prepared during the one-pot protocol given in Figure 3.8. M_p vs. PDMAC DP (determined by UV/visible spectroscopy using a previously published Beer-Lambert calibration plot constructed for DDMAT in Chapter 2) for a series of PDMAC homopolymers synthesised by RAFT solution polymerisation of DMAC in dioxane using DDMAT and purified by precipitation (open black circles). Black square: M_p for the PDMAC$_{56}$ precursor prepared *via* the one-pot protocol given in Figure 3.8.

3.2.4 Characterisation of PDMAC-P(HBA-*stat*-DAAM) Nanoparticles Prepared at pH 3

The 20 % w/w dispersion of PDMAC$_{56}$-P(HBA-*stat*-DAAM)$_{264}$ diblock copolymer nano-objects prepared using this aqueous PISA formulation formed a free-standing gel at 25 °C (Figure 3.11). On cooling to 1 °C, immediate degelation occurred to produce a transparent free-flowing dispersion. On heating to 50 °C, a turbid, free-flowing dispersion was formed, while a turbid paste was formed at 70 °C. To examine the copolymer morphologies associated with these thermal transitions, TEM studies were performed on the PDMAC$_{56}$-P(HBA-*stat*-DAAM)$_{264}$ diblock copolymer nano-objects. Cross-linking of the P(HBA-*stat*-DAAM)$_{264}$ block was conducted at the desired temperature using ADH

at pH 3, as previously reported in Chapter 2 and reference 32. Cross-linking eliminated the thermoresponsive behaviour of this diblock copolymer, hence preserving the copolymer morphology at any desired temperature. Thus this cross-linking protocol enabled visualisation of pure spheres, worms, vesicles or lamellae after covalent stabilisation at 1 °C, 25 °C, 50 °C or 70 °C, respectively (Figure 3.11f-i).
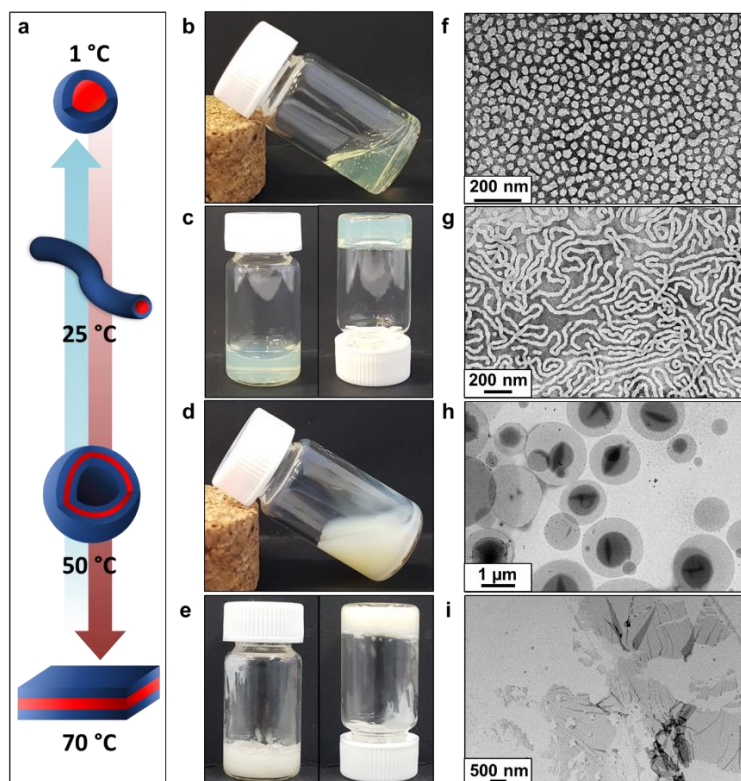
Fig. 3.11. (a) Schematic representation of the reversible morphological transitions that occur for a 20 % w/w aqueous dispersion of $PDMAC_{56}$-$P(HBA\text{-}stat\text{-}DAAM)_{264}$ diblock copolymer nano-objects on varying the temperature from 1 °C to 70 °C. Digital images show the physical appearance of this aqueous dispersion: (b) on cooling to 1 °C for 30 minutes, (c) at ambient temperature (25 °C), (d) on heating to 50 °C for 30 minutes and (e) on heating to 70 °C for 30 minutes. TEM images recorded for 0.1 % w/w aqueous dispersions of $PDMAC_{56}-P(HBA\text{-}stat\text{-}DAAM)_{264}$ after covalent stabilisation at the desired temperature using ADH at a DAAM/ADH molar ratio of 1.0: (f) spheres (crosslinked at 1 °C), (g) worms (crosslinked at 25 °C), (h) vesicles (crosslinked at 50 °C) and (i) lamellae (crosslinked at 70 °C).

Rheology studies were conducted on a 20 % w/w aqueous dispersion of PDMAC$_{56}$-P(HBA-*stat*-DAAM)$_{264}$ nano-objects as a function of temperature (Figure 3.12). As expected, a low-viscosity fluid was formed at 1 °C owing to the presence of free-flowing spherical nano-objects (see Figure 3.12a). Warming to ambient temperature-induced a sol-gel transition, producing a soft, transparent free-standing gel (Figure 3.12b). This indicates the formation of highly anisotropic worms, with multiple inter-particle contacts producing a 3D network.[33] The storage modulus (G′) exceeds the loss modulus (G″) at 17 °C, which corresponds to the critical gelation temperature (CGT). A maximum gel viscosity was observed at 25 °C (Figure 3.12a). Further heating led to a significant reduction in viscosity (and a concomitant increase in turbidity) owing to the formation of vesicles. These sphere-to-worm and worm-to-vesicle transitions proved to be remarkably reversible, with relatively little hysteresis being observed at heating/cooling rates of 1 °C min^{-1}.

Heating the turbid, free-flowing vesicular dispersion above 50 °C initially caused a further reduction in the complex viscosity (see Figure 3.12c). However, the dispersion became a turbid paste between 63 °C and 70 °C and the complex viscosity increased by approximately two orders of magnitude, which corresponds to the formation of lamellae. Significant hysteresis was observed for the lamellae-to-vesicle transition on cooling but fairly good reversibility was observed below approximately 22 °C.
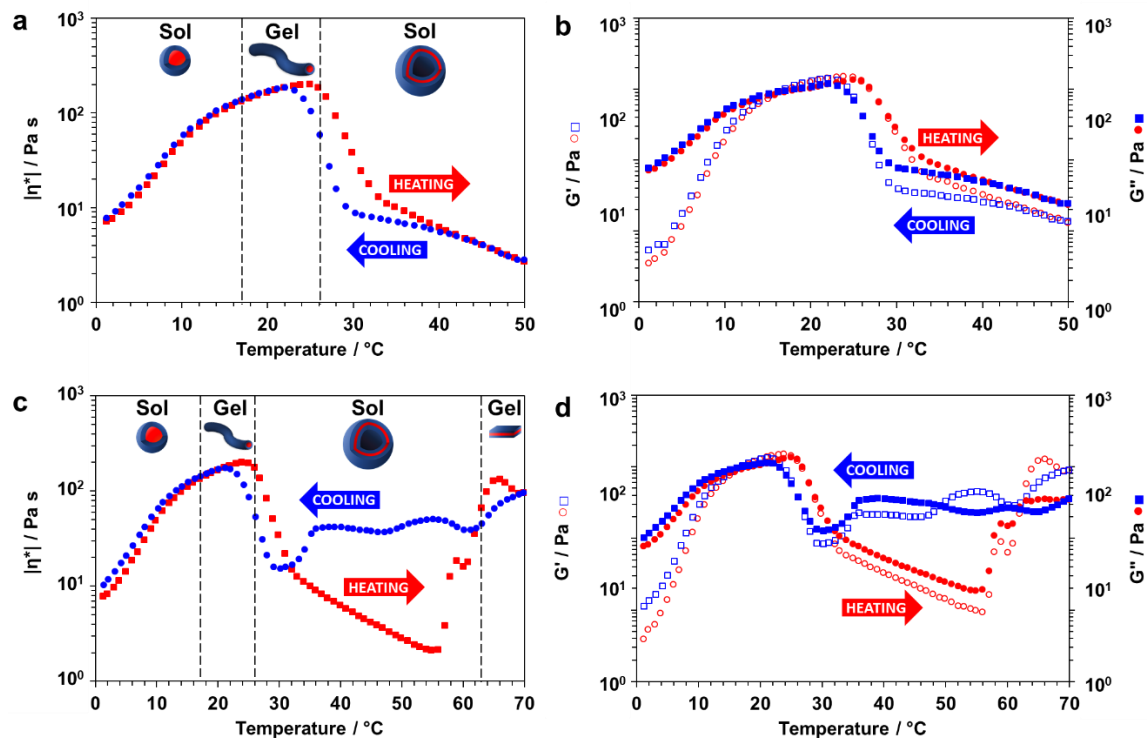
Fig. 3.12. Temperature-dependent rheological studies for a 20% w/w aqueous dispersion of PDMAC$_{56}$-P(HBA-*stat*-DAAM)$_{264}$ nano-objects at an applied strain of 1.0 % and an angular frequency of 1.0 rad s^{-1}. The dispersion was equilibrated at 1°C for 15 min prior to a thermal cycle at 1 °C min^{-1}. (a + c) Complex viscosity ($|\eta*|$) vs. temperature data for a thermal cycle from either 1 °C to 50 °C to 1 °C or 1°C to 70 °C to 1 °C. (b + d) G′ and G″ as a function of temperature for a thermal cycle from either 1 °C to 50 °C to 1 °C or 1 °C to 70 °C to 1 °C. The black dashed lines indicate the sol-gel transitions observed on heating as determined from the G′ and G″ values.

Small-angle X-ray scattering (SAXS) studies were conducted on a 1.0 % w/w aqueous dispersion of PDMAC$_{56}$-P(HBA-*stat*-DAAM)$_{264}$ nano-objects as a function of temperature at pH 3 (Figure 3.13). The gradient in the low *q* region of an *I(q)* vs. *q* plot (where *I*(q) is the scattering intensity and *q* is the scattering vector) is characteristic of the predominant copolymer morphology.[34] This gradient is close to zero at 1 °C, which suggests the presence of spheres. At 25 °C, the gradient shifts towards -1, indicating the formation of highly anisotropic worms.[1,35] On raising the temperature to 50 °C, the low *q*

gradient increases to -2, which is characteristic of bilayer (or vesicle) formation. At 70 °C, the structure factor observed at $q = 0.019$ A^{-1} indicates stacked lamellae sheets. These SAXS observations are fully consistent with the nano-object morphologies observed by TEM.
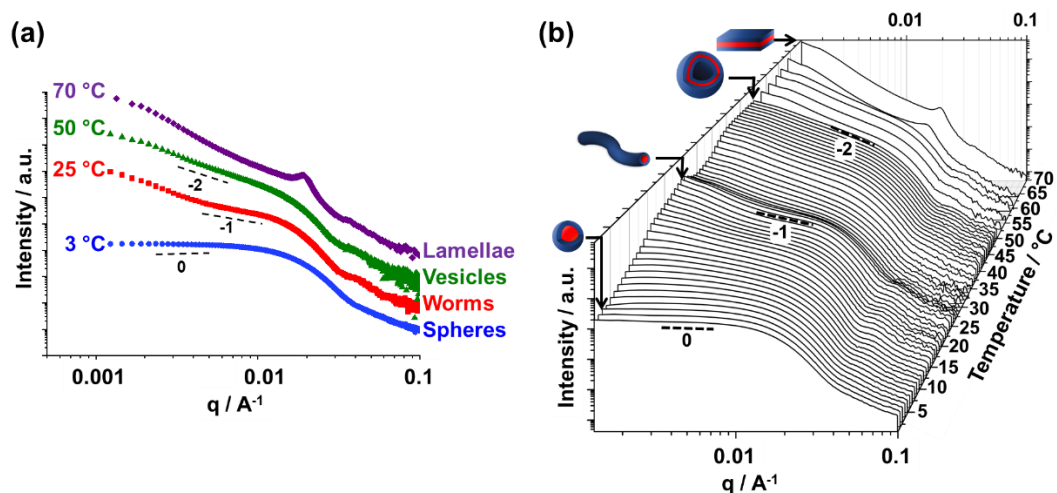
Fig. 3.13. (a) Representative double-logarithmic plot of SAXS patterns recorded for a 1.0 % w/w aqueous dispersion of thermoresponsive PDMAC$_{56}$−P(HBA-*stat*-DAAM)$_{264}$ nano-objects at 3 °C (blue data), 25 °C (red data), 50 °C (green data) and 70 °C (purple data). For guidance, black dashed lines indicate zero, -1 and -2 gradients, while the blue, green and purple data are offset by arbitrary factors to aid clarity. (b) SAXS patterns recorded for the same 1.0 % w/w aqueous dispersion of thermoresponsive PDMAC$_{56}$−P(HBA-*stat*-DAAM)$_{264}$ nano-objects between 1 °C and 70 °C using a heating rate of 1 °C min^{-1}. For guidance, black dashed lines indicate zero, -1 and -2 gradients.

Figure 3.13b shows a series of SAXS patterns recorded for a 1.0 % w/w aqueous dispersion of PDMAC$_{56}$−P(HBA-*stat*-DAAM)$_{264}$ nano-objects on heating from 1 °C to 70 °C at a heating rate of 1 °C min^{-1}. Clearly, there is a gradual increase in the low q gradient as the initial spheres are converted into first worms and then vesicles. A structure factor indicating stacked lamellae is observed at 64 °C and 70 °C. This data set confirms

that the interconversion between these four copolymer morphologies occurs rapidly on relatively short time scales even at low copolymer concentration.

DLS was used to determine the sphere-equivalent diameter for a 0.10 % w/w PDMAC$_{56}$−P(HBA-*stat*-DAAM)$_{264}$ aqueous dispersion during a thermal cycle from 2 °C to 50 °C to 2 °C (Figure 3.14). These DLS data suggest that both the sphere-to-worm and worm-to-vesicle thermal transitions occur rapidly and reversibly, with minimal hysteresis being observed even at copolymer concentrations as low as 0.10 % w/w. The excellent reversibility observed under these conditions is attributed to the relatively high mobility of the acrylic-rich core-forming block, which has a relatively low glass transition temperature.

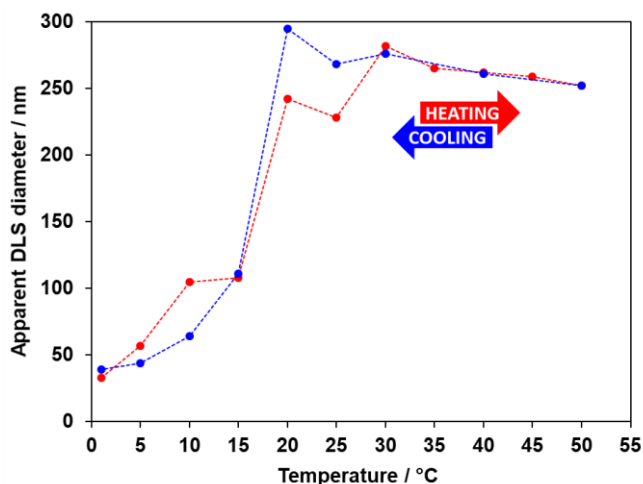Fig. 3.14. Apparent intensity-average diameter as a function of temperature as determined by DLS studies of a 0.1% w/w aqueous dispersion of PDMAC$_{56}$-P(HBA-*stat*-DAAM)$_{264}$ at pH 3. This dispersion was heated from 1 °C to 50 °C (red data) followed by cooling from 50 °C to 1 °C (blue data). The dispersion was equilibrated at each temperature for 10 min prior to DLS measurements to ensure thermal equilibration.

Variable temperature ^{1}H NMR spectroscopy studies were conducted to examine the mechanism for the unique thermoresponsive behaviour observed for this PDMAC$_{56}$-P(HBA-*stat*-DAAM)$_{264}$ diblock copolymer. Accordingly, a 20 % w/w aqueous copolymer dispersion was heated from 5 °C to 70 °C with spectra being recorded at 5 °C intervals and normalised relative to an external standard (pyridine). Partial ^{1}H NMR spectra are shown in Figure 3.15 (see Figure 3.16 for the full spectra).

^{1}H NMR signals assigned to the core-forming P(HBA-*stat*-DAAM) chains become more prominent at higher temperature, indicating progressively greater hydration for this weakly hydrophobic structure-directing block. Such spectral changes can be quantified by normalising the integrated intensity of the two C$\underline{H}_2$-OH protons assigned to the HBA repeat units relative to that of the external standard. This approach enables the *apparent* degree of hydration of the HBA repeat units within the P(HBA-*stat*-DAAM)$_{264}$ core-forming block to be calculated at any given temperature. This parameter is expressed as a percentage of the maximum value determined by ^{1}H NMR spectroscopy using CD$_3$OD (the PDMAC$_{56}$-P(HBA-*stat*-DAAM)$_{264}$ chains are molecularly dissolved in this solvent); it increases from 62 % to 83 % on heating a 20 % w/w aqueous copolymer dispersion from 5 °C to 70 °C (Figure 3.15b).
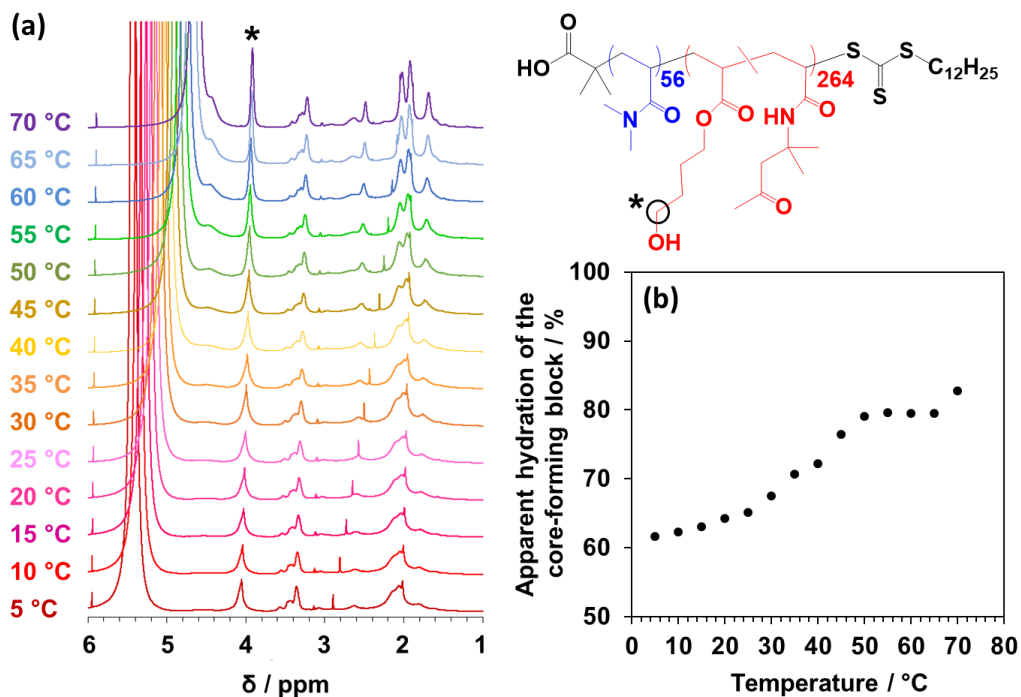
Fig. 3.15. (a) Normalised ^{1}H NMR spectra recorded for a 20% w/w aqueous dispersion of PDMAC$_{56}$−P(HBA-*stat*-DAAM)$_{264}$ nano-objects on heating from 5 °C to 70 °C. For clarity, only partial spectra in the 1–6 ppm range are shown (see Figure 3.16 for the full spectra). The signal marked with an asterisk is assigned to the two C$\underline{H}_2$-OH protons on the HBA residues. (b) Apparent degree of hydration of the hydrophobic P(HBA-*stat*-DAAM)$_{264}$ block as a function of temperature (with 100% hydration corresponding to the true diblock composition calculated by ^{1}H NMR spectroscopy for the molecularly-dissolved copolymer chains in CD$_3$OD).
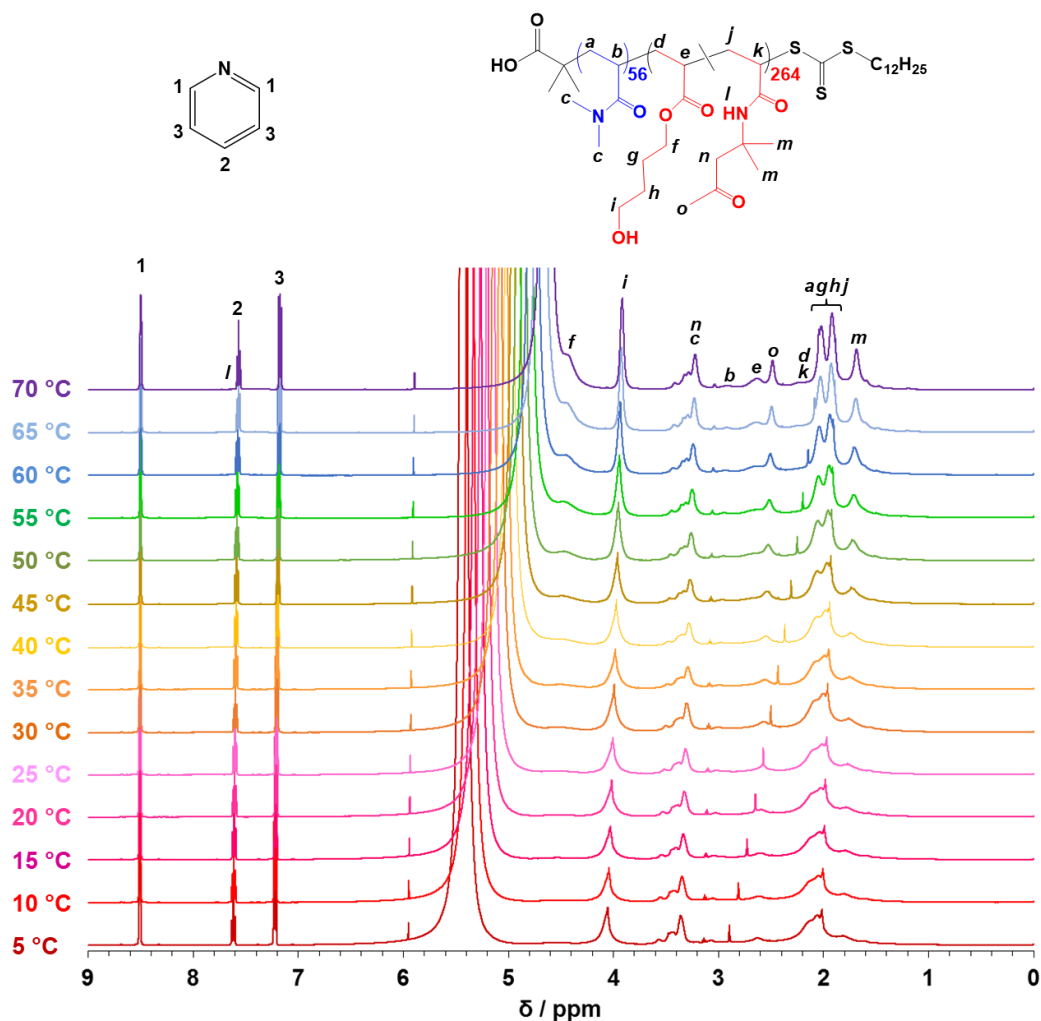
Fig. 3.16. Assigned 500 MHz ¹H NMR spectra recorded from 5 °C to 70 °C for a 20 % w/w aqueous dispersion of PDMAC₅₆−P(HBA-*stat*-DAAM)₂₆₄ nano-objects. This dispersion was equilibrated at each temperature for 10 min to ensure thermal equilibrium. All spectra were normalised relative to proton signal *1* assigned to the external standard (pyridine).

Clearly, the P(HBA-*stat*-DAAM)₂₆₄ block is partially hydrated at all temperatures and its degree of hydration increases at higher temperatures. As the hydrophobic P(HBA-*stat*-DAAM) block becomes progressively more hydrated, its volume fraction increases relative to that of the hydrophilic PDMAC stabiliser block, which leads to a subtle increase in the fractional packing parameter, *P*, for the copolymer chains, see Figure 3.17 for a schematic representation.[25,26] This accounts for the observed evolution

in morphology from spheres to worms to vesicles to lamellae that occurs on heating. Interestingly, such thermoresponsive behaviour has been recently predicted recently for a single diblock copolymer composition by Rumyantsev et al..[36] Such behaviour can be characterized as 'UCST-like', as opposed to the 'LCST-like' behaviour previously reported for an analogous amphiphilic thermoresponsive diblock copolymer, PGMA-PHPMA, that exhibited a worm-to-sphere transition on cooling from 20 °C to 5 °C.[1] This behaviour is even more unusual given that HPMA and HBA are isomeric.
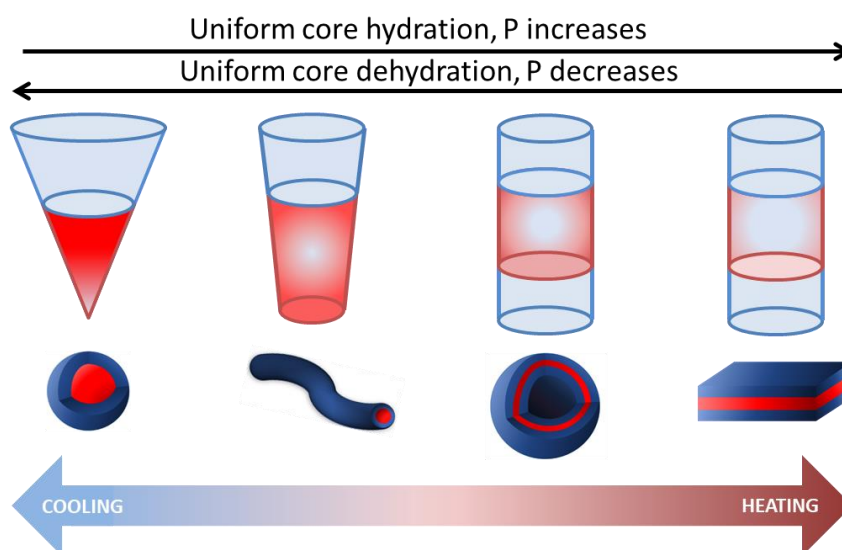
Fig. 3.17. A schematic representation of the change in the hydration of the core, and hence the packing parameter (P), on changing the dispersion temperature.

Lovett *et al.* demonstrated that deprotonation of a single carboxylic acid group located on the end of the PGMA block in a PGMA-PHPMA diblock copolymer was sufficient to allow a change in nanoparticle morphology.[29,37] Similarly, raising the solution pH of a 1 % w/w solids dispersion of the PDMAC$_{56}$−P(HBA-*stat*-DAAM)$_{264}$ nano-objects at 20 °C from pH 3 to pH 7 caused a reversible reduction in sphere-equivalent particle diameter from 333 nm (worms) to 38 nm (spheres) as judged by DLS (see Figure 3.18). This transition is attributed to deprotonation of the single carboxylic acid group located at the

end of each PDMAC steric stabiliser chain. Thus, this thermoresponsive diblock copolymer also exhibits reversible pH-responsive behaviour.
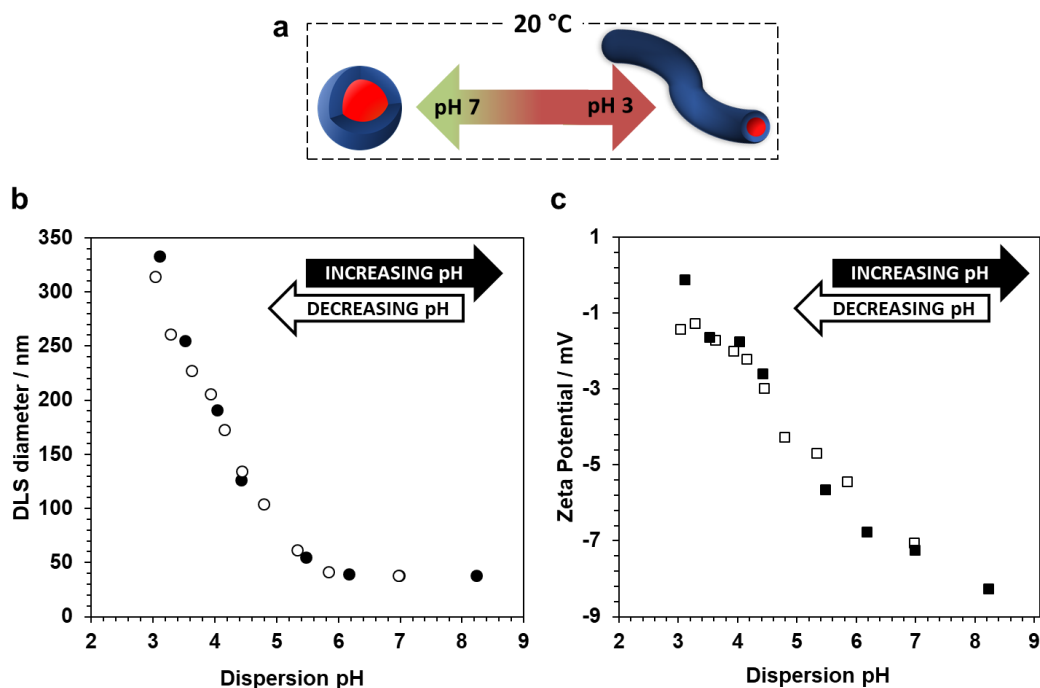
Fig. 3.18. (a) Schematic representation of the worm to sphere transition that occurs on increasing the dispersion pH from 3 to 7 at 20 °C. (b) DLS diameter recorded for a 0.10 % w/w aqueous dispersion of PDMAC$_{56}$-P(HBA-*stat*-DAAM)$_{264}$ nano-objects on increasing the PDMAC$_{56}$-P(HBA-*stat*-DAAM)$_{264}$ dispersion pH from pH 3 to pH 7 (filled circles) followed by returning the dispersion pH to pH 3 (empty circles) at 25 °C. The dispersion was equilibrated at each pH for 10 min. (c) Zeta potentials recorded for a 0.10 % w/w aqueous dispersion of PDMAC$_{56}$-P(HBA-*stat*-DAAM)$_{264}$ nano-objects on increasing the PDMAC$_{56}$-P(HBA-*stat*-DAAM)$_{264}$ dispersion pH from pH 3 to pH 7 (filled squares) followed by returning the dispersion pH to pH 3 (empty squares). The dispersion was equilibrated at each pH for 10 min.

Preliminary studies suggest that hydroxyl-functional silica nanoparticles can be readily encapsulated within such vesicles at elevated temperature (see Figure 3.19). In principle,

such payloads can be readily released on cooling to around ambient temperature because this induces a vesicle-to-worm (or vesicle to-sphere) transition.
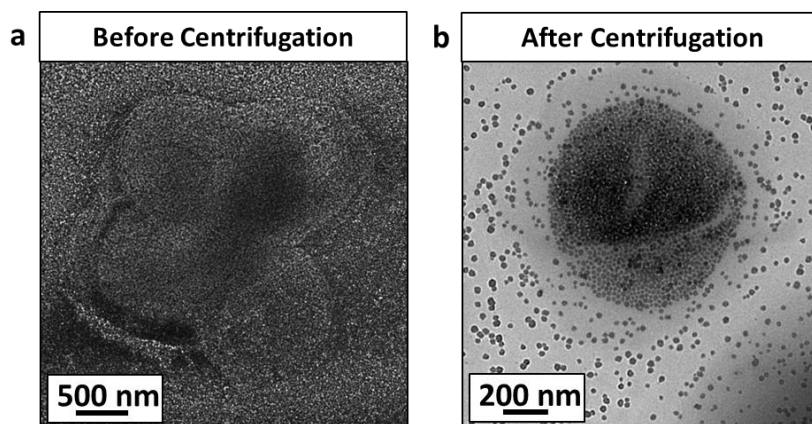
Fig. 3.19. TEM images obtained for 12 nm silica nanoparticles encapsulated within PDMAC$_{56}$-P(HBA-*stat*-DAAM)$_{264}$ vesicles at pH 3 (a) before centrifugation and (b) after six centrifuge cycles to remove most of the excess silica nanoparticles.

3.2.5 Synthesis of PDMAC-P(HBA-*stat*-DAAM) diblock copolymers at pH 7

In order for the PDMAC-P(HBA-*stat*-DAAM) thermoresponsive nano-objects to be suitable for biological-based applications, the synthesis method was modified to allow the nano-objects to be synthesised at pH 7. As previously stated, ionisation of the single carboxylic acid group located at the end of each PDMAC steric stabiliser chain caused a worm to sphere transition on increasing the solution pH from 3 to 7. Hence, esterification of the DDMAT carboxylic acid groups was necessary to directly produce higher-order morphologies, such as worms and vesicles, during the diblock copolymer synthesis at pH 7.

The esterification of DDMAT to produce Me-DDMAT was conducted in DCM using methanol as the methylating agent, see Figure 3.20.
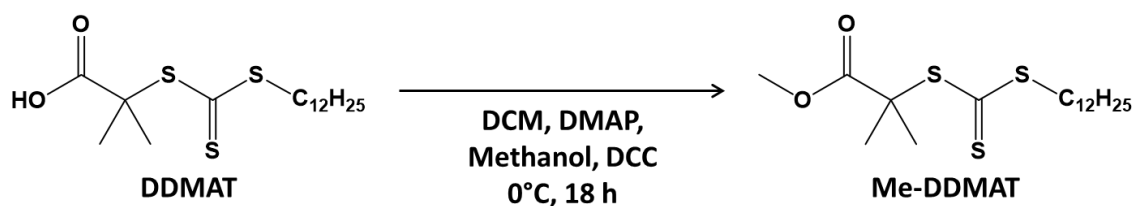
Fig. 3.20. Esterification of DDMAT using methanol as the methylating agent to produce Me-DDMAT.

The crude product was purified by column chromatography. The degree of DDMAT functionalisation was determined to be 98 % by comparison of the integrals for the dodecyl chain methyl proton signal to the methyl ester proton signal (protons *a* and *b* respectively, Figure 3.21).
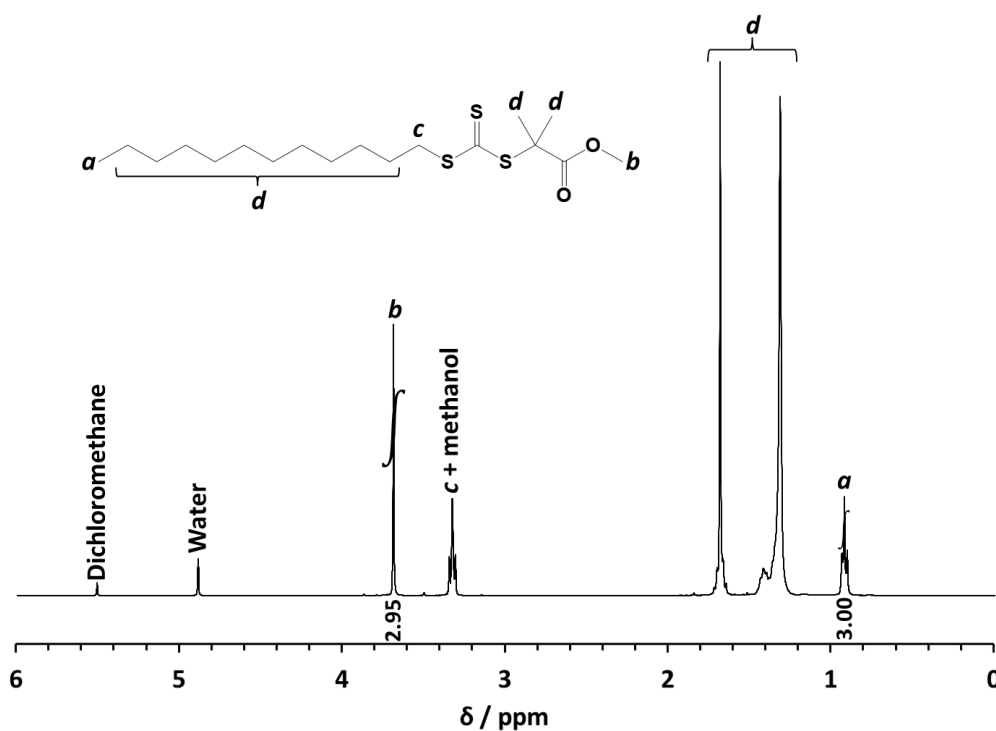
Fig. 3.21. ^{1}H NMR spectrum recorded in deuterated methanol for Me-DDMAT after purification by column chromatography. The signals labelled *a* and *b* were used to determine the degree of esterification.

The synthesis scheme for the preparation of the PDMAC-P(HBA-*stat*-DAAM) diblock copolymer at pH 7 using Me-DDMAT as the CTA is outlined in Figure 3.22. First, DMAC was polymerised in bulk (i.e. no solvent) because Me-DDMAT is insoluble even in highly concentrated aqueous solution. Due to the absence of water, ACVA was used as the initiator rather than the KPS/AscAc redox couple. The synthesis temperature was increased to 70 °C to achieve efficient decomposition of ACVA.
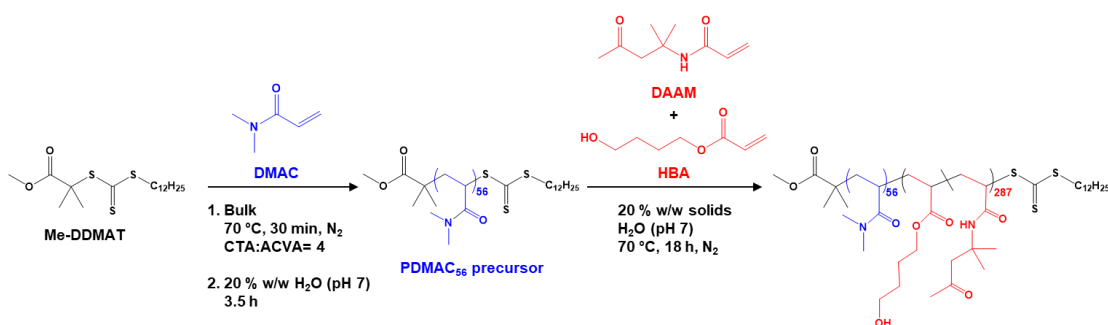
Fig. 3.22. Reaction scheme for the synthesis of the PDMAC$_{56}$ precursor *via* RAFT solution polymerisation of DMAC at 70 °C using a Me-DDMAT CTA and ACVA as the initiator. Subsequent PDMAC$_{56}$ chain extension with a binary mixture of HBA (80 mol%) and DAAM (20 mol%) *via* RAFT aqueous dispersion copolymerisation at pH 7 produced a PDMAC$_{56}$−P(HBA-*stat*-DAAM)$_{287}$ diblock copolymer.

After 30 min, the reaction mixture was diluted to 20 % w/w with pH 7 water to lower the solution viscosity. After 4 h, a small aliquot of the resulting water-soluble PDMAC precursor was removed for analysis. ^{1}H NMR spectroscopy studies confirmed that more than 99 % DMAC conversion had been achieved, see Figure 3.23. GPC analysis indicated a relatively narrow MWD ($M_w/M_n = 1.16$, see Figure 3.24). The PDMAC precursor DP was determined to be 56 by end-group analysis using UV spectroscopy using the calibration plot given in Figure 3.10.
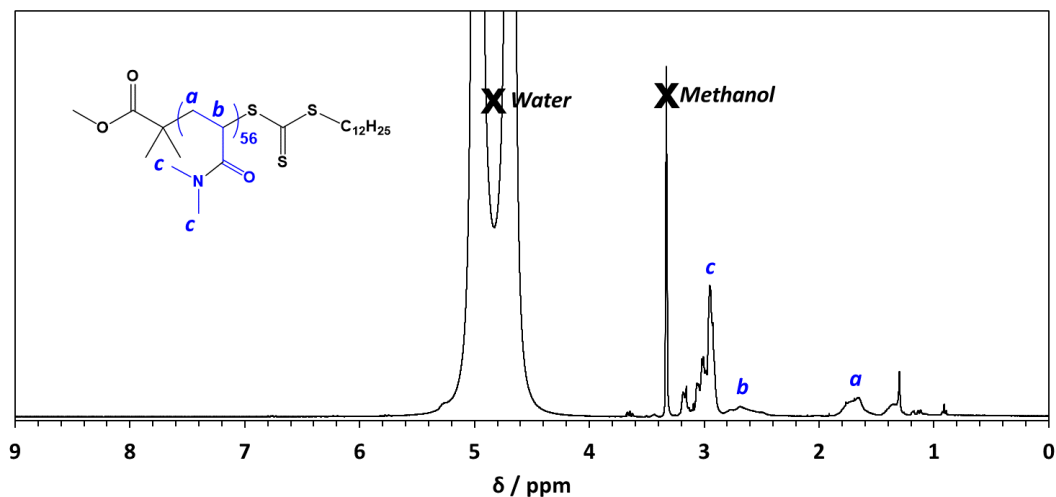
Fig. 3.23. Partially assigned ^{1}H NMR spectra recorded in CD$_3$OD for the PDMAC$_{56}$ precursor prepared at pH 7.

The 20 % w/w solution of the PDMAC$_{56}$ precursor was chain extended with HBA (80 mol%) and DAAM (20 mol%) at 20 % w/w solids to produce a PDMAC-P(HBA-*stat*-DAAM) diblock copolymer with total core target DP of 250. High HBA and DAAM conversions were achieved and the final diblock composition was determined by ^{1}H NMR spectroscopy to be PDMAC$_{56}$-P(HBA-*stat*-DAAM)$_{287}$, Figure 3.25. DMF GPC analysis showed good blocking efficiency of the PDMAC$_{56}$ precursor and a narrow MWD (M_w/M_n = 1.24) for the final diblock copolymer (see Figure 3.24).
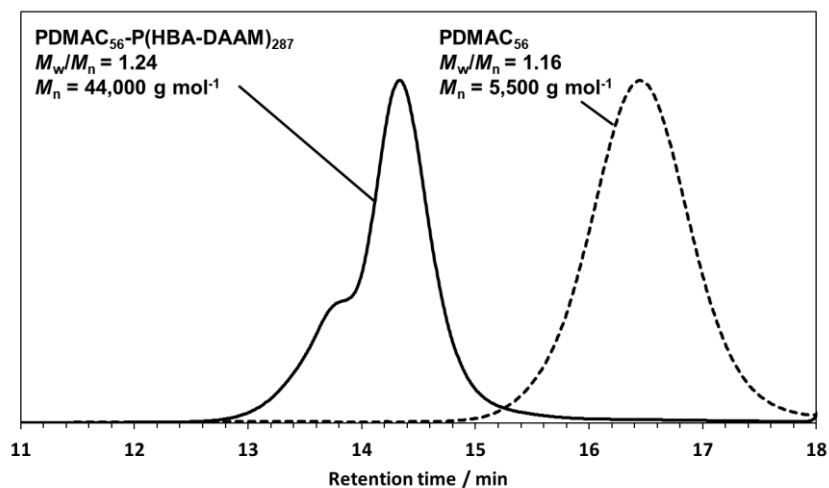
Fig. 3.24. DMF GPC chromatograms recorded for the PDMAC$_{56}$ precursor (black dashed trace) and the PDMAC$_{56}$-P(HBA-*stat*-DAAM)$_{287}$ diblock copolymer (black trace) prepared at pH 7.
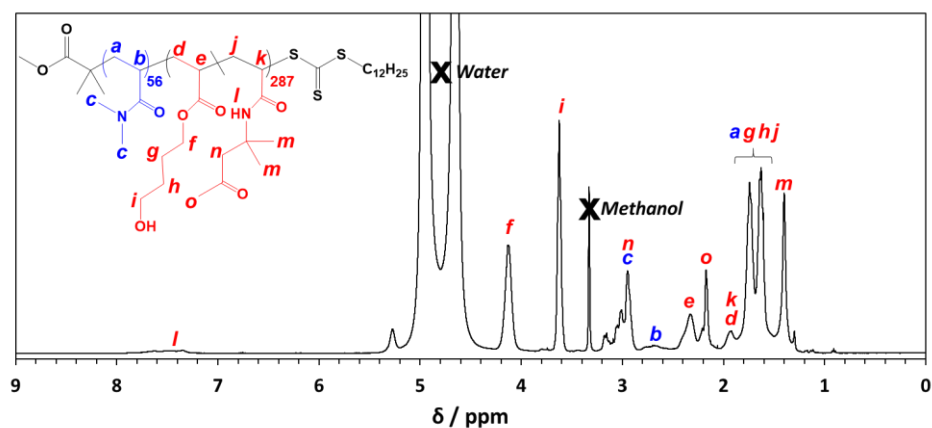
Fig. 3.25. Assigned ^{1}H NMR spectra recorded in CD$_3$OD for the PDMAC$_{56}$–P(HBA-*stat*-DAAM)$_{287}$ diblock copolymer prepared in the one-pot protocol outlined in Figure 3.22.

3.2.6 Characterisation of PDMAC-P(HBA-*stat*-DAAM) Nanoparticles Prepared at pH 7

Images of the as-prepared 20 % w/w PDMAC$_{56}$-P(HBA-*stat*-DAAM)$_{287}$ diblock copolymer dispersion at 25 °C and on heating and cooling are provided in Figure 3.26. At 25 °C the dispersion formed a transparent, free-standing gel. On cooling to 1 °C, a transparent, free-flowing dispersion was formed. On heating to 50 ° C a free-flowing turbid dispersion was formed.
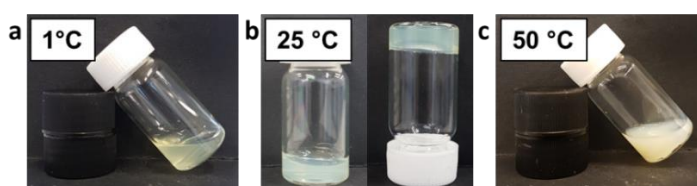
Fig. 3.26. Digital images showing the physical appearance of the PDMAC$_{56}$-P(HBA-*stat*-DAAM)$_{287}$ aqueous dispersion at 1 °C, 25 °C and 50 °C after 30 minutes equilibrium at each temperature.

Rheology studies were conducted on the 20 % w/w aqueous dispersion of PDMAC$_{56}$-P(HBA-*stat*-DAAM)$_{287}$ nano-objects as a function of temperature (see Figure 3.27). A low-viscosity fluid was formed at 1 °C suggesting the presence of spheres. Warming the dispersion induced a sol-gel transition at 24 °C owing to the formation of worms. Further heating to 29 °C led to degelation and a significant reduction in viscosity due to a worm to vesicle transition.
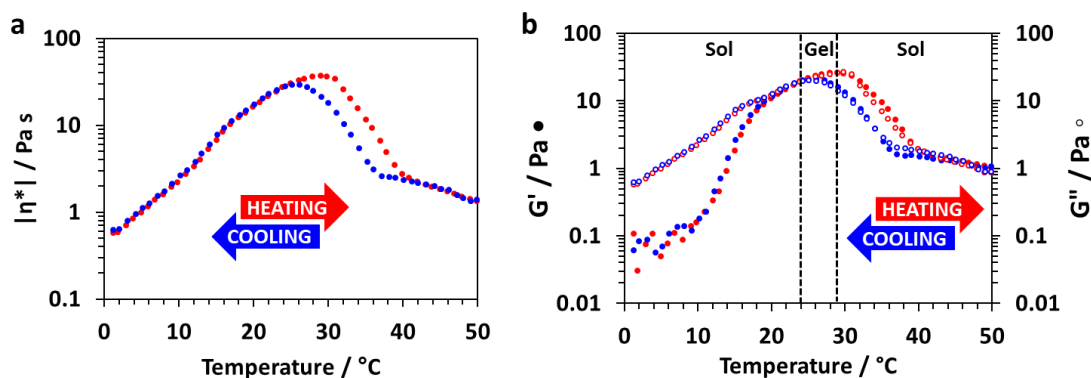
Fig. 3.27. Temperature-dependent rheological studies for 20 % w/w aqueous dispersion of PDMAC$_{56}$-P(HBA-*stat*-DAAM)$_{287}$ nano-objects at an applied strain of 1.0 % and an angular frequency of 1.0 rad s^{-1}. The dispersions were equilibrated at 1 °C for 15 min prior to a thermal cycle from 1 °C to 50 °C to 1 °C at 1 °C min^{-1}. (a) Complex viscosity ($|\eta^*|$) vs. temperature (b) G′ and G″ vs. temperature. The black dashed lines indicate the sol-gel and gel-sol transitions.

For biologically relevant applications it is important to consider the properties of the diblock copolymer nano-objects when dispersed in a biological culture medium such as NutriStem. The PDMAC$_{56}$-P(HBA-*stat*-DAAM)$_{287}$ 20 % w/w solids aqueous dispersion was freeze-dried and then redispersed at 20 % w/w solids in NutriStem by gently stirring overnight at 3 °C. This temperature was chosen to aid re-dispersion as demonstrated by Canton *et al.*.[2]

After re-dispersion in NutriStem and heating to room temperature, a free-standing gel was formed, see Figure 3.28a. Rheological studies were conducted on this NutriStem dispersion, see Figure 3.28. The rheology results for PDMAC$_{56}$-P(HBA-stat-DAAM)$_{287}$ dispersed in NutriStem are summarised in Table 3.1 along with the rheology results for the aqueous PDMAC$_{56}$-P(HBA-*stat*-DAAM)$_{287}$ dispersion for comparison.
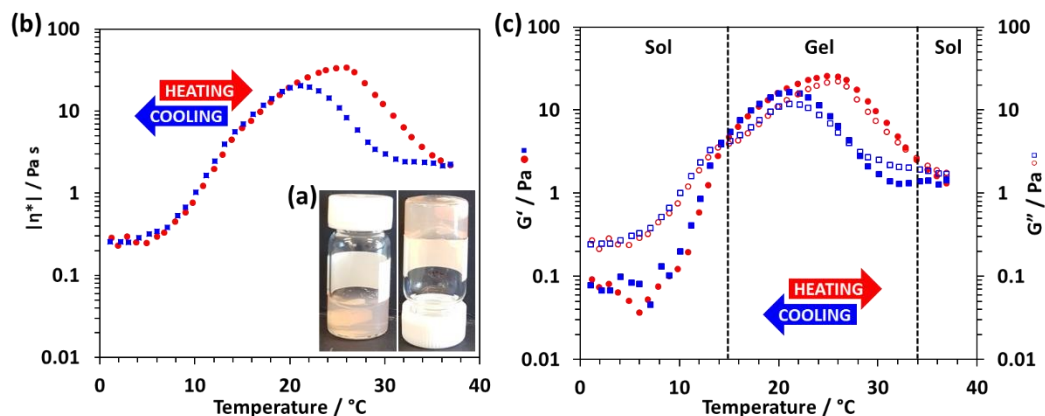
Fig. 3.28. (a) Digital image of the PDMAC$_{56}$-P(HBA-*stat*-DAAM)$_{287}$ nano-objects at 20 °C after re-dispersion in NutriStem. Temperature-dependent rheological studies for a 20 % w/w aqueous dispersion of PDMAC$_{56}$-P(HBA-*stat*-DAAM)$_{287}$ nano-objects dispersed in NutriStem at an applied strain of 1.0 % and an angular frequency of 1.0 rad s^{-1}. The dispersion was equilibrated at 1 °C for 15 minutes prior to a thermal cycle from 1 °C to 37 °C to 1 °C at 1 °C min^{-1}. (b) Complex viscosity ($|\eta^*|$) vs. temperature data (c) G' and G" as a function of temperature.

Table 3.1. Rheology data for 20 % w/w dispersion of the PDMAC$_{56}$-P(HBA-*stat*-DAAM)$_{287}$ nano-objects dispersed in either water or NutriStem.

	Water	**NutriStem**
G' 1 °C	0.05 Pa	0.09 Pa
G" 1 °C	0.80 Pa	0.27 Pa
Viscoelastic region	25 – 29 °C	15 – 34 °C
Max G'	41.3 Pa	25.6 Pa
T at Max G'	29 °C	25 °C

On cooling to 1 °C, low viscosity fluids were formed for both dispersions. On heating, both dispersions underwent sol-gel transitions. However, in NutriStem there is a broader gel region with the CGT occurring at 15 °C and the CDT occurring at 34 °C as opposed

to 25 °C and 29 °C respectively when dispersed in water. Despite the broader gel region for NutriStem a lower maximum G′ was observed compared to water, 25.6 Pa and 41.3 Pa respectively. A high worm-gel viscosity is preferable for certain potential biological applications such as cell storage as it allows less polymer to be used.[2] However, the unprecedented reversible morphological transitions witnessed for this PDMAC$_{54}$-P(HBA-*stat*-DAAM)$_{287}$ dispersion could be useful in encapsulation and release applications.

3.3 Conclusions

In summary, a series of new amphiphilic PDMAC-PHBA and PDMAC-P(HBA-*stat*-DAAM) diblock copolymers nano-objects have been reported. All the diblock copolymers were prepared by highly convenient, one-pot aqueous protocols. In all syntheses, high monomer conversions were achieved and efficient chain extension of the PDMAC precursors with HBA and DAAM was demonstrated by DMF GPC analysis.

Rheological studies conducted on the PDMAC$_{54}$-PHBA$_y$ diblock copolymer nano-objects prepared at pH 3 showed that cooling the dispersions induced a gel-sol transition whilst heating the dispersions initially resulted in a gel-sol transition but further heating induced a second sol-gel transition. These transitions were reversible in all cases however, some hysteresis was seen which became more prominent on increasing the total core DP. Furthermore, it was found that the transition temperatures were dependent on the total core DP. Unfortunately, due to the low glass transition temperature of the PHBA block TEM wasn't possible on these dispersions and cryo-TEM studies proved inconclusive.

In order to allow imaging of the dispersions by TEM, DAAM was introduced into the core by copolymerisation with HBA. These PDMAC$_{56}$-P(HBA-*stat*-DAAM)$_{264}$ diblock

copolymer nano-objects were successfully crosslinked with ADH. TEM imaging showed the formation of spheres, worms, vesicles or lamellae at 1 °C, 25 °C, 50 °C and 70 °C respectively. Rheology, DLS and SAXS showed that these morphology transitions occur rapidly and reversibly in aqueous solution at copolymer concentrations as low as 0.10 % w/w. Moreover, it was found by variable temperature ^{1}H NMR spectroscopy that these morphological transitions occur due to uniform swelling of the nano-object core with water on heating. Furthermore, it was demonstrated that these nano-objects undergo a reversible pH-induced transition. Finally, initial encapsulation studies were conducted to show that silica nanoparticles can be readily encapsulated within the vesicle core.

The diblock copolymer synthesis was repeated at pH 7 using Me-DDMAT as the CTA to produce PDMAC$_{56}$-P(HBA-*stat*-DAAM)$_{287}$ diblock copolymer nano-objects. Rheology showed a reversible sol-gel-sol transition on heating from 1 °C to 50 °C followed by cooling back to 1 °C. The dispersion was successfully freeze-dried and redispersed in a biological growth medium, NutriStem. The resulting free-standing gel was found to degel on cooling and heating.

These new systems could provide excellent models for studying the kinetics and mechanism(s) of block copolymer self-assembly in solution and such dispersions could be used for encapsulation studies.

3.4 Experimental

3.4.1 Materials

DMAC (≥ 98.5 %), L-ascorbic acid (AcsAc) (≥ 98 %), KPS (≥ 99 %), pyridine (99.8 %), DDMAT (98 %), ACVA (98 %) and KCl (≥ 99 %) were purchased from Sigma-Aldrich (UK). 4-dimethylaminopyridine (DMAP) (≥ 99 %), *N*,*N*' dicyclohexylcarbodiimide (DCC) (99 %), DAAM (99 %) and ADH (≥ 98 %) were purchased from Alfa Aesar (UK). All chemicals were used as received. Methanol was purchased from Fisher Scientific (UK). Hexane, HCl and DMF were purchased from VWR chemicals (UK). Anhydrous DCM was obtained from an in-house Grubbs purification system. All solvents were HPLC-grade. HBA was kindly donated by Scott Bader Ltd. (Wollaston, UK) and was purified by solvent extraction before use (see below for further details). CD_3OD was purchased from Cambridge Isotope Laboratories (UK). 1,1,2,2-Tetrachloroethane-d_2 was purchased from Goss Scientific Ltd (UK). Deionized water was adjusted to pH 3 using HCl and used for all experiments.

3.4.2 Purification of HBA

HBA (100 g) was washed with *n*-hexane (20 × 100 mL) to remove diacrylate impurities. Residual solvent was removed by rotary evaporation to yield purified HBA (70 g, 70%) as a viscous, colourless fluid. ^{1}H NMP (400 MHζ, $\Psi\Delta_3O\Delta$) δ 6.37 (1H, δδ), 6.15 (1H, δδ), 5.87 (1H, δδ), 4.18 (2H, τ), 3.59 (2H, τ), 1.67 (4H, μ).

3.4.3 One-pot Synthesis of $PDMAC_{54}$-$PHBA_{244}$ Diblock Copolymer Nano-Objects by RAFT Aqueous Dispersion Polymerisation at pH 3

Step 1 Synthesis of PDMAC precursor

KPS (11.1 mg 0.04 mmol, CTA/KPS molar ratio = 4.0) and AscAc (7.2 mg 0.04 mmol, CTA/AscAc molar ratio = 4.0) and acidified water (0.19 mL, adjusted to pH 3 with HCl)

were added to a 50 mL round-bottomed flask. DDMAT (0.06 g, 0.16 mmol) and DMAC (0.70 g, 7.1 mmol, target DP = 43) were weighed into a 14 mL vial. Both the round bottom flask and vial were purged with nitrogen gas for 15 min to remove oxygen. The DMAC/DDMAT solution was then added to the round bottom flask to produce an 80% w/w aqueous solution. The sealed flask was immersed into an oil bath set at 30 °C for 30 min with continuous stirring. The sealed reaction vessel was removed from the oil bath and a further portion of degassed acidified water (2.9 g, pH 3 adjusted to pH 3 with HCl) was added. The flask was agitated for 30 minutes to produce a 20% w/w aqueous solution, which was stirred for a further 3 h at 30 °C. A 0.1 mL aliquot was removed for ^{1}H NMR spectroscopy and GPC analysis.

^{1}H NMR spectroscopy studies indicated that > 99% DMAC conversion was achieved within 4 h, as determined by comparing the DMAC vinyl proton signals at 5.5–7.0 ppm to that of the PDMAC methyl protons signal at 2.8–3.2 ppm. A mean DP of 54 was determined for the PDMAC precursor prepared during the one-pot protocol. This DP was calculated using a calibration curve of M_p vs. DP, which was constructed for a series of nine PDMAC homopolymers, which were prepared and characterised by DMF GPC and UV-visible absorption spectroscopy in Chapter 2.

Step 2 Chain extension of PDMAC with HBA

HBA (4.5 g, 31.5 mmol) and acidified water (18.1 mL, adjusted to pH 3 with HCl) were added to a 24 mL vial and the resulting solution was purged with nitrogen for 30 min. The HBA and target DP was 290. The degassed HBA/water solution was added to the sealed round bottom flask from step 1, containing the PDMAC precursor. The sealed flask was immersed into an oil bath set at 30 °C for 18 h with continuous stirring to produce a transparent free-standing gel.

^{1}H NMR spectroscopy studies indicated that more than 99 % monomer conversion was achieved for HBA within 18 h, as determined by comparison of the HBA vinyl signals in the 5.0 – 7.0 ppm region to the polymer signal at 2.3 ppm. DMF GPC analysis gave an M_n of 56 500 g mol^{-1} and an M_w/M_n of 1.24. A PHBA DP of 244 was determined by ^{1}H NMR spectroscopy. PDMAC$_{54}$-PHBA$_{218}$ and PDMAC$_{54}$-PHBA$_{269}$ diblock copolymers were prepared in the same manner. High monomer conversions (> 99%) were achieved for both syntheses. DMF GPC analysis indicated an M_n of 52 200 g mol^{-1} and an M_w/M_n of 1.29 for PDMAC$_{54}$-PHBA$_{218}$ and an M_n of 60 800 g mol^{-1} and an M_w/M_n of 1.29 for PDMAC$_{54}$-PHBA$_{269}$.

3.4.4 One-pot Synthesis of PDMAC$_{56}$-P(HBA-stat-DAAM)$_{264}$ Diblock Copolymer Nano-objects by RAFT Aqueous Dispersion Polymerisation at pH 3

Step 1 Synthesis of PDMAC precursor

KPS (9.3 mg 0.034 mmol, CTA/KPS molar ratio = 4.0) and AscAc (6.0 mg 0.034 mmol, CTA/AscAc molar ratio = 4.0) and acidified water (0.16 mL, adjusted to pH 3 with HCl) were added to a 50 mL round-bottomed flask. DDMAT (0.050 g, 0.137 mmol) and DMAC (0.58 g, 5.89 mmol, target DP = 43) were weighed into a 14 mL vial. Both the round bottom flask and vial were purged with nitrogen gas for 15 min to remove oxygen. The DMAC/DDMAT solution was then added to the round bottom flask to produce an 80 % w/w aqueous solution. The sealed flask was immersed into an oil bath set at 30 °C for 30 minutes with continuous stirring. The sealed reaction vessel was removed from the oil bath and a further portion of degassed acidified water (2.44 g, pH 3 adjusted to pH 3 with HCl) was added. The flask was agitated for 30 minutes to produce a 20 % w/w aqueous solution, which was stirred for a further 3 h at 30 °C. A 0.1 mL aliquot was removed for ^{1}H NMR spectroscopy and GPC analysis.

^{1}H NMR spectroscopy studies indicated that > 99% DMAC conversion was achieved within 4 h, as determined by comparing the DMAC vinyl proton signals at 5.5–7.0 ppm to that of the PDMAC methyl protons signal at 2.8–3.2 ppm. DMF GPC analysis indicated a M_n of 6100 g mol^{-1} and a M_w/M_n of 1.23, respectively. A mean DP of 56 was determined for the PDMAC precursor prepared during the one-pot protocol. This DP was calculated using a calibration curve of M_p vs. DP, which was constructed for a series of nine PDMAC homopolymers, which were previously prepared and characterised by DMF GPC and UV-visible absorption spectroscopy in Chapter 2. The DDMAT CTA efficiency during the one-pot protocol was calculated to be 77% by comparing the experimental PDMAC DP of 56 to the target DP of 43.

Step 2 Chain extension of PDMAC with HBA and DAAM

HBA (2.53 g, 17.55 mmol), DAAM (0.743 g, 4.39 mmol) and acidified water (13.1 mL, adjusted to pH 3 with HCl) were added to a 24 mL vial and the resulting comonomer solution was purged with nitrogen for 30 min. The PHBA and PDAAM target DPs for this RAFT aqueous dispersion copolymerisation were 129 and 32 respectively ([HBA]/[DAAM] = 4) accounting for the removal of 0.1 mL PDMAC solution for analysis in step 1 and assuming 100% CTA efficiency. The degassed HBA/DAAM comonomer solution was added to the sealed round bottom flask from step 1, containing the PDMAC precursor. The sealed flask was immersed into an oil bath set at 30 °C for 18 h with continuous stirring to produce a transparent free-standing gel.

^{1}H NMR spectroscopy studies indicated that more than 99 % monomer conversion was achieved for both DAAM and HBA within 18 h, as determined by comparing the DAAM/HBA vinyl proton signals at 5.5–7.0 ppm to that of the PHBA oxymethylene protons signal at 3.6 ppm and the overlapping PHBA backbone proton signal and

PDAAM methyl protons signal at 2.0 - 2.5 ppm. DMF GPC analysis indicated an M_n of 49 200 g mol^{-1} and an M_w/M_n of 1.16. An overall HBA/DAAM DP of 264 was determined by ^{1}H NMR spectroscopy.

3.4.5 Post-polymerisation Cross-linking using ADH

The protocol used for cross-linking the PDMAC$_{56}$−P(HBA-*stat*-DAAM)$_{264}$ nano-objects was as follows. The as-synthesised PDMAC$_{56}$−P(HBA-*stat*-DAAM)$_{264}$ 20% w/w nanoparticle dispersion (0.25 g) was added to a 14 mL vial and diluted to 5 % w/w solids using acidified water (distilled water adjusted to pH 3 with HCl). The 5 % w/w dispersion was equilibrated at the desired temperature for 24 h. ADH (11.3 mg, 0.065 mmol; DAAM/ADH molar ratio = 1.0) was added to the vial, using hand-shaking to ensure uniform mixing. Cross-linking was conducted at the desired temperature for 24 h.

3.4.6 Methylation of DDMAT

DDMAT (4.30 g, 11.8 mmol) was dissolved in anhydrous dichloromethane (30 ml) in a 100 ml round-bottomed flask, which was cooled to 0 °C by immersing in an ice bath. DMAP (0.29 g, 2.4 mmol) and excess anhydrous methanol (2.0 g) were added to the stirred solution at 0 °C. DCC (2.72 g, 13.2 mmol) was added gradually over 5 min. This reaction mixture was allowed to warm up to 20 °C and stirred continuously for 16 h at this temperature prior to filtration to remove the insoluble side-product (dicyclohexyl urea). Column chromatography was used to purify the product using DCM as the eluent. This solvent was removed under vacuum to afford Me-DDMAT as an orange oil (4.21 g, 94%). ^{1}H NMR spectroscopy studies indicated a degree of esterification of 98 %.

3.4.7 One-pot Synthesis of PDMAC$_{56}$-P(HBA-stat-DAAM)$_{287}$ Diblock Copolymer Nano-objects by RAFT Aqueous Dispersion Polymerisation at pH 7

Step 1 Synthesis of PDMAC precursor

ACVA (0.9 mg 0.01 mmol, CTA/ACVA molar ratio = 4.0), Me-DDMAT (0.01 g, 0.03 mmol) and DMAC (0.11 g, 1.14 mmol, target DP = 43) were weighed into a 14 mL vial. The vial was purged with nitrogen gas for 15 min to remove oxygen. The sealed vial was immersed into an oil bath set at 70 °C for 30 min with continuous stirring. The sealed reaction vessel was removed from the oil bath and a portion of degassed acidified water (0.50 g, pH 3 adjusted to pH 3 with HCl) was added. The vial was agitated for 30 minutes to produce a 20 % w/w aqueous solution, which was stirred for a further 3 h at 70 °C. A 0.1 mL aliquot was removed for ^{1}H NMR spectroscopy and GPC analysis.

^{1}H NMR spectroscopy studies indicated that > 99% DMAC conversion was achieved within 4 h, as determined by comparing the DMAC vinyl proton signals at 5.5–7.0 ppm to that of the PDMAC methyl protons signal at 2.8–3.2 ppm. DMF GPC analysis indicated a M_n of 5500 g mol^{-1} and a M_w/M_n of 1.16, respectively. A mean DP of 56 was determined for the PDMAC precursor prepared during the one-pot protocol. This DP was calculated using a calibration curve of M_p vs. DP, which was constructed for a series of nine PDMAC homopolymers, which were previously prepared and characterised by DMF GPC and UV-visible absorption spectroscopy in Chapter 2.

Step 2 Chain extension of PDMAC with HBA and DAAM

HBA (0.61 g, 4.2 mmol), DAAM (0.17 g, 1.1 mmol) and acidified water (3.1 mL, adjusted to pH 3 with HCl) were added to a 14 mL vial and the resulting comonomer solution was purged with nitrogen for 30 min. The degassed HBA/DAAM comonomer solution was added to the sealed vial from step 1, containing the PDMAC precursor. The

sealed flask was immersed into an oil bath set at 70 °C for 18 h with continuous stirring to produce a transparent free-standing gel.

^{1}H NMR spectroscopy studies indicated that more than 99% monomer conversion was achieved for both DAAM and HBA within 18 h, as determined by comparing the DAAM/HBA vinyl proton signals at 5.5–7.0 ppm to that of the PHBA oxymethylene protons signal at 3.6 ppm and the overlapping PHBA backbone proton signal and PDAAM methyl protons signal at 2.0 - 2.5 ppm. DMF GPC analysis indicated an M_n of 44 000 g mol^{-1} and an M_w/M_n of 1.24. An overall HBA/DAAM DP of 287 was determined by ^{1}H NMR spectroscopy.

3.4.8 Silica Encapsulation

A 10 % w/w dispersion of PDMAC$_{56}$−P(HBA-*stat*-DAAM)$_{264}$ (0.5 g) was added to a vial. CC401 silica sol (0.5 g, 40 % w/w in water) was added to a second vial. The vials were cooled to 1 °C and equilibrated for 1 hour. The silica sol was added to the 10 % w/w dispersion of PDMAC$_{56}$−P(HBA-*stat*-DAAM)$_{264}$ and hand-shaking was used to ensure uniform mixing. The vial was heated to 50 °C (inducing a morphological transition of the PDMAC$_{56}$−P(HBA-*stat*-DAAM)$_{264}$ nano-objects from spheres to vesicles) and equilibrated for 1 hour. ADH (5.7 mg, 0.032 mmol; DAAM/ADH molar ratio = 1.0) was added to the vial, using hand-shaking to ensure uniform mixing. Cross-linking was conducted at 50 °C for 24 h. The crosslinked vesicle dispersion was diluted to 1 % w/w nanoparticles using pH 3 HCl/H$_2$O. Centrifugation was conducted on 1 mL aliquots to remove excess silica (6 x 1 minute at 4000 rpm).

3.4.9 Polymer Characterisation

^{1}H NMR spectroscopy

^{1}H NMR spectra were recorded in CD$_3$OD using a 400 MHz Bruker Avance III HD 400 spectrometer with 16 scans being averaged per spectrum.

Variable Temperature ^{1}H NMR spectroscopy

^{1}H NMR spectra were recorded using a 500 MHz Bruker Avance-500 spectrometer. An outer tube contained the as-synthesised 20% w/w aqueous dispersion of PDMAC-P(HBA-*stat*-DAAM) nano-objects and an inner capillary tube contained the pyridine standard in C$_2$D$_2$Cl$_4$. Spectra were recorded from 5 °C to 70 °C at 5 °C intervals with an equilibrium time of 10 min at each temperature.

Gel permeation chromatography (GPC)

Copolymer molecular weight distributions were assessed using DMF GPC. The set-up comprised a PL guard column and two Agilent PL gel 5 μm Mixed-C columns connected in series to an Agilent 1260 Infinity GPC system equipped with both refractive index and UV-visible detectors operating at 60°C. The GPC eluent was HPLC-grade DMF containing 10 mM LiBr and the flow rate was 1.0 mL min^{-1}. Calibration was achieved using a series of ten near-monodisperse poly(methyl methacrylate) standards (ranging in M_p from 625 to 618000 g mol^{-1}). Chromatograms were analysed using Agilent GPC/SEC software.

Variable Temperature Dynamic Light Scattering (DLS)

The 'sphere-equivalent' intensity-average diameter of diblock copolymer nano-objects was determined using the Stokes-Einstein equation, which assumes perfectly monodisperse, non-interacting spheres. All measurements were made using a Malvern Zetasizer NanoZS instrument. 1.0 mL of a dilute (0.10 % w/w) aqueous copolymer

dispersion at pH 3 (diluted using distilled water adjusted to pH 3 using HCl) was placed in a glass cuvette and heated from 1 °C to 50 °C, followed by cooling from 50 °C to 1 °C at 5 °C intervals with 10 minutes being allowed for thermal equilibration at each temperature. The intensity-average hydrodynamic diameter was determined at each temperature by averaging data over three consecutive runs.

Aqueous Electrophoresis

Zeta potential measurements were performed using a Malvern Zetasizer Nano ZS instrument on 0.1% w/w aqueous copolymer dispersions at 25 °C in the presence of 1 mM KCl. The initial copolymer dispersion was acidic (pH 3) with the solution pH being adjusted by addition of dilute NaOH to pH 8 followed by adjustment with dilute HCl to pH 3, with 10 min being allowed for equilibrium at each pH. Zeta potentials were calculated from the Henry equation using the Smoluchowski approximation. Hydrodynamic DLS diameters were also recorded during these pH experiments. All data were averaged over three consecutive runs.

UV−Visible Absorption Spectroscopy

UV−visible absorption spectra were recorded between 200 and 800 nm using a PC-controlled UV-1800 spectrophotometer at 25°C using a 1.0 cm path length quartz cell. The DPs for a series of nine PDMAC homopolymers were determined using a molar extinction coefficient of 16300 ± 160 mol^{-1} dm^3 cm^{-1} for DDMAT as reported in Chapter 2.

Transmission Electron Microscopy (TEM)

Copper/palladium TEM grids (Agar Scientific, UK) were coated in-house to yield a thin film of amorphous carbon. The coated grids were then subjected to a glow discharge for

30 s. An individual 10.0 µL droplet for each 0.10% w/w aqueous copolymer dispersion was placed on a freshly-treated TEM grid for 1 min and then carefully blotted with filter paper to remove excess solution. To ensure sufficient electron contrast, uranyl formate (9.0 µL of a 0.75% w/w solution) was absorbed onto the sample-loaded grid for 30 s and then carefully blotted to remove excess stain. Each grid was then dried using a vacuum hose. Imaging was performed using a FEI Tecnai Spirit 2 microscope operating at 80 kV and fitted with an Orius SC1000B camera. Particle sizes were calculated using image J. An average size was calculated by analysing 100 particles.

Rheology

An AR-G2 rheometer equipped with a variable-temperature Peltier plate and a 40 ml 2° aluminium cone was used for all experiments. Temperature sweeps were conducted using a constant percentage strain of 1.0% and a constant angular frequency of 1.0 rad s^{-1}. Before the temperature sweep, the aqueous copolymer dispersion was equilibrated at 1 °C for 15 min. A ramp rate of 1 °C min^{-1} was used for all experiments.

Small Angle X-Ray scattering (SAXS)

SAXS patterns were recorded at a synchrotron source (ESRF, station ID02, Grenoble, France) using monochromatic X-ray radiation (X-ray wavelength λ = 0.0995 nm, scattering vector q ranging from 0.0015 to 0.15 Å^{-1}, where $q = 4\pi \sin \theta/\lambda$ and θ is one-half of the scattering angle) and a Ravonix MX-170HS CCD detector. A glass capillary of 2 mm diameter was used as a sample holder and the temperature was controlled using a heating/cooling capillary holding stage (Linkam Scientific Instruments Ltd., Tadworth, UK). Measurements were conducted on a 1.0% w/w aqueous dispersion of PDMAC$_{56}$−P(HBA-*stat*-DAAM)$_{264}$ particles in pH 3 water (adjusted using HCl). Scattering data was recorded from 5 °C to 70 °C at a heating rate 1 °C min^{-1}. Scattering

data were reduced (normalisation and integration) using standard routines available at the

beamline and were further analysed using Irena SAS macros for Igor Pro.

References

(1)   Blanazs, A.; Verber, R.; Mykhaylyk, O. O.; Ryan, A. J.; Heath, J. Z.; Douglas, C. W. I.; Armes, S. P. Sterilizable Gels from Thermoresponsive Block Copolymer Worms. *J. Am. Chem. Soc.* **2012**, *134*, 9741–9748.

(2)   Canton, I.; Warren, N. J.; Chahal, A.; Amps, K.; Wood, A.; Weightman, R.; Wang, E.; Moore, H.; Armes, S. P. Mucin-Inspired Thermoresponsive Synthetic Hydrogels Induce Stasis in Human Pluripotent Stem Cells and Human Embryos. *ACS Cent. Sci.* **2016**, *2*, 65–74.

(3)   Mable, C. J.; Gibson, R. R.; Prevost, S.; McKenzie, B. E.; Mykhaylyk, O. O.; Armes, S. P. Loading of Silica Nanoparticles in Block Copolymer Vesicles during Polymerization-Induced Self-Assembly: Encapsulation Efficiency and Thermally Triggered Release. *J. Am. Chem. Soc.* **2015**, *137*, 16098–16108.

(4)   Scarpa, J. S.; Mueller, D. D.; Klotz, I. M. Slow Hydrogen-Deuterium Exchange in a Non-α-Helical Polyamide. *J. Am. Chem. Soc.* **1967**, *89*, 6024–6030.

(5)   Heskins, M.; Guillet, J. E. Solution Properties of Poly(N-Isopropylacrylamide). *J. Macromol. Sci.* **1968**, *2*, 1441–1455.

(6)   Schild, H. G. Poly(N-Isopropylacrylamide): Experiment, Theory and Application. *Prog. Polym. Sci.* **2003**, *17*, 163–249.

(7)   Aoyagi, T.; Ebara, M.; Sakai, K.; Sakurai, Y.; Okano, T. Novel Bifunctional Polymer with Reactivity and Temperature Sensitivity. *J. Biomater. Sci. Polym. Ed.* **2000**, *11*, 101–110.

(8)   Yoshida, T.; Aoyagi, T.; Kokufuta, E.; Okano, T. Newly Designed Hydrogel with Both Sensitive Thermoresponse and Biodegradability. *J. Polym. Sci. Part A Polym. Chem.* **2003**, *41*, 779–787.

(9)   Maeda, T.; Yamamoto, K.; Aoyagi, T. Importance of Bound Water in Hydration-Dehydration Behavior of Hydroxylated Poly(N-Isopropylacrylamide). *J. Colloid Interface Sci.* **2006**, *302*, 467–474.

(10)   Hoogenboom, R. Poly(2-Oxazoline)s: A Polymer Class with Numerous Potential Applications. *Angew. Chem. Int. Ed.* **2009**, *48*, 7978–7994.

(11)   Hoogenboom, R.; Schlaad, H. Thermoresponsive Poly(2-Oxazoline)s, Polypeptoids, and Polypeptides. *Polym. Chem.* **2017**, *8*, 24–40.

(12)   Luxenhofer, R.; Han, Y.; Schulz, A.; Tong, J.; He, Z.; Kabanov, A. V.; Jordan, R. Poly(2-Oxazoline)s as Polymer Therapeutics. *Macromol. Rapid Commun.* **2012**, *33*, 1613–1631.

(13)   Schlaad, H.; Diehl, C.; Gress, A.; Meyer, M.; Levent Demirel, A.; Nur, Y.; Bertin, A. Poly(2-Oxazoline)s as Smart Bioinspired Polymers. *Macromol. Rapid Commun.* **2010**, *31*, 511–525.

(14)   Park, J. S.; Akiyama, Y.; Winnik, F. M.; Kataoka, K. Versatile Synthesis of End-Functionalized Thermosensitive Poly(2-Isopropyl-2-Oxazolines). *Macromolecules* **2004**, *37*, 6786–6792.

(15) Jeong, B.; Kim, S. W.; Bae, Y. H. Thermosensitive Sol-Gel Reversible Hydrogels. *Adv. Drug Deliv. Rev.* **2012**, *64*, 154–162.

(16) Idziak, I.; Avoce, D.; Lessard, D.; Gravel, D.; Zhu, X. X. Thermosensitivity of Aqueous Solutions of Poly(*N,N*-Diethylacrylamide). *Macromolecules* **1999**, *32*, 1260–1263.

(17) Arndt, K. F.; Schmidt, T.; Reichelt, R. Thermo-Sensitive Poly(Methyl Vinyl Ether) Micro-Gel Formed by High Energy Radiation. *Polymer* **2001**, *42*, 6785–6791.

(18) Van Durme, K.; Verbrugghe, S.; Du Prez, F. E.; Van Mele, B. Influence of Poly(Ethylene Oxide) Grafts on Kinetics of LCST Behavior in Aqueous Poly(N-Vinylcaprolactam) Solutions and Networks Studied by Modulated Temperature DSC. *Macromolecules* **2004**, *37*, 1054–1061.

(19) Yu, L.; Ding, J. Injectable Hydrogels as Unique Biomedical Materials. *Chem. Soc. Rev.* **2008**, *37*, 1473–1481.

(20) Malcolm, G. N.; Rowlinson, J. S. The Thermodynamic Properties of Aqueous Solutions of Polyethylene Glycol, Polypropylene Glycol and Dioxane. *Trans. Faraday Soc.* **1957**, *53*, 921–931.

(21) Portenkirchner, E.; Oppelt, K.; Ulbricht, C.; Egbe, D. a. M.; Neugebauer, H.; Knör, G.; Sariciftci, N. S. Electrocatalytic and Photocatalytic Reduction of Carbon Dioxide to Carbon Monoxide Using the Alkynyl-Substituted Rhenium(I) Complex (5,5′-Bisphenylethynyl-2,2′-Bipyridyl)Re(CO)3Cl. *J. Organomet. Chem.* **2012**, *716*, 19–25.

(22) Kim, Y. J.; Matsunaga, Y. T. Thermo-Responsive Polymers and Their Application as Smart Biomaterials. *J. Mater. Chem. B* **2017**, *5*, 4307–4321.

(23) Glatzel, S.; Badi, N.; Päch, M.; Laschewsky, A.; Lutz, J. F. Well-Defined Synthetic Polymers with a Protein-like Gelation Behavior in Water. *Chem. Commun.* **2010**, *46*, 4517–4519.

(24) Seuring, J.; Bayer, F. M.; Huber, K.; Agarwal, S. Upper Critical Solution Temperature of Poly(N-Acryloyl Glycinamide) in Water: A Concealed Property. *Macromolecules* **2012**, *45*, 374–384.

(25) Israelachvil, J. N.; Mitchell, D. J.; Ninham, B. W. Theory of Self-Assembly of Hydrocarbon Amphiphiles into Micelles and Bilayers. *J. Chem. Soc. Faraday Trans* **1975**, *72*, 1525–1568.

(26) Antonietti, M.; Förster, S. Vesicles and Liposomes: A Self-Assembly Principle Beyond Lipids. *Adv. Mater.* **2003**, *15*, 1323–1333.

(27) Blanazs, A.; Armes, S. P.; Ryan, A. J. Self-Assembled Block Copolymer Aggregates: From Micelles to Vesicles and Their Biological Applications. *Macromol. Rapid Commun.* **2009**, *30*, 267–277.

(28) Ma, Y.; Gao, P.; Ding, Y.; Huang, L.; Wang, L.; Lu, X.; Cai, Y. Visible Light Initiated Thermoresponsive Aqueous Dispersion Polymerization-Induced Self-Assembly. *Macromolecules* **2019**, *52*, 1033–1041.

(29) Lovett, J. R.; Warren, N. J.; Armes, S. P.; Smallridge, M. J.; Cracknell, R. B.

Order-Order Morphological Transitions for Dual Stimulus Responsive Diblock Copolymer Vesicles. *Macromolecules* **2016**, *49*, 1016–1025.

(30)   Kim, S. Y.; Lee, K. E.; Han, S. S.; Jeong, B. Vesicle-to-Spherical Micelle-to-Tubular Nanostructure Transition of Monomethoxy-Poly(Ethylene Glycol)-Poly(Trimethylene Carbonate) Diblock Copolymer. *J. Phys. Chem. B* **2008**, *112*, 7420–7423.

(31)   Abbas, S.; Li, Z.; Hassan, H.; Lodge, T. P. Thermoreversible Morphology Transitions of Poly(Styrene-b-Dimethylsiloxane) Diblock Copolymer Micelles in Dilute Solution. *Macromolecules* **2007**, *40*, 4048–4052.

(32)   Byard, S. J.; Williams, M.; Mckenzie, B. E.; Blanazs, A.; Armes, S. P. Preparation and Cross-Linking of All-Acrylamide Diblock Copolymer Nano-Objects via Polymerization-Induced Self-Assembly in Aqueous Solution. *Macromolecules* **2017**, *50*, 1482–1493.

(33)   Lovett, J. R.; Derry, M. J.; Yang, P.; Hatton, F. L.; Warren, N. J.; Fowler, P. W.; Armes, S. P. Can Percolation Theory Explain the Gelation Behavior of Diblock Copolymer Worms? *Chem. Sci.* **2018**, *9*, 7138–7144.

(34)   Glatter, O.; Kratky, O. *Small Angle X-Ray Scattering*; Academic Press: London, 1982; Vol. 130.

(35)   Fielding, L. A.; Lane, J. A.; Derry, M. J.; Mykhaylyk, O. O.; Armes, S. P. Thermo-Responsive Diblock Copolymer Worm Gels in Non-Polar Solvents. *J. Am. Chem. Soc.* **2014**, *136*, 5790–5798.

(36)   Rumyantsev, A. M.; Leermakers, F. A. M.; Zhulina, E. B.; Potemkin, I. I.; Borisov, O. V. Temperature-Induced Re-Entrant Morphological Transitions in Block-Copolymer Micelles. *Langmuir* **2019**, *35*, 2680–2691.

(37)   Lovett, J. R.; Warren, N. J.; Ratcliffe, L. P. D.; Kocik, M. K.; Armes, S. P. pH-Responsive Non-Ionic Diblock Copolymers : Ionization of Carboxylic Acid End-Groups Induces an Order-Order Morphological Transition. *Angew. Chem. Int. Ed.* **2015**, *54*, 1279–1283.

Chapter 4

Salt Tolerant, Cationic, Sterically-stabilised Diblock Copolymer Nanoparticles

4.1 Introduction

It has been recognised for more than a century that charge-stabilised particles can aggregate in the presence of salt.[1,2] This phenomenon can be explained in terms of DLVO theory[3,4] and is commercially exploited for the industrial manufacture of latex gloves.[5] Faraday was the first to demonstrate that protein-stabilised particles typically exhibit significantly better colloidal stability in the presence of added salt: indeed, some of his gelatin-coated gold sols remain stable more than 160 years after their synthesis.[6] For certain applications such as enhanced oil recovery, colloidal dispersions that can exhibit *extreme* salt tolerance (up to the saturation point) at both ambient and elevated temperature are desirable.[7–13]

Recently, various polyelectrolytes have been used to simultaneously confer both charge and steric stabilisation (so-called electrosteric stabilisation) onto *inorganic* particles for such high salt applications. For example, Bagaria *et al.* physically adsorbed statistical copolymers comprising PAMPS and PAA onto the surface of ~100 nm iron oxide nanoparticles.[9] Poly(AMPS-*stat*-AA) coated iron nanoparticles remained colloidally stable in a mixture of 1.4 M NaCl and 0.2 M CaCl$_2$ at both room temperature and 90 °C for up to 1 month. In a later publication, the same team showed that iron nanoparticles resisted aggregation in a mixture of 1.4 M NaCl and 0.2 M CaCl$_2$ if poly(AMPS-*stat*-AA) chains were grafted onto the nanoparticle surface.[10]

Similarly, salt-tolerant polymer latexes have been synthesised by free radical aqueous dispersion polymerisation. For example, Cho *et al.* prepared submicrometer-sized polyacrylamide particles in the presence of 1.8 - 2.3 M ammonium sulfate. The particles were sterically-stabilised by PATAC.[14] In closely-related work, Aijun *et al.* reported the preparation of colloidally stable, cationic latex particles in the presence of 1.9 - 2.5 M

ammonium sulfate *via* aqueous dispersion copolymerisation of acrylamide with MATAC, again using PATAC as the steric stabiliser.[15]

Thus far, the morphology of salt-tolerant polymer particles has been confined to spheres. This is no doubt because such formulations have been based on conventional FRP. In contrast, controlled radical polymerisation techniques such as RAFT polymerisation enable the synthesis of well-defined, functional diblock copolymers.[16–27] Moreover, it is now well-established that, by choosing a suitable selective solvent, a range of diblock copolymer nano-objects can be prepared in the form of concentrated aqueous dispersions *via* RAFT-mediated PISA.[28–36]

In Chapter 2, the preparation and characterisation of a series of PDMAC-PDAAM diblock copolymer nano-objects synthesised *via* RAFT aqueous dispersion polymerisation was reported. Moreover, the post-polymerisation reaction of the pendent ketone group on the DAAM residues with ADH was demonstrated. Such cross-linking allows covalently-stabilised nano-objects to be produced in the form of concentrated aqueous dispersions.

In the present Chapter, this latter PISA formulation has been modified by incorporating PATAC as either the sole or supplementary cationic steric stabiliser block. Accordingly, either PATAC, PDMAC or a binary mixture of PDMAC and PATAC homopolymer precursors was chain-extended with DAAM *via* RAFT aqueous dispersion copolymerisation to produce ($[n]$ PATAC$_x$ + $[1-n]$ PDMAC$_y$)-PDAAM$_z$ diblock copolymer nanoparticles, where n denotes the mole fraction of PATAC. Pure sphere, worm and vesicle morphologies could be obtained depending on the precise PISA formulation. The effect of varying n (for a fixed x, y and z) on the cationic character of spherical nanoparticles has been studied. Moreover, the effect of increasing the PDAAM DP on the mean sphere diameter has been investigated for both a series of

PATAC$_{100}$-PDAAM$_z$ and (0.1 PATAC$_{100}$ + 0.9 PDMAC$_{67}$)-PDAAM$_z$ diblock copolymer spheres. DLS has been used to study the colloidal stability of these new diblock copolymer nanoparticles in concentrated aqueous solutions of both KCl and ammonium sulfate. Finally, the ([n] PATAC$_{100}$ + [1-n] PDMAC$_{67}$)-PDAAM$_{1500}$ spherical nanoparticles have been covalently-stabilised *via* reaction of the ketone groups within the core-forming PDAAM chains with ADH.

4.2 Results and Discussion

4.2.1 Synthesis of PATAC Homopolymer Precursors *via* RAFT Solution Polymerisation

The RAFT solution polymerisation of ATAC was conducted in a 94:6 methanol/water mixture at 44 °C using Me-DDMAT as the CTA, as outlined in Figure 4.1. Methanol was required for Me-DDMAT dissolution.
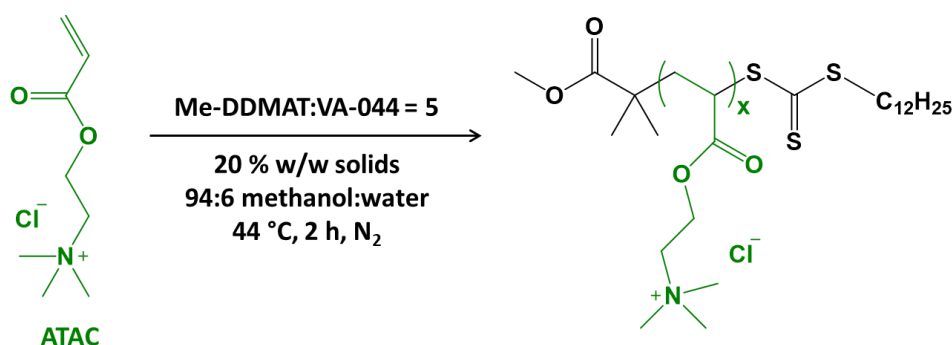
Fig. 4.1. Reaction scheme for RAFT solution polymerisation of ATAC in a methanol/water mixture using Me-DDMAT as the CTA.

The synthesis and characterisation of Me-DDMAT was presented in Chapter 3. Two PATAC homopolymers were prepared with mean DPs of 91 and 100 (target DPs of 80 and 100 respectively), as determined by UV/vis spectroscopy using a Beer-Lambert plot constructed for Me-DDMAT, see Figure 4.2. A representative ^{1}H NMR spectrum for PATAC$_{100}$ is provided in Figure 4.3. Aqueous GPC analysis indicated narrow MWDs ($M_w/M_n \leq 1.19$) for these precursors, see Figure 4.4.
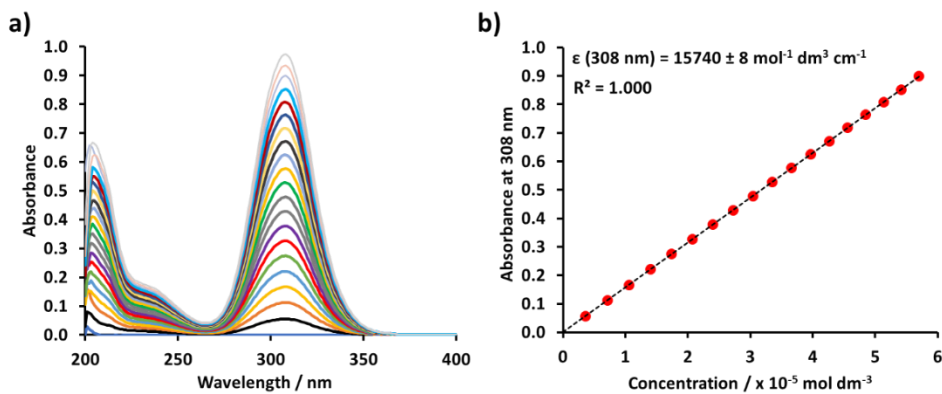
Fig. 4.2. (a) UV/visible absorption spectra recorded for Me-DDMAT in methanol for Me-DDMAT concentrations ranging from 3.6 µM to 62.5 µM. (b) Beer-Lambert calibration plot constructed for Me-DDMAT in methanol to calculate the molar extinction coefficient (ε) at the absorption maximum at 308 nm.
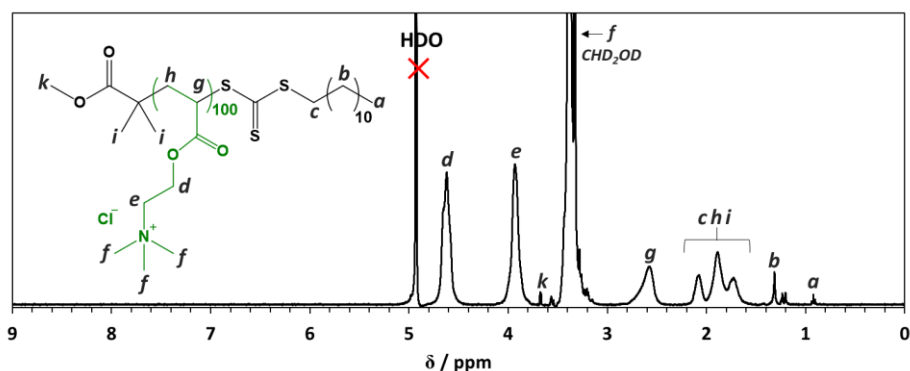
Fig. 4.3. ^{1}H NMR spectrum recorded for the PATAC$_{100}$ homopolymer in CD$_3$OD.
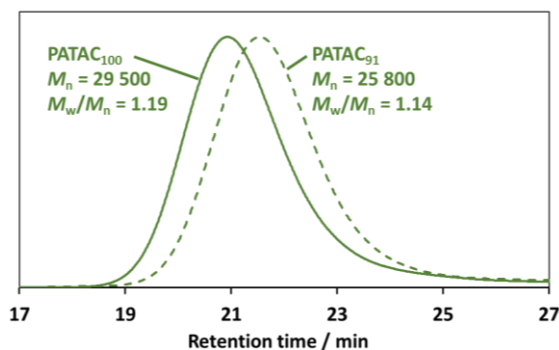
Fig. 4.4. Aqueous GPC traces recorded for the PATAC$_{91}$ and PATAC$_{100}$ homopolymer precursors.

4.2.2 Synthesis of the PDMAC Homopolymer Precursors *via* RAFT Solution Polymerisation

The RAFT solution polymerisation of DMAC was conducted in dioxane at 70 °C using Me-DDMAT as the CTA, as outlined in Figure 4.5. Two PDMAC homopolymers were prepared with DPs of 37 and 67, as determined by end-group analysis using UV spectroscopy. A representative ^{1}H NMR spectrum of PDMAC$_{67}$ is provided in Figure 4.6. DMF GPC analysis indicated narrow MWDs ($M_w/M_n \leq 1.15$) for these precursors, see Figure 4.7.
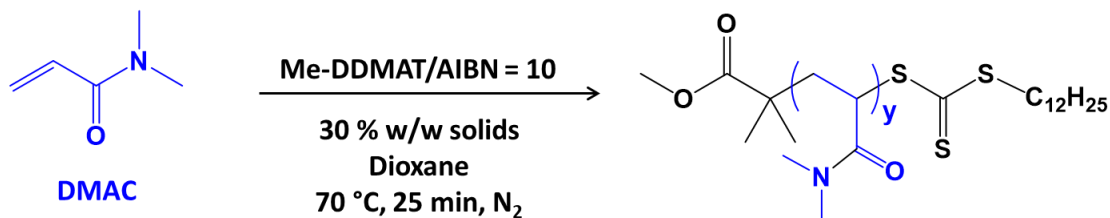

Fig. 4.5. Reaction scheme for RAFT solution polymerisation of DMAC in dioxane using Me-DDMAT as the CTA.
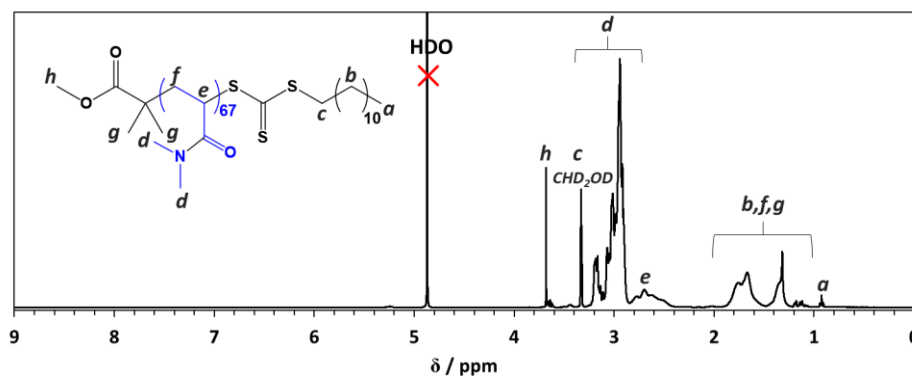
Fig. 4.6. ^{1}H NMR spectrum recorded for the PDMAC$_{67}$ homopolymer in CD$_3$OD.
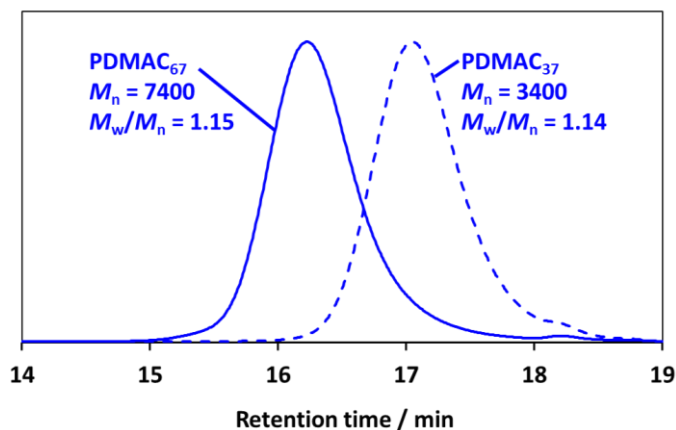
Fig. 4.7. DMF GPC chromatograms recorded for the PDMAC$_{37}$ and PDMAC$_{67}$ homopolymer precursors.

4.2.3 RAFT Aqueous Dispersion Polymerisation of DAAM

A series of ([n] PATAC$_x$ + [1-n] PDMAC$_y$)-PDAAM$_z$ diblock copolymer nanoparticles were synthesised by simultaneous chain extension of a binary pair of PATAC and PDMAC precursors *via* RAFT aqueous dispersion polymerisation of DAAM at 56 °C, see Figure 4.8. Experiments for which $n = 0$ or $n = 1$ were also conducted to provide diblock copolymer spheres with either zero or maximum cationic character, respectively. These nanoparticle syntheses were conducted at 20 % w/w solids. DAAM conversions of more than 99 % were routinely achieved for such PISA syntheses as determined by ^{1}H NMR spectroscopy studies conducted in deuterated methanol (the integral for the residual vinyl signals at 5.4−6.4 ppm was compared to that of the methyl signal assigned to the PDAAM chains at 2.2 ppm, see Figure 4.9).
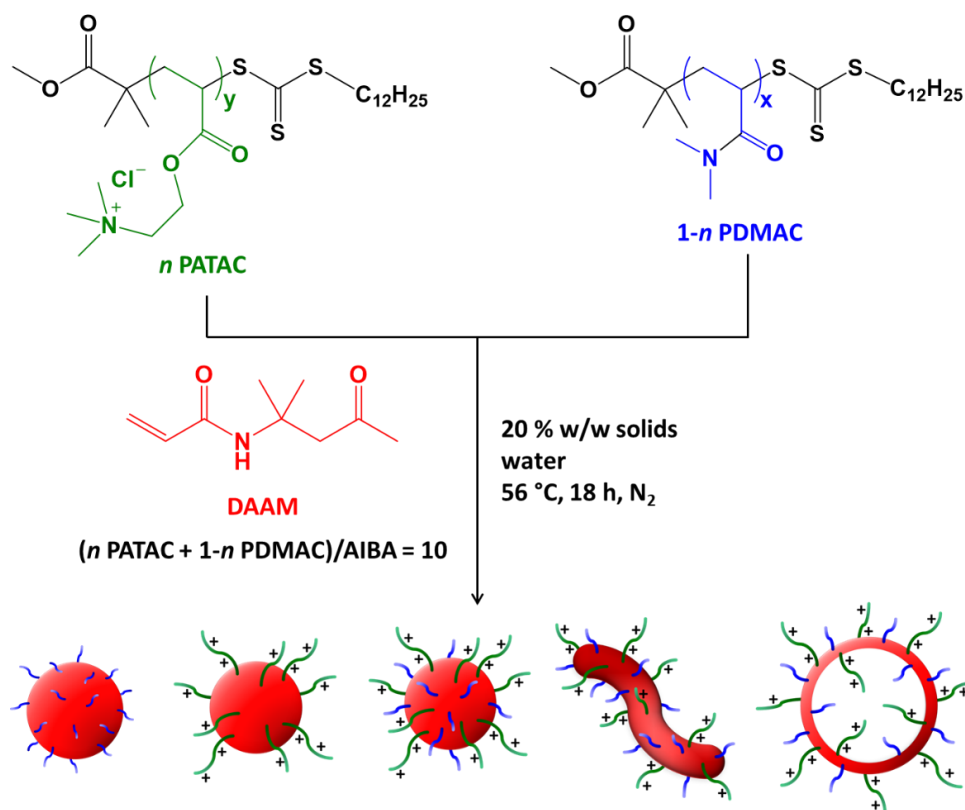
Fig. 4.8. Chain extension of either PATAC, PDMAC or a binary mixture of PATAC and PDMAC precursors *via* RAFT aqueous dispersion polymerisation of DAAM to produce either neutral or cationic diblock copolymer nanoparticles.
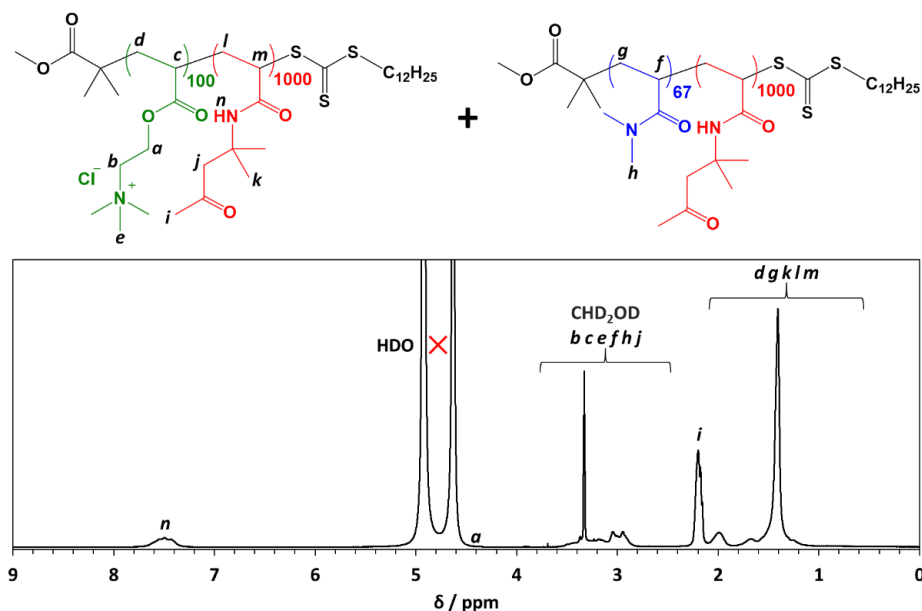
Fig. 4.9. ^{1}H NMR spectrum recorded in CD$_3$OD for the (0.1 PATAC$_{100}$ + 0.9 PDMAC$_{67}$)-PDAAM$_{1000}$ diblock copolymer.

149

Unfortunately, GPC analysis could not be conducted on the PATAC-PDAAM diblock copolymer because no suitable eluent could be identified that would solubilise the cationic PATAC and the hydrophobic PDAAM blocks. The same problem was also encountered for the GPC analysis of nanoparticles comprising binary mixtures of PATAC-PDAAM and PDMAC-PDAAM diblock copolymer chains. However, GPC analysis of the neutral $PDMAC_{67}$-$PDAAM_{1500}$ diblock copolymer chains (i.e., for $n = 0$) indicated a high blocking efficiency (minimal $PDMAC_{67}$ precursor contamination) and a relatively narrow MWD ($M_w/M_n = 1.50$) see Figure 4.10. A summary of the characterisation data obtained for all of the ($[n]$ $PATAC_x$ + $[1-n]$ $PDMAC_y$)-$PDAAM_x$ diblock copolymer nanoparticles prepared in this study is given in Table 4.1.
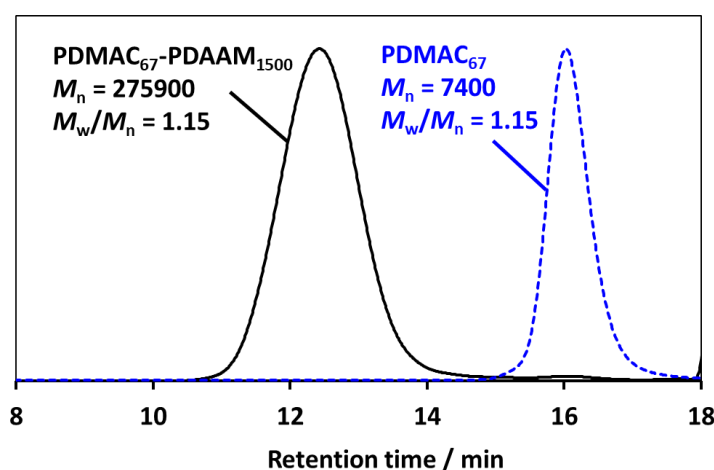
Fig. 4.10. DMF GPC chromatograms recorded for the $PDMAC_{67}$-$PDAAM_{1500}$ diblock copolymer and the $PDMAC_{67}$ homopolymer precursor trace is provided for reference.

Table 4.1. Summary of the characterisation data obtained for the ([n] PATAC$_x$ + [1-n] PDMAC$_y$)-PDAAM$_z$ diblock copolymer nanoparticles prepared in this study.

Entry	x	y	z	n	DLS diameter[a] / nm	Zeta Potential[b] /mV	Assigned morphology[c]
1	100	-	100	1.00	75 ± 20	50	Spheres
2	100	-	300	1.00	95 ± 18	34	Spheres
3	100	-	500	1.00	97 ± 20	35	Spheres
4	100	-	700	1.00	101 ± 17	35	Spheres
5	100	-	1000	1.00	122 ± 20	34	Spheres
6	100	-	1500	1.00	154 ± 44	33	Spheres
7	100	-	2000	1.00	206 ± 45	37	Spheres
8	-	67	1500	0.00	271 ± 111	1	Spheres
9	100	67	1500	0.10	204 ± 32	16	Spheres
10	100	67	1500	0.25	177 ± 29	28	Spheres
11	100	67	1500	0.50	145 ± 22	32	Spheres
12	100	67	1500	0.75	144 ± 19	38	Spheres
13	100	67	100	0.10	66 ± 19	29.1	Spheres
14	100	67	200	0.10	80 ± 21	30.9	Spheres
15	100	67	300	0.10	96 ± 22	27.7	Spheres
16	100	67	400	0.10	106 ± 21	28.9	Spheres
17	100	67	500	0.10	114 ± 17	29.6	Spheres
18	100	67	600	0.10	122 ± 22	27.4	Spheres
19	100	67	700	0.10	129 ± 12	26.6	Spheres
20	100	67	800	0.10	138 ± 30	26.5	Spheres
21	100	67	900	0.10	144 ± 18	26.2	Spheres
22	100	67	1000	0.10	165 ± 16	19.5	Spheres
23	100	67	1250	0.10	180 ± 21	19.2	Spheres
24	100	67	1750	0.10	256 ± 60	16.3	Spheres
25	100	67	2000	0.10	296 ± 40	7.9	Spheres
26	91	37	90	0.10	195 ± 89	33	Worms
27	91	67	300	0.10	196 ± 34	40	Vesicles
28	91	67	400	0.10	194 ± 19	37	Vesicles
29	91	67	900	0.10	221 ± 38	34	Vesicles

[a] Intensity-average diameter determined by DLS analysis of 0.1 % copolymer dispersions at 20°C in 1.0 mM KCl obtained using the Stokes-Einstein equation. Standard deviations were calculated using the polydispersity index (PDI) ($STD\ DEV = \sqrt{PDI} \times DLS\ diameter$). [b] Zeta potentials of 0.1 % copolymer dispersions at 20°C in 1.0 mM KCl. [c] Morphologies assigned from TEM analysis on 0.1 % copolymer dispersions in water.

4.2.4 PATAC-PDAAM Nanoparticle Characterisation

It is reported in the literature that the use of relatively long non-ionic blocks in RAFT aqueous dispersion polymerisation syntheses almost invariably result in kinetically-trapped spheres.[37,38] The same constraint applies for PISA syntheses performed using polyelectrolytic stabiliser blocks regardless of their mean DP.[39–43] This is probably because strong mutual electrostatic repulsion between nanoparticles prevent their 1D fusion to form worms during the PISA synthesis.[28,29,35] Indeed, in this work all of the $PATAC_{100}$-$PDAAM_z$ diblock copolymers ($n = 1.00$) formed well-defined spherical nanoparticles as determined by TEM studies, see Figure 4.11. Moreover, the mean particle diameter increased monotonically as the PDAAM DP (z) was systematically increased from 100 to 2000. A systematic increase in intensity-average particle diameter from 75 to 206 nm was indicated by DLS studies performed in 1.0 mM KCl, see Table 4.1, entries 1-7.
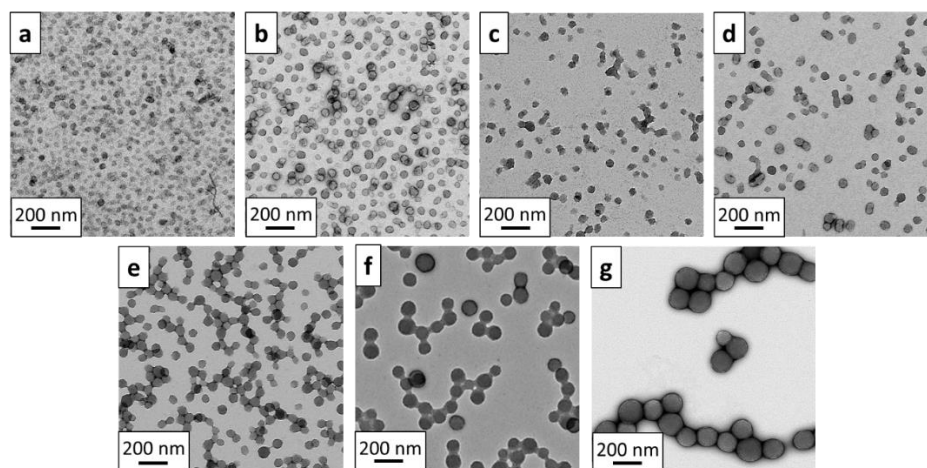
Fig. 4.11. Representative TEM images obtained for (a) $PATAC_{100}$-$PDAAM_{100}$ (b) $PATAC_{100}$-$PDAAM_{300}$ (c) $PATAC_{100}$-$PDAAM_{500}$ (d) $PATAC_{100}$-$PDAAM_{700}$ (e) $PATAC_{100}$-$PDAAM_{1000}$ (f) $PATAC_{100}$-$PDAAM_{1500}$ (g) $PATAC_{100}$-$PDAAM_{2000}$.

Zeta potential measurements were conducted on each of the seven aqueous dispersions of $PATAC_{100}$-$PDAAM_z$ spherical nanoparticles (where z = 100 – 2000) dispersed in 1.0 mM KCl at pH 7-8, see Table 4.1. In each case, these nanoparticles proved to be highly cationic, exhibiting zeta potentials of at least +33 mV with little or no particle size dependence.

4.2.5 Salt Tolerance of ([*n*] PATAC + [1-*n*] PDMAC)-PDAAM Dispersions

A 20 % w/w aqueous dispersion of $PATAC_{100}$-$PDAAM_{1500}$ nanoparticles was diluted to 0.1 % w/w *via* hand-mixing for 10 min using aqueous KCl solutions ranging from 1.0 to 4.0 M. DLS analysis was conducted on these dispersions using literature data to calculate the relatively high solution viscosity in each case.[44] The intensity-average particle diameters are provided in Figure 4.12. DLS is strongly biased towards the presence of aggregates because the scattered light intensity scales as the sixth power of the particle radius.[45] Hence, a 50 nm particle will scatter 10^6 as much light as a 5 nm particle. Thus it is well-known that this technique is well-suited for assessing the incipient flocculation of various types of colloidal dispersions.[46–49] In the present work, aqueous dispersions were judged to be colloidally unstable if a significant increase in their intensity-average particle diameter and DLS polydispersity index (which is expressed as a standard deviation) was observed.

The $PATAC_{100}$-$PDAAM_{1500}$ nanoparticles remained colloidally stable in the presence of 1.0 to 4.0 M KCl. In fact, a modest reduction in intensity-average particle diameter was observed compared to that obtained for the same dispersion in 1.0 mM KCl (from 154 ± 44 nm in 1.0 mM KCl to 134 ± 53 nm in 4.0 M KCl). This is attributed to efficient electrostatic screening in the highly salty media which leads to relaxation of the initially highly stretched cationic $PATAC_{100}$ stabiliser chains and hence a thinner coronal layer.[50]

Fig. 4.12. Plot of intensity-average DLS diameter against KCl concentration for 0.1 % w/w aqueous dispersions of $PATAC_{100}$-$PDAAM_{1500}$ nanoparticles prepared using aqueous KCl solutions ranging from 1 mM to 4.0 M (Standard deviations were calculated from the DLS PDI).

The $PATAC_{100}$-$PDAAM_{1500}$ nanoparticles exhibited excellent resistance towards flocculation even in the presence of 4.0 M KCl. In view of this observation, these dilute aqueous dispersions were stirred for 115 days at 20 ˚C with their colloidal stability being periodically monitored by DLS analysis, see Figure 4.13.

Fig. 4.13. Plot of intensity-average DLS diameter against time for 0.1 % w/w aqueous dispersions of $PATAC_{100}$-$PDAAM_{1500}$ nanoparticles prepared using aqueous KCl solutions ranging from 1.0 M to 4.0 M (Standard deviations were calculated from the PDI determined by DLS).

After almost four months ageing under such conditions, no significant increase in apparent particle size was observed for these PATAC$_{100}$-PDAAM$_{1500}$ nanoparticles. Thus, further salt resistance studies were conducted using 1.0 to 4.0 M ammonium sulfate. The molar ionic strength (*I*) of this 1:2 salt is significantly higher than that of a 1:1 electrolyte such as KCl according to Equation 4.1 where *c* is the molar concentration of ion *i* and *z* is the charge of ion *i*.[51]

$$I = \frac{1}{2} \sum_{i=1}^{n} c_i z_i^2 \qquad \textbf{4.1}$$

The initial 20 % w/w aqueous dispersion of PATAC$_{100}$-PDAAM$_{1500}$ nanoparticles was diluted to 0.1 % w/w using up to 4.0 M ammonium sulfate and mixed for 10 minutes prior to DLS analysis, see Figure 4.14.
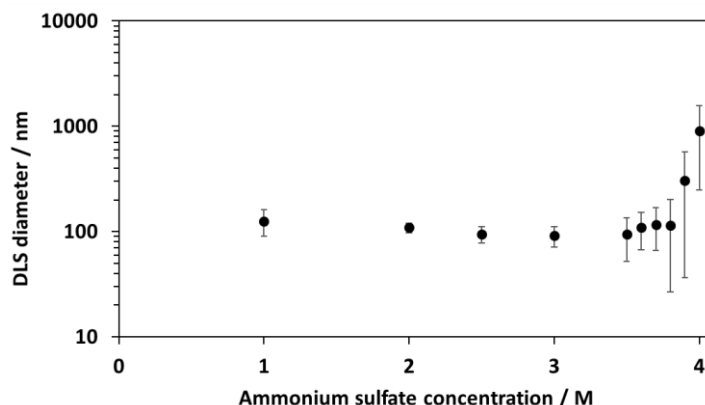
Fig. 4.14. Plot of intensity-average DLS diameter against ammonium sulfate concentration for 0.1 % w/w aqueous dispersions of PATAC$_{100}$-PDAAM$_{1500}$ nanoparticles prepared using aqueous ammonium sulfate solutions ranging from 1.0 to 4.0 M (Standard deviations were calculated from the PDI determined by DLS).

Remarkably, colloidal stability was retained up to 3.0 M ammonium sulfate. However, an increase in the dispersity of the nanoparticles was observed in 3.5 – 3.8 M ammonium sulfate. Aggregation was eventually observed at 3.9 M and 4.0 M ammonium sulfate,

with floccations of 305 ± 269 nm and 906 ± 659 nm respectively being formed under such conditions. It is perhaps worth emphasizing that this demonstration of colloidal stability in the presence of 3.0 M ammonium sulfate compares quite favourably with several recent reports of salt-tolerant nanoparticles.[9,10,14,15]

The PATAC$_{100}$-PDAAM$_{1500}$ nanoparticles were aged for 115 days at 20 °C in up to 4.0 M ammonium sulfate, see Figure 4.15. At the highest salt concentration, nanoparticle flocculation was observed immediately. However, nanoparticles dispersed in up to 3.0 M ammonium sulfate exhibited no significant increase in apparent particle size after 115 days, indicating high resistance towards flocculation under such conditions.
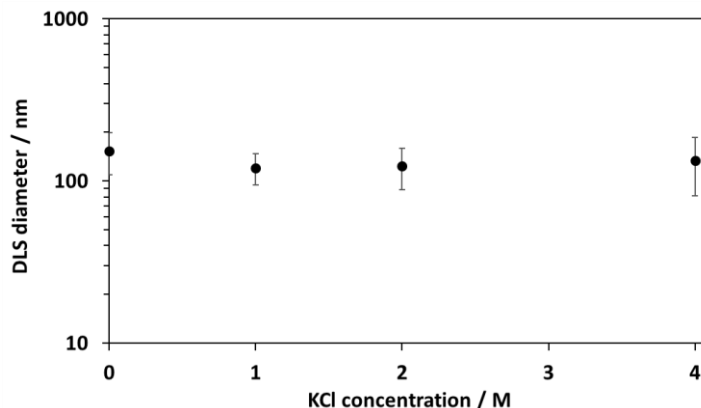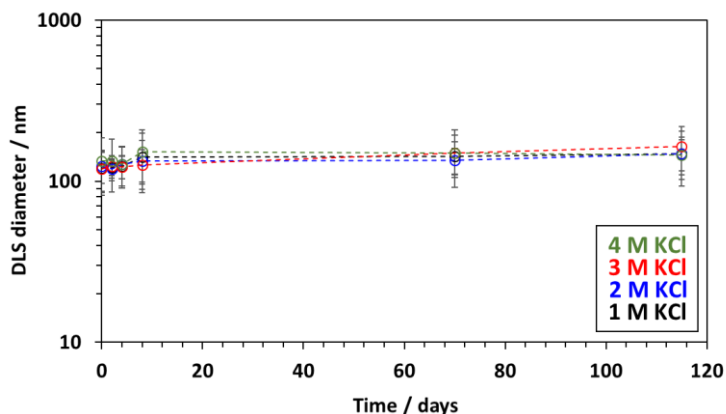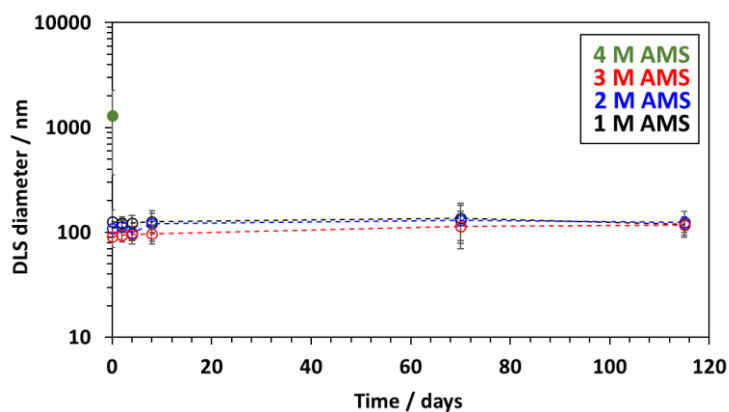

Fig. 4.15. Plot of intensity-average DLS diameter against time for 0.1 % w/w aqueous dispersions of PATAC$_{100}$-PDAAM$_{1500}$ nanoparticles prepared using aqueous ammonium sulfate (AMS) solutions ranging from 1.0 to 4.0 M (Standard deviations were calculated from the PDI determined by DLS).

On systematically varying *n* from 0.00 to 1.00 at a fixed *z* value of 1500, the zeta potential determined at pH 7 increased from essentially zero (+1 mV) when using the non-ionic PDMAC$_{67}$ stabiliser block alone to +16 mV at $n = 0.10$, +28 mV at $n = 0.25$ and +32 mV at $n = 0.50$. Thereafter, no significant change in zeta potential was observed for the $0.5 < n \leq 1.00$ interval (see entries 6 and 8 – 12 in Table 4.1). Clearly, incorporating further

cationic $PATAC_{100}$ chains into the sterically-stabilised nanoparticles has no discernible additional effect on their electrophoretic behaviour.

The salt resistance of a series of aqueous dispersions of ($[n]$ $PATAC_{100}$ + $[1-n]$ $PDMAC_{67}$)-$PDAAM_{1500}$ nanoparticles was examined when varying n from 0.00 to 1.00. As-synthesised 20 % w/w nanoparticle dispersions were diluted to 0.1 % w/w using aqueous KCl solutions ranging from 1 mM up to 4.0 M, see Figure 4.16.
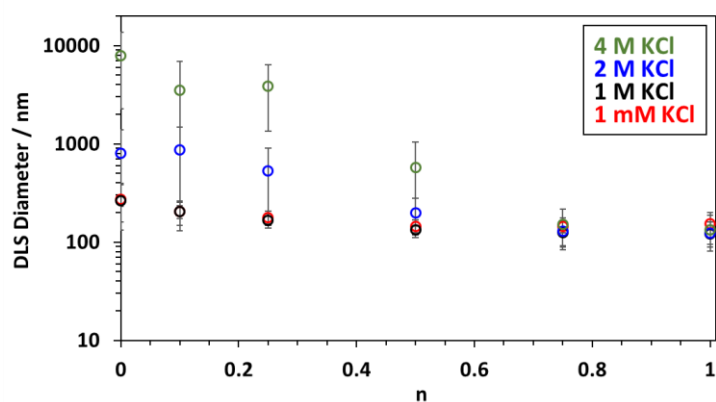
Fig. 4.16. Apparent DLS diameters determined for 0.1 % w/w aqueous dispersions of ($[n]$ $PATAC_{100}$ + $[1-n]$ $PDMAC_{67}$)-$PDAAM_{1500}$ spherical nanoparticles after 10 minutes of mixing in either 0.001, 1.0, 2.0 or 4.0 M KCl, where n is varied from 0.00 to 1.00 (Standard deviations were calculated from the PDI determined by DLS).

In all cases, the ($[n]$ $PATAC_{100}$ + $[1-n]$ $PDMAC_{67}$)-$PDAAM_{1500}$ nanoparticles proved to be colloidally stable on dilution with 1.0 M KCl within 10 min of their addition to the concentrated salt solution. However, only those nanoparticles containing a relatively high proportion of cationic PATAC stabiliser chains (i.e. $n = 0.75$ or $n = 1.00$) remained colloidally stable when diluted using 2.0 or 4.0 M KCl. This is perhaps surprising given the relatively high cationic zeta potentials determined in the presence of 1.0 mM KCl for those nanoparticles prepared using $n \geq 0.25$. This suggests that the colloidal stability

depends on a sufficiently high charge density within the coronal stabiliser layer, rather than the nanoparticle zeta potential.

4.2.6 Colloidal Stability at 90 °C

For applications such as enhanced oil recovery, good colloidal stability is required at elevated temperatures for extended time periods.[7–13] Hence the colloidal stability of $PATAC_{100}$-$PDAAM_{1500}$ nanoparticles was also briefly investigated at 90 °C. The as-synthesised 20 % w/w copolymer dispersion was diluted to 0.1 % w/w using aqueous KCl solutions ranging from 1.0 mM to 4.0 M. These dilute aqueous dispersions were aged for six days at 90 ˚C with their colloidal stability being periodically monitored by DLS analysis, see Figure 4.17. Literature values were used for the solution viscosities of 1.0 - 4.0 M KCl aqueous solutions at 90 ˚C.[52]
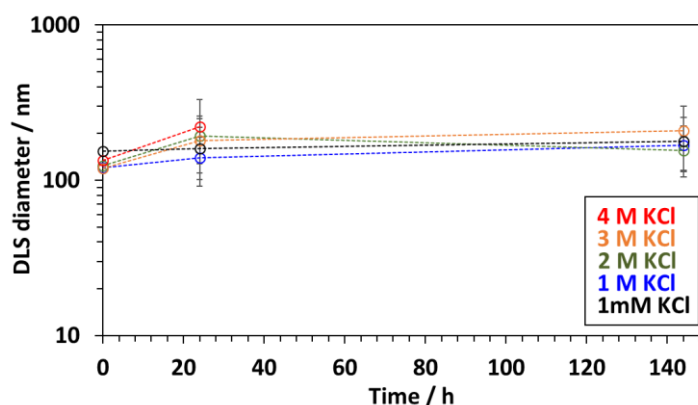
Fig. 4.17. Plot of intensity-average DLS diameter against time at 90 °C for 0.1 % w/w aqueous dispersions of $PATAC_{100}$-$PDAAM_{1500}$ nanoparticles prepared using aqueous KCl solutions ranging from 1.0 mM to 4.0 M (Standard deviations were calculated from the PDI determined by DLS).

After 6 days at 90 °C, the dispersions diluted with 1.0 mM to 3.0 M KCl remained stable. However, the 4.0 M KCl dispersion only remained stable for 24 hours at 90 °C after which flocculation occurred which made the sample unsuitable for DLS analysis. However, these results still compare favourably with those stated in the recent literature.[10–13]

4.2.7 Covalent Stabilisation of Diblock Copolymer Spheres

In principle, covalent stabilisation of the PDAAM-based nanoparticles prepared in this study can be achieved by reaction of ADH with the pendent ketone groups located within the hydrophobic core-forming PDAAM block.[38] Accordingly, selected ($[n]$ PATAC$_{100}$ + $[1\text{-}n]$ PDMAC$_{67}$)-PDAAM$_{1500}$ spheres were crosslinked using the protocol reported in Chapter 2: ADH was added to 20 % w/w aqueous copolymer dispersions (DAAM/ADH molar ratio = 10), which were then stirred for 6 h at 20 °C. TEM and DLS studies were conducted on (i) dilute aqueous dispersions of the spherical nanoparticles before cross-linking and (ii) dilute methanolic dispersions of the same nanoparticles after cross-linking, see Figure 4.18 and Table 4.2. The latter protocol confirmed that the crosslinked nanoparticles remained intact in methanol, which is a good solvent for PDAAM, in all cases. Such covalent stabilisation may be useful for enhanced oil recovery, because it should provide access to physically robust nanoparticles that can remain intact under demanding conditions (e.g. high pressure, elevated temperature and strong salinity).
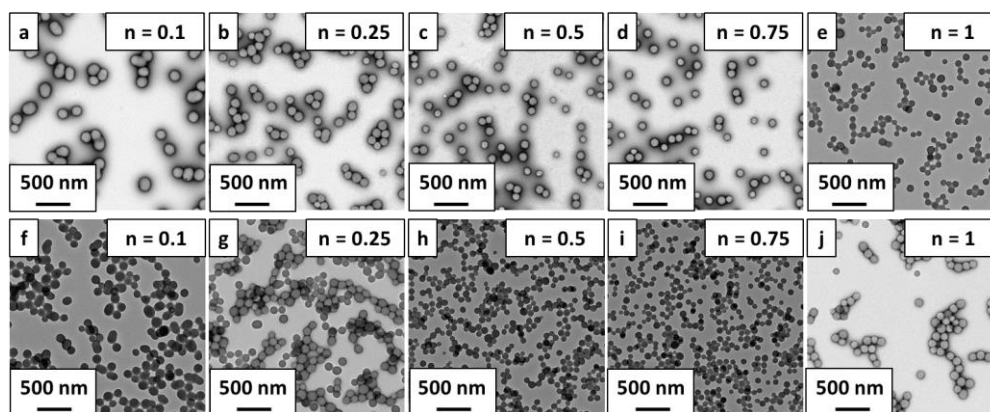
Fig. 4.18. TEM images obtained for ($[n]$ PATAC$_{100}$ + $[1\text{-}n]$ PDMAC$_{67}$)-PDAAM$_{1500}$ diblock copolymer 0.1% w/w nanoparticle dispersions where (a-e) are aqueous dispersions before cross-linking and (f-j) are methanolic dispersions after cross-linking with ADH at a DAAM/ADH molar ratio = 10.

Table 4.2. Intensity-average particle diameters obtained for ([*n*] PATAC$_{100}$ + [1-*n*] PDMAC$_{67}$)-PDAAM$_{1500}$ diblock copolymer 0.1% w/w nanoparticle dispersions in water before crosslinking and methanol after crosslinking.

n	Aqueous dispersion[a] DLS diameter[c] / nm	Methanolic dispersion[b] DLS diameter[c] / nm
0.10	188 ± 37	215 ± 19
0.25	158 ± 26	175 ± 23
0.50	144 ± 21	153 ± 24
0.75	144 ± 19	149 ± 22
1.00	163 ± 24	167 ± 17

[a] 0.1% w/w nanoparticle aqueous dispersion before cross-linking. [b] 0.1% w/w nanoparticle methanolic dispersion after cross-linking with ADH at a DAAM/ADH molar ratio = 10. [c] Intensity-average diameter determined by DLS analysis of 0.1 % copolymer dispersions at 20 °C in 1.0 mM KCl obtained using the Stokes-Einstein equation. Errors were calculated using the polydispersity index (PDI) ($Error = \sqrt{PDI} \times DLS\ diameter$).

4.2.8 Synthesis of Cationic Block Copolymer Worms and Vesicles

The synthesis of so-called 'higher-order' morphologies such as worms and vesicles *via* PISA requires the efficient 1D fusion of spheres on the time scale of the RAFT dispersion polymerisation.[28,29,35,53] Since electrosteric stabilisation strongly inhibits such sphere-sphere fusion events, it is inherently difficult to produce worms and vesicles by chain extension of a polyelectrolytic homopolymer precursor.[39–42] However, worms and vesicles can be readily produced by chain extension of a judicious binary mixture of cationic and non-ionic precursors.[41,42]

In this present study, it was found that only spherical nanoparticles could be produced when a binary mixture of PATAC$_{100}$ and PDMAC$_{67}$ homopolymers was chain extended with DAAM ($x = 100 – 2000$) even when *n* was as low as 0.10 (see Table 4.1, entries 13-25). A monotonic increase in the mean sphere diameter was observed when increasing the PDAAM DP, see Figures 4.19 and 4.20a. The lack of higher-order morphologies is attributed to the steric barrier imposed by the relatively long PATAC and PDMAC stabiliser blocks.[37] Interestingly, the nanoparticle zeta potential was reduced from

+29 mV to +8 mV when increasing the PDAAM DP from 100 to 2000 for this series of (0.1 PATAC$_{100}$ + 0.9 PDMAC$_{67}$)-PDAAM$_x$ spheres, see Figure 4.20b. This is presumably because larger spheres possess lower surface charge densities as the inter-separation distance between neighbouring PATAC chains is increased.
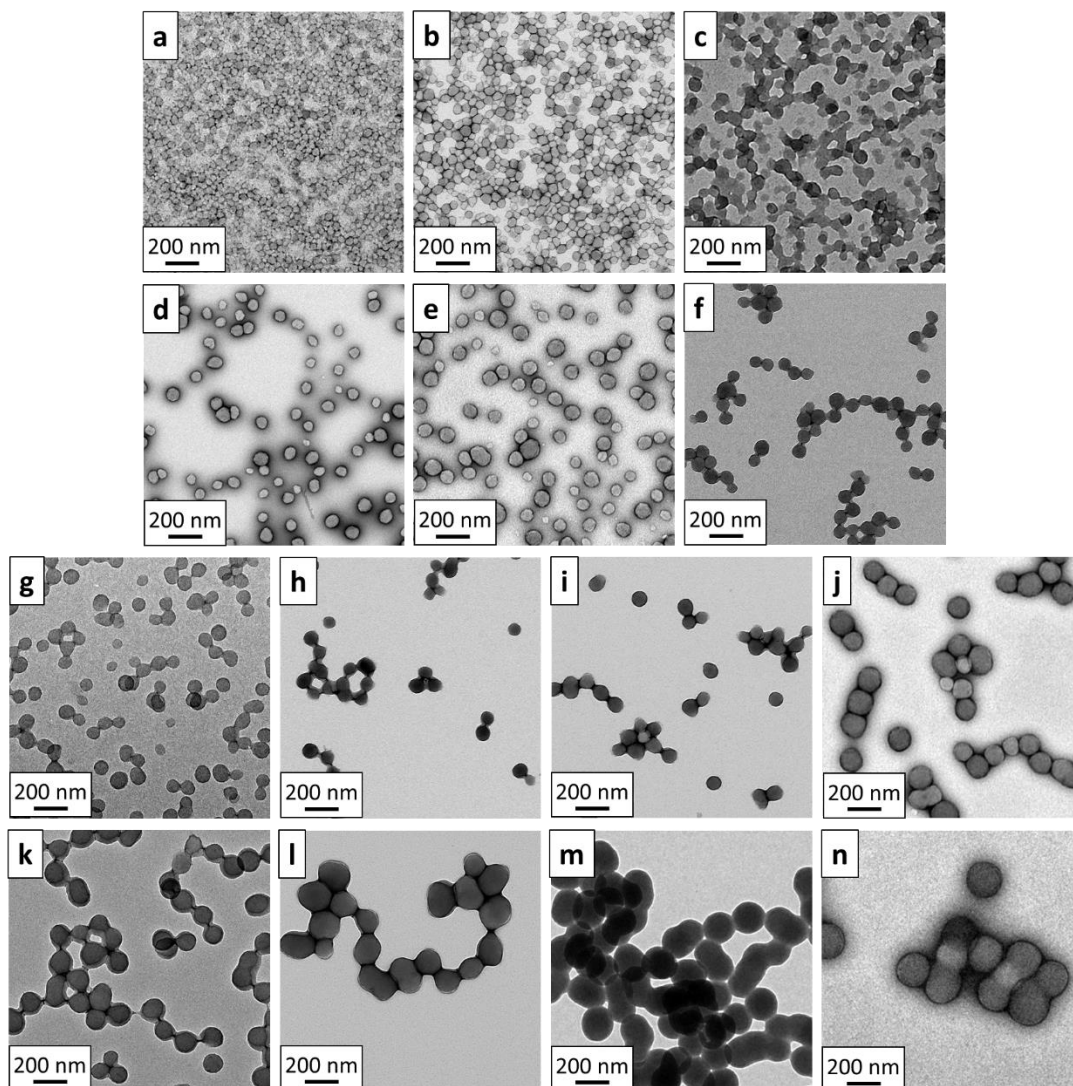
Fig. 4.19. Representative TEM images obtained for 0.1% w/w (0.1 PATAC$_{100}$ + 0.9 PDMAC$_{67}$)-PDAAM$_x$ diblock copolymer dispersions: a) $x = 100$ b) $x = 200$ c) $x = 300$ d) $x = 400$ e) $x = 500$ f) $x = 600$ g) $x = 700$ h) $x = 800$ i) $x = 900$ j) $x = 1000$ k) $x = 1250$ l) $x = 1500$ m) $x = 1750$ n) $x = 2000$.
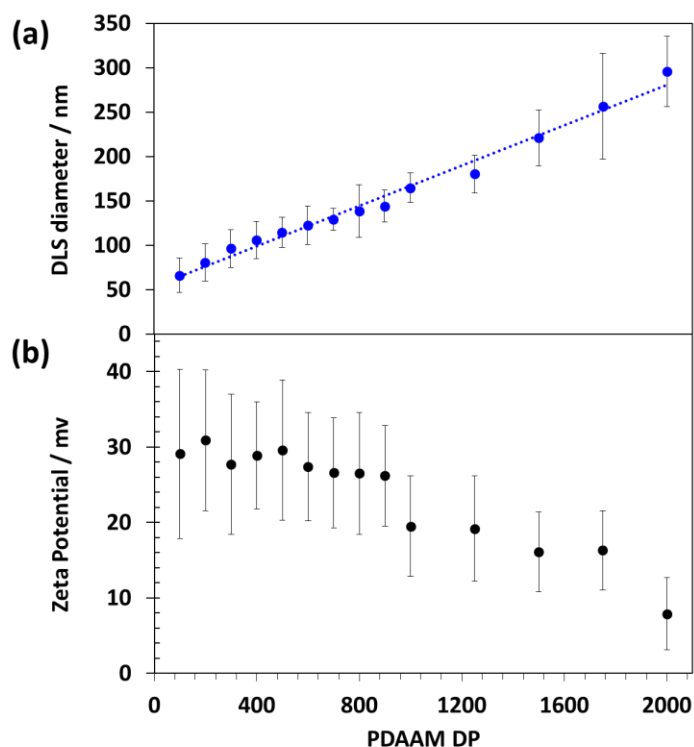
Fig. 4.20. (a) Relationship between intensity-average diameter, determined at 20 °C by DLS analysis of 0.10 % dispersions of (0.1 $PATAC_{100}$ + 0.9 $PDMAC_{67}$)-$PDAAM_x$ spheres in the presence of 1.0 mM KCl and PDAAM DP. Standard deviations were calculated using the DLS PDI (b) Relationship between zeta potential, determined at 20 °C by aqueous electrophoresis studies of 0.10 % dispersions of (0.1 $PATAC_{100}$ + 0.9 $PDMAC_{67}$)-$PDAAM_x$ spheres in the presence of 1.0 mM KCl at pH 7-8 and PDAAM DP.

It was found that a shorter PDMAC stabiliser block was required to allow access to higher order morphologies. Thus, chain extension of a binary mixture of 0.9 $PDMAC_{37}$ and 0.1 $PATAC_{100}$ targeting PDAAM DPs of 300 to 900 resulted in the formation of a series of well-defined vesicles (entries 27 - 29, Table 4.1, see Figure 4.21 for representative TEM images). Despite the relatively low $PATAC_{100}$ stabiliser density within the coronal layer, such vesicles proved to be highly cationic, with zeta potentials ranging from +34 mV to +40 mV. The (0.1 $PATAC_{100}$ + 0.9 $PDMAC_{37}$)-$PDAAM_{900}$ vesicles were selected for salt tolerance studies. An as-synthesised 20 % w/w dispersion was diluted to

0.1% w/w using a series of aqueous KCl solutions ranging from 1.0 mM to 4.0 M. The DLS data indicate that these cationic vesicles remained reasonably stable in the presence of up to 1.0 M KCl but significant flocculation was observed at higher salt concentrations, see Figure 4.21d. This is not surprising given that markedly lower salt tolerance was also observed for cationic spheres prepared using a binary mixture of 0.10 PATAC and 0.90 PDMAC stabiliser blocks.
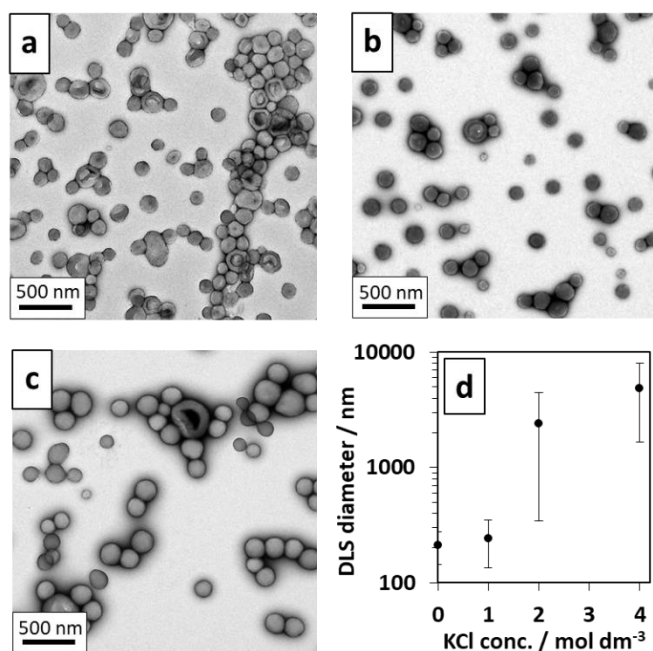
Fig. 4.21. Representative TEM images obtained for
(a) $(0.1 \text{ PATAC}_{100} + 0.9 \text{ PDMAC}_{37})\text{-PDAAM}_{300}$ vesicles,
(b) $(0.1 \text{ PATAC}_{100} + 0.9 \text{ PDMAC}_{37})\text{-PDAAM}_{600}$ vesicles and
(c) $(0.1 \text{ PATAC}_{100} + 0.9 \text{ PDMAC}_{37})\text{-PDAAM}_{900}$ vesicles d) Apparent DLS diameter
against KCl concentration for a 0.1% w/w dispersion of
$(0.1 \text{ PATAC}_{100} + 0.9 \text{ PDMAC}_{37})\text{-PDAAM}_{900}$ vesicles prepared by diluting the
as-synthesised 20% w/w vesicle dispersion using a range of KCl solutions.

Cationic worms could also be prepared by using a binary mixture of 0.1 PATAC_{91} and 0.9 PDMAC_{37} precursors to target a PDAAM DP of 90. As expected, these worms formed a free-standing gel owing to multiple inter-worm contacts.[54] The worms proved to be

highly cationic with a zeta potential of +33 mV being observed in 1.0 mM KCl (see entry 26, Table 4.1). A representative TEM image is provided in Figure 4.22 (see inset). The salt tolerance of these (0.1 PATAC$_{91}$ + 0.9 PDMAC$_{37}$)-PDAAM$_{90}$ worms was assessed by DLS, see Figure 4.22. The as-synthesised 20 % w/w worm dispersion was diluted to 0.1 % w/w using aqueous KCl solutions ranging from 1.0 mM to 4.0 M and mixed for 10 min prior to analysis. The worms remained colloidally stable up to 2.0 M KCl, with significant flocculation being observed at higher salt concentrations. This colloidal stability is surprising given that spheres and vesicles prepared with the same PATAC mole fraction flocculated in 2.0 M KCl. This is an interesting result given that worm-like micelles have been shown to be more efficient thickeners than water-soluble polymers and are currently being investigated for the oil industry.[55–57]
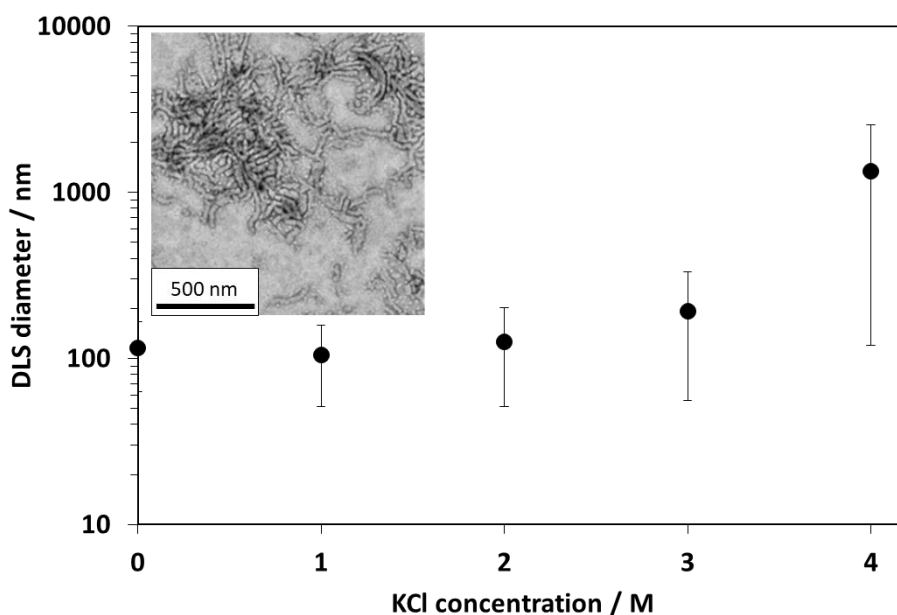
Fig. 4.22. (a) Representative TEM image obtained for (0.1 PATAC$_{91}$ + 0.9 PDMAC$_{37}$)-PDAAM$_{90}$ worms. (b) Apparent DLS diameter against KCl concentration for a 0.1% w/w aqueous dispersion of (0.1 PATAC$_{91}$ + 0.9 PDMAC$_{37}$)-PDAAM$_{90}$ worms prepared by diluting the as-synthesised 20% w/w worm dispersion using a range of KCl solutions.

4.3 Conclusions

A series of new cationic diblock copolymer spherical nanoparticles have been prepared *via* RAFT aqueous dispersion polymerisation of DAAM using either a quaternised PATAC precursor as a steric stabiliser block or a binary mixture of this cationic precursor plus a non-ionic PDMAC steric stabiliser. These nanoparticles exhibited surprisingly strong resistance towards flocculation in highly salty aqueous media. In particular, DLS studies confirmed that highly cationic spheres prepared using PATAC as the sole steric stabiliser remained colloidally stable in the presence of either 4.0 M KCl or 3.0 M ammonium sulfate for almost four months when stored at 20 °C. Moreover, this nanoparticle dispersion remained stable in 3.0 M KCl at 90 °C for six days. However, spheres prepared using binary mixtures of both PATAC and PDMAC stabiliser blocks proved to be significantly less tolerant towards added salt, despite exhibiting similarly cationic zeta potentials. Thus the latter parameter is not necessarily a good predictor of salt tolerance for such colloidal dispersions. Moreover, cationic block copolymer worms and vesicles could also be prepared using this PISA formulation by utilising a relatively low mol fraction of the cationic PATAC block as a steric stabiliser. These latter dispersions also exhibited reasonably good salt tolerance, with worms retaining their colloidal stability in the presence of up to 2.0 M KCl while vesicles resisted flocculation up to 1.0 M KCl. Such nanoparticles are likely to be excellent model systems for understanding the behaviour of aqueous colloidal dispersions in the presence of relatively high concentrations of electrolyte. Finally, we report the facile cross-linking of the $([n]\,\text{PATAC}_{100} + [1\text{-}n]\,\text{PDMAC}_{67}) - \text{PDAAM}_{1500}$ diblock copolymer spheres by reaction of ADH with the pendent ketone groups in the PDAAM block using the protocol reported in Chapter 2.

4.4 Experimental

4.4.1 Materials

DMAC ($\geq$ 98.5 %), DDMAT (98 %), dioxane and AIBA (97 %) were purchased from Sigma-Aldrich UK and used as received. DAAM (99 %) and ADH ($\geq$ 98 %) were purchased from Alfa Aesar (UK) and were used as received. AIBN (98 %) was purchased from Molekula (UK) and was used as received. VA-044 was purchased from Wako Chemicals (Japan) and was used as received. Diethyl ether, KCl ($\geq$ 99 %) and ammonium sulfate ($\geq$ 99 %) were purchased from VWR Chemicals. DCM, methanol and acetonitrile were purchased from Fisher Scientific (UK). All solvents were HPLC-grade. Deuterated methanol was purchased from Cambridge Isotope Laboratories (UK). Finally, ATAC was kindly donated by BASF (Germany) in the form of an 80 % w/w aqueous solution.

4.4.2 Synthesis of PDMAC *via* RAFT Solution Polymerisation

A typical protocol for the synthesis of a PDMAC$_{67}$ precursor was conducted as follows. Me-DDMAT (2.00 g, 5.30 mmol), AIBN (87.0 mg 0.53 mmol, Me-DDMAT/AIBN molar ratio = 10), and DMAC (34.12 g, 0.34 mol) were weighed into a 500 mL round-bottom flask. Dioxane (84.5 mL) was added to produce a 30 % w/w solution, which was purged with nitrogen for 1 h. The sealed flask was immersed into an oil bath set at 70 °C for 25 minutes and the polymerisation was subsequently quenched by immersing the flask in an ice bath, followed by exposure to air. The final DMAC conversion was 95%, as judged by ^{1}H NMR spectroscopy. The crude polymer was purified by precipitation into a ten-fold excess of diethyl ether (twice). The resulting PDMAC homopolymer was isolated by filtration and dissolved in deionised water, any residual diethyl ether/dioxane was removed under reduced pressure, and the resulting aqueous solution was freeze-dried for 48 h. The purified PDMAC precursor was obtained as a yellow solid. End-group analysis using UV-visible absorption spectroscopy indicated a mean DP of 67. DMF GPC analysis

indicated an M_n of 7 400 g mol^{-1} and an M_w/M_n of 1.14. A PDMAC$_{37}$ was also prepared using the same protocol. In this case DMF GPC analysis indicated an M_n of 3 400 g mol^{-1} and an M_w/M_n of 1.15.

4.4.3 Synthesis of PATAC *via* RAFT Solution Polymerisation

A typical protocol for the synthesis of a PATAC$_{100}$ precursor was conducted as follows. Me-DDMAT (0.600 g, 1.58 mmol), VA-044 (0.10 g 0.317 mmol, Me-DDMAT/VA-044 molar ratio = 5.0), and ATAC (30.69 g, 0.13 mol, supplied as an 80% aqueous solution) were weighed into a 250 mL round-bottom flask. Methanol (94.45 mL) and water (0.43 mL) were added to produce a 20% w/w solution, which was purged with nitrogen for 1 h. The sealed flask was immersed into an oil bath set at 44 °C for 2 h and the polymerisation was subsequently quenched by immersing the flask in ice, followed by exposure to air. The final ATAC conversion was 96%, as judged by ^{1}H NMR spectroscopy. Methanol was removed under reduced pressure, followed by purification of the polymer by precipitation into a ten-fold excess of acetonitrile. The precipitate was redissolved in water and precipitated once more into excess acetonitrile. The crude PATAC was dissolved in deionised water, any residual solvent was removed under reduced pressure, and the resulting aqueous solution was freese-dried for 48 h. The purified PATAC was obtained as a yellow solid. End-group analysis using UV-visible absorption spectroscopy indicated a mean DP of 100. DMF GPC analysis indicated M_n and M_w/M_n values of 29 500 g mol^{-1} and an M_w/M_n of 1.19, respectively. A PATAC$_{91}$ precursor was prepared using the same protocol. Aqueous GPC analysis indicated an M_n of 25 800 g mol^{-1} and an M_w/M_n of 1.14.

4.4.4 Synthesis of (0.9 PDMAC$_{67}$ + 0.1 PATAC$_{100}$)-PDAAM$_{1500}$ Diblock Copolymer Spheres by RAFT Aqueous Dispersion Polymerisation

The typical protocol for the synthesis of (0.9 PDMAC$_{67}$ + 0.1 PATAC$_{100}$)-PDAAM$_{1500}$ spheres at 20% w/w solids was conducted as follows. The PDMAC$_{67}$ precursor (0.8 g, 0.114 mmol), PATAC$_{100}$ precursor (0.25 g, 0.013 mmol), AIBA initiator (3.40 mg, 0.013 mmol, [PDMA$_{67}$ + PATAC$_{100}$]/AIBA molar ratio = 10) and DAAM monomer (32.14 g, 0.19 mol; target DP = 1500) were weighed into a 250 mL round-bottomed flask. Deionised water (131.8 mL) was then added to afford a 20% w/w aqueous solution, which was degassed for 1 h at 4 °C prior to immersion in an oil bath set at 56 °C. This reaction solution was stirred for 18 h and then quenched by exposure to air. The DAAM monomer conversion was more than 99% as judged by ^{1}H NMR spectroscopy. All other PISA syntheses were conducted at 20 % w/w solids using the same protocol. A summary of the characterisation data for all of the ([*n*] PATAC$_x$ + [1-*n*] PDMAC$_y$)-PDAAM$_z$ diblock copolymers prepared in this study is provided in Table 4.1.

4.4.5 Post-polymerisation Cross-linking of Diblock Copolymer Spheres

The following protocol was used for cross-linking spherical nanoparticles. A 20 % w/w aqueous dispersion of (0.9 PDMAC$_{67}$ + 0.1 PATAC$_{100}$)-PDAAM$_{1500}$ spheres (99.0 g) prepared using the previously stated protocol was adjusted to pH 4 using HCl. This nanoparticle dispersion was added to a 250 mL round-bottomed flask along with ADH (ADH; 1.99 g, 11.4 mmol, DAAM/ADH molar ratio = 10.0) and the reaction solution was stirred at 25 °C for 6 h.

4.4.6 Polymer Characterisation

^{1}H NMR Spectroscopy

All NMR spectra were recorded using a 400 MHz Bruker Avance III HD 400 spectrometer in CD$_3$OD at 25 °C. Typically, 64 scans were required to ensure high-quality spectra.

End-Group Analysis via UV−Visible Absorption Spectroscopy

UV−visible absorption spectra were recorded between 200 and 800 nm using a PC-controlled UV-1800 spectrophotometer operating at 25 °C and equipped with a 1 cm path length quartz cell. A Beer−Lambert curve was constructed using a series of eighteen Me-DDMAT solutions of varying concentration in methanol. The absorption maximum at 308 nm assigned to the trithiocarbonate end-group[58] was used for this calibration plot, and Me-DDMAT concentrations were selected such that the absorbance always remained below unity. The mean DPs for the PDMAC and PATAC stabilisers were determined using the molar extinction coefficient of 15 740 ± 80 mol^{-1} dm^3 cm^{-1} calculated for Me-DDMAT.

Gel Permeation Chromatography (GPC)

The MWD for the PATAC stabiliser block was assessed using aqueous GPC. An acidic aqueous buffer containing 0.5 M acetic acid and 0.3 M NaH$_2$PO$_4$ was adjusted to pH 2 using concentrated HCl and used as an eluent for aqueous GPC analysis of the cationic PATAC precursor. The GPC instrument comprised an Agilent 1260 Infinity series degasser and pump, two Agilent PL 8 µm Aquagel-OH 30 columns and one 8 µm Aquagel-OH 40 column in series. These columns were calibrated using ten near-monodisperse poly(ethylene oxide) standards ranging from 1080 g mol^{-1} to 905 000 g mol^{-1}. A refractive index detector operating at 30 °C was used at a flow rate of 1.0 mL min^{-1}.

The molecular weight distribution of the PDMAC stabiliser block and the PDMAC-PDAAM copolymer were assessed using DMF GPC. The GPC instrument comprised two Agilent PL gel 5 μm Mixed-C columns and a guard column connected in series to an Agilent 1260 Infinity GPC system equipped with both refractive index and UV−visible detectors (only the refractive index detector used) operating at 60 °C. The GPC eluent was HPLC-grade DMF containing 10 mM LiBr at a flow rate of 1.0 mL min^{-1} and DMSO was used as a flow-rate marker. Calibration was achieved using a series of ten near-monodisperse poly(methyl methacrylate) standards (ranging in M_{p} from 625 to 618 000 g mol^{-1}). Chromatograms were analysed using Agilent GPC/SEC software.

Transmission Electron Microscopy (TEM)

Copper/palladium TEM grids (Agar Scientific, UK) were coated in-house to yield a thin film of amorphous carbon. The coated grids were then subjected to a glow discharge for 30 s. Individual 10.0 μL droplets of 0.1% w/w aqueous copolymer dispersions were placed on freshly-treated grids for 1 min and then carefully blotted with filter paper to remove excess solution. To ensure sufficient electron contrast, uranyl formate (9.0 μL of a 0.75% w/w solution) was absorbed onto the sample-loaded grid for 20 s and then carefully blotted to remove excess stain. Each grid was then dried using a vacuum hose. Imaging was performed using a FEI Tecnai Spirit 2 microscope fitted with an Orius SC1000B camera operating at 80 kV.

Dynamic Light Scattering (DLS) at 20 °C

All measurements were made on 0.1% w/w aqueous copolymer dispersions in 1.0 cm cuvette cells; scattered light was detected at 173° and data were averaged over three consecutive runs. Sphere-equivalent intensity-average diameters were calculated for diblock copolymer nano-objects *via* the Stokes−Einstein equation, which assumes perfectly monodisperse, non-interacting spheres. According to its manufacturer, this

Nano ZS instrument set-up has an upper limit particle diameter of approximately 6 μm. The solution viscosity was taken to be that of pure water for nanoparticles prepared in 1.0 mM KCl. For DLS studies performed in the presence of higher salt concentrations, the solution viscosity was calculated for each salt concentration using literature data, see Table 4.3.[44]

Table 4.3. KCl and ammonium sulfate solution viscosities used for DLS analysis at 20 °C.[44]

Salt	Concentration / M	Viscosity / Pa s
KCl	1.0	0.9912
KCl	2.0	0.9964
KCl	3.0	1.0246
KCl	4.0	1.0403
AMS	1.0	1.2559
AMS	2.0	1.6497
AMS	2.5	2.0868
AMS	3.0	2.5303
AMS	3.5	2.9415
AMS	3.6	3.1055
AMS	3.7	3.1055
AMS	3.8	3.2764
AMS	3.9	3.4540
AMS	4.0	3.6383

Dynamic Light Scattering (DLS) at 90 °C

All measurements were made on 0.1% w/w aqueous copolymer dispersions in 1.0 cm cuvette cells; scattered light was detected at 173° and data were averaged over three consecutive runs. Sphere-equivalent intensity-average diameters were calculated for diblock copolymer nano-objects via the Stokes−Einstein equation, which assumes perfectly monodisperse, non-interacting spheres. According to its manufacturer, this Nano ZS instrument set-up has an upper limit particle diameter of approximately 6 μm. The solution viscosity was taken to be that of pure water for nanoparticles prepared in

1.0 mM KCl. For DLS studies performed in the presence of higher salt concentrations,

the solution viscosity was calculated for each salt concentration using literature data, see

Table 4.4.[52]

Table 4.4. KCl solution viscosities used for DLS analysis at 90 °C.[52]

Salt	Concentration / M	Viscosity / Pa s
KCl	1.0	0.3364
KCl	2.0	0.3480
KCl	3.0	0.3600
KCl	4.0	0.3723

Aqueous Electrophoresis

Zeta potentials were determined for 0.1% w/w aqueous copolymer dispersions at 20 °C

in the presence of 1.0 mM KCl using the Malvern Zetasizer Nano ZS instrument described

above using its default settings and a palladium Uzgiris-type dip electrode.[59] The

instrument uses the Smoluchowski model to calculate zeta potentials from electrophoretic

mobilities using the Henry equation.[60]

References

(1)   Selmi, F. Studi Sulla Dimensione Di Cloruro d'argento. *Nuovi Ann. delle Sci. Nat. di Bol.* **1845**, *IV*, 146.

(2)   Graham, T. On the Properties of Silicic Acid and Other Analogous Colloidal Substances. *J. Chem. Soc.* **1864**, No. 17, 318–327.

(3)   Derjaguin, B.; Landau, L. Theory of the Stability of Strongly Charged Lyophobic Sols and of the Adhesion of Strongly Charged Particles in Solution of Electrolytes. *Acta Physicochim. U.R.S.S* **1941**, *14*, 633–662.

(4)   Verwey, E.; Overbeek, Jt. *Theory of the Stability of Lyophobic Colloids*; Elsevier: Amsterdam, 1948.

(5)   Groves, R.; Routh, A. F. Film Deposition and Consolidation during Thin Glove Coagulant Dipping. *J. Polym. Sci. Part B Polym. Phys.* **2017**, *55*, 1633–1648.

(6)   Faraday, M. The Bakerian Lecture - Experimental Relations of Gold (and Other Metals) to Light. *Philos. Trans. R. Soc. A* **1857**, *147*, 145–181.

(7)   Kotsmar, C.; Yoon, K. Y.; Yu, H.; Ryoo, S. Y.; Barth, J.; Shao, S.; Prodanović, M.; Milner, T. E.; Bryant, S. L.; Huh, C.; et al. Stable Citrate-Coated Iron Oxide Superparamagnetic Nanoclusters at High Salinity. *Ind. Eng. Chem. Res.* **2010**, *49*, 12435–12443.

(8)   Hwang, C. C.; Wang, L.; Lu, W.; Ruan, G.; Kini, G. C.; Xiang, C.; Samuel, E. L. G.; Shi, W.; Kan, A. T.; Wong, M. S.; et al. Highly Stable Carbon Nanoparticles Designed for Downhole Hydrocarbon Detection. *Energy Environ. Sci.* **2012**, *5*, 8304–8309.

(9)   Bagaria, H. G.; Yoon, K. Y.; Neilson, B. M.; Cheng, V.; Lee, J. H.; Worthen, A. J.; Xue, Z.; Huh, C.; Bryant, S. L.; Bielawski, C. W.; et al. Stabilization of Iron Oxide Nanoparticles in High Sodium and Calcium Brine at High Temperatures with Adsorbed Sulfonated Copolymers. *Langmuir* **2013**, *29*, 3195–3206.

(10)   Bagaria, H. G.; Xue, Z.; Neilson, B. M.; Worthen, A. J.; Yoon, K. Y.; Nayak, S.; Cheng, V.; Lee, J. H.; Bielawski, C. W.; Johnston, K. P. Iron Oxide Nanoparticles Grafted with Sulfonated Copolymers Are Stable in Concentrated Brine at Elevated Temperatures and Weakly Adsorb on Silica. *ACS Appl. Mater. Interfaces* **2013**, *5*, 3329–3339.

(11)   Kini, G. C.; Yu, J.; Wang, L.; Kan, A. T.; Biswal, S. L.; Tour, J. M.; Tomson, M. B.; Wong, M. S. Salt- and Temperature-Stable Quantum Dot Nanoparticles for Porous Media Flow. *Colloids Surfaces A Physicochem. Eng. Asp.* **2014**, *443*, 492–500.

(12)   Ranka, M.; Brown, P.; Hatton, T. A. Responsive Stabilization of Nanoparticles for Extreme Salinity and High-Temperature Reservoir Applications. *ACS Appl. Mater. Interfaces* **2015**, *7*, 19651–19658.

(13)   Sun, X.; Zhang, Y.; Chen, G.; Gai, Z. Application of Nanoparticles in Enhanced Oil Recovery: A Critical Review of Recent Progress. *Energies* **2017**, *10*, 345.

(14)   Cho, M. S.; Yoon, K. J.; Song, B. K. Dispersion Polymerization of Acrylamide in

Aqueous Solution of Ammonium Sulfate : Synthesis and Characterisation. *J. Appl. Polym. Sci.* **2002**, *83*, 1397–1405.

(15) Aijun, G.; Yiran, G.; Lili, Z.; Jun, L.; Dong, L.; Peng, L. Preparation of Cationic Polyacrylamide Microsphere Emulsion and Its Performance for Permeability Reduction. *Pet. Sci.* **2014**, *11*, 408–416.

(16) Chiefari, J.; Chong, Y. K. B.; Ercole, F.; Krstina, J.; Jeffery, J.; Le, T. P. T.; Mayadunne, R. T. A.; Meijs, G. F.; Moad, C. L.; Moad, G.; et al. Living Free-Radical Polymerization by Reversible Addition-Fragmentation Chain Transfer: The RAFT Process. *Macromolecules* **1998**, *31*, 5559–5562.

(17) Qiu, J.; Charleux, B.; Matyjaszewski, K. Controlled/Living Radical Polymerization in Aqueous Media: Homogeneous and Heterogeneous Systems. *Prog. Polym. Sci.* **2001**, *26*, 2083–2134.

(18) Hill, M. R.; Carmean, R. N.; Sumerlin, B. S. Expanding the Scope of RAFT Polymerization: Recent Advances and New Horizons. *Macromolecules* **2015**, *48*, 5459–5469.

(19) Zhou, W.; Qu, Q.; Xu, Y.; An, Z. Aqueous Polymerization-Induced Self-Assembly for the Synthesis of Ketone-Functionalized Nano-Objects with Low Polydispersity. *ACS Macro Lett.* **2015**, *4*, 495–499.

(20) Mitsukami, Y.; Donovan, M. S.; Lowe, A. B.; McCormick, C. L. Water-Soluble Polymers. 81. Direct Synthesis of Hydrophilic Styrenic-Based Homopolymers and Block Copolymers in Aqueous Solution via RAFT. *Macromolecules* **2001**, *34*, 2248–2256.

(21) Lai, J. T.; Filla, D.; Shea, R. Functional Polymers from Novel Carboxyl-Terminated Trithiocarbonates as Highly Efficient RAFT Agents. *Am. Chem. Soc. Polym. Prepr. Div. Polym. Chem.* **2002**, *35*, 6754–6756.

(22) McCormick, C. L.; Lowe, A. B. Aqueous RAFT Polymerization: Recent Developments in Synthesis of Functional Water-Soluble (Co)Polymers with Controlled Structures. *Acc. Chem. Res.* **2004**, *37*, 312–325.

(23) Moad, G.; Rizzardo, E.; Thang, S. H. Living Radical Polymerization by the RAFT Process. *Aust. J. Chem.* **2005**, *58*, 379–410.

(24) Perrier, S.; Takolpuckdee, P. Macromolecular Design via Reversible Addition-Fragmentation Chain Transfer (RAFT)/Xanthates (MADIX) Polymerization. *J. Polym. Sci. Part A Polym. Chem.* **2005**, *43*, 5347–5393.

(25) Lowe, A. B.; McCormick, C. L. Reversible Addition-Fragmentation Chain Transfer (RAFT) Radical Polymerization and the Synthesis of Water-Soluble (Co)Polymers under Homogeneous Conditions in Organic and Aqueous Media. *Prog. Polym. Sci.* **2007**, *32*, 283–351.

(26) Zetterlund, P. B.; Kagawa, Y.; Okubo, M. Controlled/Living Radical Polymerization in Dispersed Systems. *Chem. Rev.* **2008**, *108*, 3747–3794.

(27) Zhang, X.; Boissé, S.; Zhang, W.; Beaunier, P.; D'Agosto, F.; Rieger, J.; Charleux, B. Well-Defined Amphiphilic Block Copolymers and Nano-Objects Formed in Situ via RAFT-Mediated Aqueous Emulsion Polymerization. *Macromolecules*

2011, *44*, 4149–4158.

(28)   Canning, S. L.; Smith, G. N.; Armes, S. P. A Critical Appraisal of RAFT-Mediated Polymerization-Induced Self-Assembly. *Macromolecules* **2016**, *49*, 1985–2001.

(29)   Warren, N. J.; Armes, S. P. Polymerization-Induced Self-Assembly of Block Copolymer Nano-Objects via RAFT Aqueous Dispersion Polymerization. *J. Am. Chem. Soc.* **2014**, *136*, 10174–10185.

(30)   Charleux, B.; Delaittre, G.; Rieger, J.; D'Agosto, F. Polymerization-Induced Self-Assembly: From Soluble Macromolecules to Block Copolymer Nano-Objects in One Step. *Macromolecules* **2012**, *45*, 6753–6765.

(31)   Derry, M. J.; Fielding, L. A.; Armes, S. P. Polymerization-Induced Self-Assembly of Block Copolymer Nanoparticles via RAFT Non-Aqueous Dispersion Polymerization. *Prog. Polym. Sci.* **2016**, *52*, 1–18.

(32)   Tan, J.; Sun, H.; Yu, M.; Sumerlin, B. S.; Zhang, L. Photo-PISA: Shedding Light on Polymerization-Induced Self-Assembly. *ACS Macro Lett.* **2015**, *4*, 1249–1253.

(33)   Jiang, Y.; Xu, N.; Han, J.; Yu, Q.; Guo, L.; Gao, P.; Lu, X.; Cai, Y. The Direct Synthesis of Interface-Decorated Reactive Block Copolymer Nanoparticles via Polymerisation-Induced Self-Assembly. *Polym. Chem.* **2015**, *6*, 4955–4965.

(34)   Zhou, D.; Dong, S.; Kuchel, R. P.; Perrier, S.; Zetterlund, P. B. Polymerization Induced Self-Assembly: Tuning of Morphology Using Ionic Strength and PH. *Polym. Chem.* **2017**, *8*, 3082–3089.

(35)   Khor, S. Y.; Quinn, J. F.; Whittaker, M. R.; Truong, N. P.; Davis, T. P. Controlling Nanomaterial Size and Shape for Biomedical Applications via Polymerization-Induced Self-Assembly. *Macromol. Rapid Commun.* **2019**, *40*, 1–22.

(36)   Karagoz, B.; Esser, L.; Duong, H. T.; Basuki, J. S.; Boyer, C.; Davis, T. P. Polymerization-Induced Self-Assembly (PISA)-Control over the Morphology of Nanoparticles for Drug Delivery Applications. *Polym. Chem.* **2014**, *5*, 350–355.

(37)   Blanazs, A.; Ryan, A. J.; Armes, S. P. Predictive Phase Diagrams for RAFT Aqueous Dispersion Polymerization: Effect of Block Copolymer Composition, Molecular Weight, and Copolymer Concentration. *Macromolecules* **2012**, *45*, 5099–5107.

(38)   Byard, S. J.; Williams, M.; Mckenzie, B. E.; Blanazs, A.; Armes, S. P. Preparation and Cross-Linking of All-Acrylamide Diblock Copolymer Nano-Objects via Polymerization-Induced Self-Assembly in Aqueous Solution. *Macromolecules* **2017**, *50*, 1482–1493.

(39)   Semsarilar, M.; Ladmiral, V.; Blanazs, A.; Armes, S. P. Anionic Polyelectrolyte-Stabilized Nanoparticles via RAFT Aqueous Dispersion Polymerization. *Langmuir* **2012**, *28*, 914–922.

(40)   Semsarilar, M.; Ladmiral, V.; Blanazs, A.; Armes, S. P. Cationic Polyelectrolyte-Stabilized Nanoparticles via RAFT Aqueous Dispersion Polymerization. *Langmuir* **2013**, *29*, 7416–7424.

(41)   Williams, M.; Penfold, N. J. W.; Lovett, J. R.; Warren, N. J.; Douglas, C. W. I.;

Doroshenko, N.; Verstraete, P.; Smets, J.; Armes, S. P. Bespoke Cationic Nano-Objects via RAFT Aqueous Dispersion Polymerisation. *Polym. Chem.* **2016**, *7*, 3864–3873.

(42)   Penfold, N.; Ning, Y.; Verstraete, P.; Smets, J.; Armes, S. P. Cross-Linked Cationic Diblock Copolymer Worms Are Superflocculants for Micrometer-Sized Silica Particles. *Chem. Sci.* **2016**, *7*, 6894–6904.

(43)   Chaduc, I.; Girod, M.; Antoine, R.; Charleux, B.; D'Agosto, F.; Lansalot, M. Batch Emulsion Polymerization Mediated by Poly(Methacrylic Acid) MacroRAFT Agents: One-Pot Synthesis of Self-Stabilized Particles. *Macromolecules* **2012**, *45*, 5881–5893.

(44)   Weast, R. *Handbook of Chemistry and Physics*, 66th Edi.; CRC Press: Florida.

(45)   Kumar, N.; Kumbhat, S. *Concise Concepts of Nanoscience and Nanomaterials*; Scientific Publishers: Jodhpur, 2018.

(46)   Munro, D.; Goodall, A. R.; Wilkinson, M. C.; Randle, K.; Hearn, J. Study of Particle Nucleation, Flocculation, and Growth in the Emulsifier-Free Polymerization of Styrene in Water by Total Intensity Light Scattering and Photon Correlation Spectroscopy. *J. Colloid Interface Sci.* **1979**, *68*, 1–13.

(47)   Weitz, D.; Huang, J.; Lin, M.; Sung, J. Dynamics of Diffusion-Limited Kinetic Aggregation. *Phys. Rev. Lett.* **1984**, *53*, 1657–1660.

(48)   Ditsch, A.; Laibinis, P. E.; Wang, D. I. C.; Hatton, T. A. Controlled Clustering and Enhanced Stability of Polymer-Coated Magnetic Nanoparticles. *Langmuir* **2005**, *21*, 6006–6018.

(49)   Gregory, J. Monitoring Particle Aggregation Processes. *Adv. Colloid Interface Sci.* **2009**, *147–148*, 109–123.

(50)   Fuoss, R. M.; Strauss, U. P. Electrostatic Interaction of Polyelectrolytes and Simple Electrolytes. *J. Polym. Sci.* **1948**, *3*, 602–603.

(51)   Lewis, G. N.; Randall, M. The Activity Coefficient of Strong Electrolytes. *J. Am. Chem. Soc.* **1921**, *43*, 1112–1154.

(52)   Kestin, J.; Khalifa, E. H.; Correia, R. J. Tables of the Dynamic and Kinematic Viscosity of Aqueous KCl Solutions in the Temperature Range 25–150 °C and the Pressure Range 0.1–35 MPa. *J. Phys. Chem. Ref. Data* **1981**, *10*, 57–70.

(53)   Blanazs, A.; Madsen, J.; Battaglia, G.; Ryan, A. J.; Armes, S. P. Mechanistic Insights for Block Copolymer Morphologies: How Do Worms Form Vesicles? *J. Am. Chem. Soc.* **2011**, *133*, 16581–16587.

(54)   Lovett, J. R.; Derry, M. J.; Yang, P.; Hatton, F. L.; Warren, N. J.; Fowler, P. W.; Armes, S. P. Can Percolation Theory Explain the Gelation Behavior of Diblock Copolymer Worms? *Chem. Sci.* **2018**, *9*, 7138–7144.

(55)   Yang, J. Viscoelastic Wormlike Micelles and Their Applications. *Curr. Opin. Colloid Interface Sci.* **2002**, *7*, 276–281.

(56)   Chu, Z.; Dreiss, C. A.; Feng, Y. Smart Wormlike Micelles. *Chem. Soc. Rev.* **2013**, *42*, 7174–7203.

(57)   Wang, J.; Feng, Y.; Agrawal, N. R.; Raghavan, S. R. Wormlike Micelles versus Water-Soluble Polymers as Rheology-Modifiers: Similarities and Differences. *Phys. Chem. Chem. Phys.* **2017**, *19*, 24458–24466.

(58)   Skrabania, K.; Miasnikova, A.; Bivigou-Koumba, A. M.; Zehm, D.; Laschewsky, A. Examining the UV-Vis Absorption of RAFT Chain Transfer Agents and Their Use for Polymer Analysis. *Polym. Chem.* **2011**, *2*, 2074–2083.

(59)   Uzgiris, E. Laser Doppler Spectroscopy: Applications to Cell and Particle Electrophoresis. *Adv. Colloid Interface Sci.* **1981**, *14*, 75–171.

(60)   Hunter, R. *Zeta Potential in Colloid Science*; Academic Press: London, 1981.

Chapter 5

A Low-Viscosity Route to High

Molecular Weight Water-Soluble

Diblock Copolymers

5.1 Introduction

The ability of water-soluble polymers to increase the viscosity of aqueous solutions has been exploited for many commercial applications.[1] Both natural and synthetic water-soluble polymers are used as viscosity modifiers for pharmaceutical formulations, foodstuffs, cosmetics, paints, detergents, lubricants and fracturing fluids for oil and gas production.[1–8]

Most commercial synthetic water-soluble polymers are prepared by FRP.[9] Conducting such polymerisations either in the bulk or in solution invariably results in high-viscosity solutions even at low copolymer concentrations, owing to chain entanglements.[10] Although this is the desired final outcome for water-thickening polymers, it is very difficult to achieve efficient heat dissipation during such polymerisations, particularly when targeting high molecular weights. In order to overcome this drawback, low-viscosity polymerisation methods such as inverse emulsion, suspension or precipitation polymerisation are often used.[10–13] Such formulations enable polymerisations to be conducted at high solids while maintaining relatively low solution viscosities.[9,14] However, purification steps are often required to remove the polymerisation solvent and any excess surfactant or polymeric stabiliser. Moreover, although FRP is useful for the preparation of homopolymers, it inevitably results in broad MWDs with no scope for the preparation of diblock copolymers or other complex architectures.[15]

In principle, PISA can be used to prepare nanoparticles *in situ* from double-hydrophilic diblock copolymers when one block is rendered initially insoluble by judicious choice of reaction conditions. For example, An *et al.* prepared a series of PDMAC precursors with varying molecular weights which were then chain-extended in aqueous solution using

NIPAM at 70 °C.[16] Under such conditions, the growing PNIPAM chains are water-insoluble, so PNIPAM-core nanoparticles were formed *via* PISA. However, on cooling the dispersion to room temperature, i.e. below the LCST of PNIPAM, nanoparticle dissolution occurred to afford water-soluble diblock copolymer chains. High conversions were achieved and well-defined double-hydrophilic diblock copolymers were formed ($M_w/M_n \sim 1.20$). However, the main focus of this pioneering study was the formation of thermoresponsive nanogels *via* the addition of a bisacrylamide cross-linker, rather than targeting high molecular weight linear diblock copolymers for use as viscosity modifiers. Similarly, Cunningham *et al.* prepared a series of $PGMA_{63}$-$PNMEP_y$ diblock copolymer nanoparticles by RAFT aqueous dispersion polymerisation of NMEP at 70 °C.[17] Relatively large, partially hydrated spherical nanoparticles of up to 1 µm were formed under such conditions. Nanoparticle dissolution occurred on cooling to 20 °C, resulting in highly viscous, double-hydrophilic diblock copolymer solutions. This method enabled the synthesis of reasonably well-defined ($M_w/M_n < 1.50$), high molecular weight (92 % GMA conversion was achieved when $y = 5000$ was targeted) $PGMA_{63}$-$PNMEP_y$ diblock copolymers. Moreover, the relatively expensive PGMA precursor could be replaced with PMAA. In this case, high NMEP conversions were achieved up to $y \leq 4000$.

In this Chapter, a series of $PATAC_{100}$-$PDMAC_y$ diblock copolymer nanoparticles are prepared by RAFT aqueous dispersion polymerisation of DMAC in 2 M ammonium sulfate. PATAC was chosen as the stabiliser block because this cationic polyelectrolyte remains soluble in highly salty aqueous media[18,19] as confirmed in Chapter 4 of this Thesis. Conversly, PDMAC homopolymers are insoluble in 2 M ammonium sulfate but soluble in aqueous media. A series of $PATAC_{100}$-$PDMAC_y$ diblock copolymer nanoparticles were synthesised at 10 % w/w solids using a one-shot batch polymerisation process in combination with a low-temperature initiator. Nanoparticle dissolution on

dilution with deionized water was studied by DLS and ^{1}H NMR spectroscopy. The thickening behaviour of the resulting fully water-soluble double-hydrophilic diblock copolymers has been examined using rheology measurements to determine the solution viscosity. Finally, a monomer-starved feed protocol has been developed for the synthesis of high molecular weight diblock copolymer nanoparticles in the form of relatively concentrated dispersions.

5.2 Results and Discussion

5.2.1 Homopolymerisation of ATAC

The synthesis and characterisation of the PATAC$_{100}$ precursor used in this work is described in Chapter 4.

5.2.2 Homopolymerisation of DMAC

The RAFT solution polymerisation of DMAC was conducted in 1,4-dioxane at 70 °C using DDMAT as the CTA, as described in Chapter 2. A PDMAC homopolymer was prepared with a mean DP of 135, as determined by UV-visible absorption spectroscopy using the Beer-Lambert calibration plot constructed for DDMAT in Chapter 2.

5.2.3 Solubility Studies in Ammonium Sulfate Solutions

Solubility studies were conducted on the PATAC$_{100}$ and PDMAC$_{135}$ homopolymers using aqueous ammonium sulfate solutions ranging from 0.1 M to 2.0 M. A small portion of each homopolymer was stirred in the ammonium sulfate solutions for 30 min at 20 °C. As expected,[18,19] the PATAC$_{100}$ precursor formed transparent solutions at all salt concentrations and hence was judged to be fully soluble in each case, see Fig. 5.1a. The PDMAC$_{135}$ homopolymer also formed transparent solutions for ammonium sulfate concentrations ranging from 0.1 M to 0.5 M. However, PDMAC$_{135}$ became sparingly soluble (forming a cloudy solution) when added to 1.0 M ammonium sulfate and was judged to be water-insoluble in both 1.5 M and 2.0 M ammonium sulfate, see Fig. 5.1b.
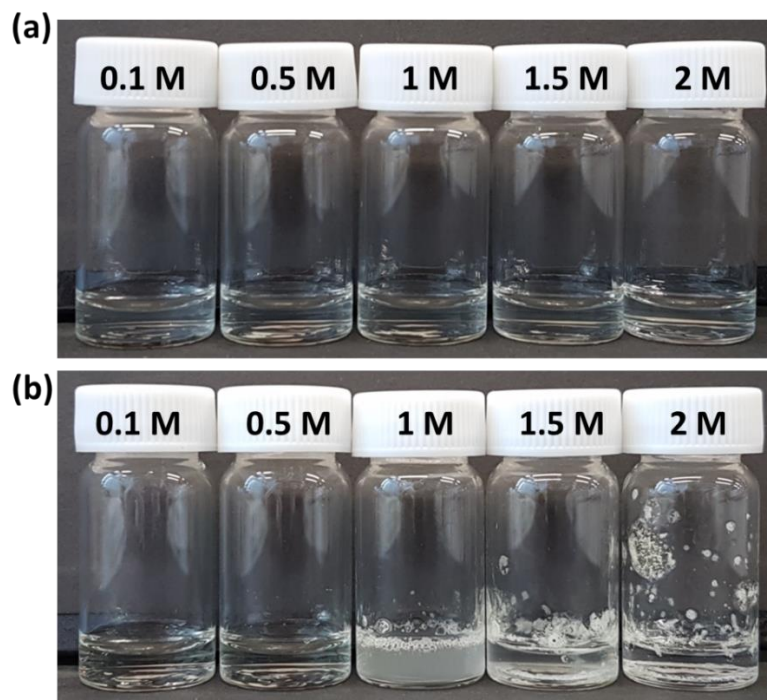
Fig. 5.1. Digital photographs showing the visual appearance of aqueous solutions containing 0.1 M to 2.0 M ammonium sulfate recorded at 20 °C 30 min after addition of (a) PATAC$_{100}$ homopolymer and (b) PDMAC$_{135}$ homopolymer.

5.2.4 RAFT Aqueous Dispersion Polymerisation of DMAC

Preliminary solubility studies confirmed that the PATAC$_{100}$ homopolymer was soluble in 2.0 M ammonium sulfate whereas the PDMAC$_{135}$ homopolymer was water-insoluble under such conditions. Hence chain extension of the PATAC$_{100}$ homopolymer with DMAC in 2.0 M ammonium sulfate under RAFT aqueous dispersion conditions should result in the formation of PDMAC-core diblock copolymer nanoparticles. Moreover, a kinetically-trapped spherical morphology is expected because it is well-known that using a polyelectrolyte-based steric stabiliser usually prevents sphere-sphere fusion during PISA,[20–22] which is a pre-requisite for the formation of either worms or spheres.

Accordingly, chain extension of the $PATAC_{100}$ homopolymer with DMAC was conducted at 10 % w/w solids in 2.0 M ammonium sulfate at 44 °C for 18 h using VA-044 as a water-soluble, low-temperature initiator, see Figure 5.2.
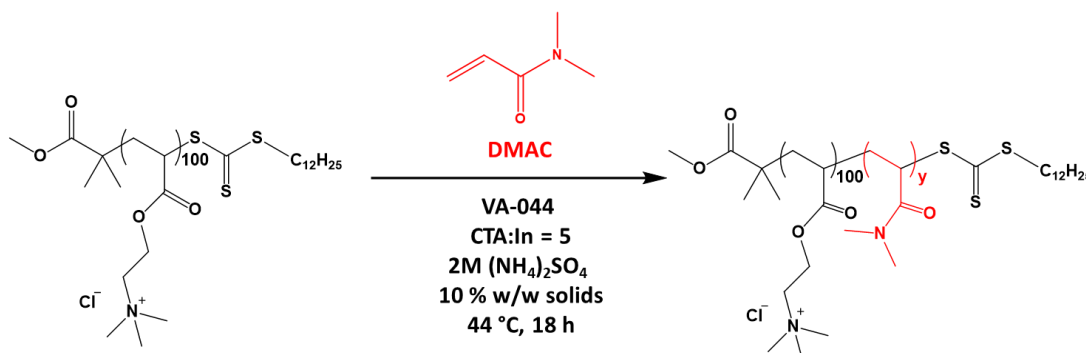

Fig. 5.2. Reaction scheme for the RAFT aqueous dispersion polymerisation of DMAC at 44 °C using a $PATAC_{100}$ precursor in 2.0 M ammonium sulfate to form $PATAC_{100}$-$PDMAC_y$ diblock copolymer nanoparticles at 10 % w/w solids.

A series of $PATAC_{100}$-$PDMAC_y$ diblock copolymer nanoparticles were prepared with y = 500, 1000, 2000, 4000 and 8000. High DMAC conversions (> 99 %) were achieved in all cases as determined by ^{1}H NMR spectroscopy (the integrated DMAC vinyl proton signals in the 5.0 – 7.0 ppm region were compared to the integrated signal *h*, see Figure 5.3). Unfortunately, preliminary aqueous GPC analysis of the $PATAC_{100}$-$PDMAC_{500}$ diblock copolymer suggests inefficient blocking of the $PATAC_{100}$ precursor, see Figure 5.4. Integration of the biomodal chromatogram suggests that there is approximately 39 % of the $PATAC_{100}$ does not chain extend. The reasons for this are not understood yet and require further investigation. Nevertheless, all of the resulting aqueous dispersions were free-flowing and became increasingly turbid when targeting higher PDMAC DPs, see Figure 5.5.
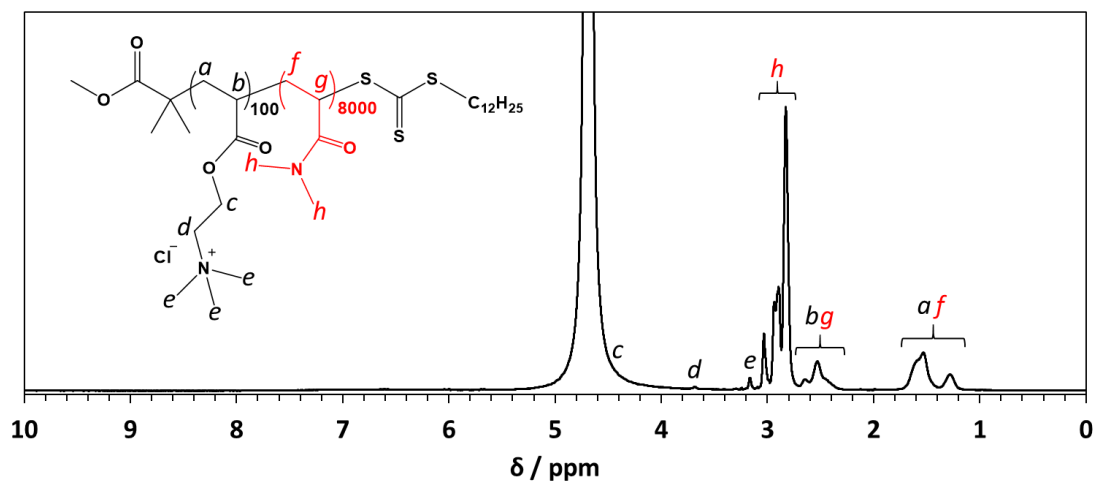
Fig. 5.3. Representative ^{1}H NMR spectrum recorded for a PATAC$_{100}$-PDMAC$_{8000}$ diblock copolymer molecularly dissolved in D$_2$O.
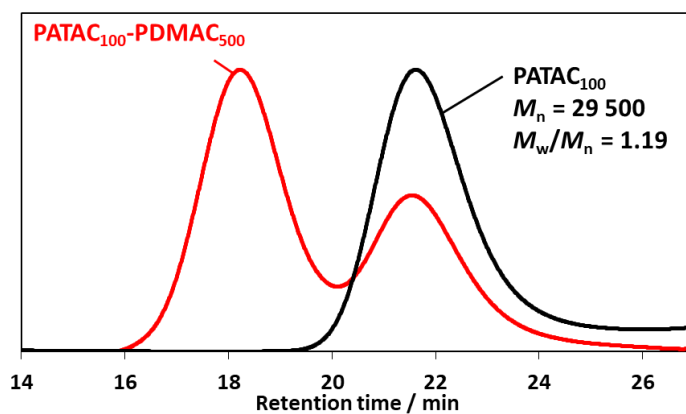

Fig. 5.4. Aqueous GPC traces recorded for the PATAC$_{100}$ homopolymer precursor and the PATAC$_{100}$-PDMAC$_{500}$ diblock copolymer.

Fig. 5.5. Digital photograph recorded for a series of five 2.5 % w/w aqueous dispersions of PATAC$_{100}$-PDMAC$_y$ diblock copolymer nanoparticles (where y = 500 – 8000) in 2.0 M ammonium sulfate. Targeting higher PDMAC DPs clearly leads to greater turbidity.

The as-synthesised 10 % w/w aqueous dispersions were diluted to 0.1 % w/w solids using a 2.0 M ammonium sulfate solution for DLS analysis, see Table 5.1. As expected, DLS analysis shows a systematic increase in mean particle diameter from 94 to 698 nm on increasing the target PDMAC DP from 500 to 8000. Moreover, the DLS polydispersities were relatively low (0.02 to 0.14), which indicates relatively narrow particle size distributions.

Table 5.1. Summary of DLS data obtained for 0.1 % w/w aqueous dispersions of PATAC$_{100}$-PDMAC$_y$ diblock copolymer nanoparticles in 2.0 M ammonium sulfate at 20 °C.

PDMAC DP	Intensity-average particle diameter[a] / nm	PDI	Derived count rate / Kcps
500	94	0.06	17 700
1000	136	0.14	45 000
2000	173	0.07	54 200
4000	476	0.02	22 500
8000	698	0.09	20 800

[a] Intensity-average diameter determined by DLS analysis. The solution viscosity of an aqueous solution of 2.0 M ammonium sulfate at 20 °C is 1.65 Pa s.[23]

As mentioned above, the PATAC$_{100}$ and PDMAC$_{135}$ homopolymers are both soluble in 0.5 M ammonium sulfate, see Fig 5.1. Hence, a four-fold dilution of the as-synthesised 10 % w/w nanoparticle dispersions using deionised water should result in complete nanoparticle dissolution to afford water-soluble diblock copolymer chains. Indeed, transparent, viscous solutions were formed when each of the 10 % w/w aqueous nanoparticle dispersions were diluted with water, see Figure 5.6.
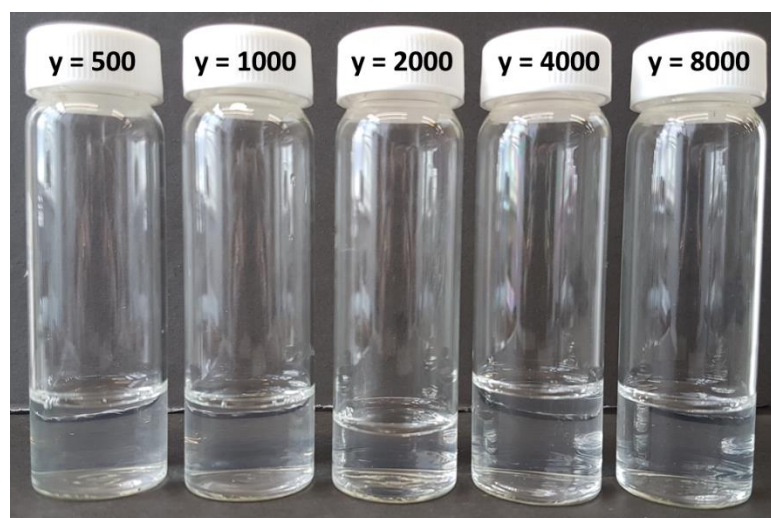
Fig. 5.6. Digital photograph recorded for five 2.5% w/w aqueous solutions of PATAC$_{100}$-PDMAC$_y$ in 0.5 M ammonium sulfate. The loss of turbidity compared to that observed in Figure 5.5 indicates complete nanoparticle dissolution.

The as-synthesised 10 % w/w PATAC$_{100}$-PDMAC$_y$ dispersions were diluted to 0.1 % w/w solids using 0.5 M ammonium sulfate for DLS studies. The intensity-average diameters and derived count rates are provided in Table 5.2. There is a significant reduction in both the intensity-average diameter and derived count rate for each sample compared to the as-synthesised 2.0 M ammonium sulfate nanoparticle dispersions. These results suggest complete nanoparticle dissolution to form aqueous solutions of PATAC$_{100}$-PDMAC$_y$ diblock copolymer chains. The mean particle diameter increases from 31 nm to 71 nm on increasing the target PDMAC DP from 500 to 8000. This is attributed to the greater

hydrodynamic volume occupied by the molecularly-dissolved copolymer chains, which most likely adopt a random coil conformation in aqueous solution, as the PDMAC is increased. This interpretation is consistent with the much lower derived count rates compared to those reported in Table 5.2. Finally, it is perhaps worth noting that the DLS polydispersities are relatively high, which suggests a relatively broad molecular weight distribution for these diblock copolymer chains.

Table 5.2 Summary of DLS data obtained for a series of $PATAC_{100}$-$PDMAC_y$ diblock copolymers in 0.5 M aqueous ammonium sulfate at 20 °C.

PDMAC DP	Intensity-average particle diameter[a] / nm	PDI	Derived count rate / Kcps
500	31	0.51	303
1000	35	0.36	414
2000	49	0.33	665
4000	63	0.28	835
8000	71	0.40	832

[a] Intensity-average diameter determined by DLS analysis. The solution viscosity of an aqueous solution of 0.5 M ammonium sulfate at 20 °C is 1.11 Pa s.[23]

The extent of nanoparticle dissolution was further investigated using ^1H NMR spectroscopy. A $PATAC_{100}$-$PDMAC_{500}$ diblock copolymer was synthesised in a 2.0 M ammonium sulfate/D_2O solution using the same synthesis route outlined in Figure 5.2. ^1H NMR spectra were recorded for 2.5 % w/w $PATAC_{100}$-$PDMAC_{500}$ dispersions/solutions in the presence of 2.0 M, 1.5 M, 1.0 M, 0.75 M or 0.50 M ammonium sulfate solutions prepared using D_2O, see Figure 5.7a. The $PATAC_{100}$-$PDMAC_{500}$ diblock copolymer was synthesised in D_2O to minimise the water (HDO) signal in the ^1H NMR spectra. A $PATAC_{100}$-$PDMAC_{500}$ diblock copolymer composition was chosen to (i) minimise the increase in viscosity associated with nanoparticle

dissolution (since this leads to broader NMR signals) and (ii) to achieve sufficient resolution of the PDMAC signals.

The spectra shown in Figure 5.7a were normalised to the signal assigned to the two protons adjacent to the quaternary amine in the PATAC block ($CH_2N(CH_3)_3$, see signal marked with an asterisk). The latter proton signal remains fully solvated regardless of the ammonium sulfate concentration. The signal assigned to the six equivalent protons on the methyl groups in the PDMAC block (*a* on Figure 5.7a) are visible in 2.0 M ammonium sulfate showing that these nanoparticles are partially hydrated in 2.0 M ammonium sulfate. Clearly, signal *a* becomes more prominent on reducing the ammonium sulfate concentration, suggesting a greater degree of hydration for this block. The spectra recorded using 0.50 M and 0.75 M ammonium sulfate were identical, see Figure 5.7b.

The integrated signals *e* and *h* correspond to the composition of the fully solvated PATAC$_{100}$-PDMAC$_{500}$ diblock copolymer as determined in D$_2$O (i.e. in the absence of any ammonium sulfate). This demonstrates that lowering the ammonium sulfate concentration from 2.0 M to 0.50 M *via* four-fold dilution of the as-synthesised 10 % w/w PATAC$_{100}$-PDAMC$_{500}$ nanoparticles using deionised water is sufficient to cause complete nanoparticle dissolution.

(a)

(b)
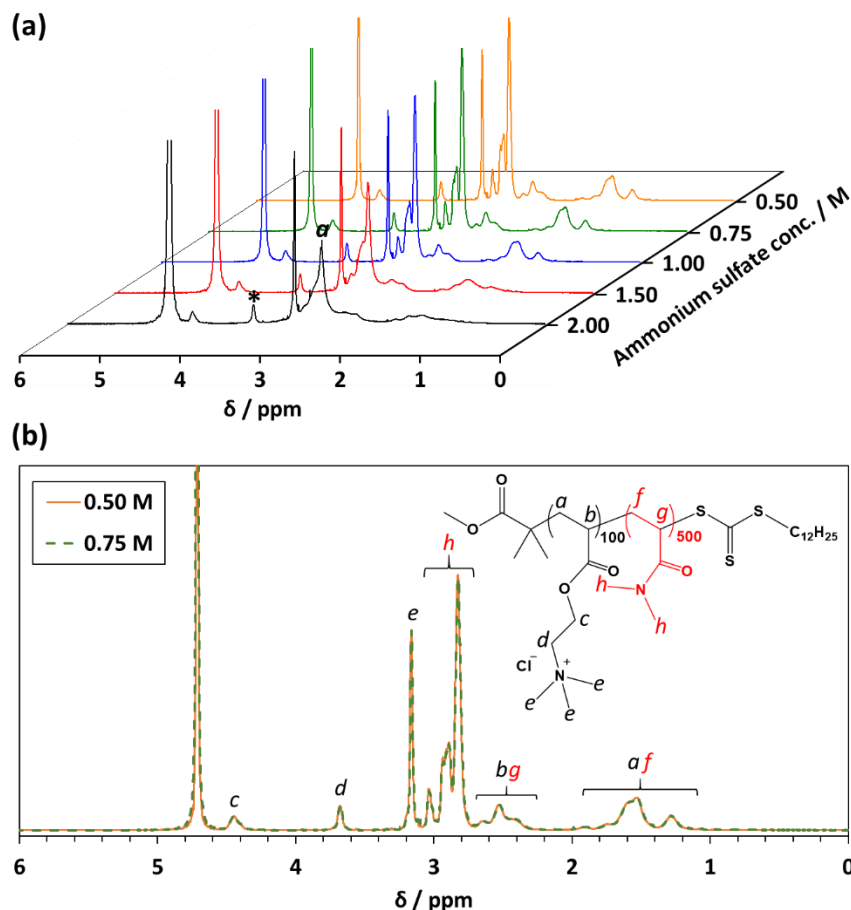
Fig. 5.7. (a) ^{1}H NMR spectra recorded for five 2.5 % w/w PATAC$_{100}$-PDMAC$_{500}$ diblock copolymer dispersions/solutions prepared in 2.0 M, 1.5 M, 1.0 M, 0.75 M or 0.50 M ammonium sulfate using D$_2$O. All spectra are normalised to the signal marked with an asterisk, which corresponds to the two protons adjacent to the quaternary amine in the PATAC block (CH_2N(CH$_3$)$_3$). The signal marked *a* corresponds to the six equivalent methyl protons in the PDMAC block. (b) Overlaid spectra for PATAC$_{100}$-PDMAC$_{500}$ recorded in 0.75 M (green) and 0.5 M (orange) ammonium sulfate, respectively.

5.2.5 Rheological Studies

Rotational rheology measurements were conducted to examine the thickening behaviour conferred by the double-hydrophilic PATAC$_{100}$-PDMAC$_y$ diblock copolymers in aqueous solution. Measurements were conducted on each of the five PATAC$_{100}$-PDMAC$_y$ diblock copolymers (where y = 500 to 8000) at 2.5 % w/w solids in

either 0.5 M or 2.0 M ammonium sulfate. This copolymer concentration was chosen because it corresponds to the maximum concentration that can be achieved after a four-fold dilution of the as-synthesised 10 % w/w copolymer dispersions with water. Shear sweeps were conducted on each sample from 0.1 s^{-1} to 50 s^{-1} at 20 °C. Data obtained for copolymer dispersions in 2.0 M and 0.5 M ammonium sulfate are shown in Figure 5.8a and Figure 5.8b respectively. The data was plotting using the target DP however, this will be incorrect given that there is 39 % PATAC$_{100}$ contamination but it is assumed that all of the reactions will contain the same level of contamination and are therefore comparable.

According to Figure 5.8a, the PATAC$_{100}$-PDMAC$_y$ nanoparticles formed in 2.0 M ammonium sulfate have dispersion viscosities that are comparable to that of water (which is shown as a black dashed line). When targeting $y = 500$ to 8000, the viscosity of the PATAC$_{100}$-PDMAC$_y$ nanoparticle dispersions is independent of both copolymer molecular weight and nanoparticle diameter. Inspecting Figure 5.8b, the PATAC$_{100}$-PDMAC$_y$ solution viscosities at 2.5 % w/w solids in 0.5 M ammonium sulfate are comparable to that of water for $y = 500 – 2000$. Targeting a PDMAC DP greater than 2000 is required to observe a significant thickening effect. This suggests that a PDMAC DP of approximately 2000 is the critical DP (DP$_c$) where copolymer chains become entangled at this particular copolymer concentration. This inflection point is more readily apparent when plotting $\log(\eta_0)$ against $\log(\text{PDMAC DP})$ where η_0 is the zero shear viscosity (see Figure 5.9). The latter parameter was determined by extrapolation of the viscosity vs. shear rate data in the linear constant viscosity regime to zero shear. For the PATAC$_{100}$-PDMAC$_{8000}$ copolymer, only a narrow linear region between 0.1 s^{-1} and 1.0 s^{-1} was observed (see inset in Figure 5.8b) prior to shear-thinning behaviour. According to

the literature, above the DP_c a power-law relationship between η_0 and DP should be observed with a numerical exponent of 3.4 (Equation 5.1).[24]

$$\eta_0 = K[DP]^{3.4} \qquad\qquad 5.1$$

Indeed, a power-law relationship of 3.4 was calculated for the $PATAC_{100}$-$PDMAC_y$ diblock copolymer chains in 0.5 M ammonium sulfate solution when *y* exceeded 2000.
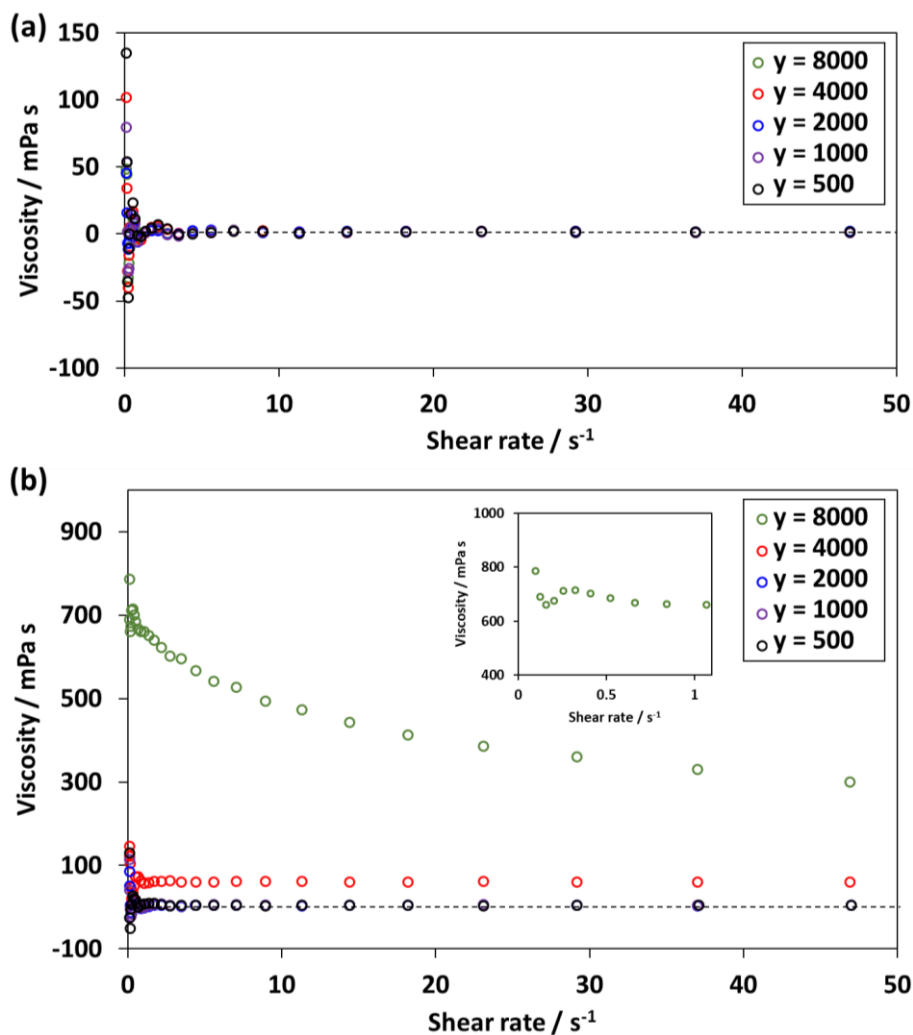
Fig. 5.8. Rotational rheology data recorded for $PATAC_{100}$-$PDMAC_y$ diblock copolymers where *y* = 500 to 8000: (a) dispersion viscosity against shear rate for $PATAC_{100}$-$PDMAC_y$ *dispersions* in 2.0 M ammonium sulfate; (b) solution viscosity against shear rate for $PATAC_{100}$-$PDMAC_y$ *solutions* in 0.5 M ammonium sulfate. The inset shows the linear constant viscosity region observed for the $PATAC_{100}$-$PDMAC_{8000}$ diblock copolymer. The black dashed lines indicate the viscosity of deionised water.

Fig. 5.9. Relationship between $\log(\eta_0)$ and $\log$(PDMAC DP), where η_0 is the zero shear viscosity, for a series of PATAC$_{100}$-PDMAC$_y$ aqueous solutions in 0.50 M ammonium sulfate at 20 °C.

5.2.6. Maximising Thickening Performance

There are two obvious approaches for maximising the thickening effect after the four-fold dilution of the PATAC$_{100}$-PDMAC$_y$ formulation. Firstly, since the solution viscosity depends on th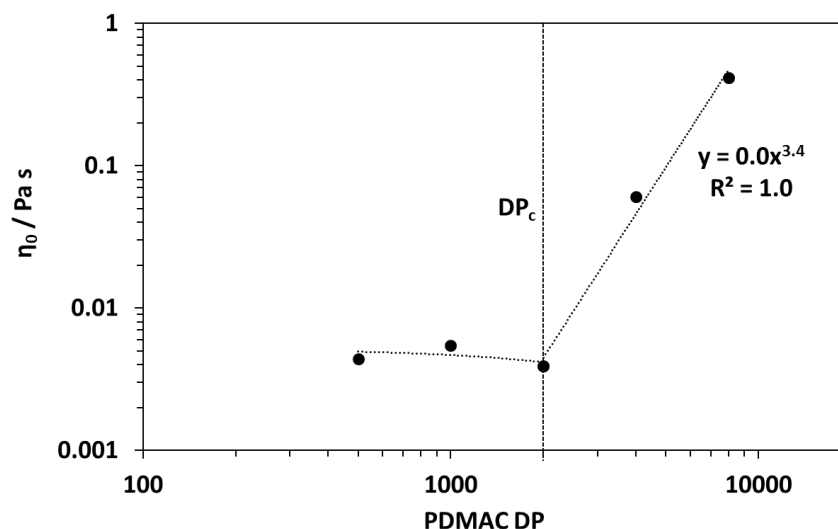e copolymer molecular weight, higher PDMAC DP can be targeted. Secondly, the overall solids content (or copolymer concentration) can be raised for this PISA formulation, which should increase the solution viscosity and also lower the DP$_c$.[25] In principle, combining these two strategies should enable the maximum solution viscosity to be achieved.

Unfortunately, increasing the PDMAC target DP up to 10000 and the copolymer concentration up to 20 % w/w solids using the one-shot batch protocol shown in Figure 5.2 resulted in phase separation of the DMAC monomer from the 2.0 M ammonium sulfate aqueous solution. This suggests that the solubility limit of the monomer was exceeded under these conditions.

To overcome this problem, the synthesis protocol was modified to enable continuous addition of the monomer into the reaction solution. This was achieved using a syringe pump and this 'monomer-starved feed' set-up is shown in Figure 5.10. The modified reaction scheme for the synthesis of $PATAC_{100}$-$PDMAC_{10000}$ diblock copolymer nanoparticles at a copolymer concentration of 40 % w/w solids is summarised in Figure 5.11.
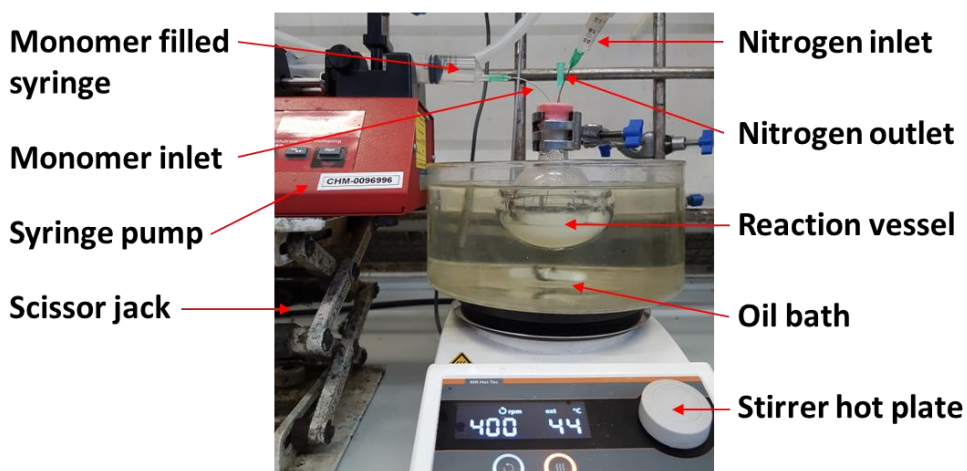

Fig. 5.10. Digital image showing the experimental set-up for the monomer-starved feed protocol used to prepare $PATAC_{100}$-$PDMAC_{10000}$ at 40 % w/w solids.
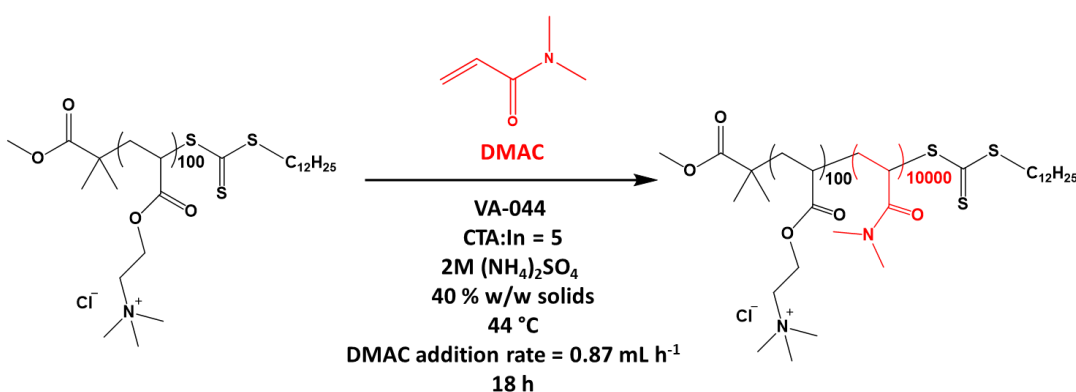

Fig. 5.11. Reaction scheme for the chain extension of a $PATAC_{100}$ precursor with DMAC in 2.0 M ammonium sulfate at 44 °C using a monomer-starved feed protocol.

DMAC was added to the reaction vessel over the first 6 h of the polymerisation at a feed

rate of 0.87 mL h^{-1}. The final DMAC conversion was judged to be 98% as determined by

^{1}H NMR spectroscopy. A turbid, free-flowing dispersion was obtained after 18 h at 44 °C,

see Figure 5.12. DLS analysis indicated an intensity-average diameter of 635 nm for the

PATAC$_{100}$-PDMAC$_{10000}$ dispersion diluted to 0.1 % w/w solids using 2.0 M ammonium

sulfate solution. A four-fold dilution of the as-synthesised 40 % w/w

PATAC$_{100}$-PDMAC$_{10000}$ nanoparticle dispersion with water resulted in the formation of

a transparent free-standing gel, see Figure 5.12.
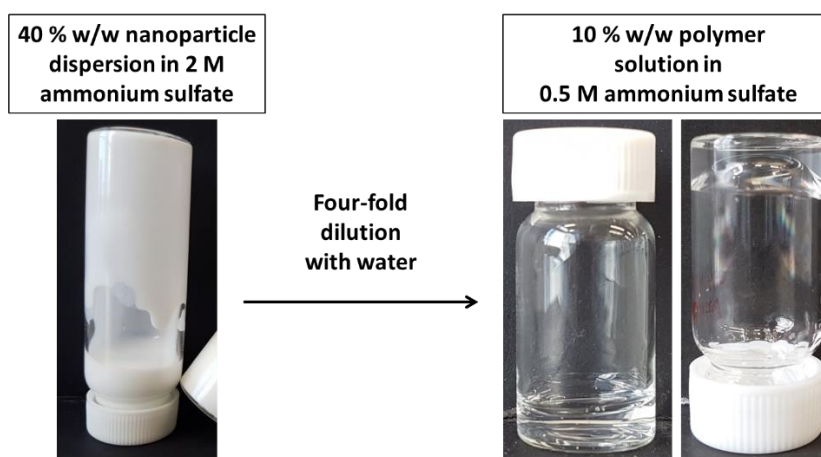
Fig. 5.12. Left-hand image: a low-viscosity, turbid, free-flowing 40 % w/w aqueous
dispersion of PATAC$_{100}$-PDMAC$_{10000}$ nanoparticles in 2.0 M ammonium sulfate
prepared using a monomer-starved feed protocol. Right-hand image: four-fold dilution
of the same PATAC$_{100}$-PDMAC$_{10000}$ nanoparticles with deionised water affords a
10 % w/w transparent, free-standing gel owing to complete nanoparticle dissolution.

As expected, targeting a higher target DP for a more concentrated formulation clearly has

a profound effect on the viscosity modification performance. DLS analysis of a

0.1 % w/w solution of this molecularly-dissolved PATAC$_{100}$-PDMAC$_{10000}$ diblock

copolymer in 0.5 M ammonium sulfate gave an intensity-average diameter of 81 nm,

which is consistent with the 71 nm diameter obtained previously for a

$PATAC_{100}$-$PDMAC_{8000}$ diblock copolymer. In view of the high transparency of the solution and the ^1H NMR spectroscopy results obtained for shorter copolymer chains, this suggests that complete nanoparticle dissolution has occurred under these conditions.

Whilst it is clearly possible to produce $PATAC_{100}$-$PDMAC_{10000}$ diblock copolymers using this monomer-starved feed protocol, unfortunately, there were issues with reproducibility with several reactions resulting in no DMAC conversion. This is in part the result of the very low levels of added initiator. In principle, this problem could be alleviated by conducting PISA syntheses on a much larger (kg) scale.

5.3 Conclusions

A series of $PATAC_{100}$-$PDMAC_y$ diblock copolymer nanoparticles (where $y = 500 - 8000$) have been prepared by exploiting the insolubility of PDMAC in 2.0 M ammonium sulfate at 44 °C. ^1H NMR spectroscopy studies confirmed that high DMAC conversions (> 99 %) were achieved for this RAFT aqueous dispersion polymerisation formulation, which is conducted at 10 % w/w solids using a one-shot batch protocol. GPC analysis showed inefficient blocking of the $PATAC_{100}$ hompolymer resulting in 39 % homopolymer contaimation. Nevertheless, DLS analysis indicated the *in situ* formation of nanoparticles with sphere-equivalent diameters of 94 nm to 698 nm. Rotational rheology measurements conducted on the 2.0 M ammonium sulfate dispersions confirmed that the aqueous dispersion viscosity is comparable to that of water and is independent of both the PDMAC DP and the nanoparticle diameter. Four-fold dilution of such aqueous dispersions using deionized water resulted in nanoparticle dissolution, as confirmed by both DLS and ^1H NMR spectroscopy analysis. This is because the water-insoluble PDMAC block initially formed in the presence of 2.0 M ammonium sulfate becomes water-soluble in the presence of 0.75 M ammonium sulfate (or lower salt concentrations).

Rheology measurements conducted on 2.5 % w/w $PATAC_{100}$-$PDMAC_y$ diblock copolymer aqueous solutions formed in the presence of 0.5 M ammonium sulfate indicated that PDMAC DPs of more than 2000 are required to achieve a significant thickening effect. A monomer-starved feed protocol was developed to allow the synthesis of a $PATAC_{100}$-$PDMAC_{10000}$ diblock copolymer at 40 % w/w solids. A nanoparticle-to-copolymer chain transition was induced by a four-fold dilution with deionized water to afford a transparent, free-standing gel. The work presented in this Chapter offers a highly convenient, wholly aqueous low-viscosity route to high molecular weight water-soluble polymers. It is perhaps worth emphasising that such high DP formulations require so little RAFT agent that its colour, cost and malodour become negligible, which is ideal for industrial scale-up. However, further refinement and optimisation is required to improve the reproducibility of such PISA formulations, particularly when conducted in concentrated solution under monomer-starved conditions and to improve the blocking efficiency of the PATAC homopolymer.

5.4 Experimental

5.4.1 Materials

DMAC ($\geq$ 98.5 %), DDMAT (98 %), D_2O and 1,4-dioxane and were purchased from Sigma-Aldrich UK and used as received. AIBN (98 %) was purchased from Molekula (UK) and was used as received. VA-044 was purchased from Wako Chemicals (Japan) and was used as received. Diethyl ether and ammonium sulfate were purchased from VWR Chemicals. Methanol was purchased from Fisher Scientific (UK). All solvents were HPLC-grade. Deuterated methanol (99 %) was purchased from Cambridge Isotope Laboratories (UK).

5.4.2 PATAC$_{100}$-PDMAC$_y$ Synthesis using a Batch Polymerisation Method

The typical protocol for the synthesis of PATAC$_{100}$-PDMAC$_{1000}$ spheres at 10 % w/w solids was conducted as follows. A PATAC$_{100}$ precursor (0.15 g, 0.008 mmol), VA-044 initiator (0.50 mg, 0.0015 mmol, PATAC$_{100}$/VA-044 molar ratio = 5.0) and DMAC monomer (0.75 g, 7.6 mmol; target DP = 1000) were weighed into a 14 mL vial. 2.0 M ammonium sulfate (8.1 mL) was then added to afford a 10 % w/w aqueous solution, which was degassed for 15 min at 4 °C using a stream of nitrogen gas prior to immersion of the vial in an oil bath set at 44 °C. The reaction solution was magnetically stirred for 18 h under a nitrogen atmosphere. The DMAC polymerisation was quenched by exposing the contents of the vial to air, followed by cooling the vial to ambient temperature. The DMAC monomer conversion was more than 99% as judged by ^{1}H NMR spectroscopy. All other PISA syntheses were conducted at 10 % w/w solids using the same protocol.

5.4.3 PATAC$_{100}$-PDMAC$_{10000}$ Synthesis using a Monomer-starved Feed Protocol

A PATAC$_{100}$ precursor (0.100 g, 0.0050 mmol), VA-044 (0.30 mg, 0.0010 mmol, PATAC CTA/initiator molar ratio = 5.0) and 2.0 M ammonium sulfate (7.7 mL) were

added to a 100 mL round-bottomed flask. Separately, DMAC (5.00 g, 0.050 mol) was

added to a sample vial. Each solution was degassed for 30 min at 4 °C using a stream of

nitrogen gas. The round-bottomed flask was sealed using a rubber septum and then placed

in a 44 °C oil bath with continuous magnetic stirring and a nitrogen flow. The degassed

DMAC monomer was drawn up into a syringe, which was then placed in a syringe pump

unit. The syringe outlet needle was inserted into the round-bottom flask *via* its rubber

septum. DMAC was pumped into the round-bottom flask over 6 h at a rate of 0.87 mL h^{-1}.

On completion of the DMAC addition, the nitrogen inlet was removed, the round-bottom

flask was sealed, and the reaction solution was stirred at 44 °C for a further 12 h.

^{1}H NMR spectroscopy studies in D$_2$O indicated a final DMAC conversion of 98 %.

5.4.4 Polymer Characterisation

^{1}H NMR Spectroscopy

The NMR spectrum for the PDMAC$_{135}$ homopolymer was recorded in CD$_3$OD. The NMR

spectra for the PATAC-PDMAC diblock copolymers were recorded in D$_2$O. All spectra

were obtained using a 400 MHz Bruker Avance III HD 400 spectrometer at 25 °C.

Typically, 64 scans were acquired to ensure high-quality spectra.

Gel Permeation Chromatography (GPC)

Aqueous GPC was used to assess the MWD of the PATAC$_{100}$-PDMAC$_{500}$ diblock

copolymer. An acidic aqueous buffer containing 0.5 M acetic acid and 0.3 M NaH$_2$PO$_4$

was adjusted to pH 2 using concentrated HCl and used as an eluent for aqueous GPC

analysis of the cationic PATAC precursor. The GPC instrument comprised an Agilent

1260 Infinity series degasser and pump, two Agilent PL 8 µm Aquagel-OH 30 columns

and one 8 µm Aquagel-OH 40 column in series. These columns were calibrated using ten

near-monodisperse poly(ethylene oxide) standards ranging from 1080 g mol^{-1} to

905 000 g mol^{-1}. A refractive index detector operating at 30 °C was used at a flow rate of 1.0 mL min^{-1}.

End-Group Analysis via UV−Visible Absorption Spectroscopy

UV/visible absorption spectra were recorded between 200 and 800 nm using a PC-controlled UV-1800 spectrophotometer at 25 °C using a 1 cm path length quartz cell. A Beer-Lambert curve was constructed using a series of ten DDMAT solutions in methanol (see Chapter 2). The absorption maximum at 311 nm assigned to the trithiocarbonate group[26] was used for this calibration plot and DDMAT concentrations were selected such that the absorbance always remained below unity. The mean DP for the PDMAC$_{135}$ homopolymer was determined using the molar extinction coefficient of 16300 ± 160 mol^{-1} dm^3 cm^{-1} determined for the DDMAT.

Dynamic Light Scattering (DLS)

All measurements were made on 0.1% w/w aqueous copolymer dispersions/solutions at 20 °C using 1.0 cm cuvette cells; scattered light was detected at 173° and data were averaged over three consecutive runs. Sphere-equivalent intensity-average diameters were calculated for diblock copolymer nanoparticles *via* the Stokes−Einstein equation, which assumes perfectly monodisperse, non-interacting spheres.

Rheology

Rotational rheology measurements were performed using an MCR 502 rheometer (Anton Paar, Gratz, Austria) using a Couette geometry. Measurements were performed at 20 °C with the sample gap set to 2.0 mm. Shear sweeps were conducted from 0.1 s^{-1} to 50 s^{-1}. Approximately 10 mL of copolymer dispersion was used per measurement, with a copolymer concentration of 2.5 % w/w solids.

References

(1)   *Industrial Water Souble Polymers*, First Edi.; Finch, C., Ed.; The Royal Society of Chemistry: Cambridge, 1996.

(2)   Budd, P.; Chakrabarti, S. Ultracentrifugal Studies of the Degradation of a Fracturing Fluid Polymer: Hydroxypropyl Guar. *J. Appl. Polym. Sci.* **1991**, *42*, 2191–2196.

(3)   de Lima, B. L. B.; Marques, N. do N.; Villetti, M. A.; Balaban de, R. C. HPAM-g-PEOPPO: Rheological Modifiers in Aqueous Media of High Temperature and High Ionic Strength. *J. Appl. Polym. Sci.* **2019**, *136*, 1–10.

(4)   Glomski, R. L.; Davis, L. E.; Joseph, G. A. Water Soluble Hydroxyethyl Methyl Cellulose Ether Thickener for Latex Paint. 3709876, 1973.

(5)   Kadajji, V. G.; Betageri, G. V. Water Soluble Polymers for Pharmaceutical Applications. *Polymers* **2011**, *3*, 1972–2009.

(6)   Shit, S. C.; Shah, P. M. Edible Polymers: Challenges and Opportunities. *J. Polym.* **2014**, *2014*, 1–13.

(7)   Necas, J.; Bartosikova, L. Carrageenan: A Review. *Vet. Med.* **2013**, *58*, 187–205.

(8)   Hui, Y. H.; Culbertson, J. D. *Handbook of Food Science, Technology and Engineering Volume 2*; CRC Press: Boca Raton, 2006.

(9)   *Water-Soluble Polymers: Synthesis, Solution Properties, and Applications*, First Edi.; Shalaby, S., McCormick, C. L., Butler, G., Eds.; American Chemical Society: Washington, 1991.

(10)   Hernández-Barajas, J.; Hunkeler, D. Heterophase Water-in-Oil Polymerization of Acrylamide by a Hybrid Inverse-Emulsion/Inverse-Microemulsion Process. *Polymer* **1997**, *38*, 5623–5641.

(11)   Halake, K.; Birajdar, M.; Kim, B. S.; Bae, H.; Lee, C. C.; Kim, Y. J.; Kim, S.; Kim, H. J.; Ahn, S.; An, S. Y.; et al. Recent Application Developments of Water-Soluble Synthetic Polymers. *J. Ind. Eng. Chem.* **2014**, *20*, 3913–3918.

(12)   Hernández-Barajas, J.; Hunkeler, D. J. Inverse-Emulsion Polymerization of Acrylamide Using Block Copolymeric Surfactants: Mechanism, Kinetics and Modelling. *Polymer* **1997**, *38*, 437–447.

(13)   Pabon, M.; Corpart, J. M.; Selb, J.; Candau, F. Synthesis in Inverse Emulsion and Properties of Water-Soluble Associating Polymers. *J. Appl. Polym. Sci.* **2002**, *84*, 1418–1430.

(14)   Rivera, J. G.; Barajas, J. H.; Carrillo, A. G.; Alvarado, A. F. A. Preparation of Highly Concentrated Inverse Emulsions of Acrylamide-based Anionic Copolymers as Efficient Water Rheological Modifiers. *J. Appl. Polym. Sci.* **2016**, *133*, 1–10.

(15)   Braunecker, W. A.; Matyjaszewski, K. Controlled/Living Radical Polymerization: Features, Developments, and Perspectives. *Prog. Polym. Sci.* **2007**, *32*, 93–146.

(16)   An, Z.; Shi, Q.; Tang, W.; Tsung, C. K.; Hawker, C. J.; Stucky, G. D. Facile RAFT

Precipitation Polymerization for the Microwave-Assisted Synthesis of Well-Defined, Double Hydrophilic Block Copolymers and Nanostructured Hydrogels. *J. Am. Chem. Soc.* **2007**, *129*, 14493–14499.

(17)   Cunningham, V. J.; Derry, M. J.; Fielding, L. A.; Musa, O. M.; Armes, S. P. RAFT Aqueous Dispersion Polymerization of N-(2-(Methacryloyloxy)Ethyl)Pyrrolidone: A Convenient Low Viscosity Route to High Molecular Weight Water-Soluble Copolymers. *Macromolecules* **2016**, *49*, 4520–4533.

(18)   Cho, M. S.; Yoon, K. J.; Song, B. K. Dispersion Polymerization of Acrylamide in Aqueous Solution of Ammonium Sulfate : Synthesis and Characterisation. *J. Appl. Polym. Sci.* **2002**, *83*, 1397–1405.

(19)   Song, B.; Cho, M.; Yoon, K.; Lee, D. Dispersion Polymerization of Acrylamide with Quaternary Ammonium Cationic Comonomer in Aqueous Solution. *J. Appl. Polym. Sci.* **2003**, *87*, 1101–1108.

(20)   Semsarilar, M.; Ladmiral, V.; Blanazs, A.; Armes, S. P. Anionic Polyelectrolyte-Stabilized Nanoparticles via RAFT Aqueous Dispersion Polymerization. *Langmuir* **2012**, *28*, 914–922.

(21)   Semsarilar, M.; Ladmiral, V.; Blanazs, A.; Armes, S. P. Cationic Polyelectrolyte-Stabilized Nanoparticles via RAFT Aqueous Dispersion Polymerization. *Langmuir* **2013**, *29*, 7416–7424.

(22)   Williams, M.; Penfold, N. J. W.; Lovett, J. R.; Warren, N. J.; Douglas, C. W. I.; Doroshenko, N.; Verstraete, P.; Smets, J.; Armes, S. P. Bespoke Cationic Nano-Objects via RAFT Aqueous Dispersion Polymerisation. *Polym. Chem.* **2016**, *7*, 3864–3873.

(23)   Weast, R. *Handbook of Chemistry and Physics*, 66th Edi.; CRC Press: Florida.

(24)   Barnes, H. *A Handbook of Elementary Rheology*, First Edi.; The University of Wales Institue of Non-Newtonian Fluid Mechanics: Aberystwyth, 2000.

(25)   Wang, J.; Feng, Y.; Agrawal, N. R.; Raghavan, S. R. Wormlike Micelles versus Water-Soluble Polymers as Rheology-Modifiers: Similarities and Differences. *Phys. Chem. Chem. Phys.* **2017**, *19*, 24458–24466.

(26)   Skrabania, K.; Miasnikova, A.; Bivigou-Koumba, A. M.; Zehm, D.; Laschewsky, A. Examining the UV-Vis Absorption of RAFT Chain Transfer Agents and Their Use for Polymer Analysis. *Polym. Chem.* **2011**, *2*, 2074–2083.

Chapter 6

Conclusions and Outlook

6.1 Conclusions and Outlook

The preparation of diblock copolymer nanoparticles by PISA has been extensively studied over the past decade.[1–3] Although there are still various aspects of PISA that remain poorly understood, the focus of academic research has shifted towards the preparation of functional and stimulus-responsive nanoparticles. Several groups have demonstrated that stimulus-responsive nanoparticles can be prepared using RAFT aqueous dispersion polymerisation.[4–6] However, there are still relatively few monomers that have been utilised to form the structure-directing hydrophobic block for RAFT aqueous dispersion polymerisation. This is mainly because there are relatively few monomers that are water-miscible but form water-insoluble polymers. The O'Reilly group have recently published an *in silico* method which they claim allows the prediction of suitable core-forming monomers for such PISA formulations.[7] In reality, laboratory experiments are still required to determine whether a monomer is actually suitable for RAFT aqueous dispersion polymerisation. In this regard, the aqueous solubility of the monomer appears to be a more reliable predictor than the theoretical approach. Moreover, there is currently no *in silico* method to predict whether a diblock copolymer will be stimulus-responsive.

In the first half of this Thesis, two monomers were explored for RAFT aqueous dispersion polymerisation, namely DAAM and HBA. At the time that this work was conducted, a number of groups had shown PDAAM to be a suitable core-forming block for PISA. However, only spheres and vesicles had been obtained and there were no investigations into the stimulus-responsive nature of PDAAM-based diblock copolymers. Moreover, there were no published studies in which PHBA had been used as a core-forming block for such PISA formulations.

In Chapter 2, a series of well-defined PDMAC precursors were chain-extended with DAAM *via* RAFT aqueous dispersion polymerisation to produce diblock copolymer nano-objects. It was shown for the first time that pure worms could be accessed for this PISA formulation. A detailed phase diagram was constructed which enabled the reproducible synthesis of pure spheres, worms and vesicles. Either heating or cooling these PDMAC-PDAAM nanoparticle dispersions showed that their size and morphology were relatively insensitive to changes in temperature. More specifically, only a mixture of worms and vesicles could be obtained when heating a pure worm dispersion from 20 °C to 50 °C. This weakly thermoresponsive behaviour was attributed to the relatively narrow phase space occupied by the diblock copolymer worms.

Previously, Lovett *et al.* showed that pH-responsive PGMA-PHPMA nanoparticles could be obtained by using a carboxylic acid-functionalised CTA.[4,8] Similarly, a carboxylic acid-functionalised CTA (DDMAT) was used to prepare the PDMAC-PDAAM nanoparticles. As expected, switching from pH 3 to pH 9 led to a significant change in nanoparticle zeta potential from 0 mV to approximately -30 mV. However, the PDMAC-PDAAM nanoparticles proved to be rather weakly pH-responsive: only a morphological transition from worms to a mixed phase of worms and spheres was observed under such conditions. Since this work was conducted, other research groups have reported the preparation of thermoresponsive nanoparticles using PDAAM. For example, An and co-workers prepared PDMAC$_{30}$-PDAAM$_{60-90}$ lamellae at 70 °C that formed a worm/sphere mixed phase on cooling to 20 °C, although ^{1}H NMR spectroscopy showed no evidence for a reduction in the degree of hydration of the PDAAM block at the latter temperature.[6] Ma *et al.* used PITSA to prepare PHPMAC$_{38}$-PDAAM$_{100}$ vesicles at 70 °C but on cooling to 25 °C a vesicle-to-worm transition occurred within 48 h.[9] It is

not yet clear why the PDMAC-PDAAM nanoparticles prepared in this Thesis proved to be relatively unresponsive to changes in temperature.

Chapter 2 also explored covalent stabilisation of the PDMAC-PDAAM nanoparticles using ADH; this water-soluble cross-linker reacts with the pendent ketone groups on the hydrophobic PDAAM chains to form hydrazone moieties. FT-IR spectroscopy studies provided direct evidence for this cross-linking chemistry, while DLS measurements performed in methanol (a good solvent for the PDMAC and PDAAM blocks) confirmed that covalent stabilisation could be achieved within 6 h at 25 °C using ADH/DAAM molar ratios as low as 0.075. This protocol allows the convenient preparation of covalently-stabilised spheres, worms or vesicles in the form of moderately concentrated aqueous dispersions.

In Chapter 3, PHBA was investigated as the core-forming block in a PISA formulation. A one-pot protocol was developed in which well-defined PDMAC-PHBA diblock copolymers could be prepared using DDMAT at pH 3 without any purification steps. Whereas the PDMAC-PDAAM worms prepared in Chapter 2 proved to be relatively unresponsive to changes in temperature, the PDMAC-PHBA nano-objects proved to be remarkably thermoresponsive. Rheological studies showed that heating an aqueous dispersion of PDMAC$_{54}$-PHBA$_{244}$ nano-objects from 1 °C to 20 °C resulted in an increase in dispersion viscosity and an associated sol-to-gel transition. Further heating to 25 °C resulted in a reduction in viscosity and a gel-to-sol transition. Heating up to 45 °C resulted in a second sol-to-gel transition. Moreover, the CGT could be tuned by varying the PHBA DP. However, these dispersions could not be imaged by TEM owing to the low glass transition temperature of PHBA. To overcome this problem, DAAM was introduced into the core by statistical copolymerisation with HBA. These

PDMAC$_{56}$-P(HBA-*stat*-DAAM)$_{264}$ diblock copolymer nano-objects were then crosslinked using ADH. TEM images confirmed the formation of well-defined spheres, worms, vesicles or lamellae at 1 °C, 25 °C, 50 °C or 70 °C, respectively. ^{1}H NMR spectroscopy studies showed that the morphological transitions that occurred on heating were the result of uniform plasticisation of the nanoparticle cores. Hence PHBA displays UCST-like behaviour. This observation is highly counter-intuitive given that HBA is isomeric with HPMA and Blanazs et al. have shown that PHPMA core-forming blocks display LCST-like behaviour.[10,11]

Using methylated DDMAT allowed a PDMAC$_{56}$-P(HBA-*stat*-DAAM)$_{287}$ diblock copolymer to be prepared at pH 7. Recently, Mable et al. reported that PHPMA-PGMA vesicles could be used to encapsulate and release silica nanoparticles.[12] The neutral pH PISA formulation prepared herein should enable the thermally-activated encapsulation and release of either nanoparticles or proteins/enzymes within vesicles.[13,14] Moreover, varying the diblock copolymer composition should enable the critical gelation temperature (or maximum solution viscosity) to be tuned. This opens up the possibility of using these diblock copolymer nanoparticles in cell biology applications such as a wholly synthetic gel for 3D cell culture medium[15] and/or a long-term storage medium for human stem cells.[16]

It would be useful to develop a new crosslinking mechanism for the PDMAC-PHBA nanoparticles that would enable imaging of the various copolymer morphologies without the need for DAAM comonomer incorporation. If this can be achieved, then a direct comparison between the differing thermoresponsive behaviours exhibited by the PHPMA and PHBA core-forming blocks could be made. In principle, this might be achieved by using glutaraldehyde as a crosslinker at low pH.[17] The unprecedented thermoresponsive

behaviour of the PDMAC-PHBA diblock copolymer also makes it an ideal model system for exploring the mechanism of the vesicle-to-lamellae morphological transition. A suitable crosslinking strategy would allow key transient intermediate species to be studied by TEM analysis. This would also enable the mechanism for the strong hysteresis for vesicle reformation during the cooling cycle to be examined.

In the second half of this Thesis, both salt-tolerant and salt-responsive nanoparticles were synthesised by PISA using RAFT aqueous dispersion polymerisation. In each case, PATAC was employed as a steric stabiliser block. PATAC is a cationic polyelectrolyte that remains soluble even in the presence of high salinity. In Chapter 4, PATAC$_{100}$ was used to prepare a series of PATAC$_{100}$-PDAAM$_y$ spheres. DLS analysis showed that the PATAC$_{100}$-PDAAM$_{1500}$ spheres remained stable in either 4 M KCl or 3 M ammonium sulfate for at least 115 days at 20 °C. The same dispersion also remained stable in 3 M KCl for 6 days at 90 °C. Such remarkably salt-tolerant cationic spheres can be envisaged for use in high salinity, high temperature environments, e.g. enhanced oil recovery applications.

Penfold *et al.*[18] and Williams *et al.*[19] showed that cationic worms and vesicles could be prepared by chain extension of binary mixture of neutral and cationic precursors. Indeed, simultaneous chain extension of a binary mixture of PATAC and PDMAC stabilisers using DAAM enabled the synthesis of cationic spheres, worms and vesicles. However, these nano-objects proved to be significantly less salt-tolerant, which is presumably because of the lower density of PATAC chains within the steric stabiliser layer.

In Chapter 5, high molecular weight PATAC-PDMAC diblock copolymers were prepared in a convenient, low-viscosity nanoparticle form *via* RAFT aqueous dispersion polymerisation at 10 % w/w solids by exploiting the insolubility of PDMAC in 2 M

ammonium sulfate. A four-fold dilution of such 10 % w/w PATAC-PDMAC dispersions using deionised water resulted in complete nanoparticle dissociation to afford molecularly-dissolved copolymer chains, as judged by DLS analysis and ^{1}H NMR spectroscopy. When the PDMAC DP was greater than 2000, this transition was accompanied by a significant increase in solution viscosity.

Using a monomer-starved feed protocol enabled PATACT$_{100}$-PDMAC$_{10000}$ diblock copolymer nanoparticles to be prepared at 40 % w/w solids in 2 M ammonium sulfate. A four-fold dilution of this latter dispersion with water resulted in a transparent, free-standing gel. However, preliminary aqueous GPC studies suggest relatively low blocking efficiencies for the chain extension of the PATAC$_{100}$ precursor with DMAC. Moreover, reproducibility issues were sometimes encountered when using the monomer-starved feed protocol at 40 % solids with some reactions resulting in no DMAC conversion. In principle, a one-pot synthesis conducted on a larger scale might alleviate the problems of poor blocking efficiency and irreproducibility for such syntheses as it would allow a larger quantity of intiator to be used. Furthermore, other monomers could be explored to form both the stabiliser and core-forming blocks in order to improve blocking efficiency and broaden the scope of such high salinity PISA formulations. Given the highly convenient dilution-triggered thickening effect and the fact that the cost, colour and malodour of the CTA are minimised when targeting such high copolymer DPs, these PISA syntheses are likely to offer a range of potential industrial applications.

References

(1) Derry, M. J.; Fielding, L. A.; Armes, S. P. Polymerization-Induced Self-Assembly of Block Copolymer Nanoparticles via RAFT Non-Aqueous Dispersion Polymerization. *Prog. Polym. Sci.* **2016**, *52*, 1–18.

(2) Canning, S. L.; Smith, G. N.; Armes, S. P. A Critical Appraisal of RAFT-Mediated Polymerization-Induced Self-Assembly. *Macromolecules* **2016**, *49*, 1985–2001.

(3) Warren, N. J.; Armes, S. P. Polymerization-Induced Self-Assembly of Block Copolymer Nano-Objects via RAFT Aqueous Dispersion Polymerization. *J. Am. Chem. Soc.* **2014**, *136*, 10174–10185.

(4) Lovett, J. R.; Warren, N. J.; Ratcliffe, L. P. D.; Kocik, M. K.; Armes, S. P. PH-Responsive Non-Ionic Diblock Copolymers : Ionization of Carboxylic Acid End-Groups Induces an Order-Order Morphological Transition. *Angew. Chem. Int. Ed.* **2015**, *54*, 1279–1283.

(5) Figg, C. A.; Simula, A.; Gebre, K. A.; Tucker, B. S.; Haddleton, D. M.; Sumerlin, B. S. Polymerization-Induced Thermal Self-Assembly (PITSA). *Chem. Sci.* **2015**, *6*, 1230–1236.

(6) Wang, X.; Zhou, J.; Lv, X.; Zhang, B.; An, Z. Temperature-Induced Morphological Transitions of Poly(Dimethylacrylamide)-Poly(Diacetone Acrylamide) Block Copolymer Lamellae Synthesized via Aqueous Polymerization-Induced Self-Assembly. *Macromolecules* **2017**, *50*, 7222–7232.

(7) Foster, J. C.; Varlas, S.; Couturaud, B.; Jones, J. R.; Keogh, R.; Mathers, R. T.; O'Reilly, R. K. Predicting Monomers for Use in Polymerization-Induced Self-Assembly. *Angew. Chem. Int. Ed.* **2018**, *57*, 15733–15737.

(8) Lovett, J. R.; Warren, N. J.; Armes, S. P.; Smallridge, M. J.; Cracknell, R. B. Order-Order Morphological Transitions for Dual Stimulus Responsive Diblock Copolymer Vesicles. *Macromolecules* **2016**, *49*, 1016–1025.

(9) Ma, Y.; Gao, P.; Ding, Y.; Huang, L.; Wang, L.; Lu, X.; Cai, Y. Visible Light Initiated Thermoresponsive Aqueous Dispersion Polymerization-Induced Self-Assembly. *Macromolecules* **2019**, *52*, 1033–1041.

(10) Verber, R.; Blanazs, A.; Armes, S. P. Rheological Studies of Thermo-Responsive Diblock Copolymer Worm Gels. *Soft Matter* **2012**, *8*, 9915–9922.

(11) Blanazs, A.; Verber, R.; Mykhaylyk, O. O.; Ryan, A. J.; Heath, J. Z.; Douglas, C. W. I.; Armes, S. P. Sterilizable Gels from Thermoresponsive Block Copolymer Worms. *J. Am. Chem. Soc.* **2012**, *134*, 9741–9748.

(12) Deng, R.; Derry, M. J.; Mable, C. J.; Ning, Y.; Armes, S. P. Using Dynamic Covalent Chemistry to Drive Morphological Transitions: Controlled Release of Encapsulated Nanoparticles from Block Copolymer Vesicles. *J. Am. Chem. Soc.* **2017**, *139*, 7616–7623.

(13) Blackman, L. D.; Varlas, S.; Arno, M. C.; Houston, Z. H.; Fletcher, N. L.; Thurecht, K. J.; Hasan, M.; Gibson, M. I.; O'Reilly, R. K. Confinement of Therapeutic Enzymes in Selectively Permeable Polymer Vesicles by

Polymerization-Induced Self-Assembly (PISA) Reduces Antibody Binding and Proteolytic Susceptibility. *ACS Cent. Sci.* **2018**, *4*, 718–723.

(14)   Blackman, L. D.; Varlas, S.; Arno, M. C.; Fayter, A.; Gibson, M. I.; O'Reilly, R. K. Permeable Protein-Loaded Polymersome Cascade Nanoreactors by Polymerization-Induced Self-Assembly. *ACS Macro Lett.* **2017**, *6*, 1263–1267.

(15)   Simon, K. A.; Warren, N. J.; Mosadegh, B.; Mohammady, M. R.; Whitesides, G. M.; Armes, S. P. Disulfide-Based Diblock Copolymer Worm Gels: A Wholly-Synthetic Thermoreversible 3D Matrix for Sheet-Based Cultures. *Biomacromolecules* **2015**, *16*, 3952–3958.

(16)   Canton, I.; Warren, N. J.; Chahal, A.; Amps, K.; Wood, A.; Weightman, R.; Wang, E.; Moore, H.; Armes, S. P. Mucin-Inspired Thermoresponsive Synthetic Hydrogels Induce Stasis in Human Pluripotent Stem Cells and Human Embryos. *ACS Cent. Sci.* **2016**, *2*, 65–74.

(17)   Mansur, H. S.; Sadahira, C. M.; Souza, A. N.; Mansur, A. A. P. FTIR Spectroscopy Characterization of Poly (Vinyl Alcohol) Hydrogel with Different Hydrolysis Degree and Chemically Crosslinked with Glutaraldehyde. *Mater. Sci. Eng. C* **2008**, *28*, 539–548.

(18)   Penfold, N. J. W.; Whatley, J. R.; Armes, S. P. Thermoreversible Block Copolymer Worm Gels Using Binary Mixtures of PEG Stabilizer Blocks. *Macromolecules* **2019**, *52*, 1653–1662.

(19)   Williams, M.; Penfold, N. J. W.; Lovett, J. R.; Warren, N. J.; Douglas, C. W. I.; Doroshenko, N.; Verstraete, P.; Smets, J.; Armes, S. P. Bespoke Cationic Nano-Objects via RAFT Aqueous Dispersion Polymerisation. *Polym. Chem.* **2016**, *7*, 3864–3873.